EVALUATING SITE EFFECTS FOR ESTIMATION OF SEISMIC GROUND RESPONSE: A PRACTICAL APPROACH

by

Barbaros Çetiner

B.S., Civil Engineering, Istanbul Technical University, 2008

Submitted to the Kandilli Observatory and
Earthquake Research Institute in partial
fulfillment of the requirements for the degree of
Master of Science

Graduate Program in Earthquake Engineering

Boğaziçi University

2013

To my family

ACKNOWLEDGEMENTS

In the course of the preparation of this thesis, I have directly and indirectly benefited from the valuable contributions of a number of individuals. I would like to thank Professor M. Atilla Ansal for, throughout my Masters studies, sharing his vision of the expanses of ground response analysis practices that require further advancement. His thoughts helped me acquire a broader understanding of this significant engineering problem, and resultantly develop the essential theoretical knowledge which formed the basis of this study. I want to express my gratitude to Associate Professor Aslı Kurtuluş for her truthful appreciation of my academic endeavors, and sincere belief to my intellect. Last but not least, I would like thank Dr. Gökçe Tönük for her attentiveness to help whenever I came across a hurdle during my studies. Her empathy and alacrity gave me important support which simply cannot be overlooked.

ABSTRACT

EVALUATING SITE EFFECTS FOR ESTIMATION OF SEISMIC GROUND RESPONSE: A PRACTICAL APPROACH

Expansion of scientific methodologies to estimate the probable extents of ground motion effects in earthquake-prone areas is crucial for proper planning, investigation, and design of engineering structures. In this regard, accurate estimation of site effects instigated by the terminal geological structure at a considered location, in the presence of a seismic tremor, plays a particularly significant role. The key emphasis of this document is to develop a practical ground response analysis procedure comprised of a line of objective, well-outlined and simple-but-adept individual processes to address this aspect of the problem. In this study, to achieve that goal, a total of 1188 ground response analyses were performed for a combination of ground motion selection/scaling and equivalent-linear site response analysis techniques – all of which by itself constitute the current agreed practice within their parts – at 10 accelerometer sites. Each location evaluated herein was selected so that the recording station is a part of the Turkish Strong Ground Motion Network, with readily accessible, detailed geotechnical and geophysical reports; and at least a single earthquake event record, that correspond to the 10 per cent exceedance level in 50 years, existing. This allowed for a direct comparison of the result patterns obtained using each analysis component with the actual earthquake response; thus a truthful appraisal of how changing different parts of the overall procedure is reflected in the attained approximation level. For each station, the main output of the proposed method is a uniform hazard spectrum (UHS), fashioned in a similar way as that in major seismic codes. Therefore, as an auxiliary outcome of this assessment, a case study presenting the insufficiency of the currently adopted site factors for faithful estimation of site effects, and a vital application regarding how the suggested approach may play a role in improving the existing seismic code practice is as well provided.

ÖZET

ZEMİN YÜZEYİNDE SİSMİK YER HAREKETİNİN TAHMİNİNDE YEREL ZEMİN ETKİLERİNİN BELİRLENMESİ: UYGULAMAYA YÖNELİK BİR YAKLAŞIM

Deprem olma olasılığı bulunan bölgelerde, gözlemlenebilecek yer hareketlerinin boyutlarını değerlendirmek ve böylelikle mühendislik yapıları için daha güvenilir planlama, çözümleme ve tasarım yapılabilmesini sağlamak açısından, mevcut bilimsel yöntemlerin iyileştirilmesi mühim bir yer tutmaktadır. Bu bağlamda, sismik sarsıntılardan dolayı zemin yüzeyinden mühendislik anakayasına kadar uzanan tabakalaşmada oluşan etkilerin hassas bir biçimde belirlenmesi önemli bir rol oynamaktadır. İşbu tez çalışmasının amacı, bu konuda uygulamada gözlemlenen eksikliği, nesnel, iyi belirlenmiş ve basit-ama-gerçekçi bir yöntemler dizisi yardımıyla oluşturulan edimsel bir zemin davranış analizi aracılığıyla iyileştirmektir. Belirtilen amacı gerçekleştirmek adına, yerine getirilen çalışmada – her biri kendi içinde, an itibariyle, kabul görmüş uygulamaları oluşturan – çeşitli deprem kaydı seçme/ölçekleme ve eşlenik-lineer zemin tepkisi hesaplama teknikleri birleşimleri kullanmak suretiyle, 10 adet ivmeölçer noktasında, toplamda 1188 zemin davranış analizi yapılmıştır. Çözümlemeler kapsamında incelenen her münferit noktanın seçimi sırasında ilgili istasyonun Türkiye Ulusal Kuvvetli Yer Hareketi Ağı'nın bir parçası olması, kolayca erişilebilir, kapsamlı geoteknik ve jeofizik bilgileri bulunması ve 50 yılda yüzde 10 aşılma olasılığına karşılık gelen, en az bir deprem olayı kaydetmiş olması kıstasları göz önünde bulundurulmuştur. Böylece herhangi bir analiz yöntemi bileşeni ile elde edilen sonuç düzeninin gerçek deprem etkisi ile kıyaslanması; bu sayede de ilgili unsurlardaki değişikliklerin, hesaplanan değerlerin, kaydedilmiş tepkilere yaklaşım mertebelerini nasıl etkilediği gözlemlenebilmiştir. Ele alınan her bir yer için, ana çıktı olarak, bütün önde gelen deprem yönetmeliklerinde deprem tehlikesini ifade etmek adına benimsenmiş olan, sabit tehlike spektrumu hesaplanmıştır. Dolayısıyla, belirtilen karşılaştırmalara ek olarak, bu araştırmada, mevcut yönetmeliklerde benimsenen zemin katsayılarının yetersizliğini belirten bir vaka

incelemesi serisi ve önerilen yöntemin bu eksikliklerin giderilmesinde sahip olabileceği önemli konumu sahneleyen bir uygulama da bu çalışma ile birlikte sunulmuş olmaktadır.

TABLE OF CONTENTS

LIST OF FIGURES

LIST OF TABLES

LIST OF SYMBOLS/ABRREVIATIONS

$a(t)$	Initial (unscaled) earthquake time history
A	Incident wave amplitude
A_0	Amplitude of harmonic loading on a SDOF system
b	Amplitude coefficients related with $f(t)$
B	Reflected wave amplitude
c_{ik}	*S*pectral response at t_i resulting from the application of $f_k(t)$
C	SDOF response amplitudes at instants when tuning is needed
f	Frequency of vibration
$f(t)$	Set of adjustment functions used for wavelet calculations
F_{ij}	Transfer function relating disp. amplitudes of *i*th and *j*th strata
G	Shear modulus
G^*	Complex shear modulus
$h_i(t)$	Acceleration impulse-response function for a SDOF system
k	Wave number
k^*	Complex wave number
M_L	Local magnitude
M_s	Surface magnitude
M_w	Moment magnitude
P_i	Polarity of peak oscillator response at *i*th w and ξ pair
Q_γ	Effective shear strain ratio
R_{jb}	Joyner-Boore distance
SF_i	Scaling factor for the *i*th event
SA	Spectral acceleration
SA_i^{UHS}	Spectral acceleration value of the *i*th data point on a UHS
S_s	Spectral acceleration for short periods according to PSHA
S_1	Spectral acceleration for a 1-second period according to PSHA
t	Time
t_i	Time at which the maximum oscillator response is observed

T	Period of vibration
u	Ground displacement along the direction of wave stresses
$\ddot{u}$	Ground acceleration along the direction of wave stresses
υ	Propagation velocity along the direction of wave stresses
V_s	Shear-wave velocity
V_{s30}	Mean shear-wave velocity down to 30m from ground surface
w	Circular frequency
w_n	Natural circular frequency
W	Peak energy stored in a system per loading cycle
z	Location of the point at which stresses\strains are calculated
α^*	Complex impedance ratio
$\delta a(t)$	Adjustment time series compatible with the spectral misfit
ΔR_i	Spectral misfit at ith frequency/damping ratio pair
Δt_k	Time difference between t_k and the locus of wavelet
ΔW	Energy dissipated within a system per loading cycle
η	Material viscosity
ϕ	Phase angle
γ	Shear strain
γ_{eff}	Effective shear strain level signifying a transient loading case
γ_{max}	Max. shear strain level resulting from a transient loading case
γ	Frequency-dependent duration adjustment factor
ξ	Damping ratio (Fraction of critical damping)
μ	Mean squared error
ψ_i	Peak ground acceleration value of the ith event
ψ_{haz}	Peak ground acceleration determined for a location as per PSHA
ρ	Material density
τ	Time lag
ζ	Shear stress
DSI	General Directorate of State Hydraulic Works of Turkey

GMPE	Ground motion prediction equation
GRG	Generalized Reduced Gradient
IGVAnet	Istanbul Geotechnical Vertical Array Network
KiK-net	Kiban Kyoshin Network
MRDF	Modified Reduction Factor
NAF	North Anatolian fault
NGA	Next generation attenuation
NEHRP	National Earthquake Hazards Reduction Program
PDF	Partial differential equation
PEER	Pacific Earthquake Engineering Research Center
PGA	Peak ground acceleration
PGV	Peak ground velocity
PI	Plasticity index
PSHA	Probabilistic seismic hazard analysis
SDOF	Single degree of freedom system
TSGMN	Turkish Strong Ground Motion Network
TUBITAK	Scientific and Technological Research Council of Turkey
UHS	Uniform hazard spectrum

1. INTRODUCTION

For the sake of its mathematical convenience, and for developing a segmented but more specialized understanding on the principal features of complex nature of the phenomena, in determination of the surface response of ground motions affiliated with an earthquake event, the physical processes involved are considered to be influenced by three principal mechanisms; source, path and site effects. It is by convolution of these individual assemblages; one can calculate the aggregate effect of a seismic tremor to engineering structures. In reality, however, quantifying each of these mechanisms comprise significant aleatory and epistemic uncertainties. Thus, to form a well-founded theoretical approach, in accordance with this consideration, that is meaningful for engineering purposes; employing a probabilistic approach to determine the contribution of each defined component to a statistically determined overall performance level, with a definitive figure of total uncertainty, is indispensable.

In this regard, probabilistic seismic hazard analysis (PSHA) is an important tool to calculate the contribution of potential earthquake events of different magnitudes to the expected level of shaking at a particular location, and provides a collective estimate of essential ground motion parameters at desired exceedance rates [1]. Instead of the decisive viewpoint of a deterministic method, in this procedure, initially, the uncertainties in magnitude, position, and recurrence features of earthquakes; and in the variation of earthquake features by magnitude and position are exclusively computed (i.e. source mechanism). Following, using ground motion prediction equations (GMPEs), the level of ground shaking intensity estimated at the subject site is determined (i.e. path and site mechanisms), for all possible source traits, with due consideration to intrinsic uncertainties. Then as a final step, each of the uncertainties in location and magnitude characteristics of relevant earthquakes, and the predicted ground motion parameter are joined to attain the probability that the specified ground motion value will be exceeded at a given time duration [2].

In the described process, the prediction equations, i.e. GMPEs, when used in connection with PSHA, come to be a powerful tool to represent path effects. This is, indeed, expected as the effectiveness of an attenuation model is largely dictated by the relevance of its parent dataset to the deliberated seismic environment. Accordingly, from a geophysical standpoint, for earthquake events of analogous source properties, the principal path behavior – accurately speaking geometric spreading of seismic waves, and energy dissipation by the stiff-rock travelling medium [3] – in, for instance, all active tectonic regions of shallow crustal faulting[1] can be anticipated to comprise of similar attributes, irrespective of the event location (At least this is the statistical thinking implicitly adopted for categorizing uses of GMPEs). On the other hand, speaking in terms of estimating seismic ground response, the empirical means embedded in GMPEs for assessing site effects, including deep sediment response, involve limitations that vitally constraint their application to merely the geological formation classes that are adequately represented in the dataset employed for derivation of a relationship. Even further decreasing the efficacy of the developed empirical approaches is the adoption of the much-debated [4] [5] [6] [7] [8] [9] mean shear-wave velocity down to 30m from ground surface (V_{s30}) as the main correlating parameter, without exception, in every state of the art GMPE, including Next Generation Attenuation (NGA)-West2 models [10] [11] [12] [13] [14].

A sensible way that is broadly acknowledged in practice; and for geologies of lacking data, even recommended in code approaches, e.g. soil class E in NEHRP Seismic Provisions [15]; is the functional approach of benefiting from the adept fragment of PSHA results, i.e. combining source and path effects, but performing the calculations for the site effects in a separate, more detailed fashion, through using the ground shaking estimated at a reference site that is expected to display negligible nonlinear behavior while transmitting seismic waves. Depending on the established prediction relationship, definition of a reference site is typically relied upon the researcher's designation, based on the availability of data for the studied area. Nonetheless, considering the GMPEs utilized in developing probabilistic hazard maps for active tectonic areas of shallow crustal faulting such as Western United States [16], Turkey

[1] Even if "active tectonic regions of shallow crustal faulting" is, in this context, employed as an abstract example; this study is, in fact, passively limited to such environments; since the entire set of seismic hazard areas evaluated herein are identified to be located in active tectonic environments and subjected to shallow crustal earthquakes only.

[17], Italy [18], Greece [19] as a unified set, this value can be elected so that all PSHA calculations (excluding site effects) can be computed for a common locus, up to which each employed GMPE merely exhibits a fundamentally-linear soil amplification/de-amplification behavior.

Coherency computations performed by the author on downhole array recordings from various resources, including Kiban Kyoshin Network (KiK-net) and Istanbul Geotechnical Vertical Array Network (IGVAnet), for validating the linear soil behavior at a number of designated loci, points out that the V_{s30} value that distinguishes the boundary between NEHRP soil classes B and C, that is 760 m/s, (although not the most veracious) constitutes an ideal reference point for PSHA outputs (See Figure 1.1). Here selection of V_{s30} as a categorization parameter solely stems from the understanding that average shear-wave velocity for the upper 30m is by far the most accessible information for soil deposits with existing geotechnical figures. In addition, the selection of 760 m/s as a reference value, but not a higher V_{s30} at which a better coherency is expected, is justified by the thought that the nominated parameter shall not be smaller than that decided as the reference in any pertinent predictive equation; an in-depth analysis of documentation for GMPEs reveal that the least reference-level-V_{s30} designation in relationships derived for active tectonic environments subjected to shallow crustal earthquakes is, in fact, specified as 760 m/s by Boore et al. [11].

In this study, using this common locus as the profiling bedrock, a series of ground response analyses is carried out using two distinct, one-dimensional (1-D) equivalent-linear wave propagation solution procedures (hereafter simply referred to as 1-D solutions) making use of different rheological models to portray behavior of soil subjected to dynamic excitations; namely the procedure originally proposed by Schnabel at al. [20] and later modified by Idriss and Sun [21], and the method offered by Hashash et al. [22]. The reasoning for limiting herein discussion to solely 1-D solutions is mainly impelled by the popularity of such solutions among practitioners – as a consequence of the nominal number of parameters required for establishing necessary definitions – compared with the relatively demanding two- or three-dimensional codes utilizing comprehensive but elaborate soil models. Whereas the decided 1-D solution preference is predominantly manifested by the urge to inspect the

propriety of a frequency-dependent complex shear modulus formulation (i.e. in the case of the solution by Idriss and Sun; the expression developed by Udaka [23]) against frequency-independent modulus conceptions (which reflect the actual grain-slippage behavior arising under dynamic loading conditions [24] in a more fitting manner), in context of site response computation module for a site effects determination methodology.

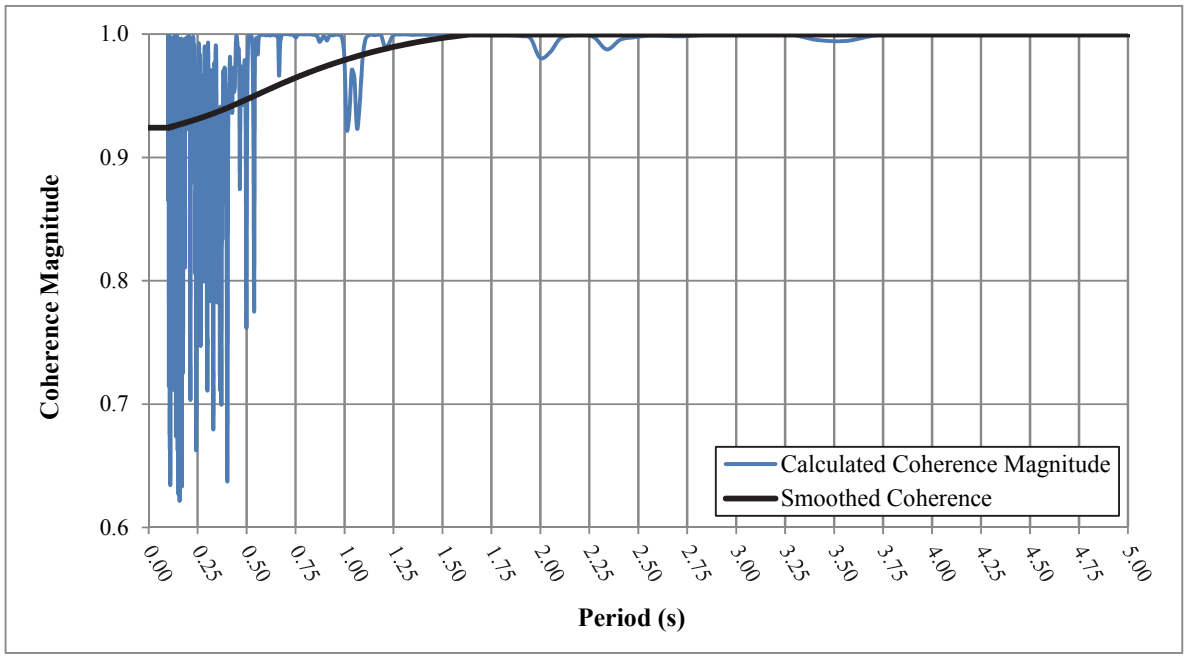

Figure 1.1. Magnitude squared coherence of the surface and borehole ground motions induced by October 23, 2004 M_w=6.8 Chuetsu Earthquake at KiK-net station NIGH15, PGA 0.189 g and 0.095 g respectively, computed using Welch's Averaged, Modified Periodogram Method [25]. The value of V_{s30} determined for this station is 740.67 m/s. Borehole acceloremeter installed within the array configuration is situated on a stiff rock deposit located at a depth of 100m, with measured shear wave velocity (V_s) of 1540 m/s

Another important facet of constructing a purposeful site effects calculation procedure is to define an input selection scheme; capable of preparing ground motion records that are pertained to the seismic environment at the appraised location, by paying satisfactory attention to the frequency content properties, hazard-compatibility and the contingent variability

features of potential events at the subject area. As PSHA, which for applications in this study is always conducted up to the surface of reference bedrock strata beneath the soil profile, produce results in the form of a ground motion parameter, e.g. peak ground acceleration (PGA), spectral acceleration (*SA*) and so on, through use of a meaningful mode of accelerogram decision, the criteria that express the seismic setting is as well fairly fulfilled. Herein, the ground response analyses are executed through three different means for establishing input records: (i) PGA scaling, (ii) Scaling to obtain the best-fit mean spectrum, and (iii) Nonstationary spectral matching via adjustment wavelets, using between 10 to 22 records per selection technique, for each case, to cogitate the aleatory unpredictability of a sesmic tremor. The only basis of restraining the adopted record selection arrangements to the itemized techniques simply resides on the opinion that these compose the most substantive set of procedures meant for this purpose.

In the following chapter, a brief discussion of the background on each of the exercised ground motion selection methods is furnished. Afterwards, the mathematical theory behind the one-dimensional equivalent-linear wave propagation solution procedures selected for carrying out computations is described.

The third chapter is structured in two main parts. The first part of the chapter offers a comprehensive discourse on the geological and geophysical properties of the Turkish Strong Ground Motion Network (TSGMN) stations that recorded the benchmark ground motion data used to assess the effectiveness of each input scaling and 1-D solution method combination to predict the ground response induced by a considerable seismic tremor (In this context, the qualitative expression “considerable” is gauged as the earthquake event that corresponds to 10 per cent exceedance rate in 50 years). Then, the calculated results for every individual combination are compared with the observed (measured) spectra. In the second part of the chapter, two-point site specific UHS are computed for each analysis location to generate code-comparable output for every single evaluated item. Then and there, comparisons between the standard spectra proposed in several significant seismic codes, in use at the present time, and the obtained spectra are delivered.

In the fourth and the final chapter, based on the results depicted in the third chapter, the recommended standardized ground response analysis methodology is outlined along with a thorough examination of its advantages and limitations. Consequently, through the findings of the realized investigations, propositions for improving the existing seismic code practice towards a more reliable planning, analysis and design exercise for engineering structures is conveyed.

2. THEORY AND BACKGROUND

In order to delineate the type of applications a procedure is intended for – that is to say the processes a technique can be validly exercised in – and to make way for constructive improvements within a developed methodology; it is of paramount importance to deliver a well-rounded background on the theory regarding the components which constitute that tool, along with the philosophy that paved the path for their existence. The primary objective of this chapter is to provide the needed contextual information related to the ground motion selection/scaling and 1-D equivalent-linear wave propagation solution methods evaluated in this study as components of a practical ground response approach. The presentation of the material follows a logical order. Therefore, as it is necessary to first establish a group of input records to execute any ground response analysis program; in the following discussion, initially, the employed ground motion selection algorithms are exhibited in a chronological manner. Then, the theoretical background of the 1-D solution by Idriss and Sun, a sequel to the groundbreaking code SHAKE [20] that inspired virtually all ground response analysis routines currently in use, followed by the theoretic essentials of the code developed by Hashash et al. (which in fact was set up to address what is perceived as the shortcomings of the preceding) are expounded.

2.1. Ground Motion Selection/Scaling Procedures

With the instrumental era of earthquake recording being only just about 124 years old today [26], there is a global shortage of recorded data; appropriate for engineering use, particularly for large-scale events (precisely speaking, ground motions with moment magnitude (M_w) greater than or equal to 6.0). As a consequence, today, more or less in every seismic assessment situation, it is required to firstly arrange a set of input motions that will sufficiently epitomize the seismic setting in an interested area.

Beginning from the earliest geotechnical/structural seismic considerations, there has been a continuous effort to conceive ways for appropriately tackling this problem. The three methods described in the following constitute the most apposite practice proposed for this intent and, as a result, shall be tested for applicability to a standardized methodology. Here, one might certainly proffer the argument that at least a single synthetic ground motion generation technique in the existing literature shall find use, as a minimum for review, in milieu of a site effects calculation approach. The main reason for not including such routines in the performed calculations is marked by the observation that, using the state-of-the-art knowledge regarding such generation methods, it is highly unlikely to achieve, let alone easy to get to, impartial parameter decision modes to produce records that are assured to depict the frequency-content and time-variation characteristics of actual earthquake recordings. The principal focus of this study, however, is to develop an objective, as well as standardized, methodology. Hence, synthetic earthquake record generation ways are simply not compatible with the goal of this research and thus not considered.

2.1.1. Preparation of Input Records by PGA Scaling

Possibly, one of the earliest appearances of the idea to rescale ground motions, in order to attain records serviceable for seismic considerations, was in the report published by Krinitzsky and Chang [27] in 1977, reflecting the state-of-the-art practice at the time. In their study, they proposed scaling of input ground motion records that were obtained at sites of fault type, site geology and fault distance traits complacent with the properties of the maximum credible earthquake determined for a subject area, to a range of either PGA or peak ground velocity (PGV) values; the choice of the controlling criteria depending on the whichever is deemed the most significant for the application; prior to use in dynamic response analysis.

In this specific study, the objective was to develop design earthquakes that can be reliably employed for analysis of critical structures, and, in that sense, the parameters PGA or PGV depict the intensity measures that were, at the moment of this study, believed to be the main correlating parameters for structural damage (most likely, because *SA* began to find relatively wide use, both as an engineering parameter and a risk index, only after 1971 [28]).

However, in the current practice, a parallel reasoning is generalized to literally any earthquake engineering situation, through implementation of the correct intensity measure (or measures); proved to correlate well with the concerned phenomenon; as target parameter/parameters for scaling. Hence, by way of this simple process, a somewhat adequate transition is ensured between PSHA results and the corresponding input motions.

As mentioned in Chapter 1, a truthful representation of site effects can only be achieved through determination of PSHA results at a valid reference level, at which merely an insignificant degree of soil (or rock) nonlinearity is anticipated. Therefore, so to perform ground response calculations, the seismic hazard results (free from site effects) shall be described at this locus, in terms of intensity measure(s) that well-relate to the ground shaking; so that the input motions obtained using a scaling procedure yields objective outcomes. In this regard, a natural selection for a scaling criterion is PGA; a parameter, by itself, observed to display a reasonably strong correlation with ground shaking intensity in numerous studies [29], [30], [31], [32], [33], [34].

Selection and scaling of input records with respect to reference-level PGA is a very straightforward practice. As in just about any ground motion selection procedure, the initial step of the process requires determination of the key source and path features of the design earthquake predicted for the subject site at respective exceedance rates, through a deterministic analysis based on the disaggregation results of PSHA. For ground response analyses, most important of these parameters can be listed as: magnitude (i.e. M_w), mechanism (e.g. strike-slip, normal, etc.), distance (to the recorded site, preferably identified as Joyner-Boore distance [R_{jb}]) and depending on the exercise, duration information of a seismic event. Once this knowledge is established, by defining these factors in intervals – except the mechanism information – suitable records are queried on the basis of the data attained from hazard results [35]. At this stage, demarcating a range for each factor is a contrivance to find adequate amount of records for analyses (given the lack of large-scale event recordings in current databases) and to eliminate bias within the selection set. As a rule of thumb, a range of $\pm$ 0.5, $\pm$ 20 km and $\pm$ 20s is frequently used for describing magnitude, distance and duration properties respectively to form the preliminary group of records. Also a vital consideration at

this phase, except in cases where directivity and directionality conditions are of particular concern, is to exclude records obtained at near-field sites to prevent unsolicited bias in the developed set.

In the next step, the input motions that are perceived to satisfy set limitations are filtered depending on their compatibility with the locus site condition. Due to widespread lack of accelerograms retrieved at stiff, rock-like sites which display average shear-wave velocities identical to that defined for the reference level, worldwide, at this phase, it is also necessary to impose the selection criterion in terms of an interval of V_{s30} values. According to the coherency computations carried out, a V_{s30} range of 680-830 m/s can function as a suitable range for this purpose, without substantial compromise from the elastic-resemblant behavior reached at deposits with measured V_{s30} value the same as that expressed for the locus constituting the base of the profiling for site effects computations, i.e. 760 m/s.

Subsequent to the second step, a record set that can be presumed to model the frequency content of the target design earthquake is obtained. At this juncture, to make these records hazard-compatible (and perform necessary amplitude adjustments), the acceleration time series saved for each record component shall be multiplied with a scale factor (SF_i) so that their PGA (ψ_i) levels are normalized to the peak ground acceleration value calculated through PSHA (ψ_{haz}). This scale factor can be described in mathematical terms as;

$$SF_i = \frac{\psi_{haz}}{\psi_i} \tag{2.1}$$

Where ψ_i is calculated such that:

$$\psi_i = \max\left(|a_i(t)|\right) \tag{2.2}$$

In Equation 2.2, $a_i\ (t)$ signifies the acceleration acceleration-time history for the i_{th} component of the final record set and the enclosing brackets "| |" stand for the absolute value.

As an example, Figures 2.1 and 2.2 provide a visual illustration of the spectral accelerations within the record set that is, in this study, put together for performing ground response analysis for Ceyhan, Adana site (at which a strike-slip earthquake of M_w=6.2 with R_{jb} roughly equal to 40 km is anticipated as the design earthquake corresponding to 475-year return period), before and after the amplitude adjustments incurred by PGA scaling respectively. The calculated hazard PGA level for the subject site is 0.34g. For engineering comparison, both figures also display the mean spectrum of the whole group of selected components and the two-point UHS calculated at the considered site based on PSHA.

It can be easily noticed that, the discussion conveyed to this point merely offers explanations regarding how PGA scaling provides means to produce hazard-compatible record sets that depict the frequency-content characteristics of potential events expected at a location without any emphasis on time-variation features of seismic occurrences and how this aspect of the problem is addressed. This facet of scaling techniques is discussed in Section 2.1.3.

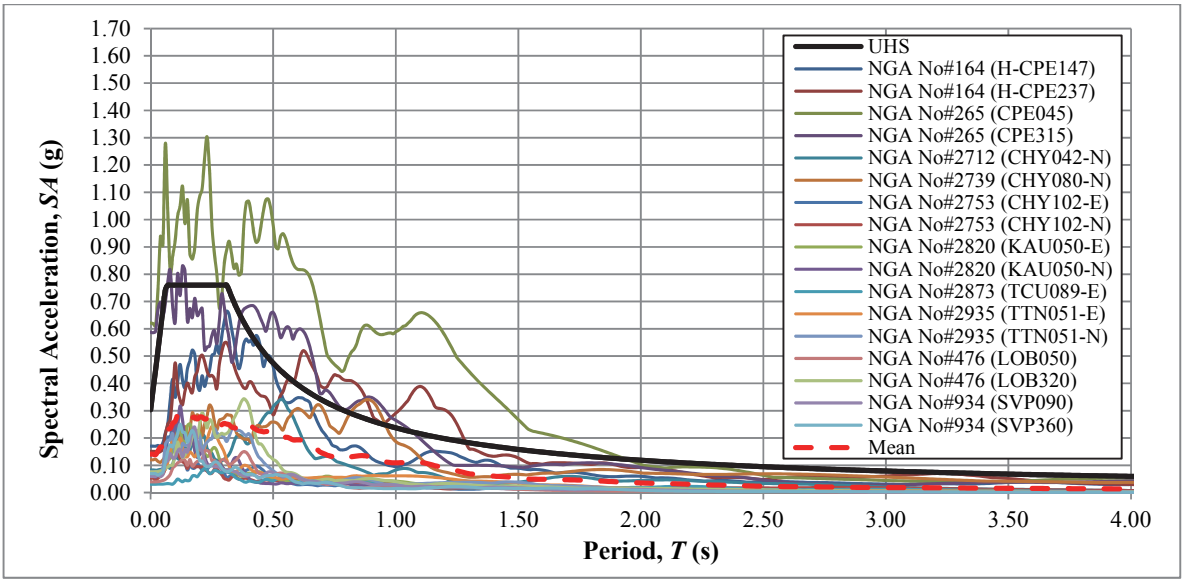

Figure 2.1. 5%-damped response spectra of 17 earthquake record components retrieved from strike-slip events of M_w=6.19-6.53 and R_{jb}=12.4-45.5 km

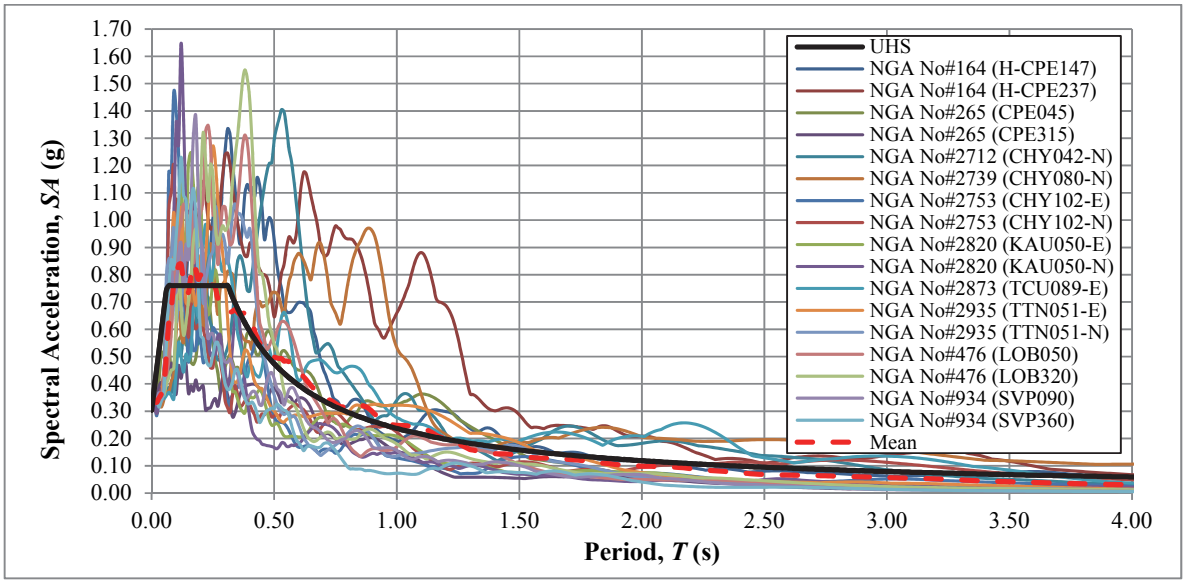

Figure 2.2. 5%-damped response spectra of earthquake record components presented in Figure 2.1 after normalization of each time series to the hazard PGA level of 0.34g

2.1.2. Preparation of Input Records by Scaling to Obtain the Best-Fit Mean Spectrum

Response spectrum, a concept first introduced by Maurice A. Biot in 1932 [36], serves as a favorable tool to compile peak response of single degree of freedom (SDOF) systems with different stiffness properties to a specific component of an earthquake motion in a compact manner. Henceforth; using of the theory of structural dynamics; it delivers a practice-oriented instrument for structural design and implementation of the lateral-force requirements in seismic codes. In view of that, describing earthquake behavior in terms of a design spectrum becomes a central concept in earthquake engineering.

Given one of the key objectives of computing seismic ground response is to evaluate the level of shaking that an engineering structure would be susceptible to at the base level, utilizing response spectra is unquestionably very crucial for describing site effects. On the other side, by performing suitable mathematical manipulations, it is possible to model the linear (or approximately linear-elastic) behavior of a reference rock layer under dynamic excitations as a series of single degree of freedom systems (SDOF) [37], therefore in theory it

can be proved that the ground shaking intensity at a rock site is extensively interrelated with the spectral accelerations determined for that site (Thus, *SA* is a significant index for describing hazard information on the transmitting base, in site effects computations). For that reason, similar to the case for PGA scaling, discussed in Section 2.1.1, a technique can be evolved such that ground motion records selected based on the affinity with the design earthquake and locus site condition can be scaled so that the spectrum represented by that set of components match the UHS determined via PSHA. Consequently, by use of response spectra both at the base of the soil profile and at the surface of an interested layer to describe earthquake behavior, the effects of surficial layers on the ground motion characteristics is identified in a simple but commanding way.

As expected, the pathway for input motion scaling to match the average spectrum of a record set with a marked UHS follows steps identical to that described for PGA scaling at 1st and 2nd stages, that is querying components with respect to a defined range of earthquake properties mirroring the seismic event properties determined to be relevant for the subject site, for an exceedance rate of 10% in 50 years, and narrowing down the attained group based on the pertinence of their V_{s30} values to the defined levels. The step at which the two approaches diverge from each other, at least in arrangement, is the final stage.

Since, UHS is a figure that is typically (but not necessarily) composed with reference to two spectral acceleration values determined through PSHA, that is the spectral acceleration values for the periods of 0.2s and 1.0s, i.e. S_s and S_1 respectively, in this scaling method, the target parameter to match input motions is not as simple as in the case of PGA scaling, where a single parameter functions as the normalization level. It is essential to define a proper scaling coefficient calculation procedure to find the optimal solution for each SF_i to obtain the best-fit mean spectrum for a record set. The most computationally-efficient way to achieve this task is to first define a quantitative measure that assesses the extent of congruity, that is the mean squared error (μ), between the mean spectrum of the subject dataset and the target UHS – in which a result of zero indicates complete-agreement – and then using an optimization routine, minimize the cumulative difference calculated via that measure to obtain a best-fit solution. Herein, this task is performed by means of the following criterion;

$$\mu = \min\left(\sum_j \left\{\frac{\sum_{i=1}^{n}\left[SA_i(T_j) \times SF_i\right]}{n} - SA_i^{UHS}(T_j)\right\}^2\right) \quad (2.3)$$

where $SA_i(T)$ denotes the spectral acceleration value of the ith event, within the evaluated ground motion set, for the period of T; n denotes the total number of records in the subject record group; T_j signifies the jth period value on the mutual period vector employed for expressing the response spectra (which is in this study defined as the 1201-point vector consisting of values starting from 0.00s and increasing at a rate of 0.01s until reaching 12.00s); SA_i^{UHS} connotes the spectral acceleration value of the ith data point on the UHS determined for the subject location via PSHA; and, finally, the function "min( )" stands for the optimization operation that minimizes the value of μ through determination of SF_i such that the best-fit tally between the mean spectrum of the appraised record assemblage and the PSHA-determined UHS is achieved.

For performing the input preparation calculations included in this document, Generalized Reduced Gradient (GRG) 2 nonlinear optimization method developed by Lasdon et al. [38] is employed to attain the desired best-fit matching. As, the considered problem is a nonlinear one, in order to improve the chance of finding the globally optimal solution using this algorithm, the code is executed using multiple starting values for SF_i (adjusted at the start to reside within a few orders of magnitude of each other to establish a well-scaled model); channeled by the course and curvature of the imposed objective function, and the auxiliary constraints. Such a tweak helps avoid the recognized pitfall of the code terminating at a peak or valley closest to the supplied initial values. Moreover, by enforcing the two supporting constrictions, in the following, on the model, the scatter within the scaled set of input motions is limited.

$$\max(SA_i) \leq 1.5S_s \quad (2.4)$$

$$\min(SA_i) \geq 0.85S_s \tag{2.5}$$

Throughout the herein optimization computations, the conditions stated in Equations 2.4 and 2.5 are fully coerced, and the iterations are concluded only when the relative change in the objective function is less than the convergence tolerance of 10^{-7} for the last five iteration steps.

Figure 2.3 demonstrates the results of the record scaling realized for the accelerogram set shown in Figure 2.1, using the discussed procedure, for preparation of input motions applicable to ground response analysis. It is palpable from the provided visual depiction that for this specific case, i.e. Ceyhan, Adana site, the mean spectrum for the obtained record assemblage turn out to be very similar to what is calculated using the PGA scaling technique, while displaying a notably diminished overall scatter from the UHS.

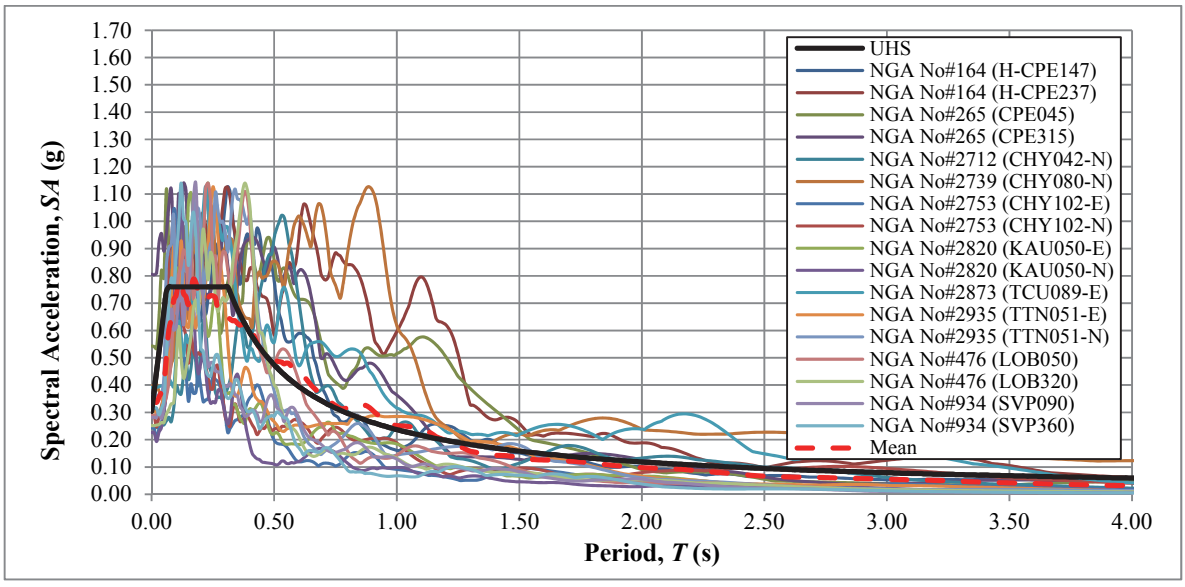

Figure 2.3. 5%-damped response spectra of earthquake record components presented in Figure 2.1 subsequent to scaling to obtain the mean spectrum that is best-fit with the PSHA-determined UHS

2.1.3. Limitations of Scaling Actual Recorded Events for Establishing Input Motions

The primary motivation of using actual recorded events to prepare input accelerograms for ground response analysis is to ascertain that the frequency content associated with an anticipated design earthquake is properly replicated for engineering use. Considering the objective ways of synthesizing time histories that satisfactorily represent the genuine earthquake tremors are virtually nonexistent, scaling of available records complacent with the seismic environment at a subject site is a facile and efficacious instrument to develop acceptable data towards analysis, design and evaluation applications. Probably, as a result of that very convenience one might easily encounter situations in practice where this approach is mistreated, by adopting beyond its range of application.

A very important consideration when employing scaling techniques in connection with actual time histories is to acknowledge the right interval of values for scaling coefficients depending on the studied problem. Obviously, a logical range for the factors shall be located around unity so that the deviation in frequency content resulting from the elastic/inelastic nonlinearity in force-deformation behavior is minimized. Nonetheless, from a pragmatic stance, this is a rarely experienced situation; as, especially for large-amplitude design events, the potential choices (retrieved on the defined locus site condition) are bound to a handful of pairs. Then the question becomes, how do we decide on the confines of applicable scaling?

Seeing the popularity of scaling methods for input preparation, surprisingly, the literature on this issue is particularly scarce. However, the recommendations of these (two) papers shall, without doubt, be a good starting point for efforts to reply this question. In their lead study on ground motion scaling, following an analysis of 187 earthquake records compiled and processed by California Institute of Technology, Krinitzsky and Chang [27] suggested that, for preparation of engineering input, no ground acceleration data shall be divided or multiplied by a factor greater than 4 and the scaling coefficients should be reserved in the proximity of 1 whenever possible without commenting on their reasoning for their argument. Ensuing this work, Vanmarcke [39], using a rather smaller dataset, containing records from 70 events, re-examined that recommendation through a more circumspect

statistical assessment utilizing acceleration amplification factor, inelastic acceleration response ratio and equivalent number of cycles as scaling invariant parameters. He concluded that the advised interval shall be more tolerable to appraisal of linear-elastic structures, hence depending on the engineering emphasis; described range shall be further narrowed.

Keeping in mind none of the of the today's seismic codes propose a restriction on the coefficient of scaling for input preparation, and some databases even adopting factors as high as 30 for establishing records at preferred amplitude ranks, both of these studies founded on highly empirical evaluations might seem to offer bold statements on this matter. Nevertheless, even if the intervals endorsed by these studies are not definitive, or possibly incorrect, the comprehension that the scaling factors used with actual time histories shall be limited is undoubtedly valid and can be proved using the present geotechnical knowledge.

To deliver a simple example to justify this opinion, analyzing downhole array records for a large–amplitude records retrieved from an M_w>6.0 seismic event occurrence can provide invaluable substantiation. Here, in order not to deviate from the main topic, we examine a single such situation; the East-West component ground-acceleration data from the October 23, 2004 M_w=6.8 Chuetsu Earthquake recorded at KiK-net station NIGH15 (The coherence results of which is demonstrated in Figure 1.1). The first step of the evaluations is to compute blind predictions of the ground response using the downhole record obtained within a granite rock geology, with a measured V_s value equal to 1540 m/s, as the rigid base motion of the profile, set up according to the available P-S logging and geological information. In this particular case, the analyses are executed using the 1-D equivalent-linear calculation scheme built in DEEPSOIL [22], and the nonlinear site response approach proposed by Hashash et al. [40] using the Modified Reduction Factor (MRDF) Pressure-Dependent Hyperbolic Model [41] to represent the cyclic behavior, and frequency-independent formulation to model damping behavior of soil/rock strata; enabling a more comprehensive depiction of nonlinear site characteristics. Figure 2.4 demonstrates how the results of the performed calculations compare with the authentic surface accelerogram.

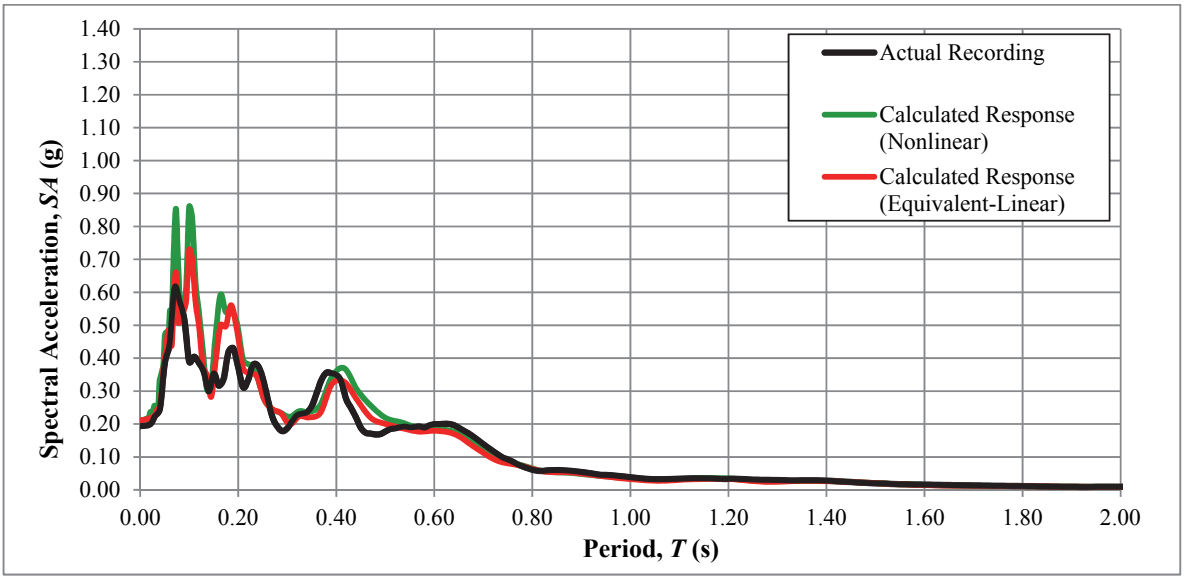

Figure 2.4. A comparison between the 5%-damped response spectra of actual East-West component surface time history retrieved at KiK-net station NIGH15 for the 2004 M_w=6.8 Chuetsu Earthquake, and the seismic responses computed using the downhole record triggered by the identical seismic tremor using 1-D equivalent-linear and nonlinear approaches

There are remarkable similarities between the actual and computed ground responses. Both the 1-D equivalent-linear and nonlinear techniques are effective in capturing the spectral behavior of the recorded time history, only mistaken by exhibiting an extra peak after the initial rise in the spectrum. On the other hand, the amplitudes are overestimated in the calculation results by a factor of 1.07 and 1.39 at the fundamental peak, and 1.38 and 1.30 at the longer-period-peak-response through equivalent-linear and nonlinear analysis techniques respectively (with solely the extent of the last significant peak being similar in both situations). This obvious discrepancy most certainly is an effect of the underestimation of damping levels within rock strata as a consequence of the probable incompatibility between the dynamic properties suggested for rock-like materials by EPRI [42], used for determination of dynamic properties – i.e. strength degradation/damping curves in equivalent-linear method and constitutive model parameters in nonlinear method – of deep-gravel and granite layers, and the characteristics of the considered formation. Even so, the attained analysis output

should be sufficient to characterize the change in frequency content of a reference time history induced by scaling techiques.

In order to keep this argument at the simplest degree as possible; herein, two different situations, where the base motion is doubled and halved in amplitude by scaling, are investigated. The ground response results for each case, calculated using the equivalent-linear and nonlinear methodologies as in the prior item, are illustrated in Figures 2.5 and 2.6 respectively. To begin with, it is clear from the shown results that the scaling performed at the base of a profile does not directly reflect to the obtained response (for instance halving the amplitude of base motion does not yield a surface response half of that observed with the full record). The actual scaling coefficients for surface accelerations calculated using equivalent-linear technique are determined as 1.65 and 0.64 respectively, by calculating the ratio of spectral response of the second peak of each spectrum. In the case of nonlinear site condition modelling; these factors are computed as 1.34 and 0.66 respectively. To be able to distinguish the effect of nonlinearity, it is vital to note that this is an upshot of amplitude reduction occuring at intermediate soil/rock layers instigated by wave scattering, but not a consequence of augmented damping resulting from stimulation of larger strain levels. In essence, the tangible effect of inelastic behavior is evident in the results for the situation with the based motion doubled.

For the condition where the base motion is set as the twice of what is recorded, irrespective of the computation methodology, the calculated results display a fundamentally different behavior from the estimation for actual surface response, where the effect of nonlinearity is proved to be trivial by coherency computations. In this situation, the influence of inelastic behavior results in a considerable stifness degradation leading to a sizeable surge in the response amplitudes, accompanied by slight period shifts, for 3^{rd} and 4^{th} peaks, eventually entailing an extensive change in frequency content. Needlees to say, this change cannot be reproduced in a scaling method, as a frequency adjustment mechnism cannot be implemented in akin procedures.

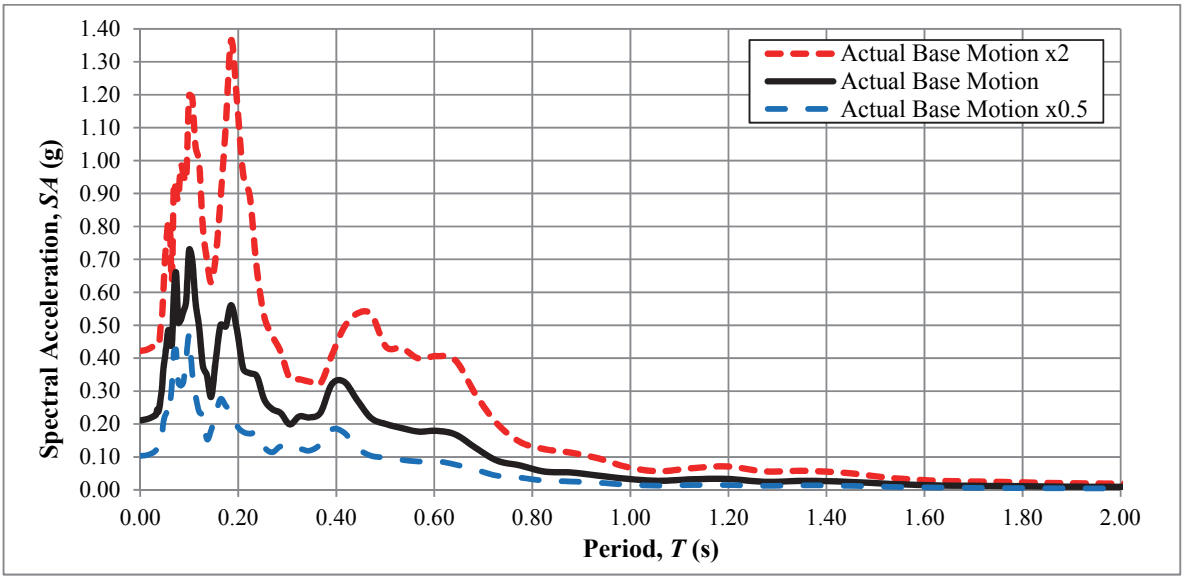

Figure 2.5. A comparison of the 5%-damped ground response results attained using actual, double and half the amplitudes of the East-West component base motion recorded at the KiK-net station NIGH15 for the 2004 M_w=6.8 Chuetsu Earthquake via equivalent-linear approach

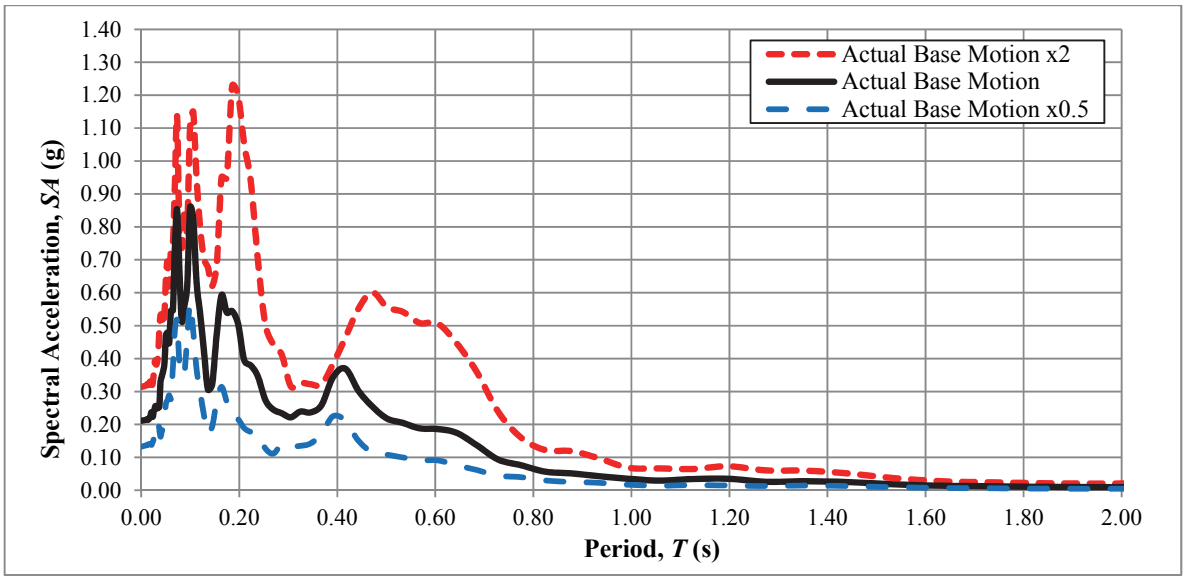

Figure 2.6. A comparison of the 5%-damped ground response results attained using actual, double and half the amplitudes of the East-West component base motion recorded at the KiK-net station NIGH15 for the 2004 M_w=6.8 Chuetsu Earthquake via nonlinear approach

Investigating the product of the analyses carried out using half the actual base motion, nonetheless, yields findings that provide completely different implications. As expected, the shape of the response spectrum for this case is virtually the duplicate of the spectrum for the estimated surface reaction; all the peaks are scaled down by approximately the same factor and the periods of the peaks are matching. Thus, as a direct corollary from the observed behavior, the scaling methods, in fact, return realistic results as long as nonlinearity threshold is not reached within the reference geology to achieve a response that satisfies target amplitude levels.

Now, going back to the starting point of this discussion, how can we decide on an appropriate range of scale factors for the scaling techniques discussed above? Although for making more generalized inferences an increased amount of analysis results is necessitated, based on the prior example, a correct range of scaling coefficients for the discussed techniques appear to be dependent on the geotechnical characteristics of the reference site where the record is acquired. With the onset of nonlinear behavior the frequency-content characteristics of the response undergo vital changes; so by having a rough idea on the dynamic properties of the interested formation, the threshold level at which this transformation occurs can be decided, using both physical or statistical techniques, depending on which is more releveant to the context. Currently, however this subject remains an open issue that certainly needs further elaboration, and at this point, from a practical stance, the best option appears to curtail the amount of scaling whenever possible, especially for the situations when the records are required to be upscaled.

The disccusion to this point focused on the constraints of scaling techniques arising from the inherent traits of a methodology. Though, another equally noteworthy exigency of using scaling techniques, borne due to the employed dataset itself, is the necessity to take into account time-variation features of seismic occurrences. Knowing that at the moment, there are not any analytical procedures available meant for this problem, practically, in all cases, this complication is dealt by using an adequate amount of time histories in the performed analyses to aptly consider aleatory unpredictability of an earthquake event (whereas the number of records deemed “adequate” depends on the exercise).

Current literature shows that, seismic response analyses executed by means of a relatively small record set will most likely display results shifted toward the prevailing response type/types within that group. Hence for obtaining meaningful outcomes, it is necessary to establish an assemblage of inputs that include a broad range of response behaviors to eliminate an overall result biased towards a particular performance. Among the existing research findings, specifically the study by Rathje et al. [35] provides significant insight regarding the matter. Using input motion groups of 5, 10 and 20 events (five suites from each) selected from an up-to-date dataset of 105 records and matched to the Abrahamson and Silva [43] response spectrum depicting a M_w=6.5 and R_{jb}=20 km, they conducted equivalent-linear analyses to observe the point when a stable median response is attained. The results indicated a difference of 15-20% between different suites of five motions, while the discrepancies are reduced to 5 to 10% when 10 and 20 motions sets are used. As a consequence, to account for the intrinsic variability of ground motion records, they suggested that at least 10 accelerograms, and preferably 20, shall be employed when the standard deviation of the surface response is of interest. In this study, this recommendation is accurately followed in all of the calculations utilizing the input motions established through the described scaling schemes.

2.1.4. Establishing Input Records by Nonstationary Spectral Matching

The techniques discussed to this point reflect the methodologies that modify actual ground motion recordings via linear scaling coefficients to adjust accelerograms for establishing a set of input motions that is compatible with the seismic hazard determined at the considered locus. These methods are simplistic processes that provide practitioners an intuitive mode of forming a record group for ground response analysis. Nonetheless, for most situations, this ease in scaling is countered by the extra effort paid in determination of design earthquake parameters for the interested site through the site-specific disaggregation analysis. Besides, as explained in the previous section, preparation of input records by scaling with respect to a constant multiplier involves two considerable drawbacks, which without proper concern may lead to significant deviation from the initial assumptions that these processes are founded on.

Spectral matching techniques – irrespective of the adopted calculation approach – do not possess any of the limitations that govern the matching methods discussed in the previous sections. Except in the cases where excessive site effects are prevalent, likewise that visible for very soft ground conditions, the effectiveness of spectral matching processes in producing records closely compatible with the target UHS (by altering the variances between the frequency content on soil and rock sites) thwart the added labor spent for establishing the preliminary earthquake record group while using scaling approaches. Moreover, by contiguous matching of target hazard spectrum, spectral matching procedures largely decrease the number of records required to satisfy reference UHS [44], without eliminating the inherent natural time-variation features of earthquake events.

From a critical viewpoint, the records generated by spectral matching practices are not realistic, even if time histories attained through certain procedures, in appearance, resemble actual earthquake records. By matching individual records to a target UHS, one, in fact, generates an accelerogram that simulates an envelope of multiple earthquakes. This smooth spectral shape obtained subsequent to spectral matching is fairly dissimilar with the spectral response of a typical earthquake ground motion, which is composed of large crests and troughs. Nonetheless, the outputs created by spectral matching processes appear to be well-suited for ground response analysis calculations, particularly for those adopting a one-dimensional computation algorithm. Therefore, a procedure constructed on a numerically-stable, nonstationary adjustment system, to serve this purpose, shall be certainly adopted for appraisal as a part of a practice-oriented ground response scheme.

Herein the nonstationary, time-domain spectral matching procedure proposed by Al Atik and Abrahamson [45] is evaluated in context of a ground response analysis methodology. Based on the author's experience with various noteworthy spectral matching processes existing in the prevailing literature, this method provides noticeably better convergence properties, computational efficiency and preserving of nonstationary characteristics of the originating time histories. In addition, the relatively simple and objective utilization of the proposed method to calculate spectrum matched records makes it one of most appropriate candidates for utilization within the framework of seismic response calculations. In the

following, a concise explanation of the spectral matching method implemented in the procedure proposed by Al Atik and Abrahamson is conveyed.

The Lilhanand and Tseng [46] algorithm employed in the spectral matching procedure by Al Atik and Abrahamson essentially comprises of a methodology that is based on altering of ground motion time series in time-domain by making use of wavelet functions. The central postulation of this computation arrangement is that the time of the peak oscillator response (t_i) generated by the originating record, for a defined frequency and damping value, is not shifted as a result of wavelet modifications. Consequently, the spectral misfit (ΔR_i) between the target UHS and response spectrum of the considered time history at a given frequency (w_i) and damping ratio (ξ_i) is described as;

$$\Delta R_i = \left(SA_i^{UHS} - SA_i\right)P_i \tag{2.6}$$

where, P_i denotes the polarity of the peak oscillator response (If the response is positive P_i=1; if the response is negative P_i = -1. Then, if one calculates a tuning series, $\delta a(t)$, to amend the initial record, $a(t)$, such that the peak oscillator response of the modifier time history at t_i equals the spectral misfit (ΔR_i) for all i, it is possible adjust the originating ground motion into a spectrum-compatible recording. Speaking in mathematical terms $\delta a(t)$ can be defined as;

$$\delta a(t) = \sum_{k=1}^{N} b_k f_k(t) \tag{2.7}$$

In Equation 2.7, $f_k(t)$ signifies the group of adjustment functions and b_k represents the pertinent amplitude coefficients that need to be established at a total of N spectrum points.

Based on the knowledge developed for the theory of random vibrations, the spectral response of the time series $\delta a(t)$ shall be calculated for a w_i and ξ_i pair as;

$$\delta R_i = \int_0^{\infty} [\delta a(\tau) h_i(t_i - \tau)]\, d\tau \tag{2.8}$$

where $h_i(t)$ denotes the acceleration impulse-response function (IRF) for a SDOF system and τ signifies the time lag used for carrying out integrations. The $h_i(t)$ is defined as $h_i(t)$=0 for values of t less than zero and such that as defined in Equation 2.9 for values of t greater than zero [47].

$$h_i(t) = \frac{-w_i}{\sqrt{1-\xi_i^2}} e^{-(w_i \xi_i t)\left[\left(2\xi_i^2 - 1\right)\sin\left(w_i t\sqrt{1-\xi_i^2}\right) - 2\xi_i\sqrt{1-\xi_i^2}\cos\left(w_i t\sqrt{1-\xi_i^2}\right)\right]} \tag{2.9}$$

Consequently, putting in the terms in Equation 2.8 into 2.7 yields;

$$\delta R_i = \sum_{k=1}^{N} b_k \int_0^{\infty} [f_k(\tau) h_i(t_i - \tau)]\, d\tau \tag{2.10}$$

Now setting the term c_{ik} to denote the spectral response at time t_i at ith w_i and ξ_i couple resulting from the application of $f_k(t)$ (i.e. the integral terms in Equation 2.10), the preceding expression is rearranged as;

$$\delta R_i = \sum_{k=1}^{N} b_k\, c_{ik} \tag{2.11}$$

Note that, as the aim of the resultant formula is to select b_k and c_{ik} so that $\delta R_i = \Delta R_i$, the equation derived in 2.11 delivers an alternative way to express the spectral misfit. Hence the amplitude of each adjustment wavelet can be determined as;

$$b = C^{-1}\delta R \tag{2.12}$$

where square matrix *C* denotes the array that includes the amplitude of each SDOF spectral response at the instant when the response characteristics need to be attuned through an alteration wavelet.

Then, substituting the Equation 2.12 into Equation 2.7, the adjustment time series at an iteration step is given by;

$$\delta a(t) = \sum_{k=1}^{N} [C^{-1}\delta R] f_k(t) \tag{2.13}$$

Subsequently the modified time series at an iteration step is calculated as;

$$a_j(t) = a_{j-1}(t) + \gamma \delta a_j(t) \tag{2.14}$$

where γ is a moderation factor, between 0 and 1, used to dampen the adjustments and $a_0(t)=a(t)$ (i.e. originating time series).

At this juncture, the only parameter that needs to be described to carry out the necessary calculations is the adjustment function, $f_k(t)$. In the method suggested by Al Atik and Abrahamson, this entity is selected so that any drift in velocity and displacement behavior induced by the computed time series is eliminated. Furthermore, to implement a computationally efficient matching procedure, the function is decided such that determination of an analytical solution for elements of *C* is possible. The following equations define the improved tapered cosine wavelet developed by Al Atik and Abrahamson to perform spectral matching computations.

$$f_k(t) = \cos\left[w_k\sqrt{1-\xi_k^2}(t - t_k + \Delta t_k)\right] e^{-\left(\frac{t-t_k+\Delta t_k}{\gamma_k}\right)^2} \tag{2.15}$$

where the frequency-dependent duration adjustment factor γ_k, and the time difference between the instant of peak oscillator response (t_k) and the locus of wavelet, Δt_k, are defined by Equation 2.16 and 2.17 respectively.

$$\gamma_k = 1.178 f_k^{-0.93} \tag{2.16}$$

$$\Delta t_k = \frac{\tan^{-1}\left(\frac{\sqrt{1-\xi_k^2}}{\xi_k}\right)}{w_k\sqrt{1-\xi_k^2}} \tag{2.17}$$

Figure 2.7 displays the results of the spectral matching computations performed using Al Atik and Abrahamson method, for the record group presented in Figure 2.1. In addition, Figure 2.8 and Figure 2.9 provide an illustration of a time series within the evaluated set (i.e. NGA No#265 (CPE045) time history recorded during, M_w=6.33; October 24, 1980; Victoria, Mexico Earthquake on a site of V_{s30}=659.6 m/s) prior and subsequent to performed calculations, and the velocity/displacement time histories determined from the matched event, respectively. As expected, the robust nonstationary method developed by Al Atik and Abrahamson prevents any unwanted drifts in the velocity and displacement characteristics of the accelerograms developed by the matching procedure. Moreover, as a result of the refined calculation modes utilized to ensure agreement with the target UHS, each accelerogram obtained through the defined process shows minute differences from the estimated hazard at the reference site condition. Therefore, the need for a large set of ground motions to develop hazard-compatible input motions to attain stable seismic response results is relieved.

By way of a rudimentary visual inspection, one can easily conclude that the Al Atik and Abrahamson technique performs significantly well, compared to the previously defined input motion preparation practices, in providing records that are in-line with PSHA results. However, the unrealistic spectral shape seen in ground motions prepared via the suggested technique lead many to the question whether such time series are meaningful for seismic analysis purposes. This inquiry shall best be responded by examining the semblance of ground response analysis results computed using each of the candidate procedures with actual

measurements. An in-depth investigation aimed to fulfill that objective is furnished in the next chapter.

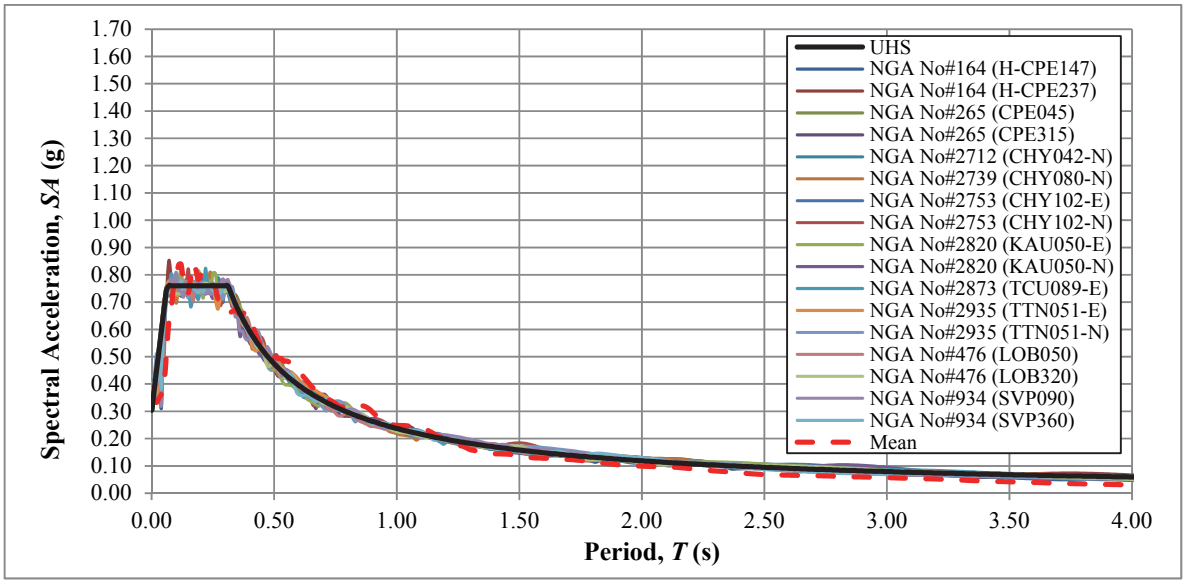

Figure 2.7. 5%-damped response spectra of earthquake record components presented in Figure 2.1 subsequent to spectral matching via Al Atik and Abrahamson technique

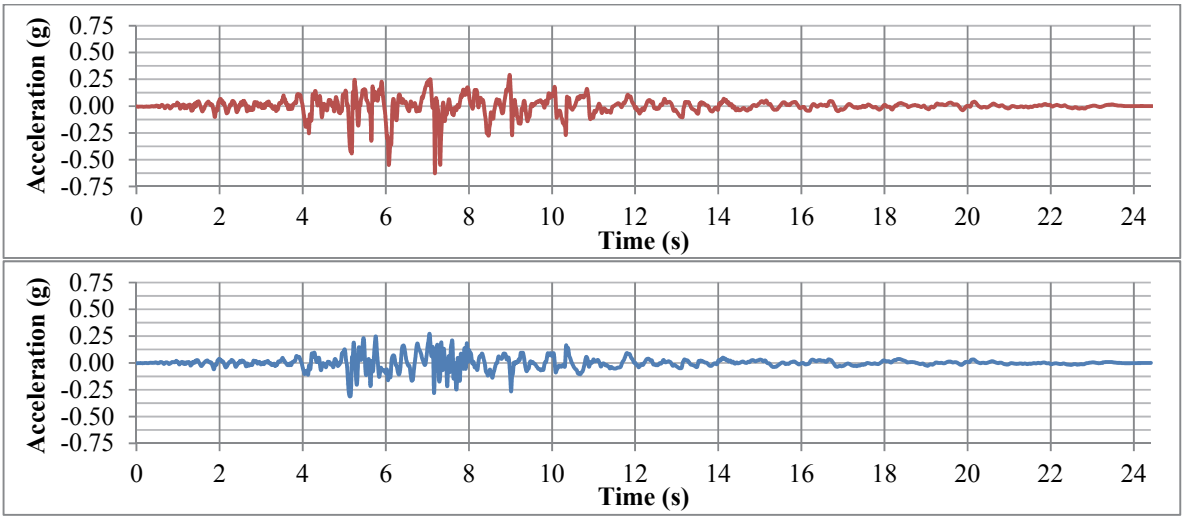

Figure 2.8. NGA No#265 (CPE045) ground acceleration times series before (Top) and after (Bottom) spectral matching via Al Atik and Abrahamson technique

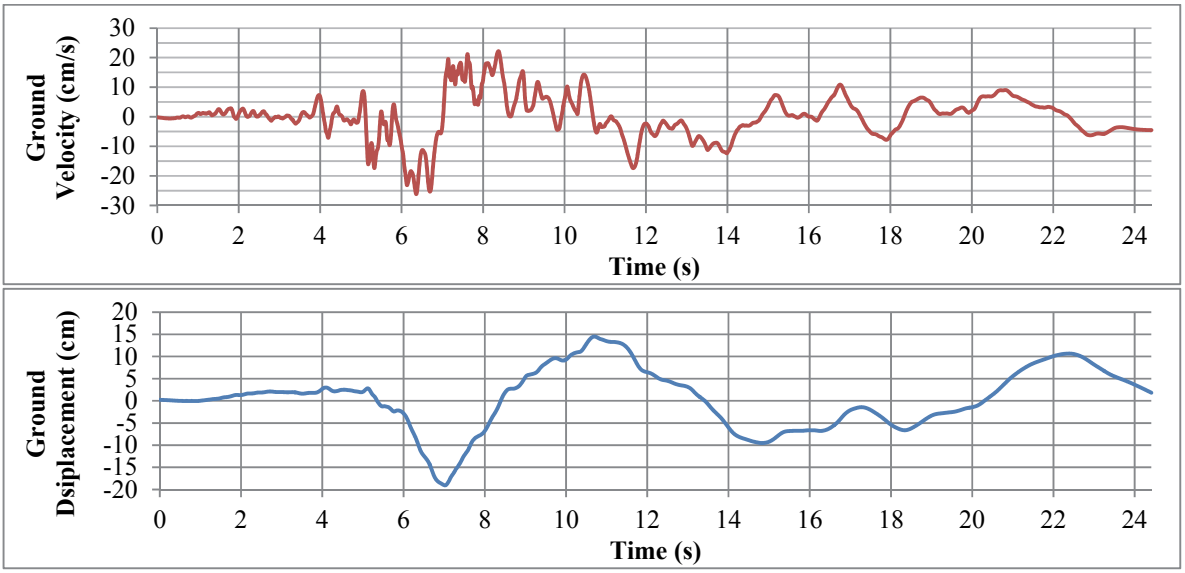

Figure 2.9. Ground velocity (Top) and ground displacement (Bottom) time series induced by the spectral-matched NGA No#265 (CPE045) acceleration time history

2.2. 1-D Equivalent-Linear Wave Propagation Solution Methods

Even tough, first emerged as an analytical site response calculation scheme, at the time, meant to deliver a viable computational efficiency by utilizing simple but appropriate modeling of the inelastic soil behavior, 1-D equivalent-linear wave-propagation solution methods are still very popular to this day among earthquake engineers. This widespread use of the one dimensional seismic response codes is mainly manifested by the convenience of modeling ground behavior through nominal amount of parameters that are consistently defined using the available geotechnical/geophysical tools in a way that closely simulates the actual earthquake behavior, if the adopted methodology is suited for the interested seismic setting (e.g. basin edge effects are negligible, etc.) [48] [49] [50] [51]. Hence, through a 1-D approach, the process of ground response computations can be carried out in a practical manner without a considerable compromise from the extensive engineering knowledge that can be extracted from a systematic line of calculation.

In this chapter, to provide a thorough understanding of the capabilities 1-D equivalent-linear site response calculation procedures, a fundamental theoretical background on the two codes evaluated in this study are provided. Both the procedure by Idriss and Sun [21], and the procedure by Hashash et al. [22] are constructed on the wave propagation theory that defines the particle motion along an infinitely long, layered rod body to define the deformation characteristics of soil strata. Therefore, to start with, the mathematical equation derived for the interested conditions are delineated. Then, in the subsequent subsections the definitions of the material models adopted in each of the subject techniques are outlined.

2.2.1. 1-D Response Analysis of Layered, Damped Soil on Elastic Half-Space Base

The one-dimensional propagation of waves of any type, along an infinitely long rod can be generalized by the partial differential equation (PDF);

$$\frac{\partial^2 u}{\partial t^2} = \upsilon^2 \frac{\partial^2 u}{\partial z^2} \tag{2.18}$$

where t represents time, u signifies the displacement along the direction of wave stresses, z stands for the depth at which stresses/strains are calculated, and υ denotes the propagation velocity along the direction of stresses exerted by the propagating waves. For instance, in the case of a vertically propagating SH-wave, that is the input motion type employed in 1-D ground response analysis calculations, $\upsilon = V_s$ (i.e. shear-wave velocity) as the upward travelling wave creates shear stresses within the transmission medium.

The solution of PDF shown in Equation 2.18 can be expressed such that, for a time instance, there is both an up-going and a down-going wave that travels at a speed that is purely dependent on the propagation medium, with the wave shape being completely independent of time and position. That is, in mathematical terms;

$$u(z,t) = f(\upsilon t - z) + g(\upsilon t + z) \tag{2.19}$$

Note that the first term in Equation 2.19 stands for an upward travelling wave, whereas the function *g* signifies a down-going wave series.

Now let us assume that the subject rod is excited by a steady-state harmonic stress that is defined as $\sigma(t)=\sigma_a \cos(wt)$ where σ_a denotes the stress amplitude and w represents the circular frequency of the loading. Then the solution described in Equation 2.19 can be defined as;

$$u(z,t) = C\cos(wt - kz) + D(wt + kz) \tag{2.20}$$

where C and D are the respective wave amplitudes, and k (wave number) is defined as w/υ. Alternatively, writing Equation 2.20 in the complex form, for an improved computational efficiency, the solution to the wave equation becomes;

$$u(z,t) = Ae^{i(wt-kz)} + Be^{i(wt+kz)} \tag{2.21}$$

To this point the wave equation is expressed in a way that, irrespective of the direction of the stresses resulting from the wave propagation along the rod, the solution is identical. Therefore, by very small manipulations in the derived solution, Equation 2.21 can be easily adapted for the interested case. Recall, from the fundamental principles of mechanics, the Hooke's Law for an elastic material under pure shear stress is defined as;

$$\zeta = G\gamma \tag{2.22}$$

where ζ denotes the shear stress, G stands for the shear modulus, and γ signifies the pertaining shear strain. This expression is established for representation of static loading conditions, in which effects of material damping are merely negligible. Nonetheless for dynamic loading conditions, the influence of damping on the overall response simply cannot be disregarded. Therefore, if the computational convenience of the expression in Equation 2.22 is desired to be conserved, one shall modify the parameter G so that the effects of damping are also embedded into this term. This is achieved by defining a complex shear modulus G^* that is calculated

using G and the relevant viscous damping ratio, ξ. Consequently by solely replacing the terms for the purely elastic case, with the parameters developed for the elastoplastic situation, and by making necessary adjustments within the stiffness parameters in the course of computations; it is possible to mutually simulate the damping and inelastic ground traits during calculation of seismic response, in an exceptionally efficient fashion. For the moment, though, establishing a solution to the wave propagation problem is the primary target, so the material models used in each of appraised site effects calculation methodologies, and the resulting G^* are investigated in the following subsections.

Based on the preceding interpretation, Equation 2.22 can be rearranged as following, so that a relationship between shear stresses and strains; compatible with the subject goal is attained

$$\zeta(z,t) = G^* \frac{\partial u}{\partial z} \tag{2.23}$$

Using Equation 2.23 the expression in Equation 2.21 is then revised as

$$u(z,t) = Ae^{i(wt-k^*z)} + Be^{i(wt+k^*z)} \tag{2.24}$$

Given, $V_s^*=\sqrt{G^*/\rho}$ and $k^*= w/V_s^*$, where ρ represents the density of travelling medium.

At this point it is necessary to introduce a local coordinate system for each soil stratum to orderly define the displacement and stress compatibility equations at individual layer boundaries. This is best achieved through the planar coordinate system shown in Figure 2.10, where the displacements at the top and bottom faces of soil layer n are described as;

$$u(z_n = 0, t) = (A_n + B_n)e^{iwt} \tag{2.25}$$

$$u(z_n = H_n, t) = \left(A_n e^{-ik_n^* H_n} + B_n e^{ik_n^* H_n}\right)e^{iwt} \tag{2.26}$$

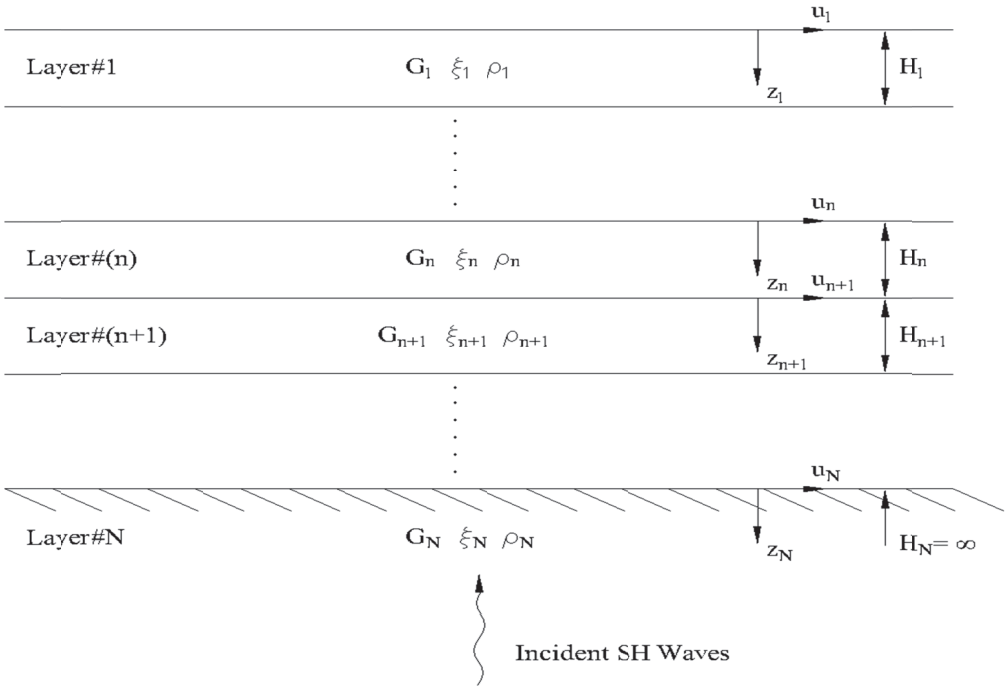

Figure 2.10. Local coordinate system adopted for defining 1-D wave propagation equations of a layered, damped soil profile founded on an elastic half-space base

Hence, once the compatibility condition is imposed at the layer boundary between strata *n* and *n+1* such that;

$$u_n(z_n = h_n, t) = u_{n+1}(z_{n+1} = 0, t) \tag{2.27}$$

the following relationship is obtained;

$$A_{n+1} + B_{n+1} = A_n e^{-ik_n^* H_n} + B_n e^{ik_n^* H_n} \tag{2.28}$$

Using the same coordinate system the shear stresses at the identical calculation points are determined through Equation 2.23 as;

$$\zeta_n(z_n = h_n, t) = ik_n^* G_n^* \left(B_n e^{ik_n^* H_n} - A_n e^{-ik_n^* H_n}\right) e^{iwt} \tag{2.29}$$

$$\zeta_{n+1}(z_{n+1} = 0, t) = ik_{n+1}^* G_{n+1}^* (B_{n+1} - A_{n+1}) e^{iwt} \tag{2.30}$$

Likewise in the case for boundary displacements, the shear stresses shall be complacent at borderlines so that;

$$\zeta_n(z_n = h_n, t) = \zeta_{n+1}(z_{n+1} = 0, t) \tag{2.31}$$

Therefore,

$$B_{n+1} - A_{n+1} = \frac{k_n^* G_n^*}{k_{n+1}^* G_{n+1}^*} \left(B_n e^{ik_n^* H_n} - A_n e^{-ik_n^* H_n}\right) \tag{2.32}$$

Equations 2.28 and 2.32 provide adequate basis to develop recursion relationships for incident and reflected wave amplitudes at any layer boundary in terms of the adjoining amplitude traits. By subtracting these expressions, then multiplying the end-product by 0.5, the incident wave amplitude, *A*, is determined as;

$$A_{n+1} = \frac{A_n}{2}(1 + \alpha_n^*) e^{-ik_n^* H_n} + \frac{B_n}{2}(1 - \alpha_n^*) e^{ik_n^* H_n} \tag{2.33}$$

Similarly, adding Equation 2.28 to Equation 2.32, subsequently multiplying resulting equation by 0.5, the reflected wave amplitude, *B*, is found such that;

$$B_{n+1} = \frac{A_n}{2}(1 - \alpha_n^*) e^{-ik_n^* H_n} + \frac{B_n}{2}(1 + \alpha_n^*) e^{ik_n^* H_n} \tag{2.34}$$

where complex impedance ratio, α_n^*, is defined as;

$$\alpha_n^* = \frac{k_n^* G_n^*}{k_{n+1}^* G_{n+1}^*} = \frac{\rho_n^* [V_s^*]_n}{\rho_{n+1}^* [V_s^*]_{n+1}} \tag{2.35}$$

Given that the shear stresses are zero for free-field conditions, using Equation 2.30 the incident and reflected wave amplitudes on the ground surface are determined to be the same, $A_1=B_1$. Thus, if the recursion formulas in Equation 2.33 and 2.44 are repetitively executed from layer 1 to *n*, the connection between surface and *n*th layer wave amplitudes are given by;

$$A_n = a_n(w)A_1 \tag{2.36}$$

$$B_n = b_n(w)B_1 \tag{2.37}$$

where, the transfer function linking the displacement amplitudes between layers *i* and *j* is defined as;

$$F_{ij}(\mathrm{w}) = \frac{|u_i|}{|u_j|} = \frac{a_i(w) + b_i(w)}{a_j(w) + b_j(w)} \tag{2.38}$$

Consequently, by means of the convenience of complex notation for describing harmonic motions, the corresponding acceleration amplitudes are calculated as;

$$|u| = w^2|\ddot{u}| \tag{2.39}$$

The key point here is, albeit the preceding relationships are derived for modeling the steady-state response of a layered soil profile residing on elastic bedrock, the calculations can be performed such that, by calculating the transfer functions for the whole suite of frequencies within the interested range and subsequently convolving the Fourier spectrum of the input motion with the attained $F_{ij}(w)$, presented findings are readjusted to any transient loading condition. Nonetheless, even so, the adopted material properties are merely elastoplastic,

which leads to a significant departure from the actual nonlinear soil behavior under dynamic loading conditions.

In equivalent-linear site effects calculation procedures, this issue is surmounted via an iterative solution that warrants the use of soil properties compatible with the ultimate strains resulting from earthquake motions. The basic thinking behind this approach is to characterize the wave series occurring as a result of a seismic event in terms of a harmonic motion. In that way, both the laboratory results used for determining strength degradation/damping properties in dynamic analyses and the derived wave propagation solutions become compliant with loading scheme used for their determination.

The iteration process begins computing the seismic response for each stratum within the evaluated soil profile by taking the elastic shear modulus, $G^{[1]}$ (extracted from V_s) and damping ratio, $\xi^{[1]}$, values as the initial soil properties. Once the shear strains resulting from the seismic tremors are determined at each layer, the effective shear strain level, $\gamma_{eff,i}$ (i.e. the harmonic-equivalent loading level for the subject motion) at stratum i is calculated as;

$$\gamma_{eff,i}^{[k]} = Q_\gamma \gamma_{max,i}^{[k]} \tag{2.40}$$

where k denotes the iteration step (e.g. for the first iteration step k=1) and Q_γ stands for the effective shear strain ratio (typically taken as 0.65). Then, based on this γ_{eff} level, the calculations are re-performed, as in the initial phase, using the new stiffness and damping values, and the identical procedure is reiterated, each time using the dynamic properties gleaned after previous iteration, until the change between successive steps are converged to a pre-defined tolerance level at each soil stratum. Figure 2.11 provides a graphical visualization of an equivalent-linearization, iteration process at a layer, in which the prescribed tolerance is reached after the 3rd iteration phase.

The discussion to this part summarizes the mathematical foundation of the wave-propagation aspect of one-dimensional site response calculation methodologies. The

theoretical basis clarified to this juncture is mutual in every other 1-D method currently used for ground response analysis purposes. The central variance between each code stems from the differences in ways to model the elastoplastic soil behavior. In the following subsections the frequency-dependent approach used in SHAKE91 and the frequency-independent outset adopted in DEEPSOIL are explained respectively.

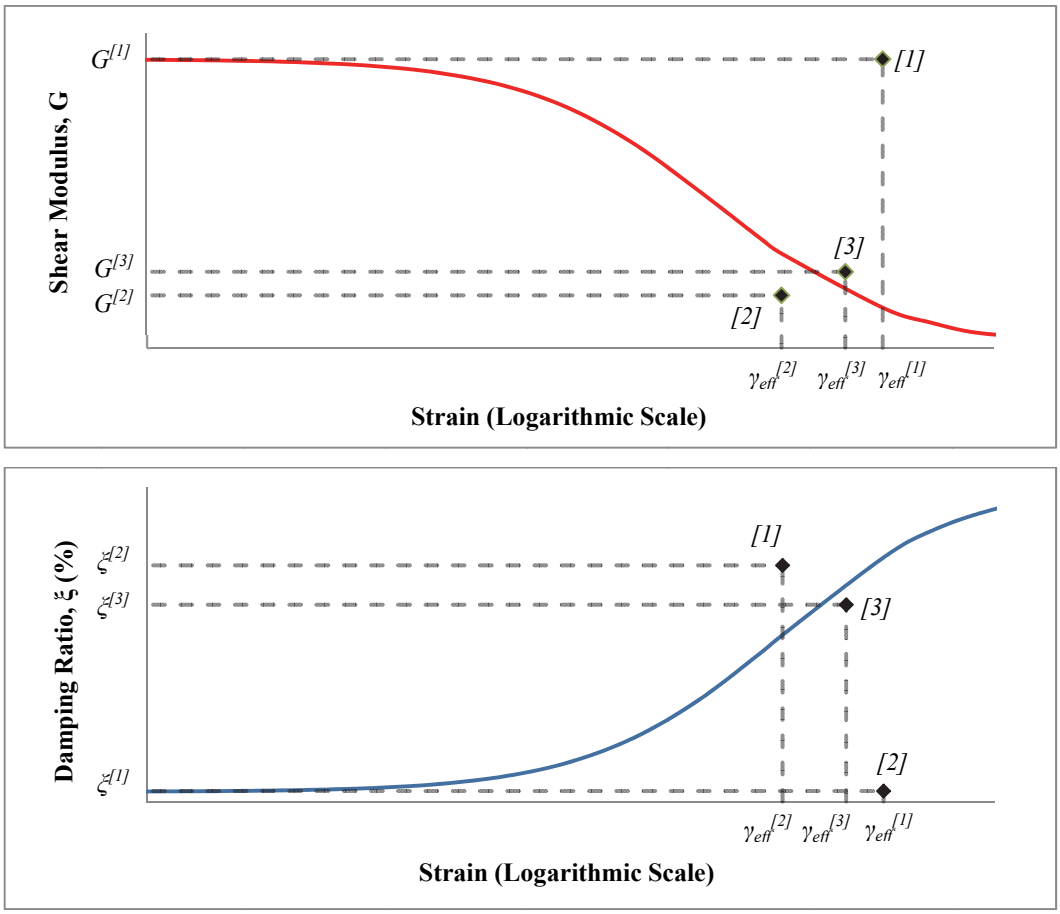

Figure 2.11. A graphical visualization of equivalent-linearization, iteration process conducted at a single soil layer

2.2.2. Frequency-Dependent Shear Modulus Formulation used in SHAKE91

The code SHAKE 91, utilizes a frequency-dependent shear modulus formulation to model the damping behavior of soil under dynamic excitations. This is a modulus construction inspired from the dynamics knowledge established for investigating earthquake effects on structures, and is a derivation from the reputable Kelvin-Voigt model used for depicting the elastoplastic characteristics of structural materials.

The complex shear modulus, developed by Udaka [23], comprises of a mathematical expression that is assembled, through back-calculation, to yield matching amplitude response with the Kelvin-Voigt model for a SDOF system, i.e. a uniform soil layer on bedrock. The purpose of this derivation is to closely simulate the solid model while conserving the computational facility of the complex notation. However, the proposed expression falls short of emulating the phase angle response prompted by the elastoplastic model to identically match the performance of a Kelvin-Voigt solid.

The complex shear modulus proposed by Udaka is given by;

$$G^* = G\left(1 - 2\xi^2 + 2i\xi\sqrt{1-\xi^2}\right) \tag{2.41}$$

Substituting the complex modulus in Equation 2.41 as the stiffness definition in the dynamic equation of motion for a SDOF system under steady-state harmonic loading as follows, the understanding dispensed in the previous paragraph can be easily tested;

$$m\ddot{u} + G\left(1 - 2\xi^2 + 2i\xi\sqrt{1-\xi^2}\right)u = A_0 e^{i\omega t} \tag{2.42}$$

where A_0 denotes the amplitude of the harmonic loading; the subject SDOF system is subjected to. The amplitude response of Equation 2.42 can be extracted by simple algebraic manipulation as;

$$u = \frac{A_0/G}{\sqrt{\left[1-\left(\frac{w}{w_n}\right)^2\right]+\left[2\xi\left(\frac{w}{w_n}\right)^2\right]}} \tag{2.43}$$

subsequently the formula for the phase angle is written as;

$$\phi = \tan^{-1}\frac{2\xi\sqrt{1-\xi^2}}{1-2\xi^2-(w/w_n)^2} \tag{2.44}$$

where w_n signifies the natural circular frequency of the interested SDOF system.

The expression in Equation 2.43 mirrors the displacement amplitude formulation for Kelvin-Voigt solid, yet the phase angle formula attained using frequency-dependent shear modulus (displayed in Equation 2.45 [52]) is greatly dissimilar with Equation 2.44.

$$\phi = \tan^{-1}\frac{2\xi(w/w_n)}{1-(w/w_n)^2} \tag{2.45}$$

Figure 2.12 demonstrates the effect of frequency-dependent material definition on ground amplification characteristics. The results displayed in the figure are calculated for 17 distinct sine wave input motion, each defined for a period value ranging from 0.05s to 2.00s, with a PGA level equal to 0.1g. The travelling medium (soil profile) for the generated harmonic base motions was selected so that the upper 10m layer is comprised of a silty-sand mixture with a unit weight equal to 16.00 kN/m^3 and V_s =250 m/s, and the underlying 10m sand stratum has a unit weight of 18.00 kN/m^3 and V_s =500 m/s (whereas the bedrock unit weight and V_s are selected as 22 kN/m^3 and 760 m/s respectively). As expected, the seismic response in each individual case comprises of a steep single peak occurring at the frequency of loading. The peaks are significantly amplified around the first two modes of the defined profiling, i.e. 0.24s and 0.08s, whereas the spectral responses for long-period loading situations are almost identical to what is witnessed at the bedrock level.

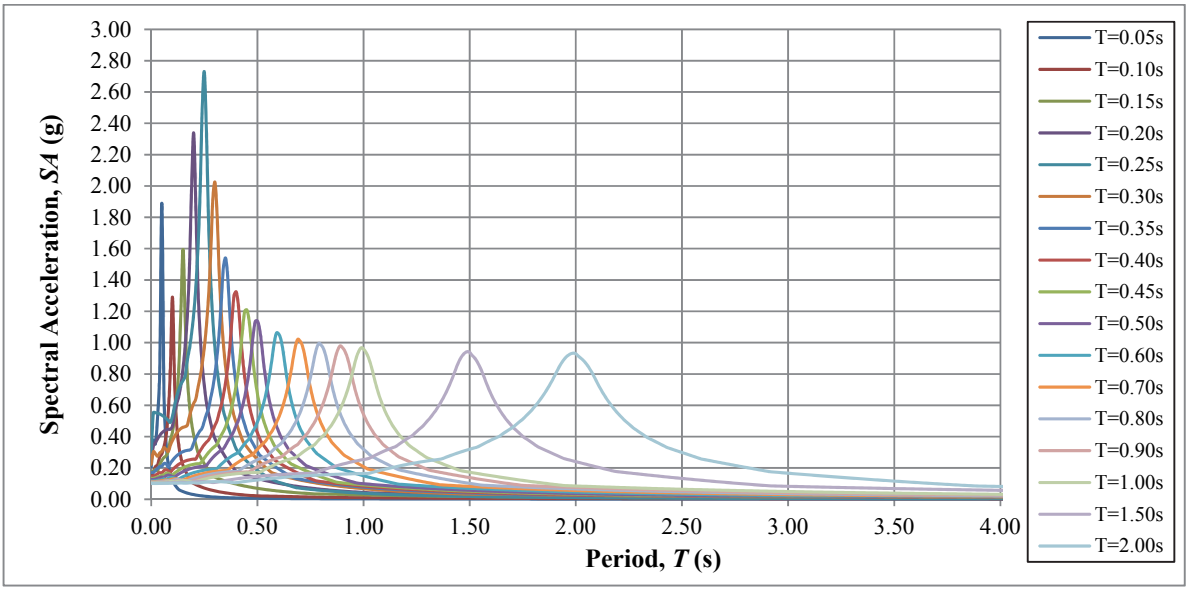

Figure 2.12. 5%-damped spectral response of a double layer soil profile on elastic bedrock to 17 harmonic base motions with loading period ranging from 0.05s to 2.00s, computed using frequency-dependent Udaka complex shear modulus formulation

2.2.3. Frequency-Independent Shear Modulus Formulation used in DEEPSOIL

The originating point of the frequency-independent Schnabel et al. [20] complex shear modulus is as well the Kelvin-Voigt rheological model. However, in derivation of the formula for defining damping characteristics, unlike in the case for frequency-dependent material definitions, this expression is formed in such a way that the damping features are controlled by the hysteretic behavior that is inherent to soils. As a result, a material description that better resembles the actual laboratory observations is ensured.

A Kelvin-Voigt solid resists shearing deformations by the combined resistance of a spring and viscous-damping dashpot constituent. This results in the stress-strain relationship

$$\zeta = G\gamma + \eta \frac{d\gamma}{dt} \tag{2.46}$$

where η denotes the material viscosity. Therefore if a Kelvin-Voigt material is subjected to a harmonic shear strain expressed as $\gamma = \gamma' \sin wt$ the resulting shear stress is described by;

$$\zeta = G\gamma' \sin wt + w\eta \cos wt \tag{2.47}$$

The stress definition formulated in Equation 2.47 defines an elliptical stress-strain loop as shown in Figure 2.13. By calculating the area of the loop the elastic energy dissipated per cycle (ΔW) is calculated as;

$$\Delta \mathrm{W} = \int_{t_0}^{t_0+T} \zeta \frac{\partial \gamma}{\partial t} dt = \pi \eta w \gamma'^2 \tag{2.48}$$

Given that, the peak energy stored in the system (W) is given by

$$\mathrm{W} = \frac{G\gamma'^2}{2} \tag{2.49}$$

damping ratio is subsequently written as;

$$\xi = \frac{1}{4\pi} \frac{\Delta W}{W} = \frac{\eta w}{2G} \tag{2.50}$$

Then, by simple arithmetic manipulation Equation 2.50 is reorganized as follows, so that the material viscosity is inversely proportional to circular frequency.

$$\eta = \frac{2G}{w} \xi \tag{2.51}$$

Therefore by making use of the viscosity definition in Equation 2.51, the damping ratio is rendered as frequency-independent (since in analyses the values for ξ are extracted from defined laboratory results).

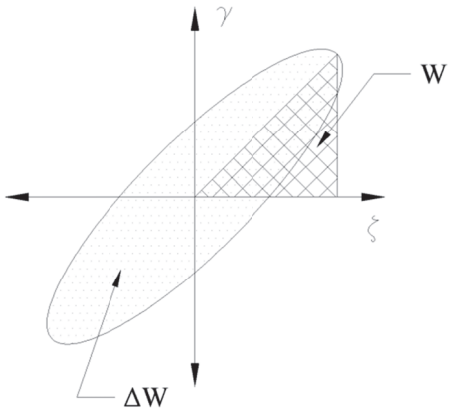

Figure 2.13. A visualization of the elliptical-shaped stress-strain loop of a Kelvin-Voigt solid along with descriptions of dissipated elastic energy (*ΔW)* and peak stored energy (*W)*

Now, getting back to the wave propagation problem, a soil profile subjected to a vertically propagating SH wave can be easily represented by a mechanism that consists of an infinite number of Kelvin-Voigt solids stacked on one another. Consequently the 1-D wave equation is determined as;

$$\rho \frac{\partial^2 u}{\partial t^2} = G \frac{\partial^2 u}{\partial z^2} + \eta \frac{\partial^3 u}{\partial z^2 \, \partial \mathrm{t}} \tag{2.52}$$

For harmonic loading conditions, the soil displacements can be defined by

$$u(z,t) = A\mathrm{e}^{\mathrm{i}\omega \mathrm{t}} \tag{2.53}$$

Putting in the expression in Equation 2.53 into 2.52, the wave equation becomes [24]

$$G^* \frac{\partial^2 A}{\partial z^2} = -\rho w^2 A \tag{2.54}$$

where complex shear modulus G^* is defined as

$$G^* = G + iw\eta = G(1 + 2i\xi) \tag{2.55}$$

It is important to note that, because Equation 2.55 is derived directly from the Kelvin-Voigt viscoelastic model, one might simply consider that the response of a SDOF system adopting the defined complex shear modulus is purely identical with that calculated using a Kelvin-Voigt solid. This is, indeed incorrect given re-performing the calculation in Equation 2.42 using 2.55, the amplitude response of the frequency-independent system is described as;

$$u = \frac{A_0/G}{\sqrt{\left[1 - \left(\frac{w}{w_n}\right)^2\right] + 2\xi^2}} \tag{2.56}$$

Figure 2.14 visualizes the effect of frequency-independent material definition on ground amplification characteristics. Displayed results clearly indicate an augmented kurtosis for amplification functions. This entails higher peaks at loading frequencies and weaker amplification at the remaining response periods.

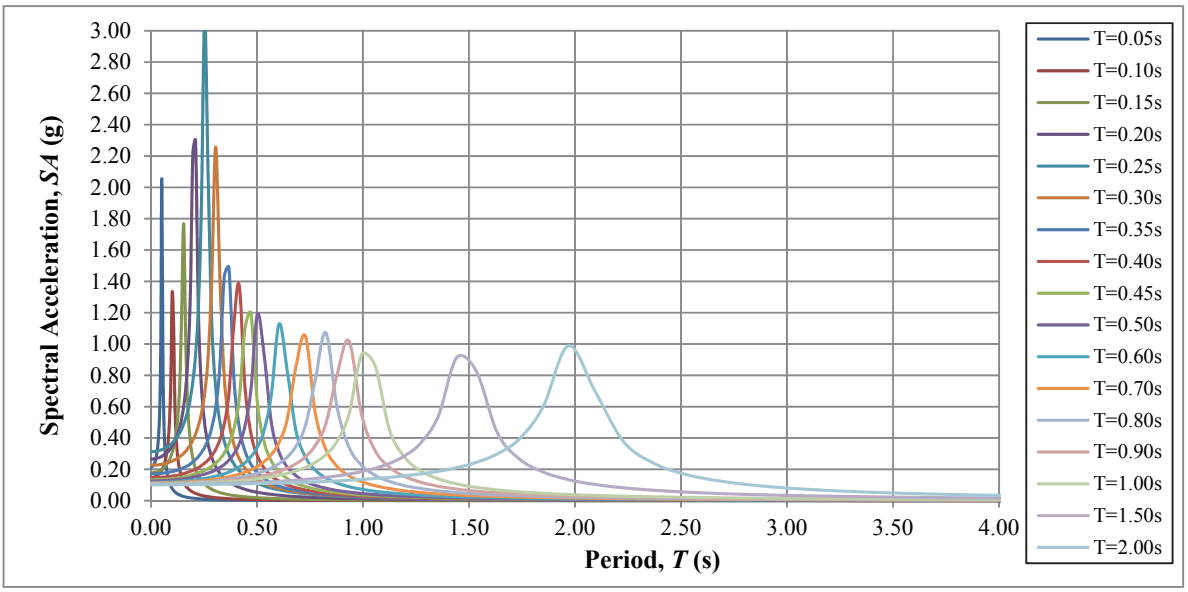

Figure 2.14. 5%-damped spectral response of the analysis case in Figure 2.12; re-computed using frequency-independent Schnabel et al. complex shear modulus formulation

3. RESULTS AND DISCUSSION

The main emphasis of this study is to develop a practice-oriented, standardized ground response analysis methodology, using simple but efficient, objective state-of-the-art constituents; each of which is a product of independent efforts of various researchers to contemplate discrete aspects of the task. A comprehensive discussion regarding the theoretical foundations and the rationale behind these separate components is delivered in the preceding. In this chapter, by pairing respective elements, as displayed in Figure 3.1, performance of six different overall procedures is examined. Provided that the effectiveness of a process cannot be inspected without the presence of reliable benchmark data, herein, these pairs are tested against ten TSGMN station locations, which recorded at least a single earthquake that is closely compatible with the design event decided for the subject location; consistent with 475 year return period. Hence, by direct comparison of results, for the set up combinations, with the reference data, the capability of every single method to capture amplification characteristics is inspected.

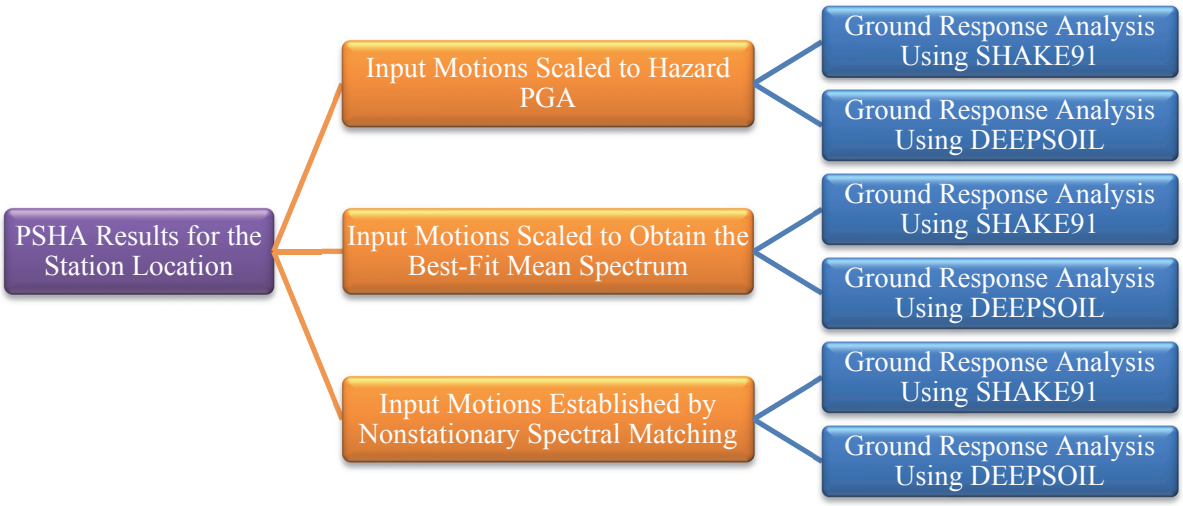

Figure 3.1. A graphical illustration of examined ground motion selection/1-D site response calculation procedure pairs, presented in a color coordinated, logical arrangement

Following section exhibits the geological and geophysical figures of Denizli (AI107), Dursunbey (AI145), Horasan (AI059), Dinar (AI137), Ceyhan (AI022), Yenisehir (AI019), Adapazari (AI005), Bolu (AI010), Duzce (AI011), and Fethiye (AI127) TSGMN stations, alongside the corresponding seismic response findings for every single assembled approach, respectively. The presented engineering knowledge regarding the evaluated sites mirror data brought together from the results of the field testing scheme undertaken within the scope of TUBITAK Project No. 105G016 (summarized in the paper published by Sandıkkaya et al. [53]), and published information extricated from various resources. On the other side, the ground response analysis outputs are structured so that every single graph shows the mean, mean + standard deviation spectral accelerations, and the benchmark response induced at an investigation point. Such visualization enables exclusive scrutiny of the effect of both the input scaling and site effects calculation modes. For maintaining the displayed outcomes at an easy-to-read layout, but not leave out an important component of the overall findings, resulting spectra attained via each method, which also include responses obtained for individual time histories, are presented in the Appendix.

Next, in Section 3.2, to reorganize the results conveyed in Section 3.1 into an effective, code-comparable shape; two-point site specific Uniform Hazard Spectra are calculated for each analysis location. Then, the ability of the subsequent product and the standardized spectrums proposed in FEMA P-750 [54], Eurocode 8 [55] and TSC07 [56] to predict the actual recorded data is assayed. This implementation is particularly significant, as it points out the existing inadequacies of current code procedures, and how the proposed technique (i.e. the method that is observed to yield results that best comply with the actual response) can create an alternative path to estimate seismic ground response, and eventually design spectrums; therefore, serve as an efficient tool to amend current practice to better estimate the effect of seismic tremors.

3.1. Ground Response Analysis Results

3.1.1. Denizli Station (AI107)

The city of Denizli, situated at the eastern foot of one of the two horst-graben systems that characterizes the seismic environment of Denizli province; i.e. the Menderes Graben configuration that extends along east-west direction (the other being northwest-southeast-oriented Gediz Graben), stands on a depression system that is, based on historical evidence [57], proved to be related with a large number of seismic activities. The geological composition of Denizli Basin is mainly governed by Neogene sedimentary rocks and Quaternary deposits. According to geotechnical investigations performed within the limits of the city, the surficial soil depositions in Denizli are set up of 20-30 m thick medium dense to dense sandy/gravelly silt sediments overlying a 15-25 m thick lean clay deposit; followed by a weak, rock-like material extending down to a depth of 75-90 m, until reaching stiffer bedrock formations.

An examination of the controlling tectonics schemes, indicate that the seismic behavior of the region is defined by shallow, normal fault systems of large-magnitude-earthquake-latency between $6.0 < M_w < 7.2$ [58]. In August 19, 1976, the prevailing extension system in the province culminated in a M_w=6.1 [59] event that resulted in 4 casualties, total collapse of 40 housing units and extensive damage in 1284 structures, merely, in the 110,000-population Denizli city [60]. TSGMN station AI107, positioned within the Meteorological Observatory building in Denizli city – roughly a R_{jb} distance of 6.43 km off the source mechanism – was the only accelerograph site that recorded this vital event (See Figure 3.2 for East-West and North-South component recorded time histories); not only storing the first strong-motion time-series in Turkey, attained in the periphery of an earthquake epicenter, but also providing valuable benchmark data for the area (as deaggragation study conducted for the region points out that this occurrence is well-suited with the design event valid for the city of Denizli). Hence, by using the horizontal components of AI107 station records as reference data, and utilizing the detailed geophysical and geotechnical information published by TUBITAK; it is

possible to examine the effectiveness of each constructed method pair for estimating seismic ground response.

Based on the PSHA results for subject site [17], estimated PGA, S_s and S_1 values at locus site condition are 0.32g, 0.70g and 0.20g respectively. So to carry out ground response analyses, it is necessary to first establish a set of records, consisting of at least 10 normal/oblique events that comply with a M_w range from 5.6 to 6.9, a R_{jb} interval that spans between 0 to 30 km, and a V_{s30} range of 600-1000 m/s (Even if this boundary is considerably different from the proposed interval of values, in this case, the decision to adjust selection criteria is justified, since the amount of records used in analyses has a greater influence on the overall results); suited to the PSHA outcome.

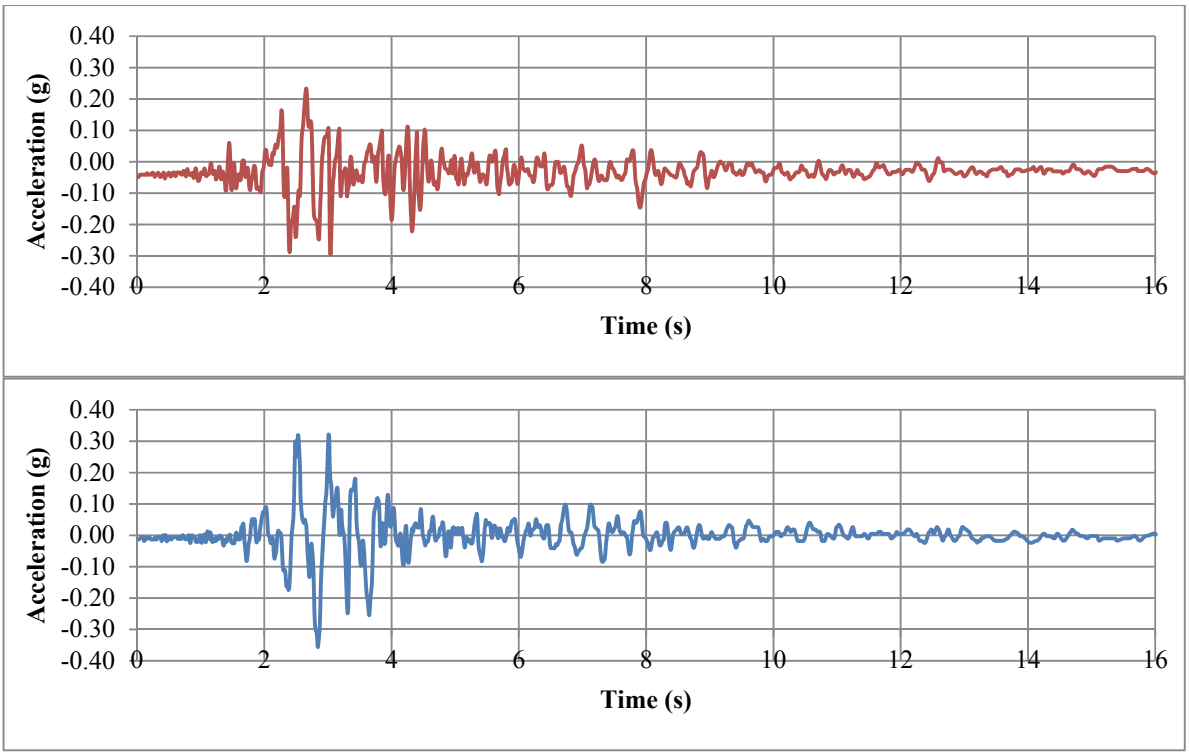

Figure 3.2. East-West (Top) and North-South (Bottom) components of the surface accelerations recorded by TSGMN Station AI107 during August 19, 1976; Denizli earthquake

Table 3.1 displays the list of 16 earthquake record components that are found to be compatible with the defined criteria, and, as a result, deemed suitable for the target application. Figures 3.3 to 3.6 exhibit the 5%-damped response spectra of unscaled record components, and the corresponding input time-histories prepared by PGA scaling, scaling to obtain the best-fit mean spectrum, and nonstationary spectral matching, respectively; along with the UHS determined for the subject location, calculated at the reference site condition as per seismic hazard results.

Table 3.1. List of earthquake time histories selected for use with the ground response analyses performed for AI107 TSGMN station

Record No.	Event	M_w	R_{jb} (km)	V_{s30} (m/s)	Record File	PGA
1	Irpinia-Italy-01 (1980)	6.90	9.5	1000.0	NGA No#284 (A-AUL000)	0.057
2	Irpinia-Italy-01 (1980)	6.90	9.5	1000.0	NGA No#284 (A-AUL270)	0.061
3	Irpinia-Italy-01 (1980)	6.90	8.1	1000.0	NGA No#285 (A-BAG270)	0.197
4	Irpinia-Italy-02 (1980)	6.20	28.7	1000.0	NGA No#295 (B-AUL270)	0.023
5	Irpinia-Italy-01 (1980)	6.90	13.3	600.0	NGA No#289 (A-CTR270)	0.173
6	Irpinia-Italy-02 (1980)	6.20	20.4	1000.0	NGA No#303 (B-STU000)	0.070
7	Irpinia-Italy-02 (1980)	6.20	20.4	1000.0	NGA No#303 (B-STU270)	0.077
8	Irpinia-Italy-02 (1980)	6.20	17.8	1000.0	NGA No#296 (B-BAG000)	0.048
9	Irpinia-Italy-02 (1980)	6.20	17.8	1000.0	NGA No#296 (B-BAG270)	0.058
10	Little Skull Montain-NV (1992)	5.65	23.8	659.6	NGA No#1741 (Lsm2000)	0.110
11	Little Skull Montain-NV (1992)	5.65	23.8	659.6	NGA No#1741 (Lsm2270)	0.086
12	Norcia-Italy	5.90	[1.7]	659.6	NGA No#156 (F-CSC-EW)	0.200
13	Norcia-Italy	5.90	[1.7]	659.6	NGA No#156 (F-CSC-NS)	0.161
14	Norcia- Italy	5.90	[31.4]	659.6	NGA No#155 (F-BEV-NS)	0.040
15	Oroville-01 (1975)	5.89	[7.8]	622.9	NGA No#106 (A-ORV037)	0.092
16	Oroville-01 (1975)	5.89	[7.8]	622.9	NGA No#106 (A-ORV307)	0.072

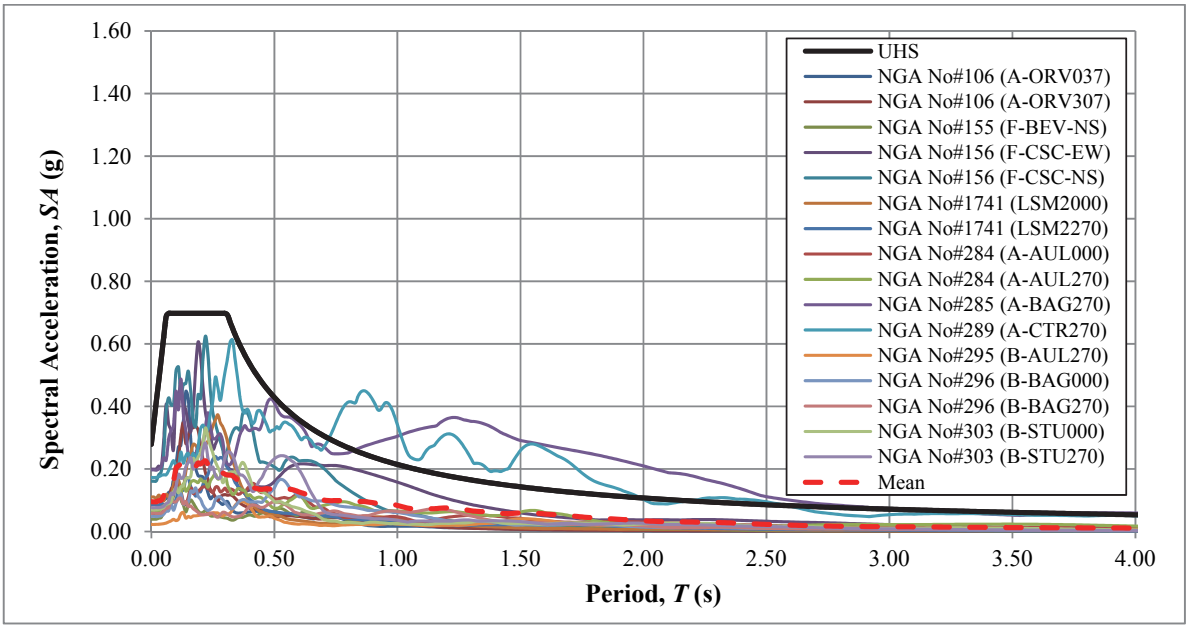

Figure 3.3. 5%-damped response spectra of earthquake record components selected for carrying out the site effects calculations for AI107 TSGMN station

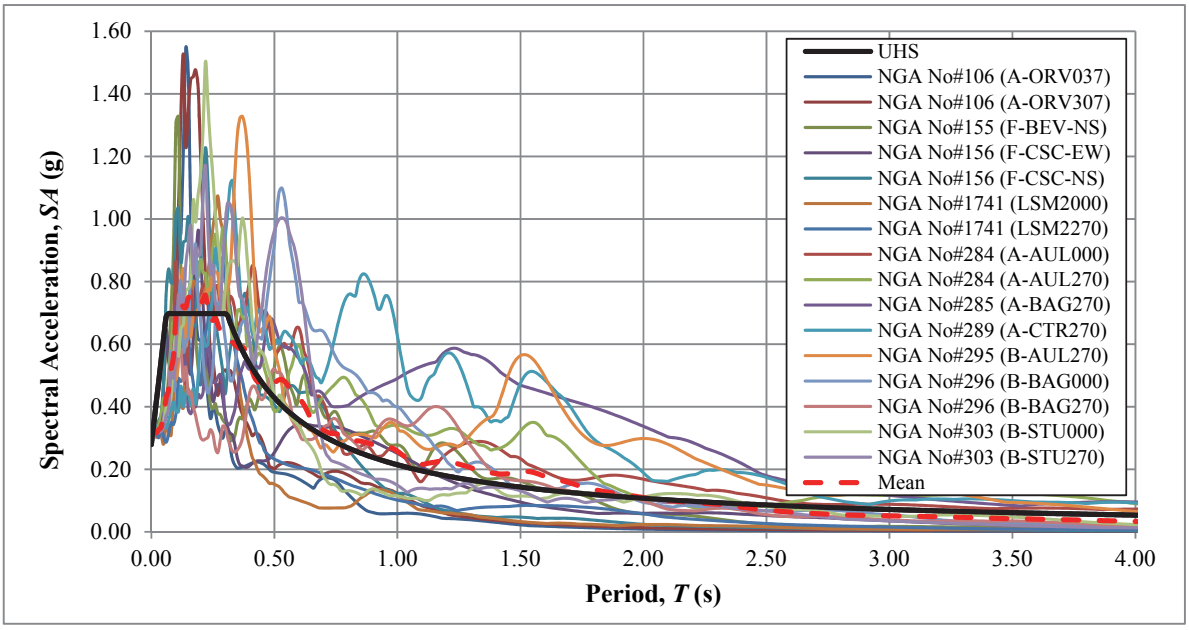

Figure 3.4. 5%-damped response spectra of earthquake record components presented in Figure 3.3 after normalization of each time series to the hazard PGA level of 0.32g

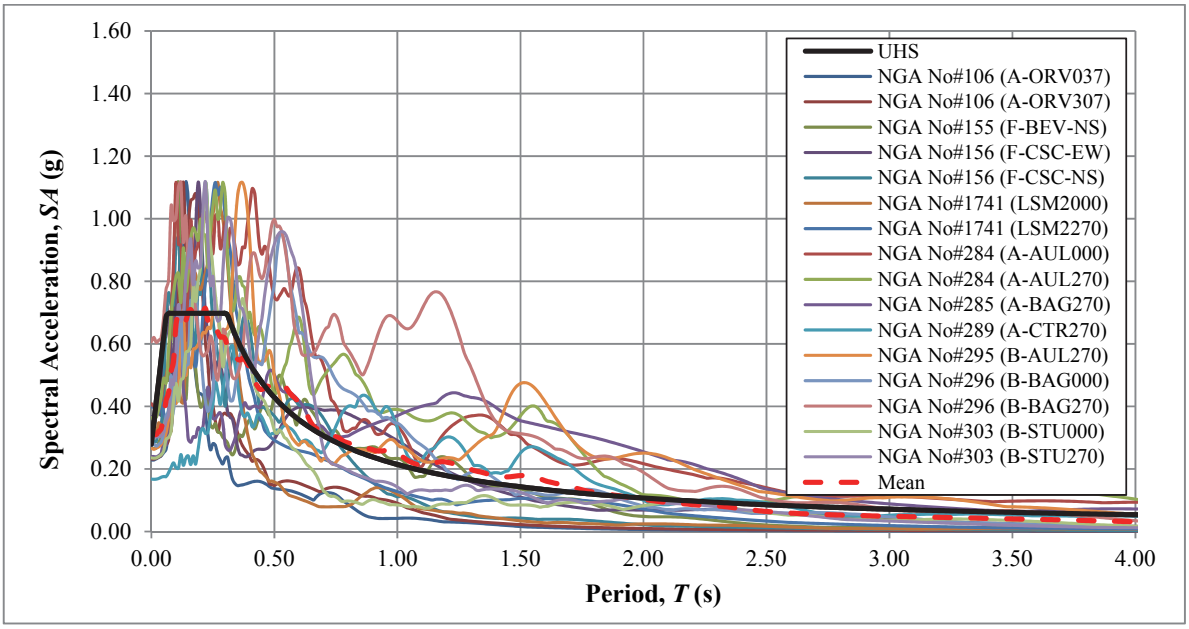

Figure 3.5. 5%-damped response spectra of earthquake record components shown in Figure 3.3 after scaling to find the mean spectrum that is best-fit with PSHA-determined UHS

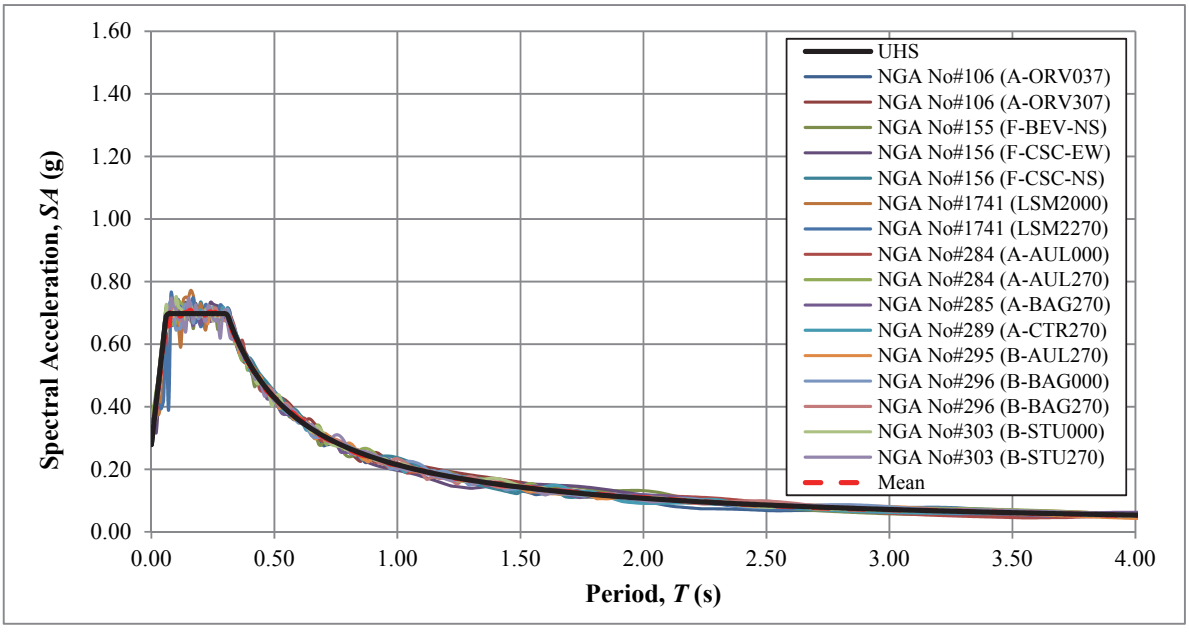

Figure 3.6. 5%-damped response spectra of earthquake record components presented in Figure 3.3 following nonstationary spectral matching as per PSHA-determined UHS

As stated by the field testing results compiled for the station site; at the top 20 m, the soil layering that underlies AI107 is defined by silty sand sedimentations with slight lean clay inclusions. Within this segment of the profile, overall plasticity index (PI) of the soil material ranges from 0 to 14 and the sand percentage shows abrupt changes, hence exhibiting a variation from sand-dominated to silt-dominated cyclic behavior at sublayers. Subsequent 17 m section of the stratification is governed by a lean clay deposition of PI=8−18. The findings of SPT and MASW tests performed in contiguity of the subject location shows that both the silty sand sedimentation and the clayey base detected at the site are amassed of fairly dense/stiff deposits with V_s values ranging from 294 m/s at surface to 443 m/s at the cessation of lean clay stratum. The ensuing rock-like layering is perceived to exhibit higher shear resistance that gradually increases towards the reference site condition. Figure 3.7 visualizes the characteristics of the soil layering beneath the AI107 station down to the decided locus.

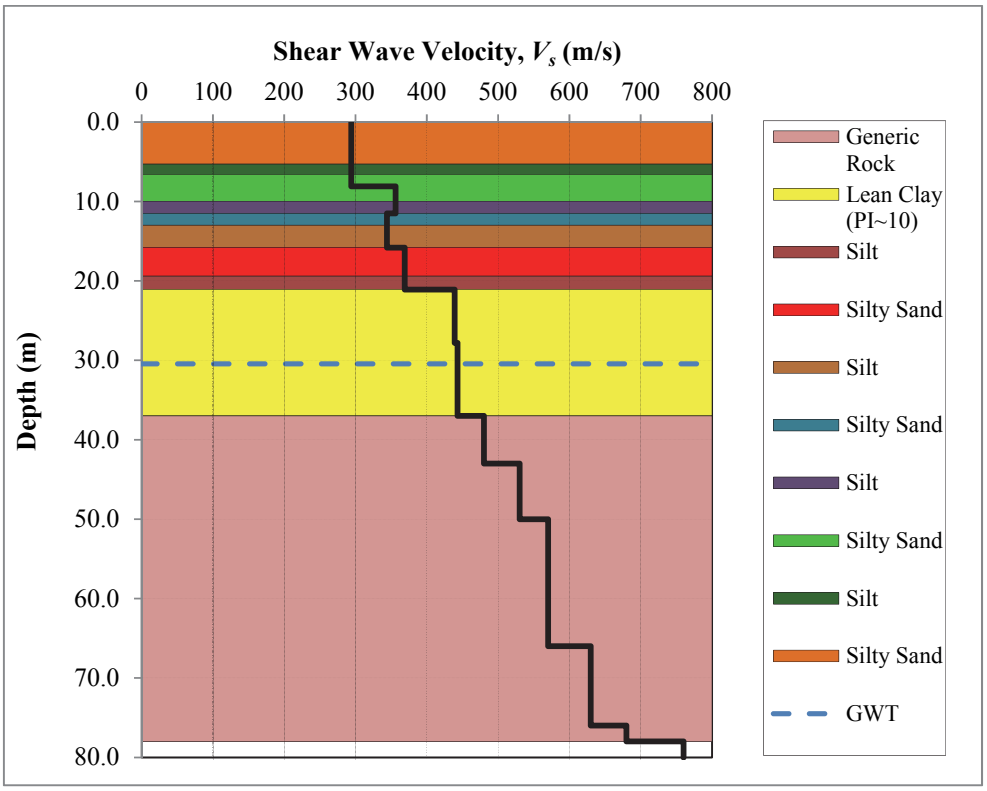

Figure 3.7. A visual depiction of soil layering, and corresponding shear-wave velocity variation underneath the AI107 station; extending down to the reference site condition

In any seismic application, be it geotechnical or structural, modelling the force-deformation behavior of involved materials is as significant of an aspect of the overall problem as the precise determination (or in the structural case idealization) of stifness properties of the interested construction, since without realistic representation of material response to dynamic excitations, either modulus degradation or the damping effect (or even both) is misinterpreted. For the purpose of carrying out the seismic response calculations for AI107 TSGMN station, in the performed analyses, the silty sand, silt, lean clay PI=10, and generic rock stratifications acknowledged according to field testing reports are expressed using the dynamic soil properties suggested by Darandeli [61], Vucetic and Dobry [62], and EPRI [42] correspondingly. Figure 3.8 conveys a graphical depiction of the employed modulus reduction/damping curves. In the performed analyses, the unit weight values of 17.30, 19.00 and 22.00 kN/m^3 are used for silty sand/clayey soils, and the generick rock material observed between depths of 32 to 37 m and 37 to 78 m respectively.

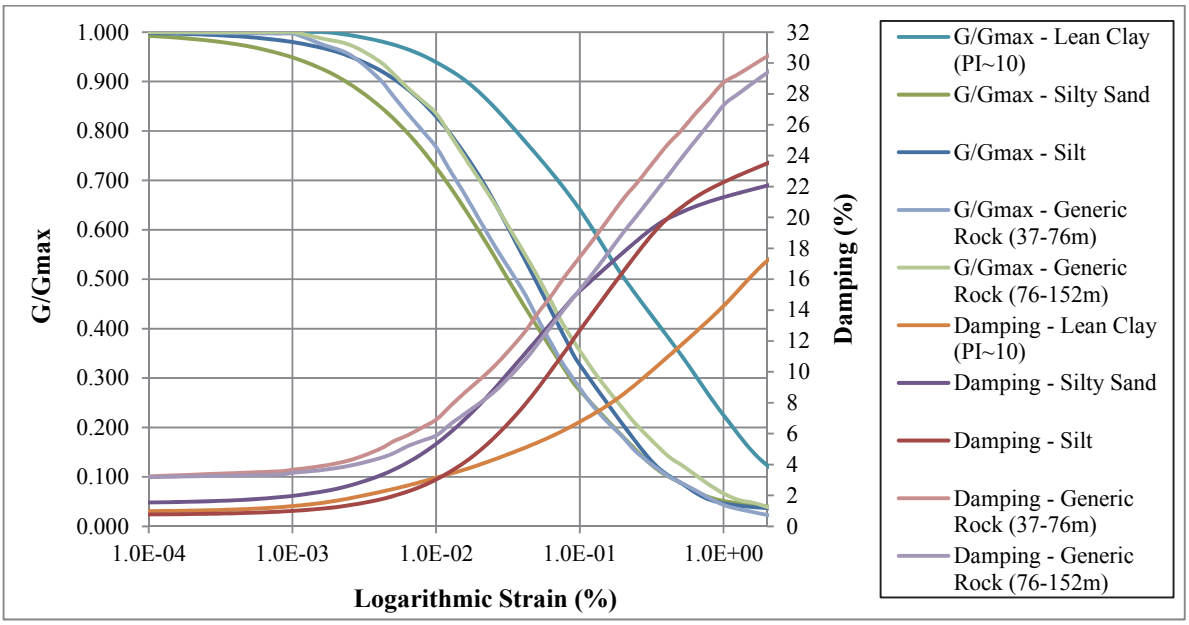

Figure 3.8. Modulus degradation and damping curves adopted for performing ground response analyses at the site of AI107 TSGMN station

Figure 3.9 and 3.10 display the mean and mean + standard deviation ground response analysis results for AI107 TSGMN station site, correspondingly obtained using each method pair. The spectral response of the the recorded components are marked by two distinct peaks, in the case of E-W direction motion, occuring at period values of 0.14s and 0.39s, and in the case of N-S direction motion, occuring at period values of 0.24s and 0.48s respectively. In all cases, the period and amplitude extents of the first peak response is more or less simulated by the calculated surface accelerations. Nonetheless, taking into consideration the shape and amplitude features of the second peak of the response spectrum for recorded ground motions, it is observed that the calculated spectral behavior, either highly overestimates the ranks of the associated amplitude values or entirely oversights the existing peak shape.

A simple comparison between Figure 3.9 and 3.10 openly reveals that this is in fact a consequence of the characteristics of program input. Time series prepared via nonstationary spectral matching exhibit merely a single peak that is concurrent with initial surge in the recorded spectrum, thus missing the seconday rise in spectral accelerations. On the other side, this shape is vastly overestimated through the input time histories prepared by the remaining input development techniques, altough the outline of response is successfully emulated. Hence, all in all, the computed output results in an incomplete representation of actual earthquake frequecy content and/or a significant overestimation of maximal spectral accelerations.

From an engineering viewpoint, approximating amplitude levels with reasonable precision appear to be more canonical, given the discrepancies in frequency-content can also be accounted for, through a well-adapted spectrum construction procedure. Then, in that case, the frequency independent calculation scheme using input motions prepared through nonstationary spectral matching technique provides a response that closely resembles the observed behavior, with a peak response ratio of approximately 1.104, as a result can be said to perform better than the remaining method pairs.

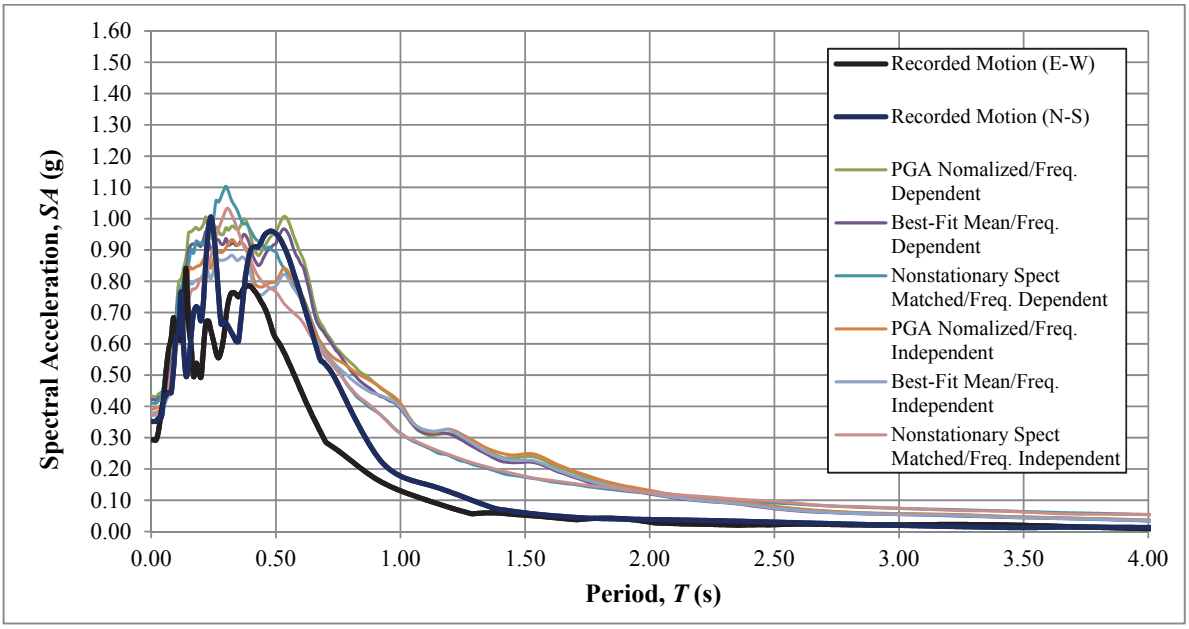

Figure 3.9. A comparison of 5%-damped mean response spectra, determined using each method pair, with the observed behavior at AI107 TSGMN station

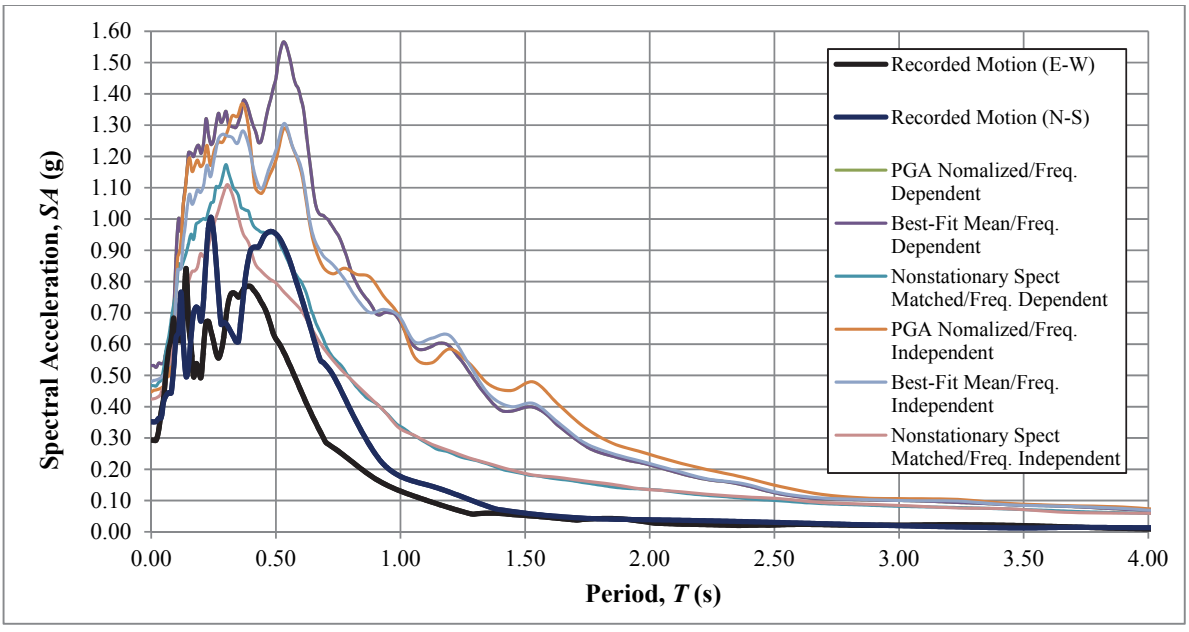

Figure 3.10. A comparison of 5%-damped mean + std. dev. response spectra, determined using each method pair, with the observed behavior at AI107 TSGMN station

3.1.2. Dursunbey Station (AI145)

Dursunbey, a city set on a group of hills on the eastern border of the Balikesir province, is situated in an active tectonics region that is governed by a number of strike-slip faulting of various sizes. This mountainous range that comprises Dursunbey is characterized by bluish/blackish sandstone, limestone and marble geologies [63]. According to geotechnical/geophysical investigations performed in the region, with a certain degree of weathering, these formations are observed continue to the ground surface; often times overlain by a 1-3 m artificial fill consisting of coarse-grained-based material.

In July 7, 1979, one of the predominant strike-slip mechanisms in the province resulted in a M_w=5.3 earthquake; triggering a raw PGA level of 0.275g. The event occurred at a R_{jb} distance of 28 km from Dursunbey and induced very little damage, mainly as a consequence of the sparsely-settled, single-story housing layout of the city. TSGMN station AI145, positioned a R_{jb} distance of 28.92 km away from the earthquake source is the single accelerometer site that recorded this occurrence (See Figure 3.11 for East-West and North-South component recorded time histories).

PSHA, and the consequent deaggragation calculations performed for the strong ground motion station site, specify that the record components of June 7, Dursunbey earthquake can indeed be employed for representing the design event for Dursunbey city. Hence, by means of taking he horizontal ground tremble data recorded by AI145 station for as a benchmark data, and taking advantage of geophysical and geotechnical field testing results published by TUBITAK, for the station location; one can investigate the validity of each evaluated method pair for calculating seismic response.

Appraisal of the probabilistic seismic hazard for the subject area [17], projected that PGA, S_s and S_1 values at the locus site condition are 0.21g, 0.46g and 0.17g respectively. In order to conduct seismic response analyses, it is essential to initially form a group of records, consisting of at least 10 strike-slip events that comply with a M_w range from 5.0 to 6.1, a R_{jb} interval that spans between 5 to 45 km and a V_{s30} range of 600-1400 m/s (Note that, this

selection range is greatly different from the proposed interval of values. However, as the number of records used in analyses has a larger impact on the attained results, herein, decision to modify selection criteria is warranted); in compliance with the PSHA findings.

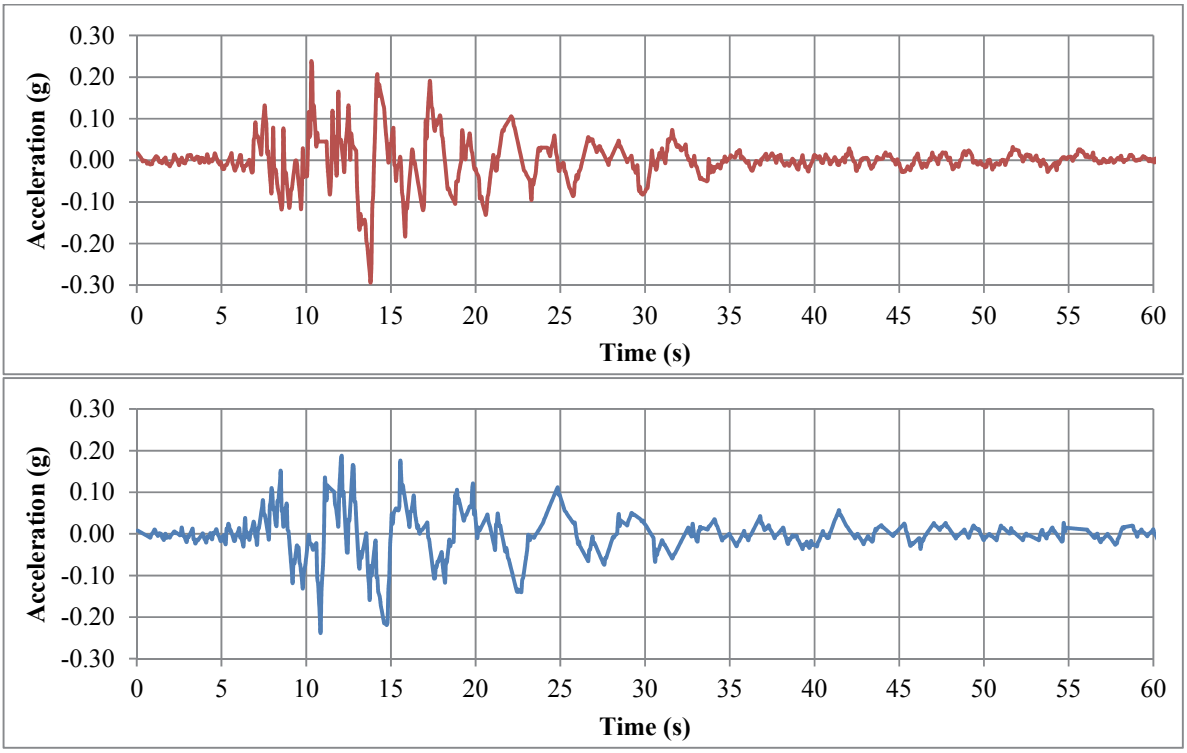

Figure 3.11. East-West (Top) and North-South (Bottom) components of the surface accelerations recorded by TSGMN Station AI145 during July 18, 1979; Asagigocek, Balikesir earthquake

Table 3.2 shows the list of 10 record components; observed to comply with the defined gauges, and, as a result, considered appropriate for the interested practice. Figures 3.12 to 3.15 display the 5%-damped response spectra of unscaled record components, and the resultant input time-series established through PGA scaling, scaling to attain the best-fit mean spectrum, and nonstationary spectral matching, correspondingly, alongside the UHS determined for the target location, calculated at the reference site condition as per seismic hazard analysis outcomes.

Table 3.2. List of earthquake time histories selected for use with the ground response analyses performed for AI145 TSGMN station

Record No.	Event	M_w	R_{jb} (km)	V_{s30} (m/s)	Record File	PGA
1	Hollister-04 (1986)	5.45	[10.7]	684.9	NGA No#501 (D-SG3205)	0.043
2	Hollister-04 (1986)	5.45	[10.7]	684.9	NGA No#501 (D-SG3295)	0.089
3	Baja California (1987)	5.50	[3.4]	659.6	NGA No#585 (CPE251)	0.890
4	Coyote Lake (1979)	5.74	10.2	1428.0	NGA No#146 (G01320)	0.133
5	Coyote Lake (1979)	5.74	5.3	597.1	NGA No#145 (CYC160)	0.156
6	Coyote Lake (1979)	5.74	5.3	597.1	NGA No#145 (CYC250)	0.276
7	Livermore-02 (1980)	5.42	[7.5]	712.8	NGA No#222 (B-LMO265)	0.197
8	Anza (Horse Canyon)-01 (1980)	5.19	[12.0]	724.9	NGA No#225 (PFT135)	0.131
9	Coalinga-08 (1983)	5.23	[17.8]	617.4	NGA No#424 (G-CSU000)	0.014
10	Coalinga-08 (1983)	5.23	[17.8]	617.4	NGA No#424 (G-CSU090)	0.016

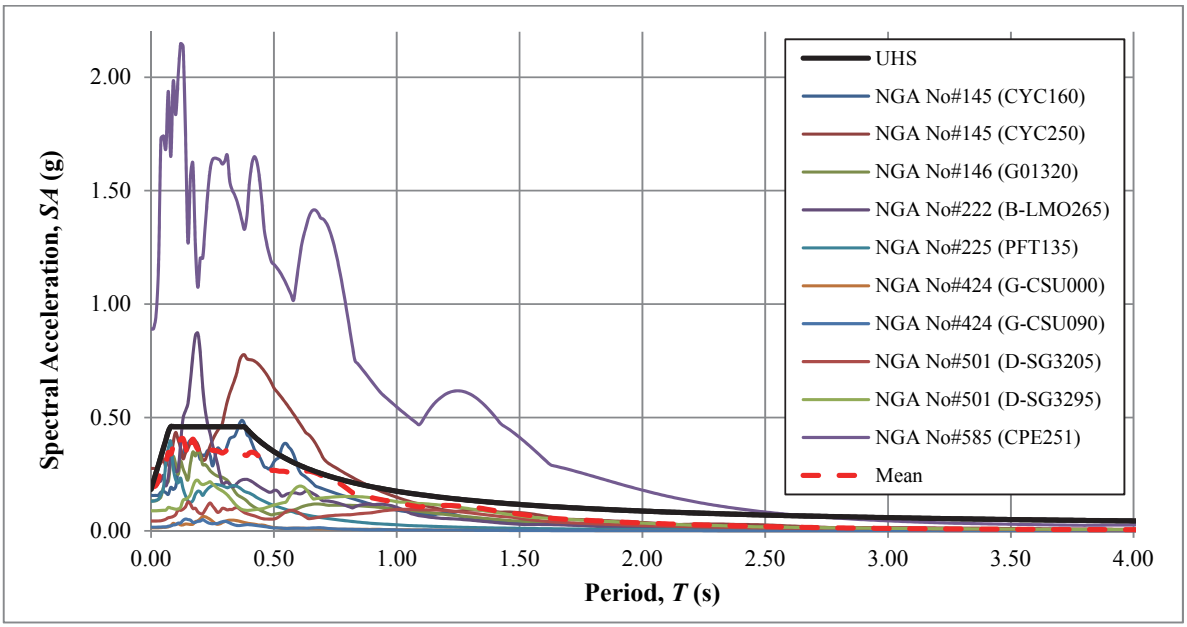

Figure 3.12. 5%-damped response spectra of earthquake record components selected for carrying out the site effects calculations for AI145 TSGMN station

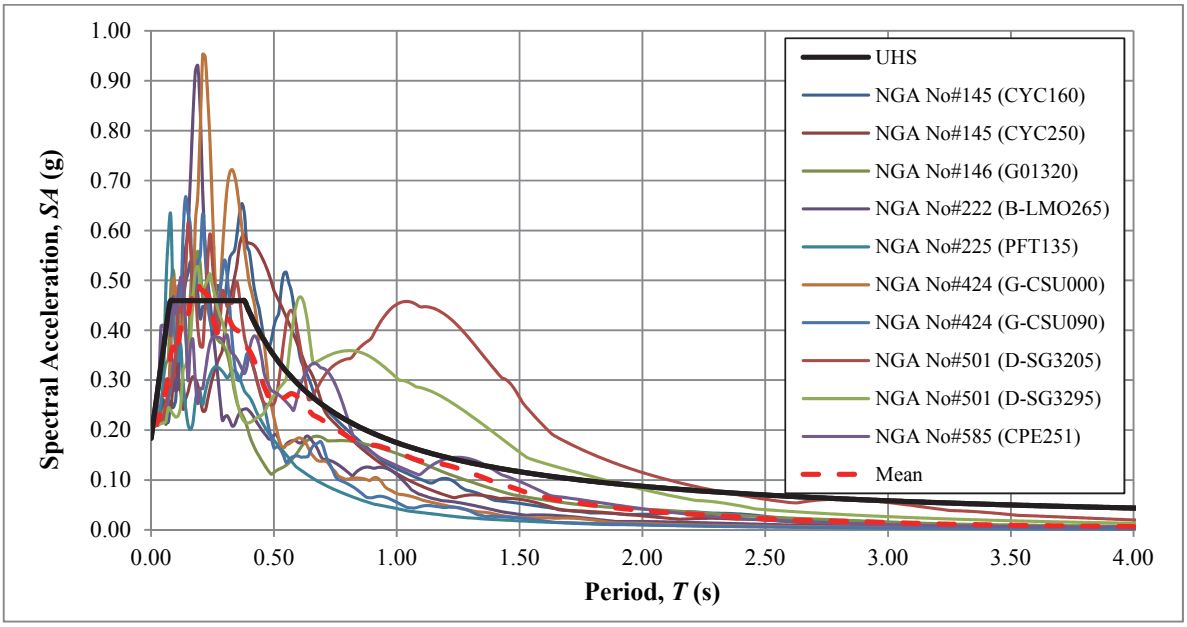

Figure 3.13. 5%-damped response spectra of earthquake record components presented in Figure 3.12 after normalization of each time series to the hazard PGA level of 0.21g

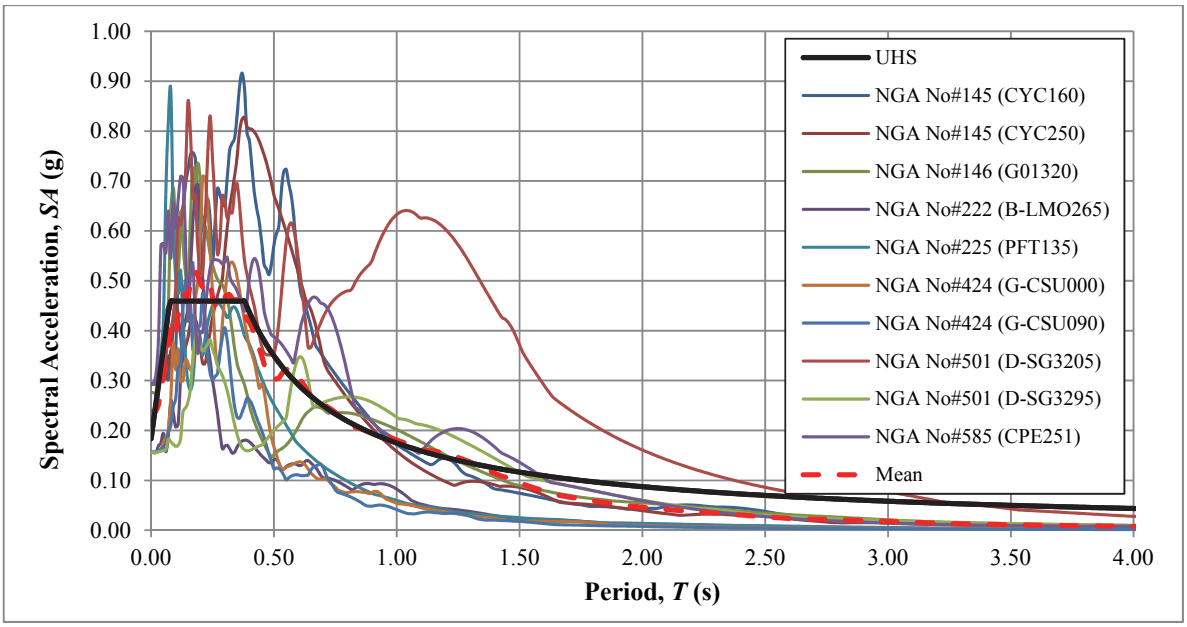

Figure 3.14. 5%-damped response spectra of earthquake record components shown in Figure 3.12 after scaling to find the mean spectrum that is best-fit with PSHA-decided UHS

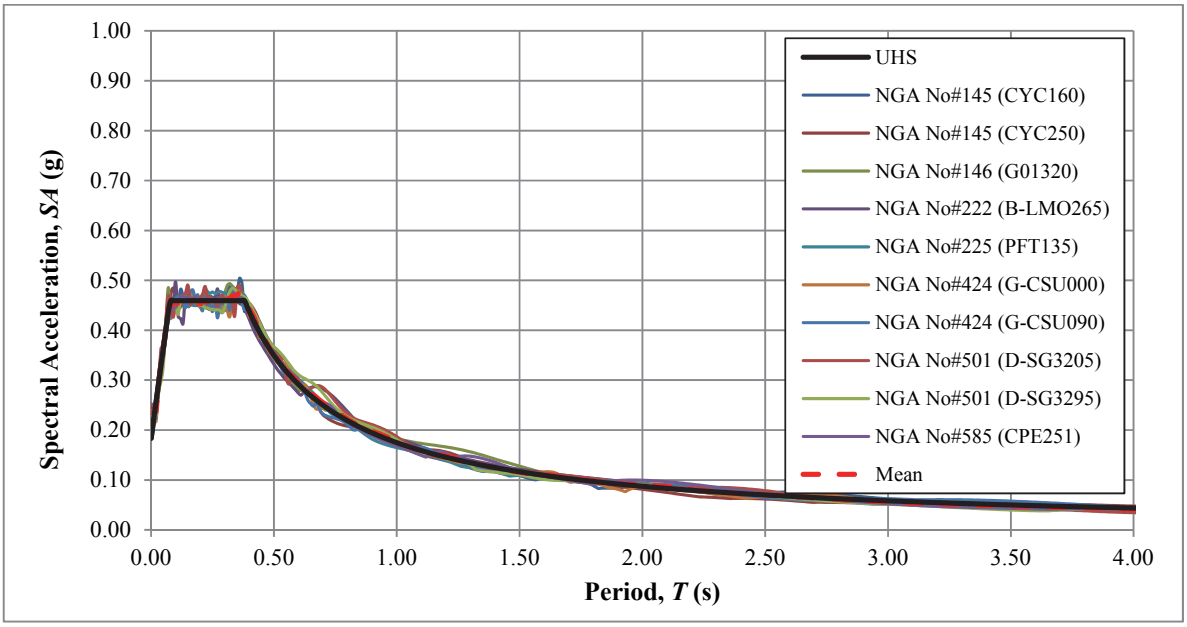

Figure 3.15. 5%-damped response spectra of the earthquake record components presented in Figure 3.12 following nonstationary spectral matching as per PSHA-determined UHS

The stratification beneath TSGMN station AI145 is characterized by a well-graded-sand-based artificial fill stratum, with a thickness of approximately 1.4 m, that caps the underlying weathered weak-rock layering (i.e. geology prevalent in the region). The product of MASW testing performed at a location that is sufficiently close to the target site indicates that both the topping artificial fill layer and the succeeding weak rock formations consist of stiff material that yields V_s measurements extending between 421 to 665 m/s from the ground surface to the locus soil condition. The stiffness features of the profiling are marked by a shear resistance that gradually strengthens with increasing depth (the sudden surge in V_s between 6.3 to 9 m being the sole exception). SPT tests performed at the station site also returns an observation that is parallel to the MASW findings. The number of penetrations at each examination depth yields a refusal situation, forcing ending of drilling at a depth of 10 m. Figure 3.16 outlines the features of soil stratification below the AI145 station down to the decided reference site condition, in a graphical manner.

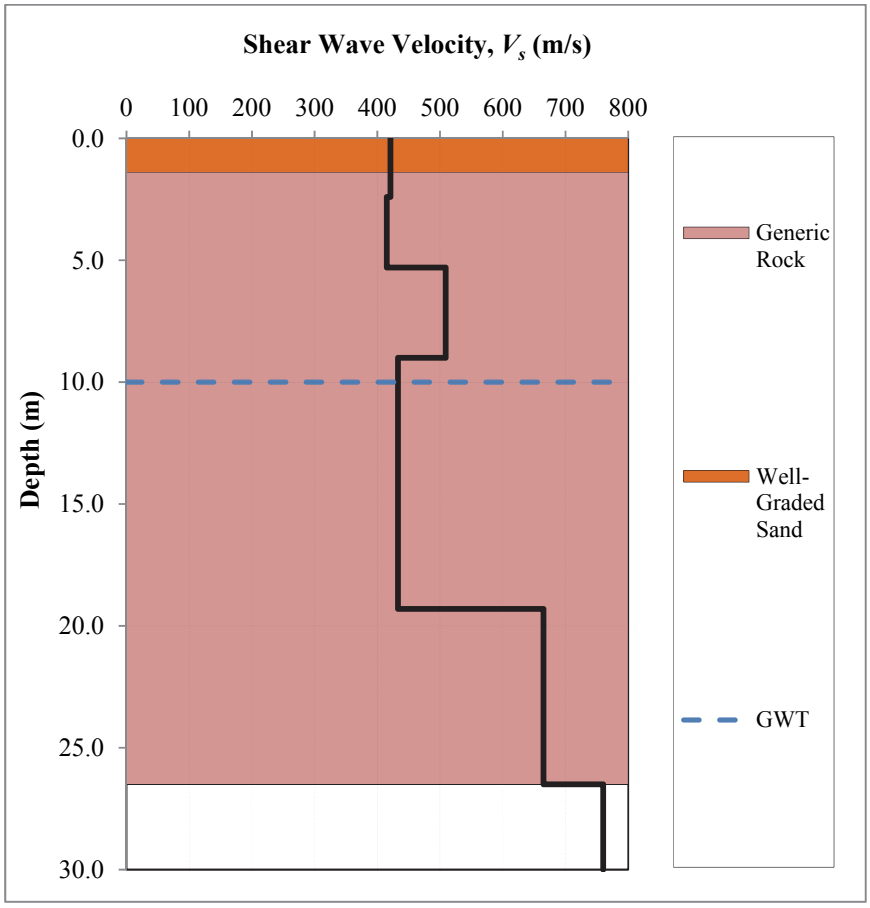

Figure 3.16. A visual depiction of soil layering and corresponding shear-wave velocity variation underneath the AI145 station; extending down to the reference site condition

In terms of modelling the dynamic behavior of involved materials, for ground response response calculations of AI145 TSGMN station, herein, the well-graded sand and generic rock stratifications identified through field observations are simulated via the dynamic soil properties suggested by Seed et al. [64] and EPRI [42] respectively. Figure 3.17 conveys a graphical description of the employed modulus reduction/damping curves. In the conducted calculations, the unit weight values of 17.30 and 20.50 kN/m^3 are used for well-graded sand, and generic rock material present between 1.4 to 26.5 m respectively. The unit weight value for the locus site is assumed as 22.00 kN/m^3.

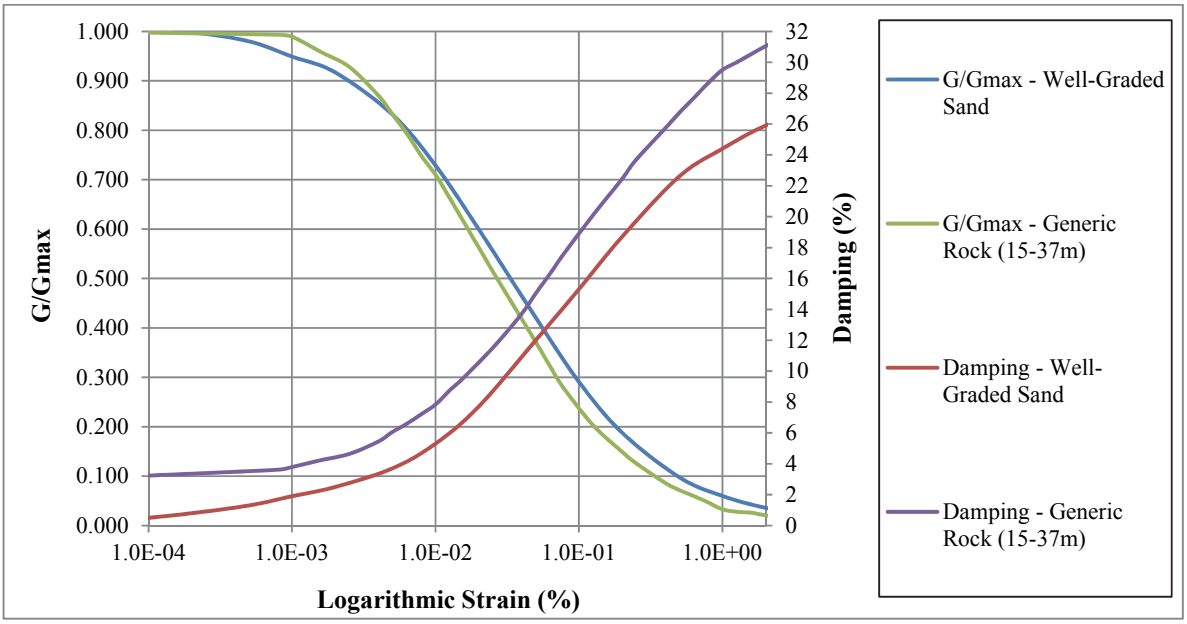

Figure 3.17. Modulus degradation and damping curves adopted for performing ground response analyses at the site of AI145 TSGMN station

Figures 3.18 and 3.19 show the seismic response analysis results for AI145 TSGMN station site, calculated using each method pair. Similar to the situation for Denizli Station, due to inadequecies of each input prepation method adopted in the performed analyses to provide a precise description of the frequency-content of bedrock-level motions, there is an apparent discrepancy between the spectrum shape of the observed and computed responses. In all cases, there is a clear tendecy of the obtained results to either miss the initial peak visible on the reponse spectra of the recorded events, roughly occuring around a period value of 0.14s (i.e. in the case of analyses conducted using records generated through nonstationary matching), or simulate the initial rise correctly but vastly overestimate secondary and third peaks (attained approximately at periods of 0.18s and 0.39s) witnessed in the spectra for observed earthquake motions. Nonetheless, speaking in terms of the peak amplitude responses, the frequency independent calculation scheme using input motions established by nonstationary spectral matching technique produces a very comparable response with the observed behavior; yielding a peak response ratio just about 1.086.

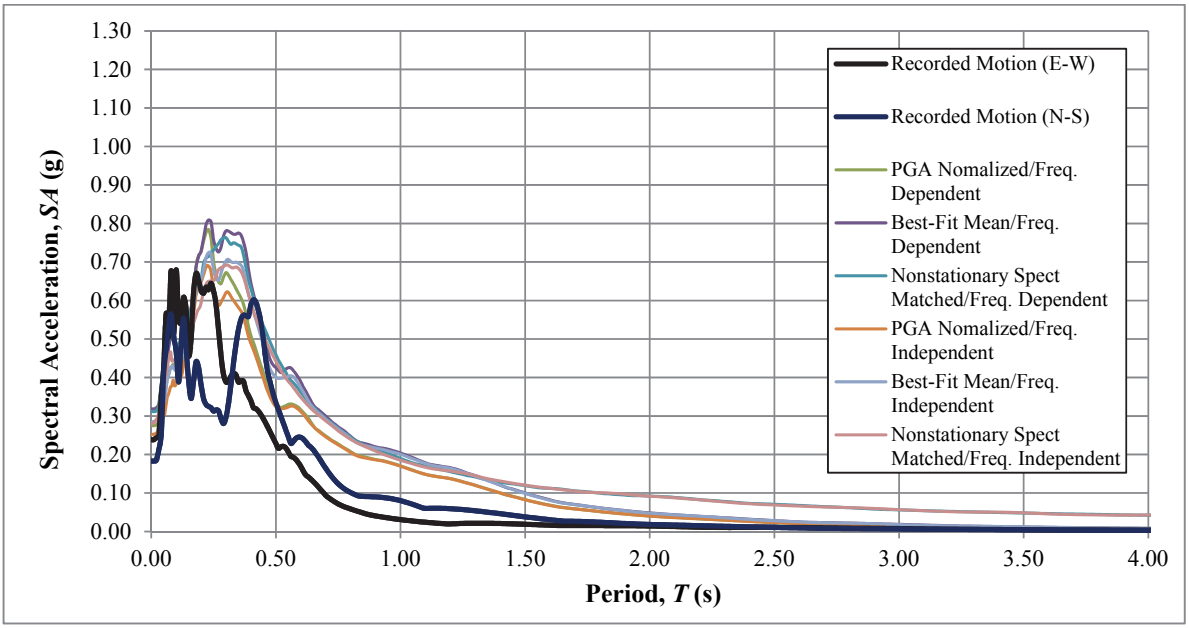

Figure 3.18. A comparison of 5%-damped mean response spectra, determined using each method pair, with the observed behavior at AI145 TSGMN station

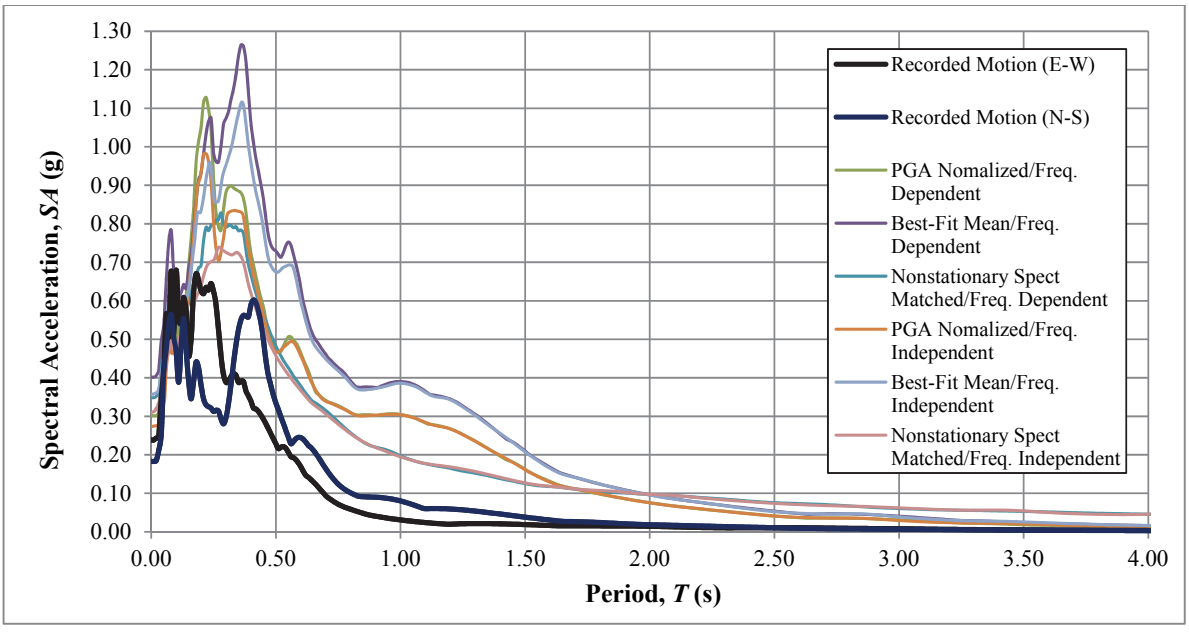

Figure 3.19. A comparison of the 5%-damped mean + std. dev. response spectra, determined via each method pair, with the observed behavior at AI145 station

3.1.3. Horasan Station (AI059)

Pasinler-Horasan Basin; the geological structure on which the city of Horasan – an administrative division of the province of Erzurum – is situated, is set up of an assemblage comprised of Neotectonic sediments that are enclosed by pre-Miocene rocks [65]. The general composition of the quaternary alluvium witnessed in the area, is constituted of unconsolidated soft clay deposits that develop into stiffer structures with depth. This sedimentation stratum shows recurrent changes in thickness, as the properties of the vertical and lateral rock body, and fault systems are fairly varied. Nonetheless, as per the geotechnical and geophysical findings reported by TUBITAK the location of the reference site condition can be approximated as approximately 45-55 m below the Horasan city.

Horasan is located in an active tectonics region that is controlled by a series of strike-slip (Dumlu and Palandoken fault groups) and extensional systems (north\northwest-south\southeast-oriented normal faulting) [66]. M_w=6.6 Horasan-Narman earthquake that happened in October 30, 1983, occurred on the northeast-southwest directed left lateral strike-slip Horasan fault (also the source of M_s=6.8, 1924 Pasinler earthquake); a part of the Palandoken fault groups [67] roughly 60 km east of Erzurum Basin. The devastating event culminated in 1155 casualties, extensive damage in 3241 buildings and moderate harm to 3007 housing structures in the provinces of Erzurum and Kars [68]. TSGMN station AI059 positioned in Horasan city center, situated at a R_{jb} distance of 22.6 km, is one of the two nearby stations that recorded this incident (See Figure 3.20 for East-West and North-South component recorded time histories).

Outcome of PSHA and the successive deaggragation study performed for the site of the strong ground motion station indicates that the October 30, 1983 Horasan-Narman earthquake, indeed, approximates the design event for Horasan city. Thus, by utilizing the horizontal components of AI059 station records as benchmark data, and making use of the detailed geophysical and geotechnical information published by TUBITAK; it is possible to test the effectiveness of each constructed method pair for the purpose of estimating seismic ground response.

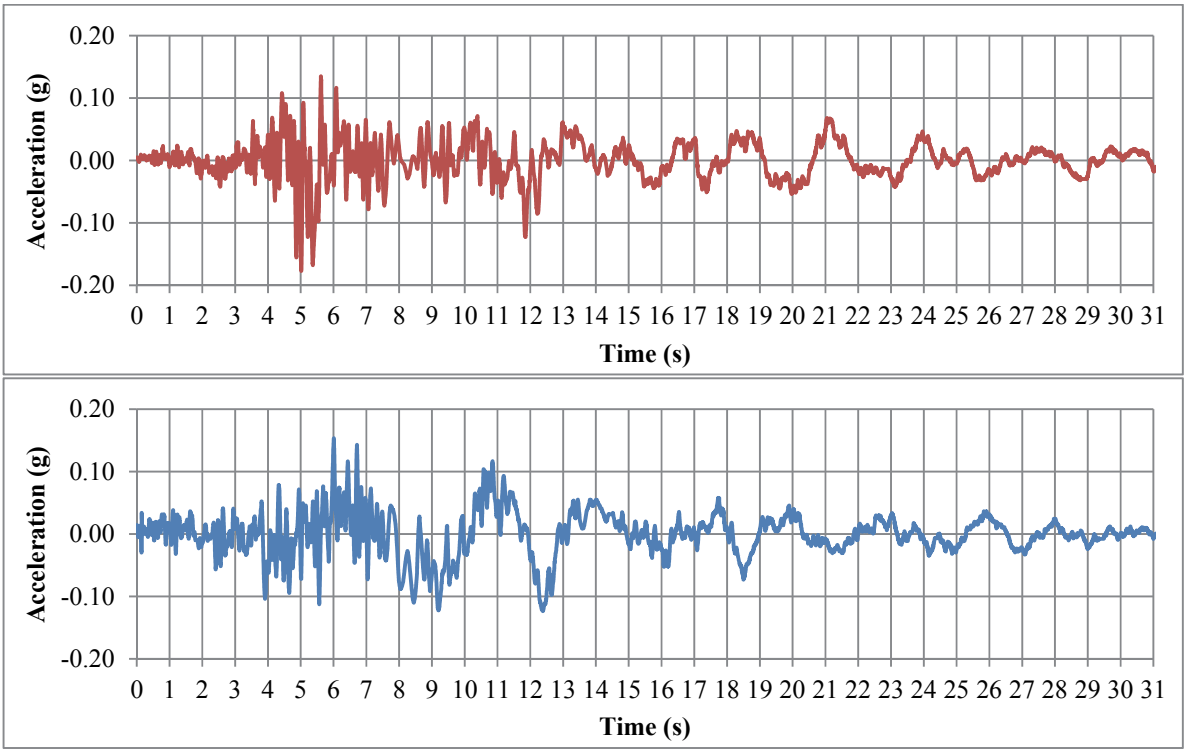

Figure 3.20. East-West (Top) and North-South (Bottom) components of the surface accelerations recorded by TSGMN Station AI059 during October 30, 1983; Horasan-Narman earthquake

According to PSHA findings for the interested site [69], estimated PGA, S_s and S_1 values at the reference site condition are 0.17g, 0.37g and 0.11g respectively. For performing seismic response analyses, it is vital to first develop a set of records, consisting of at least 10 strike-slip events, which satisfy a M_w range from 6.1 to 7.1, a R_{jb} interval that spans between 3 to 48 km and a V_{s30} range of 600-730 m/s (records from the Morgan Hill station, i.e. V_{s30}=1428 m/s being an exemption); in-line with the PSHA results. Table 3.3 displays the list of 22 earthquake record components that are found to comply with the defined criteria, and, as a result, reasoned right for the target application. Figures 3.21 to 3.24 show the 5%-damped response spectra of unscaled record components, and the agreeing input time-histories established by PGA scaling, scaling to obtain the best-fit mean spectrum, and nonstationary

spectral matching, respectively, along with the UHS determined for the subject location, calculated at the reference site condition in terms of seismic hazard results.

Table 3.3. List of earthquake time histories selected for use with the ground response analyses performed for AI059 TSGMN station

Record No.	Event	M_w	R_{jb} (km)	V_{s30} (m/s)	Record File	PGA
1	Imperial Valley-06 (1979)	6.53	15.2	659.6	NGA No#164 (H-CPE147)	0.170
2	Chi-Chi- Taiwan-04 (1999)	6.20	12.4	680.0	NGA No#2739 (CHY080-N)	0.120
3	Victoria- Mexico (1980)	6.33	13.8	659.6	NGA No#265 (CPE045)	0.621
4	Victoria- Mexico (1980)	6.33	13.8	659.6	NGA No#265 (CPE315)	0.587
5	Morgan Hill (1984)	6.19	31.9	622.9	NGA No#471 (SJL360)	0.069
6	Morgan Hill (1984)	6.19	14.9	1428.0	NGA No#455 (G01230)	0.069
7	Morgan Hill (1984)	6.19	14.9	1428.0	NGA No#455 (G01320)	0.096
8	Morgan Hill (1984)	6.19	31.9	622.9	NGA No#472 (SJR270)	0.078
9	Morgan Hill (1984)	6.19	14.9	1428.0	NGA No#472 (SJR360)	0.059
10	Kobe- Japan	6.90	7.1	609.0	NGA No#1111 (NIS090)	0.501
11	Morgan Hill (1984)	6.19	14.8	729.6	NGA No#454 (GIL067)	0.112
12	Morgan Hill (1984)	6.19	14.8	729.6	NGA No#454 (GIL337)	0.092
13	Chi-Chi- Taiwan-04 (1999)	6.20	39.3	679.9	NGA No#2753 (CHY102-E)	0.059
14	Chi-Chi- Taiwan-04 (1999)	6.20	39.3	679.9	NGA No#2753 (CHY102-N)	0.053
15	Chi-Chi- Taiwan-04 (1999)	6.20	27.2	680.0	NGA No#2873 (TCU089-E)	0.031
16	Chi-Chi- Taiwan-04 (1999)	6.20	37.5	680.0	NGA No#2935 (TTN051-E)	0.065
17	Chi-Chi- Taiwan-04 (1999)	6.20	37.5	680.0	NGA No#2935 (TTN051-N)	0.076
18	Morgan Hill (1984)	6.19	45.5	714.0	NGA No#476 (LOB320)	0.076
19	Chi-Chi- Taiwan-04 (1999)	6.20	39.7	680.0	NGA No#2820 (KAU050-E)	0.069
20	Chi-Chi- Taiwan-04 (1999)	6.20	39.7	680.0	NGA No#2820 (KAU050-N)	0.066
21	Big Bear-01 (1992)	6.46	[33.8]	684.9	NGA No#934 (SVP090)	0.059
22	Big Bear-01 (1992)	6.46	[33.8]	684.9	NGA No#934 (SVP360)	0.070

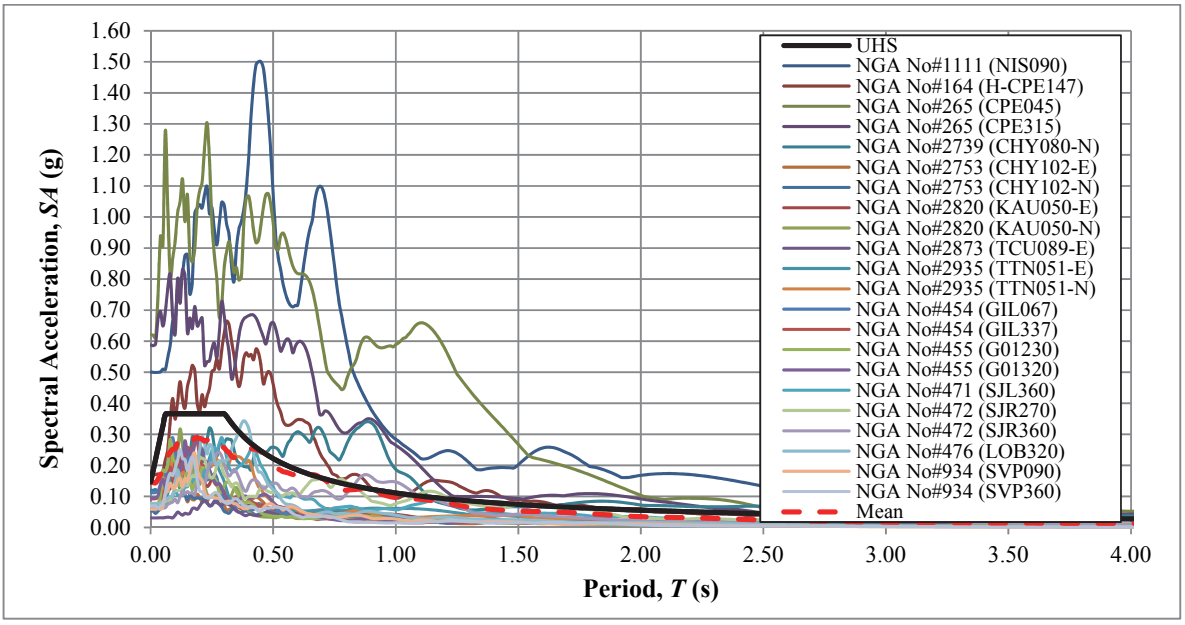

Figure 3.21. 5%-damped response spectra of earthquake record components selected for carrying out the site effects calculations for AI059 TSGMN station

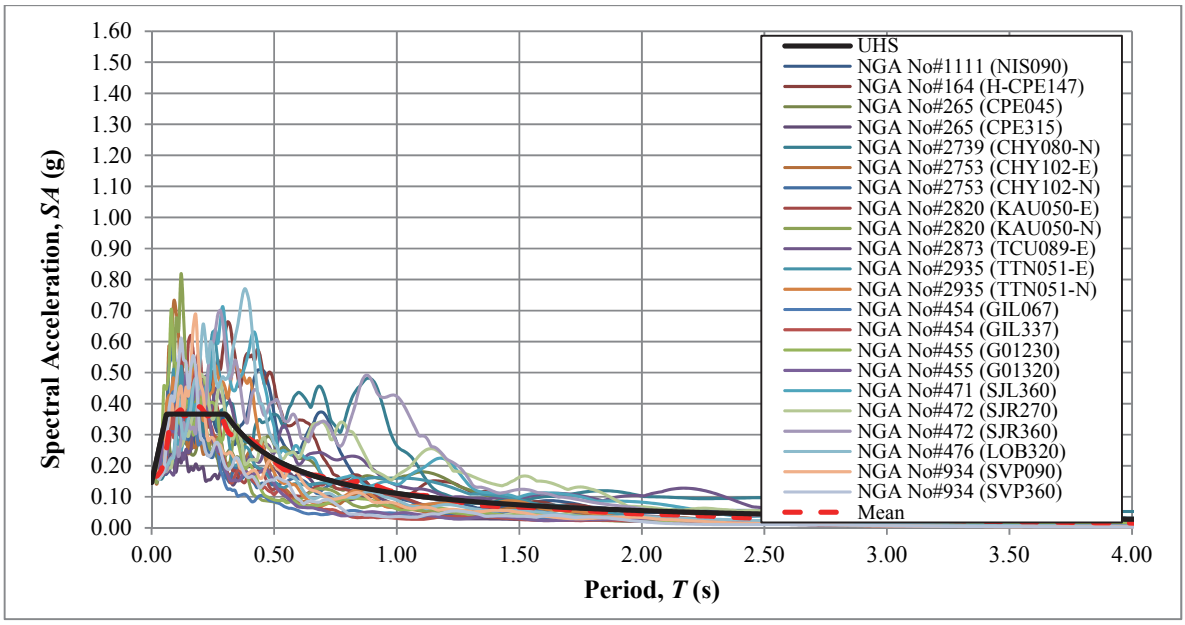

Figure 3.22. 5%-damped response spectra of earthquake record components presented in Figure 3.21 after normalization of each time series to the hazard PGA level of 0.17g

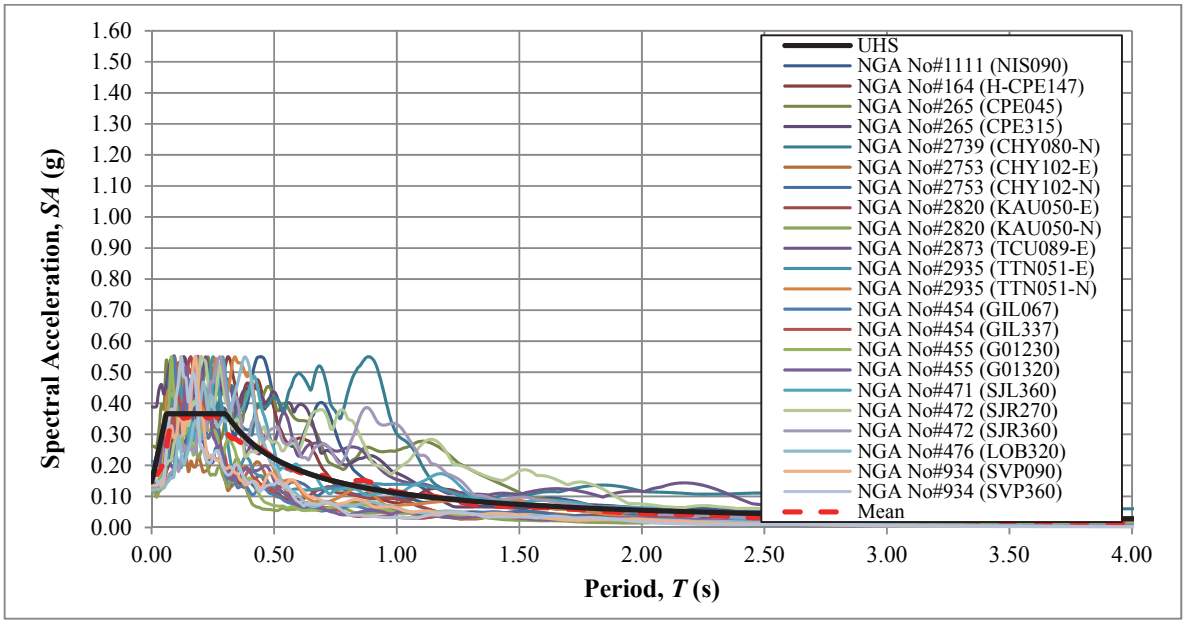

Figure 3.23. 5%-damped response spectra of earthquake record components shown in Figure 3.21 after scaling to find the mean spectrum that is best-fit with PSHA-decided UHS

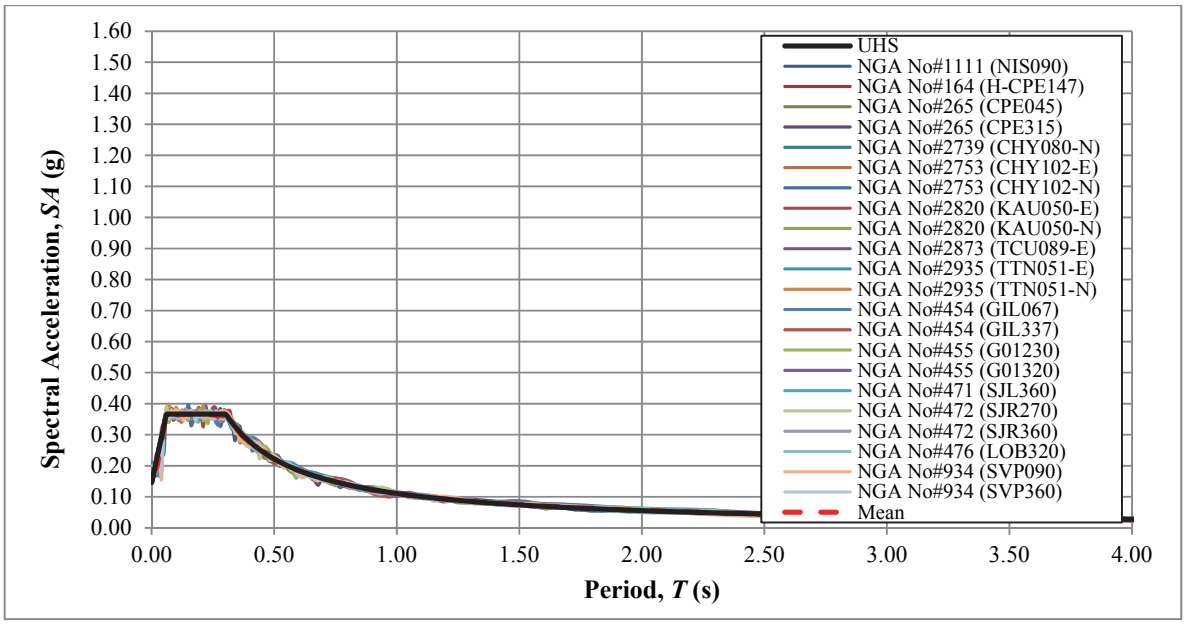

Figure 3.24. 5%-damped response spectra of earthquake record components presented in Figure 3.21 following nonstationary spectral matching as per PSHA-determined UHS

Field testing results reported for the station site indicates that the soil stratification beneath AI059 is prevailed by a clayey material with a relatively thin band of gravelly-clay layer at the top 29 m of the soil column. The plasticity of the clay layers are observed to increase with depth; indicating a steady change in the hysteretic behavior of clayey sedimentation. The results of SPT and MASW testing performed for the target location shows that the perceived clayey formations are composed of soft deposits that rapidly stiffen toward the junction where the clayey material is replaced by a weak-rock material, with V_s values ranging from 176 m/s to 509 m/s. The ensuing rock-like layering is marked by a noticeably higher shear resistance that picks up towards the locus site condition, while the joint between the clay and rock-like strata being an exception (where an abrupt reduction in the V_s profile from 509 m/s to 450 m/s is recognized). Figure 3.25 summarizes the characteristics of the soil layering beneath the AI059 station down to the decided locus, in a visual manner.

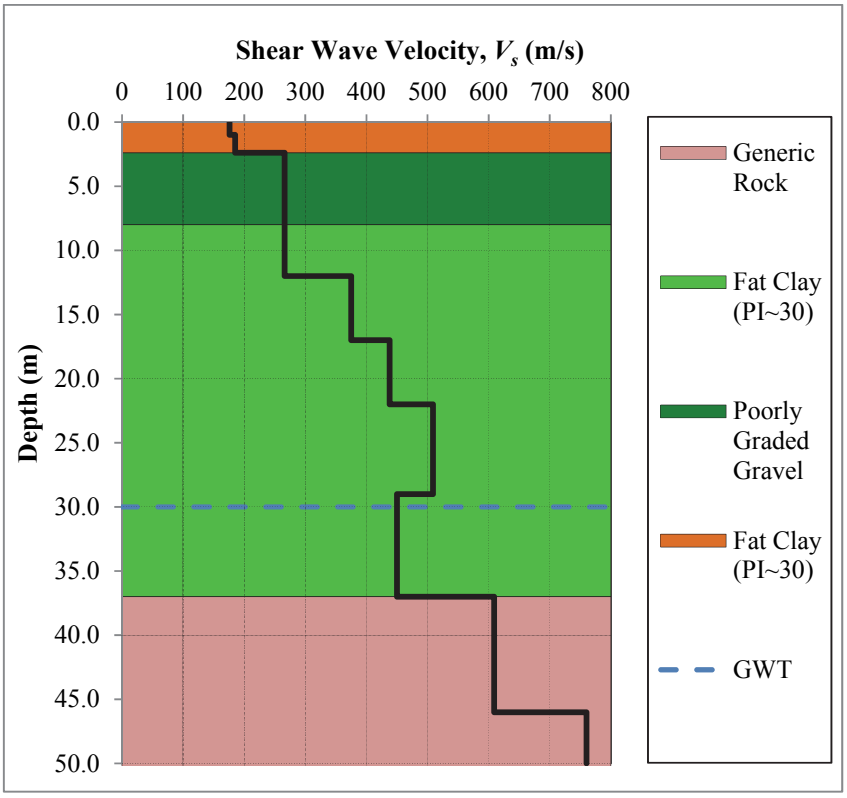

Figure 3.25. A visual depiction of soil layering and corresponding shear-wave velocity variation underneath the AI059 station; extending down to the reference site condition

So to carry out the ground reponse analyses for AI059 TSGMN station, here, the lean clay PI=15, gravelly clay and generic rock stratifications recognized in field testing reports are modeled through the dynamic soil properties published by Vucetic and Dobry [62], Seed et al. [64] and EPRI [42] respectively. Figure 3.26 provides a graphical description of the utilized modulus reduction/damping curves. In the conducted computations, the unit weight values of 17.30, 19.00, 20.50 and 22.00 kN/m^3 are used for clayey soils, gravelly clays and generic rock material present between 29 to 37 m, 37 to 46 m depths correspondingly.

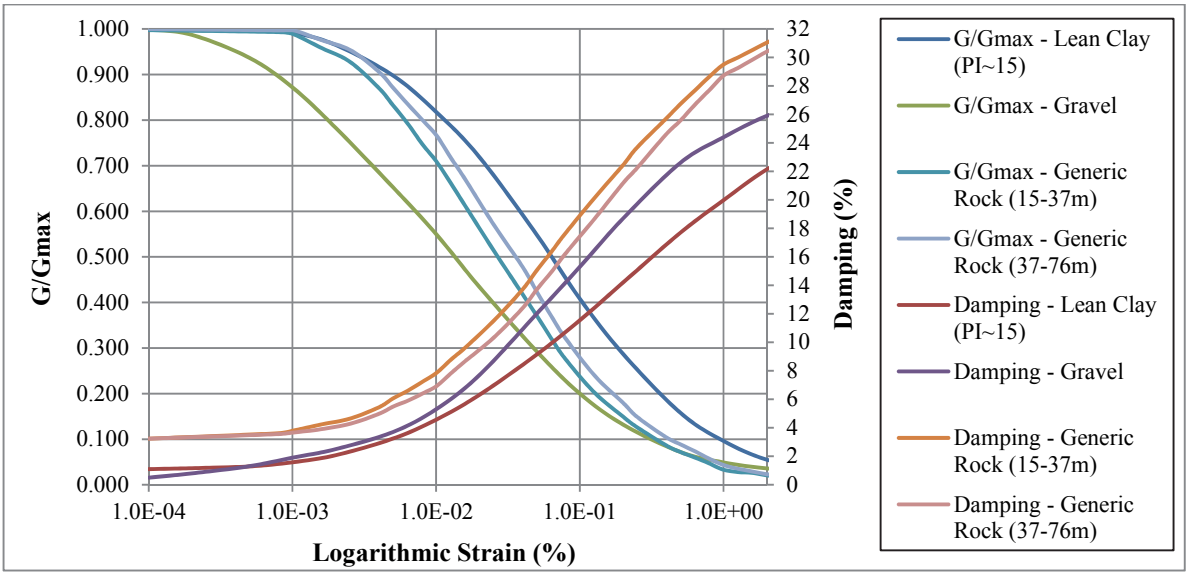

Figure 3.26. Modulus degradation and damping curves adopted for performing ground response analyses at the site of AI059 TSGMN station

Figures 3.27 and 3.28 display the seismic response analysis results for AI059 TSGMN station site, calculated using each method pair. In each situtation, computed results produce a spectral envelope that contains, virtually, all of the significant peaks on response spectra of the recorded components. Thus, more or less, the output of each method pair is effective in simulating the frequency-content traits of observed ground motion. However, judging based peak amplitude responses, the frequency independent calculation scheme using input motions established by nonstationary spectral matching technique brings about a very analogous response with the observed behavior, with a peak response ratio of around 1.125.

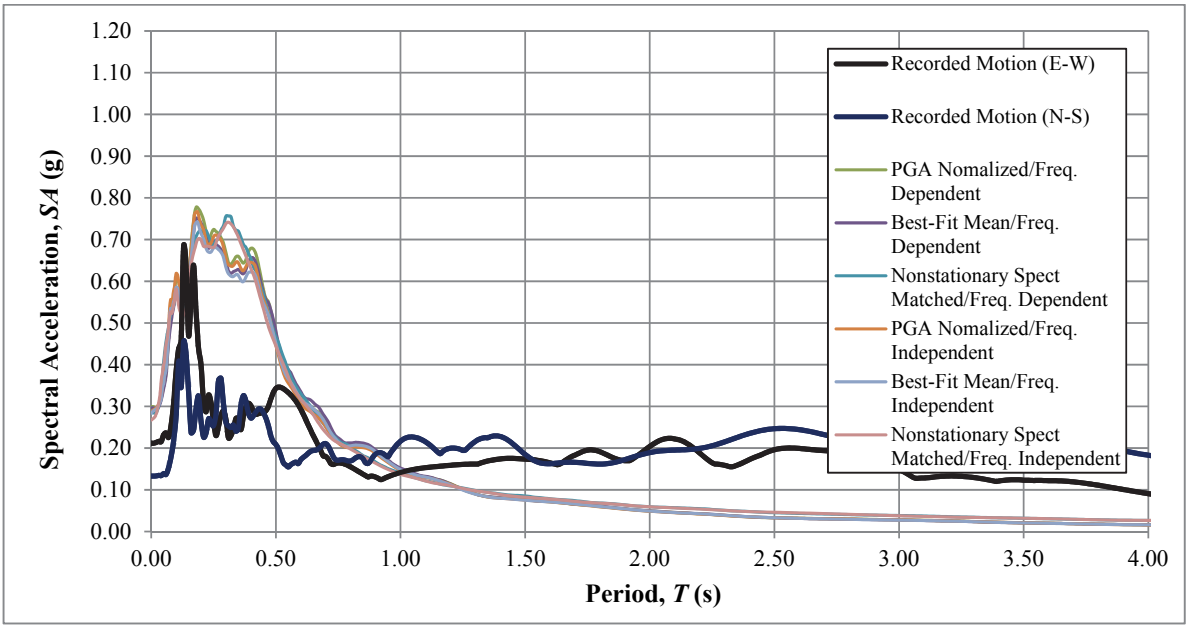

Figure 3.27. A comparison of 5%-damped mean response spectra, determined using each method pair, with the observed behavior at AI059 TSGMN station

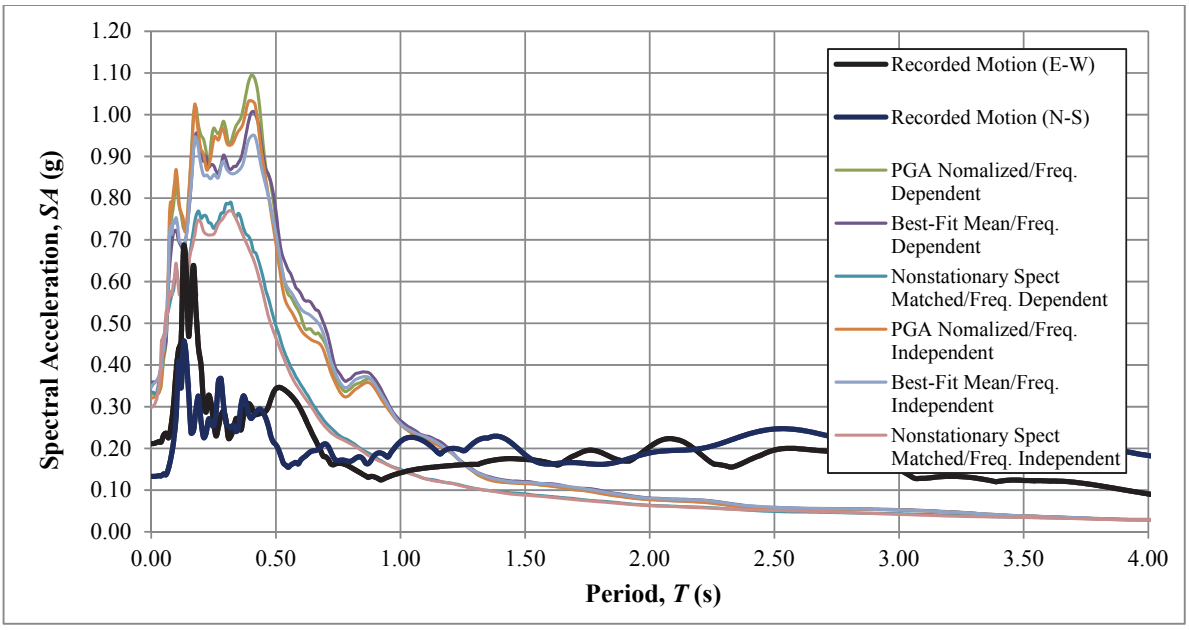

Figure 3.28. A comparison of 5%-damped mean + std. dev. response spectra, determined using each method pair, with the observed behavior at AI059 TSGMN station

3.1.4. Dinar Station (AI137)

Dinar, an administrative division of the Afyonkarahisar province, is a 25,000-population city situated on the Dinar graben formation. Dinar Graben is comprised of Plio-Quaternary alluvial sand, clay and silt sedimentations founded on clay cemented conglomerates that extend to a depth greater than 100 m. This alluvium settling is bounded on the east by the horst development that consists of limestone/conglomerates, which plunge underneath the alluvium strata at an angle of 14 degrees; thus causing a curved interface between basin edge and the sedimentation [70]. Predominantly, the alluvial deposits are composed of soft clay matter that exhibits various levels of plasticity. Microtremor testing results reported by Iyisan and Hasal [71] suggests that the thickness of this unconsolidated material ranges between 30-45 m and slowly thins out toward the basin edge.

The tectonic setting of Dinar city is characterized by two faulting systems that are located in the vicinity of the settlement; the extensional systems of North-South-oriented Akdag fault and Northwest-Southeast-oriented Dinar-Civril fault, with a small left-lateral constituent, that is known to trigger earthquake events of $6.0<M_w<7.0$ [72]. In October 1, 1995, 60 km-long Dinar-Civril normal fault, gave rise to a distressing $M_w=6.4$ event that resulted in 92 casualties, collapse of 4340 buildings and damage in 10,000 structures within the city and its surroundings [73]. TSGMN station AI137 placed in the central part of Dinar and, in fact, positioned exceptionally close the surface projection of the fault, i.e. $R_{jb}=0$ km, is one of the seven proximate stations that recorded this event (See Figure 3.29 for East-West and North-South component recorded time histories).

The PSHA-consecutive deaggragation analysis performed for the site of Dinar strong ground motion station points out that the October 1, Dinar earthquake closely takes after the design event for Dinar city. Consequently, through utilizing the horizontal components of AI137 station records as benchmark records, and making use of the comprehensive geophysical and geotechnical information published by TUBITAK, Istanbul Technical University, Iyisan and Hasal [71] and Kanlı et al. [74]; one can inspect the usefulness of each constructed method pair for assessing seismic ground response.

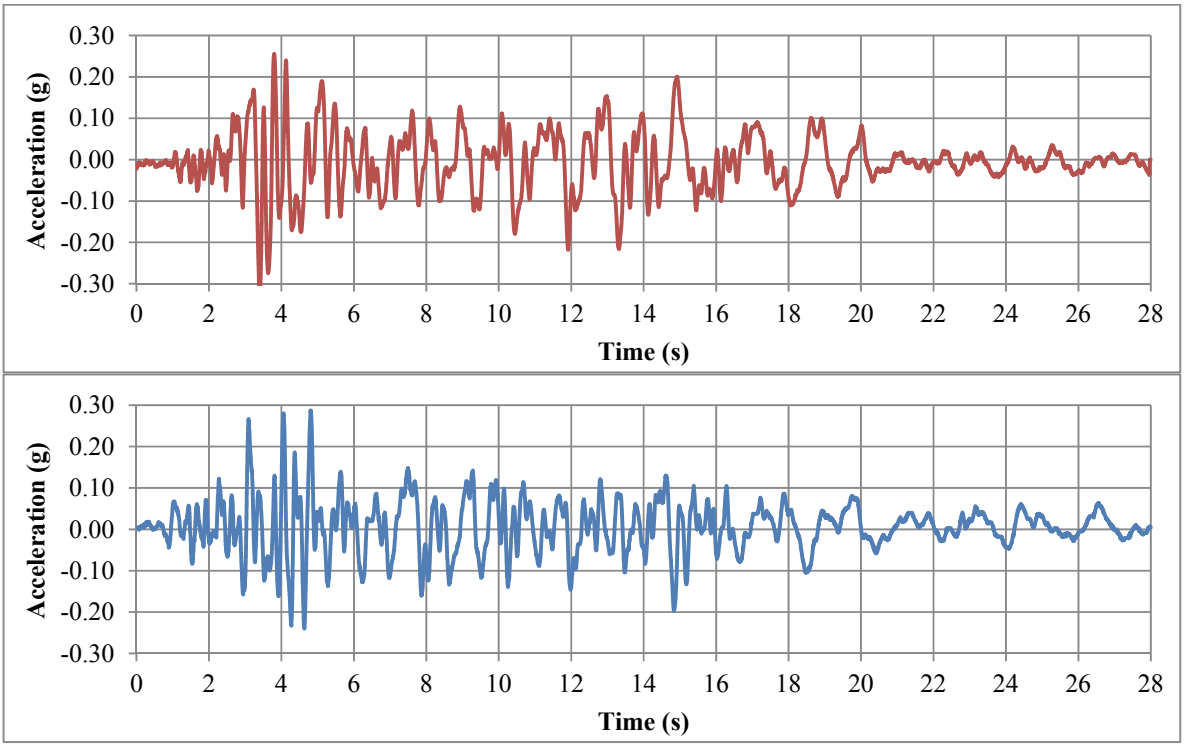

Figure 3.29. East-West (Top) and North-South (Bottom) components of the surface accelerations recorded by TSGMN Station AI137 during October 01, 1995; Dinar, Afyonkarahisar earthquake

According to PSHA results for the subject site [17], the estimated PGA, S_s and S_1 values at the reference site condition are 0.27g, 0.58g and 0.19g respectively. So for undertaking ground response calculations, it is required to initially set a group of records, containing of at least 10 normal-oblique events that content a M_w range from 5.8 to 6.9, a R_{jb} interval that ranges between 0 to 30 km, and a V_{s30} extent of 600-100 m/s (Note that this boundary is, actually, a marginally altered form of the suggested range; as it was adjusted to obtain satisfactory number of records); in compliance with the PSHA findings. Table 3.4 displays the list of the 12 earthquake record components that are found to be well-suited with the demarcated criteria, and, as a consequence, reasoned right for the subject application. Figures 3.30 to 3.33 show the 5%-damped response spectra of unscaled record components, and the pertaining input time-histories prepared by PGA scaling, scaling to obtain the best-fit mean

spectrum, and nonstationary spectral matching, respectively, along with the UHS determined for the target location, calculated at the locus site condition according to seismic hazard results.

Table 3.4. List of earthquake time histories selected for use with the ground response analyses performed for AI137 TSGMN station

Record No.	Event	M_w	R_{jb} (km)	V_{s30} (m/s)	Record File	PGA
1	Irpinia-Italy-01 (1980)	6.9	9.5	1000.0	NGA No#284 (A-AUL000)	0.057
2	Irpinia-Italy-01 (1980)	6.9	9.5	1000.0	NGA No#284 (A-AUL270)	0.061
3	Irpinia-Italy-02 (1980)	6.2	28.7	1000.0	NGA No#295 (B-AUL000)	0.018
4	Irpinia-Italy-01 (1980)	6.9	13.3	600.0	NGA No#289 (A-CTR270)	0.173
5	Irpinia-Italy-02 (1980)	6.2	20.4	1000.0	NGA No#303 (B-STU000)	0.070
6	Irpinia-Italy-02 (1980)	6.2	20.4	1000.0	NGA No#303 (B-STU270)	0.077
7	Irpinia-Italy-02 (1980)	6.2	17.8	1000.0	NGA No#296 (B-BAG270)	0.058
8	Norcia-Italy (1979)	5.9	[1.7]	659.6	NGA No#156 (F-CSC-EW)	0.200
9	Norcia-Italy (1979)	5.9	[1.7]	659.6	NGA No#156 (F-CSC-NS)	0.161
10	Norcia-Italy (1979)	5.9	[31.4]	1000.0	NGA No#155 (F-BEV-EW)	0.023
11	Norcia-Italy (1979)	5.9	[31.4]	1000.0	NGA No#155 (F-BEV-NS)	0.040
12	Oroville-01 (1975)	5.89	[7.8]	622.9	NGA No#106 (A-ORV037)	0.092

Speaking in accordance with the geological, geophysical and geotechnical knowledge collected for the station site, at the topmost 42 m, the soil layering beneath AI137 is characterized by a clayey sedimentation with thin silty sand, poorly graded sand layers. The plasticity of the clay material increases with depth, from a PI value of roughly 15 at the ground surface to 45 at the base of clay deposits. SPT and MASW findings for the station site indicate that both the clayey formations and the silt/sand-based inclusions detected at the site consist of soft deposits with V_s values extending from 149 m/s on the soil surface to 400 m/s at the base of the terminating fat clay stratum. The subsequent rock-like layering is identified to display essentially higher shear resistance with an increasing trend towards the reference site condition. Figure 3.34 outlines the features of soil layering beneath the AI022 station down to the decided reference site condition, in a graphical fashion.

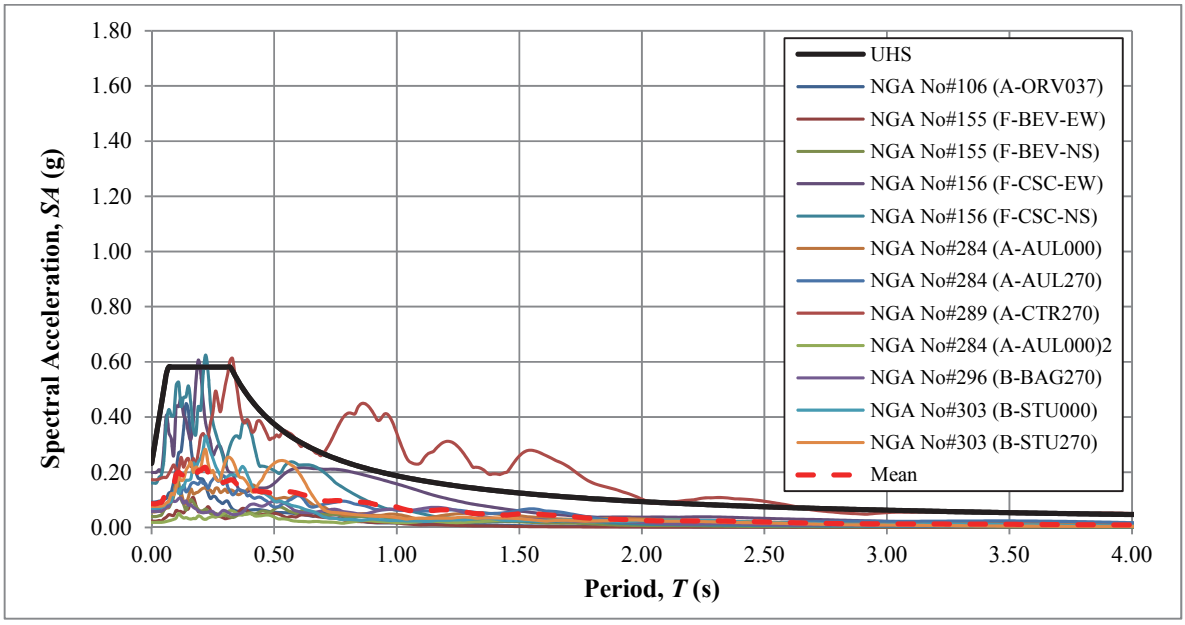

Figure 3.30. 5%-damped response spectra of earthquake record components selected for carrying out the site effects calculations for AI137 TSGMN station

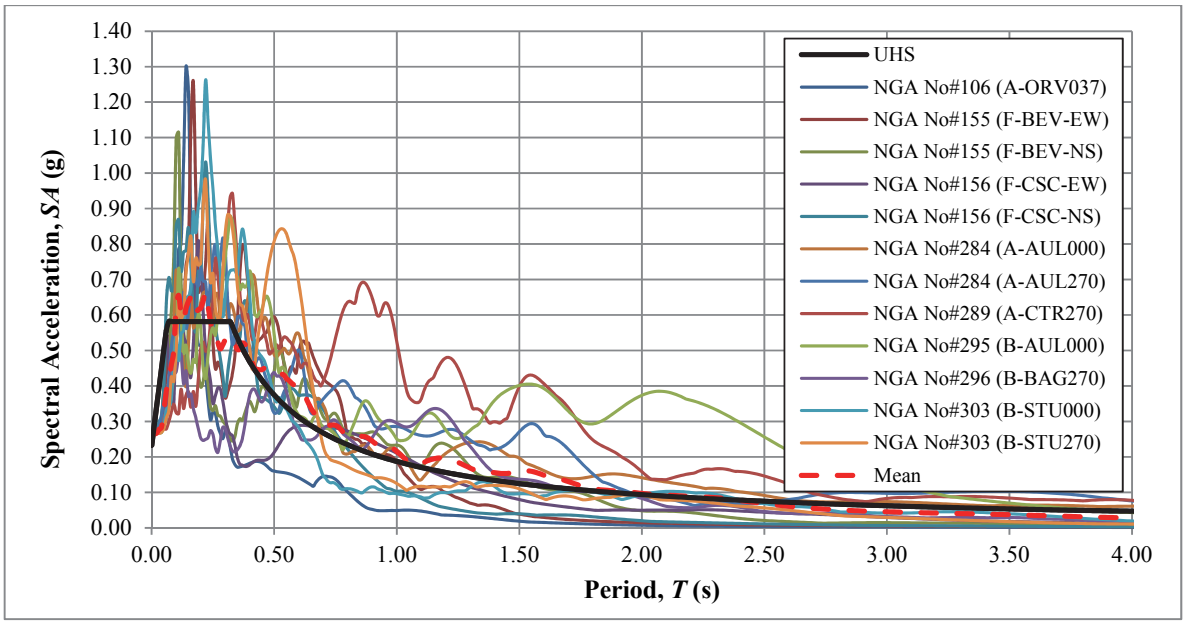

Figure 3.31. 5%-damped response spectra of earthquake record components presented in Figure 3.30 after normalization of each time series to the hazard PGA level of 0.27g

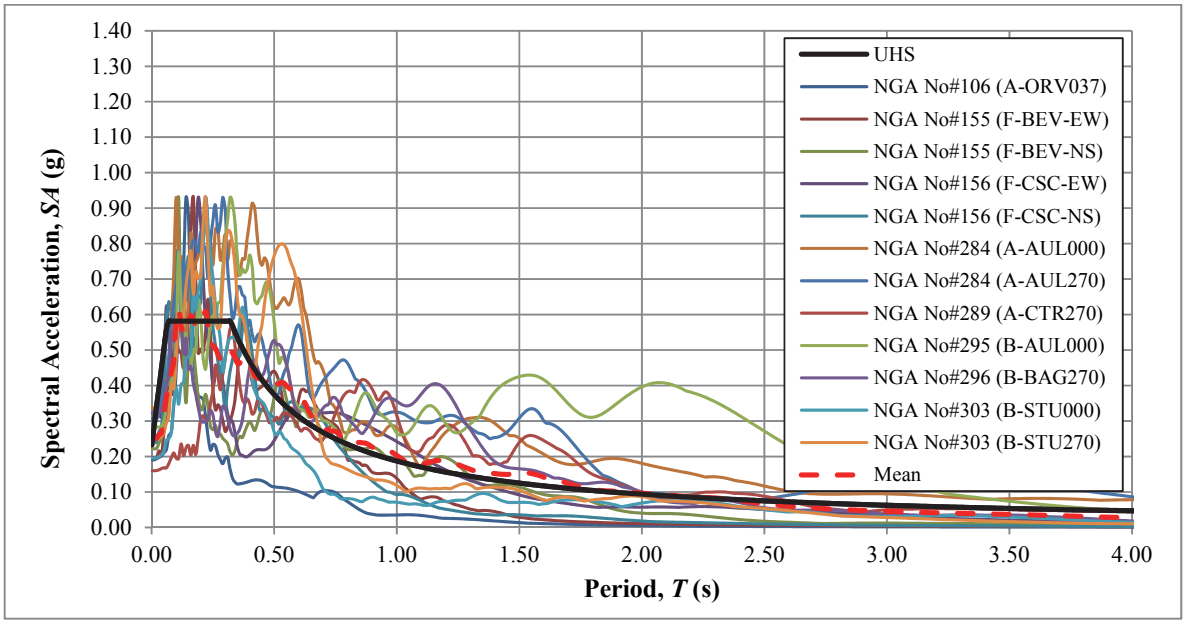

Figure 3.32. 5%-damped response spectra of earthquake record components shown in Figure 3.30 after scaling to find the mean spectrum that is best-fit with PSHA-decided UHS

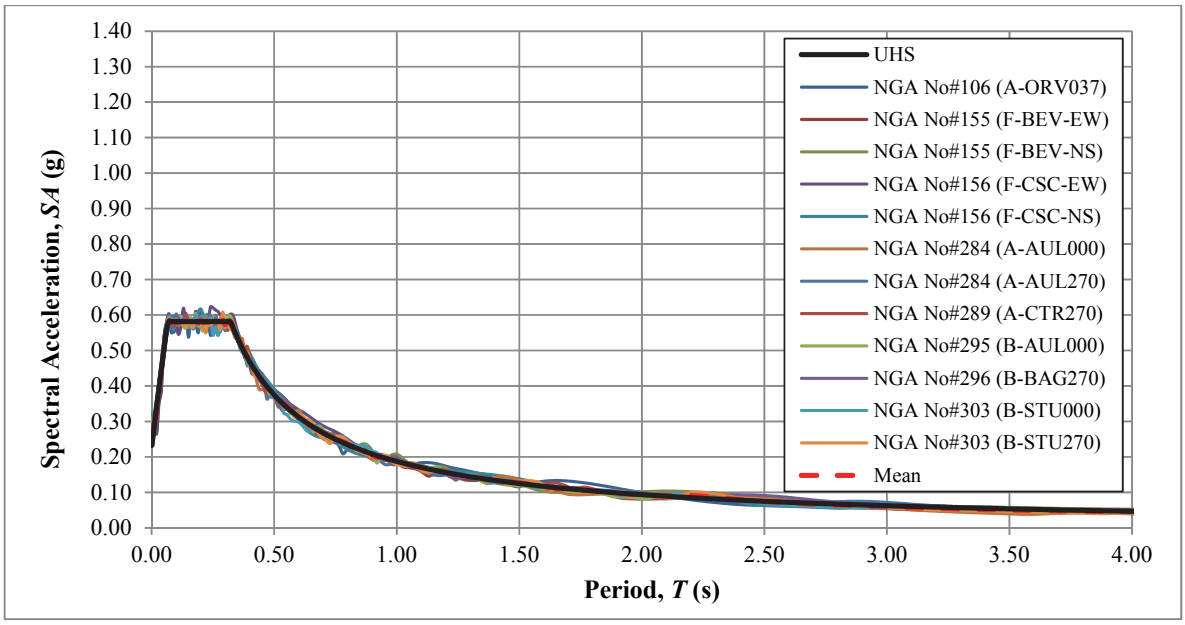

Figure 3.33. 5%-damped response spectra of earthquake record components presented in Figure 3.30 following nonstationary spectral matching as per PSHA-determined UHS

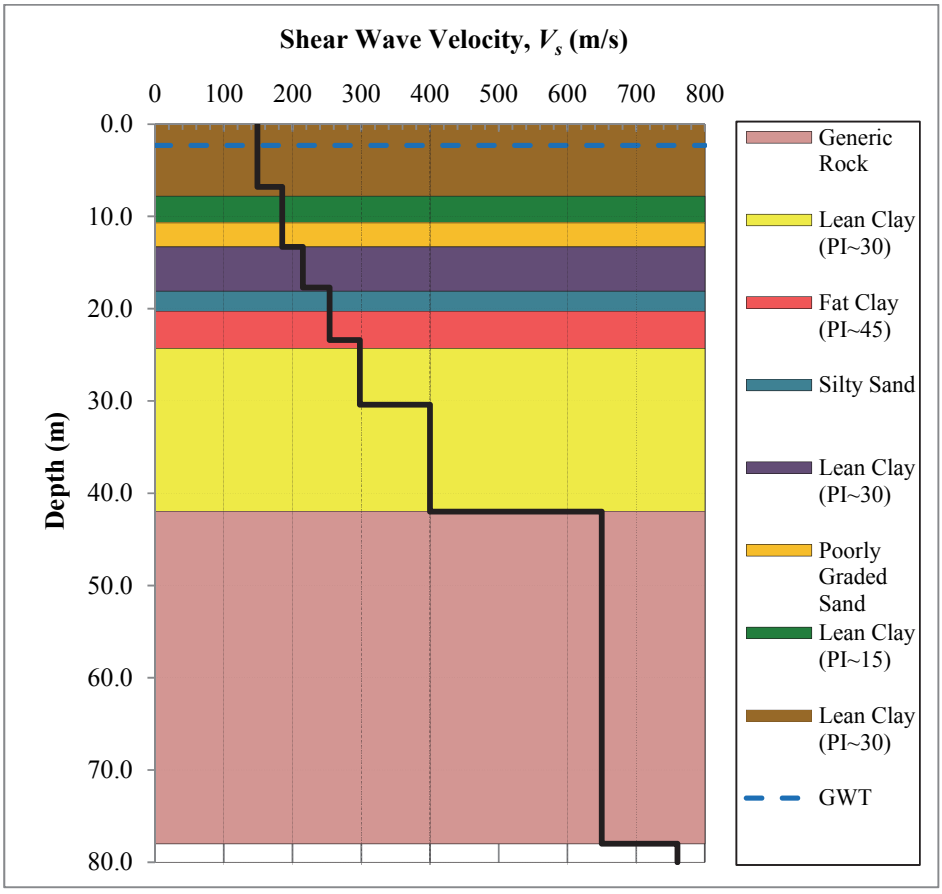

Figure 3.34. A visual depiction of soil layering and corresponding shear-wave velocity variation underneath the AI137 station; extending down to the reference site condition

During computation of seismic response for AI137 TSGMN station, the lean clay PI~15, lean clay PI~30, fat clay PI=45, silty sand, poorly graded sand and generic rock layers recognized via field observations are characterized using the dynamic soil properties suggested by Vucetic and Dobry [62], Darandeli [61], Seed et al. [64], and EPRI [42] respectively. Figure 3.35 conveys a visual illustration of the implemented modulus reduction/damping curves. For the executed analyses, the unit weight values of 17.30, 19.00, 20.50 and 22.00 kN/m^3 are used for clayey/silty soils, and generic rock material present between 42 to 60 m, 60 to 76 m and 76 to 78 m depths correspondingly.

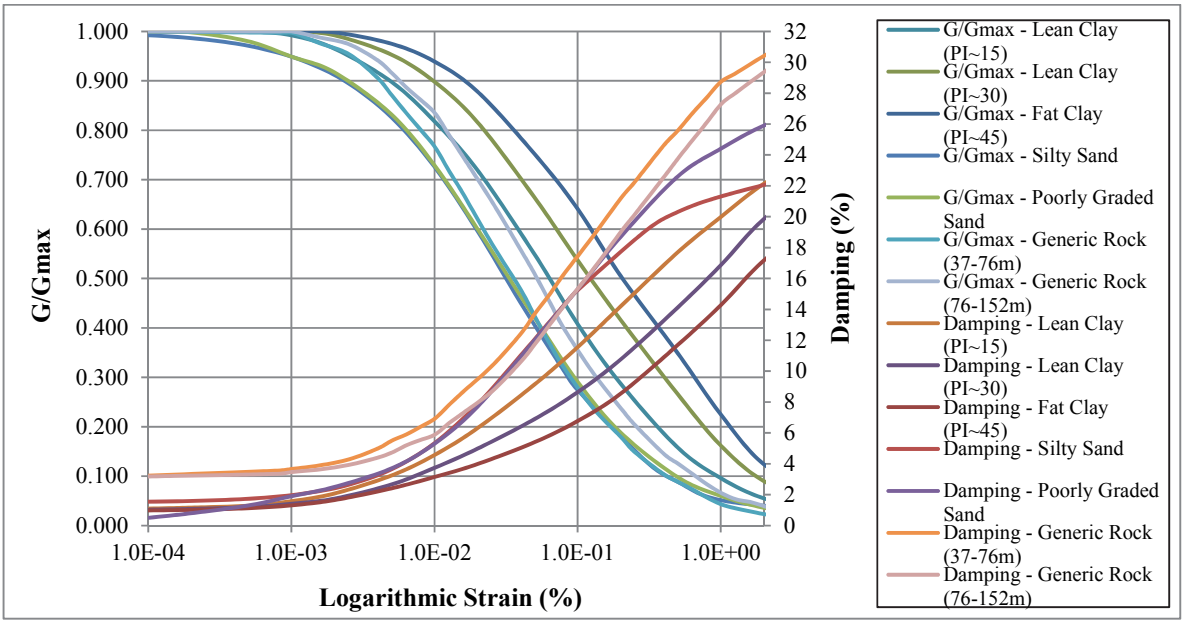

Figure 3.35. Modulus degradation and damping curves adopted for performing ground response analyses at the site of AI137 TSGMN station

Figures 3.36 and 3.37 demonstrate the results of seismic response analyses conducted for AI137 TSGMN station site. Both speaking in terms of amplitude and frequency-content characteristics, it is obvious that, each computation result falls short of approximating the spectral accelerations induced by recorded ground motions at the station site, with the best performing case (that is frequency-dependent calculation scheme utilizing PGA-normalized input motions) underestimating the observed peak response by 10.5%.

Contemplating the general trend of the outcomes perceived to this point, the observations for Dinar Station may appear to be quite vexing, but going back to the initial constraints set during construction of method pairs, it is rather straightforward to provide an account for the recognized anomaly. In the previous chapter, through explanation of the theory behind one-dimensional site effects calculation methods, the inadequacy of a one-dimensional code to model the spatial traits of a geometry, such as the basin that Dinar is situated on, is implicitly explicated. Therefore, founded on this knowledge, it is rather easy to understand that, it is plainly unlikely to catch the complex ground motion transmitting mechanisms of

shear-wave focusing and conversion of S-waves into surface waves resulting from the curvature of the basin edge/sedimentation interface using a 1-D code. In a time series, the evident effect of the former is recognized by an apparent rise in the spectral acceleration levels, while a clear manifestation of the latter is medium-to-large amplitude peaks within the long period range of a response spectrum. For subject records, the focusing effect of the basin edges (in Dinar) on the ground motion accelerograms recorded by AI137 was already suggested in the study by Bakir et al. [70]. Whereas, the presence of surface waves as consequence of wave transformation at edges is plainly palpable from the response spectra displayed for the observed time series. Thus, although from a PSHA-compatibility viewpoint the benchmark data recorded by Dinar Station is suited for the focused application, because of the major differences between the prevailing amplification mechanisms of Dinar case with the application-compatible situations, this case shall be omitted to properly decide the most effective ground response approximation procedure. Nevertheless, not excluding the results for this specific case is still well-reasoned, as such an instance provides a valuable case-study regarding the importance of imposing method constraints to attain valid and reliable results.

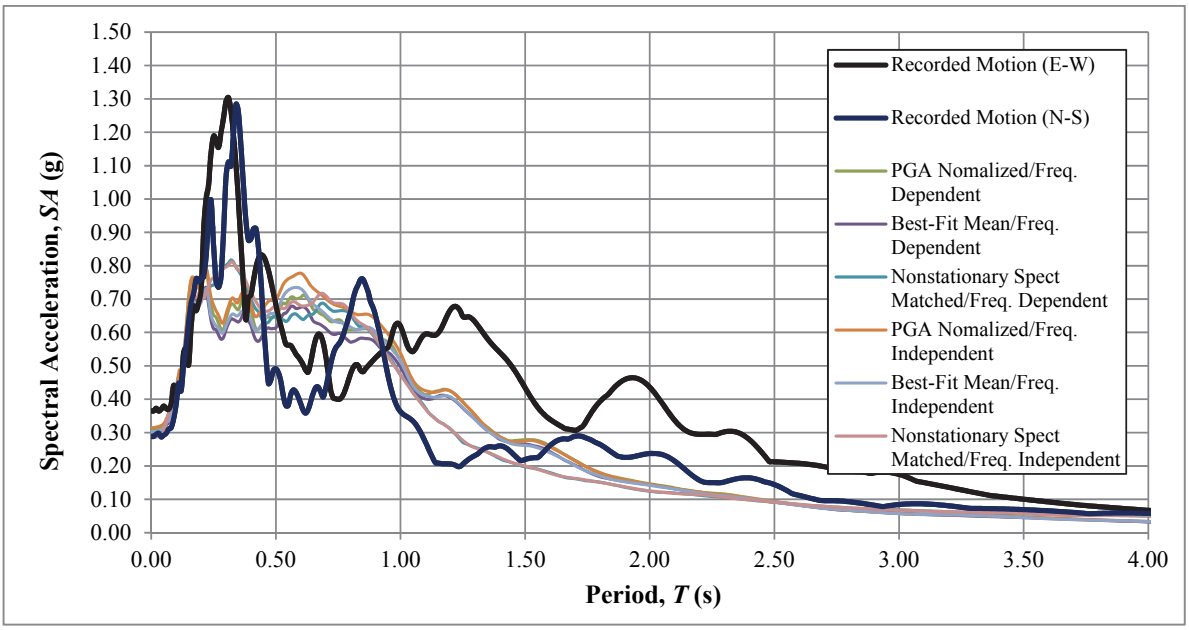

Figure 3.36. A comparison of 5%-damped mean response spectra, determined using each method pair, with the observed behavior at AI137 TSGMN station

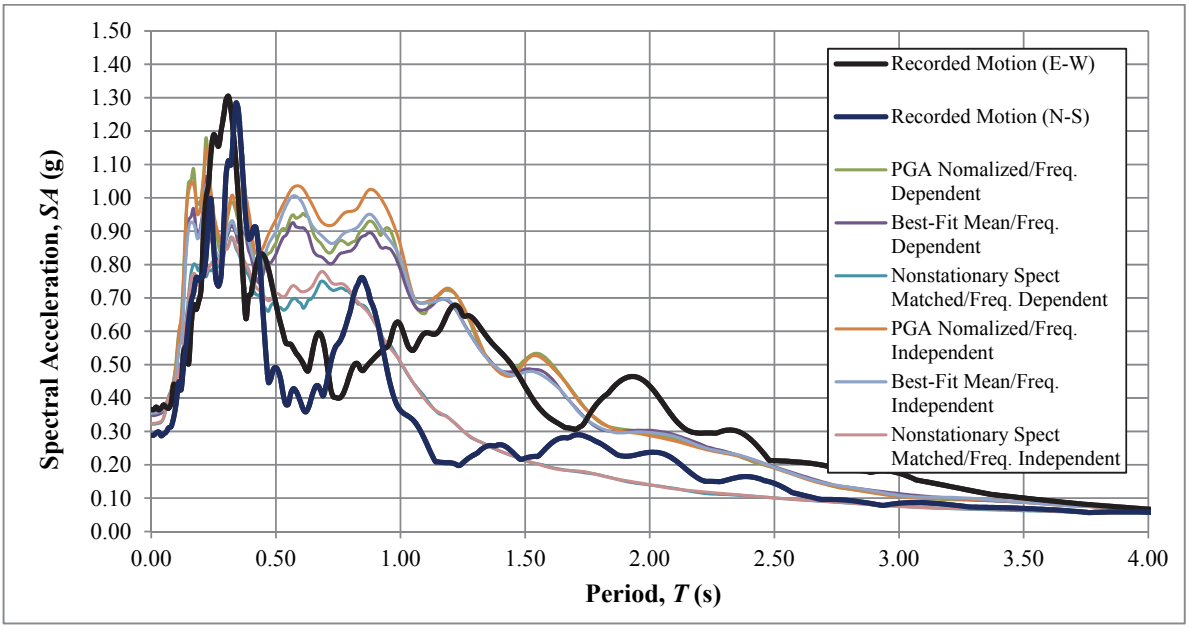

Figure 3.37. A comparison of 5%-damped mean + std. dev. response spectra, determined using each method pair, with the observed behavior at AI137 TSGMN station

3.1.5. Ceyhan Station (AI022)

Geology of the Cukurova Basin; home to the city of Ceyhan and, in the main, the province of Adana; is a complex assembly that is largely composed of a Quaternary alluvial dale that is capped with a thick layer of unconsolidated clay layer, residing on intercalated gravel, sand and silt deposits. For the most part, these formations are made up of poorly compacted deposits that range in gradation from uniform to well-graded. Field testing conducted by the General Directorate of State Hydraulic Works of Turkey (DSI) and the findings of several private companies point out that the thickness of unconsolidated material beneath the valley plains span from 100 to 300 m and progressively becomes thinner towards the northern boundary formed by Taurus Mountains [75].

The city of Ceyhan is situated in an active tectonics region that exhibits a seismic behavior that is set down to be controlled by a number of short-length strike-slip fault lines that are capable of generating earthquakes of M_w<7.0 [76]. In June 27, 1998, one of these

source mechanisms, Misis-Ceyhan left lateral strike slip fault, resulted in a significant event that caused 86 casualties, collapse of 12 reinforced concrete buildings, moderate damage in 120 structures and widespread geotechnical disturbance in the 100,000-population city alone [77]. TSGMN station AI022 in the central part of Ceyhan city, positioned at a R_{jb} distance of 40 km from the surface projection of earthquake, is one of the two nearby stations that recorded this event (See Figure 3.38 for East-West and North-South component recorded time histories).

Outcome of PSHA, and the successive deaggragation study conducted for the site of strong ground motion station indicates that the June 27, Ceyhan, Adana seismic occurrence, in fact, closely resembles the design earthquake for Ceyhan city. Therefore, by using the horizontal components of AI022 station records as reference data, and utilizing the detailed geophysical and geotechnical information published by TUBITAK, Ayhan and Bilgin [78], and Yetis [79]; it is possible to examine the effectiveness of each constructed method pair for estimating seismic ground response.

Based on the PSHA results for the subject site [17], estimated PGA, S_s and S_1 values at the locus site condition are 0.34g, 0.76g and 0.24g respectively. In order to perform ground response analyses, it is necessary to first establish a set of records, consisting of at least 10 strike-slip events that satisfy a M_w range from 5.9 to 6.5, a R_{jb} interval that spans between 10 to 50 km and a V_{s30} range of 660-830 m/s (Note that this boundary is, indeed, slightly different from the proposed extent; as it was adjusted to attain adequate amount of records); adaptable to the PSHA findings. Table 3.5 shows the list of 17 earthquake record components that are found to be compatible with the defined criteria, and, as a result, deemed suitable for the target application. Figures 3.39 to 3.42 exhibit the 5%-damped response spectra of unscaled record components, and the corresponding input time-histories prepared by PGA scaling, scaling to obtain the best-fit mean spectrum, and nonstationary spectral matching, respectively, along with the UHS calculated for the subject location, determined at the reference site condition as per seismic hazard results.

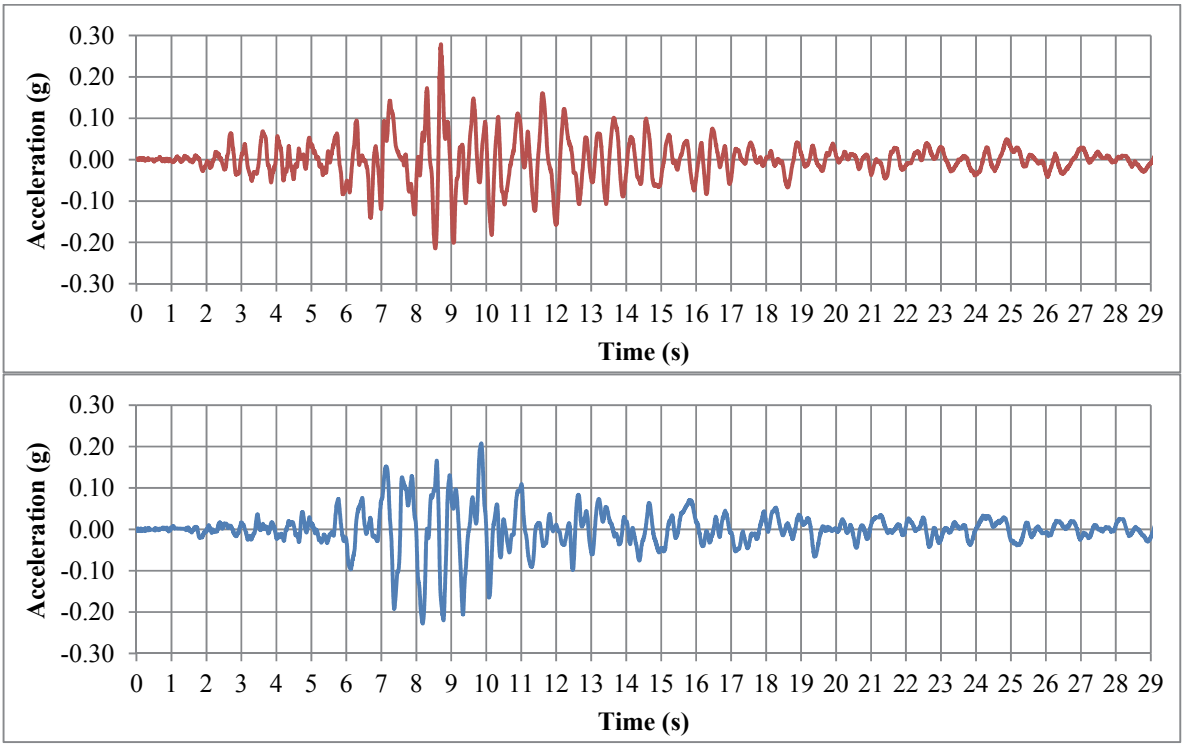

Figure 3.38. East-West (Top) and North-South (Bottom) components of the surface accelerations recorded by TSGMN Station AI022 during June 27, 1998; Ceyhan, Adana earthquake

According to the geological, geophysical and geotechnical knowledge brought together for the station site, the soil layering beneath AI022 is dominated by a clayey structure with thin bands of silts at the uppermost 33 m. A distinct feature of this geology is the increasing plasticity amongst the deepening clay layers, hence, the fluctuating hysteretic soil behavior. The results of SPT and MASW testing carried out in the periphery of the subject location points out that both the clayey formations and the silt inclusions observed at the site are composed of soft deposits with V_s values extending from 205 m/s on the soil surface to 418 m/s at the base of the finishing fat clay stratum. The following rock-like layering is identified to display substantially higher shear resistance with an ever-increasing trend towards the reference site condition, while the joining surface between the clay-dominated and rock-like strata being an exception (where, an abrupt reduction in the V_s profile from 418 m/s to 300 m/s

is recognized). Figure 3.43 summarizes the characteristics of the soil layering beneath the AI022 station down to the decided locus, in a graphical fashion.

Table 3.5. List of earthquake time histories selected for use with the ground response analyses performed for AI022 TSGMN station

Record No.	Event	M_w	R_{jb} (km)	V_{s30} (m/s)	Record File	PGA
1	Imperial Valley-06 (1979)	6.53	15.2	659.6	NGA No#164 (H-CPE147)	0.170
2	Chi-Chi-Taiwan-04 (1999)	6.53	15.2	659.6	NGA No#164 (H-CPE237)	0.151
3	Chi-Chi-Taiwan-04 (1999)	6.20	12.4	680.0	NGA No#2739 (CHY080-N)	0.120
4	Victoria-Mexico (1980)	6.33	13.8	659.6	NGA No#265 (CPE045)	0.621
5	Victoria-Mexico (1980)	6.33	13.8	659.6	NGA No#265 (CPE315)	0.587
6	Chi-Chi-Taiwan-04 (1999)	6.20	39.3	679.9	NGA No#2753 (CHY102-E)	0.059
7	Chi-Chi-Taiwan-04 (1999)	6.20	39.3	679.9	NGA No#2753 (CHY102-N)	0.053
8	Chi-Chi-Taiwan-04 (1999)	6.20	34.1	680.0	NGA No#2712 (CHY042-N)	0.083
9	Chi-Chi-Taiwan-04 (1999)	6.20	27.2	680.0	NGA No#2873 (TCU089-E)	0.031
10	Chi-Chi-Taiwan-04 (1999)	6.20	37.5	680.0	NGA No#2935 (TTN051-E)	0.065
11	Chi-Chi-Taiwan-04 (1999)	6.20	37.5	680.0	NGA No#2935 (TTN051-N)	0.076
12	Morgan Hill (1984)	6.19	45.5	714.0	NGA No#476 (LOB050)	0.039
13	Morgan Hill (1984)	6.19	45.5	714.0	NGA No#476 (LOB320)	0.076
14	Chi-Chi- Taiwan-04 (1999)	6.20	39.7	680.0	NGA No#2820 (KAU050-E)	0.069
15	Chi-Chi- Taiwan-04 (1999)	6.20	39.7	680.0	NGA No#2820 (KAU050-N)	0.066
16	Big Bear-01 (1992)	6.46	[33.8]	684.9	NGA No#934 (SVP090)	0.059
17	Big Bear-01 (1992)	6.46	[33.8]	684.9	NGA No#934 (SVP360)	0.070

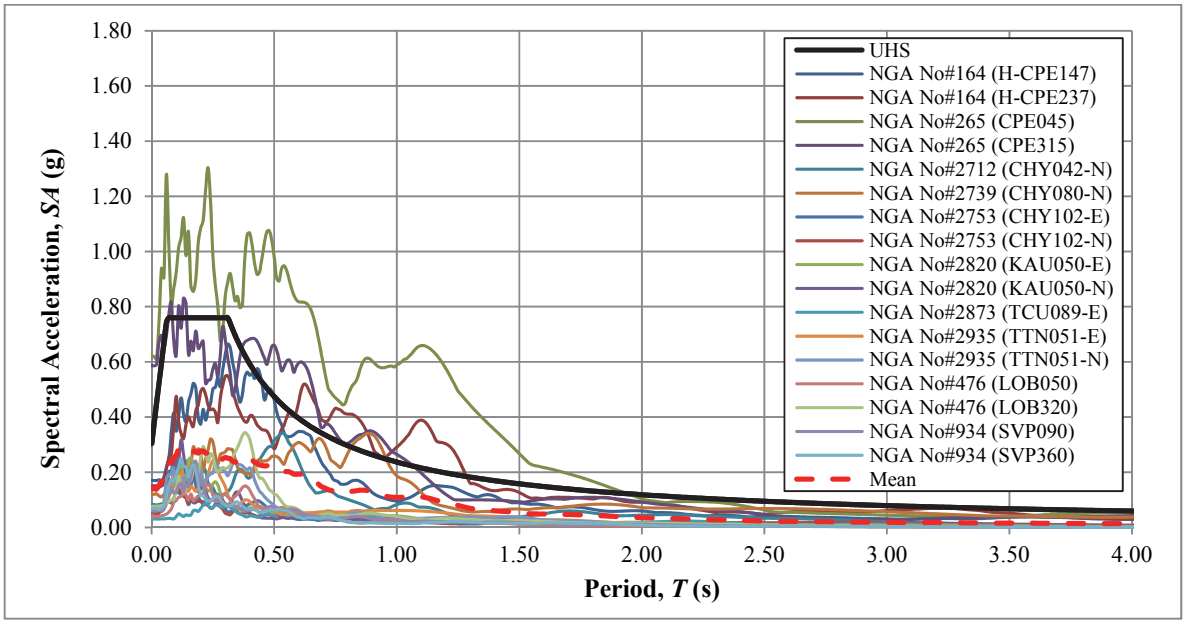

Figure 3.39. 5%-damped response spectra of earthquake record components selected for carrying out the site effects calculations for AI022 TSGMN station

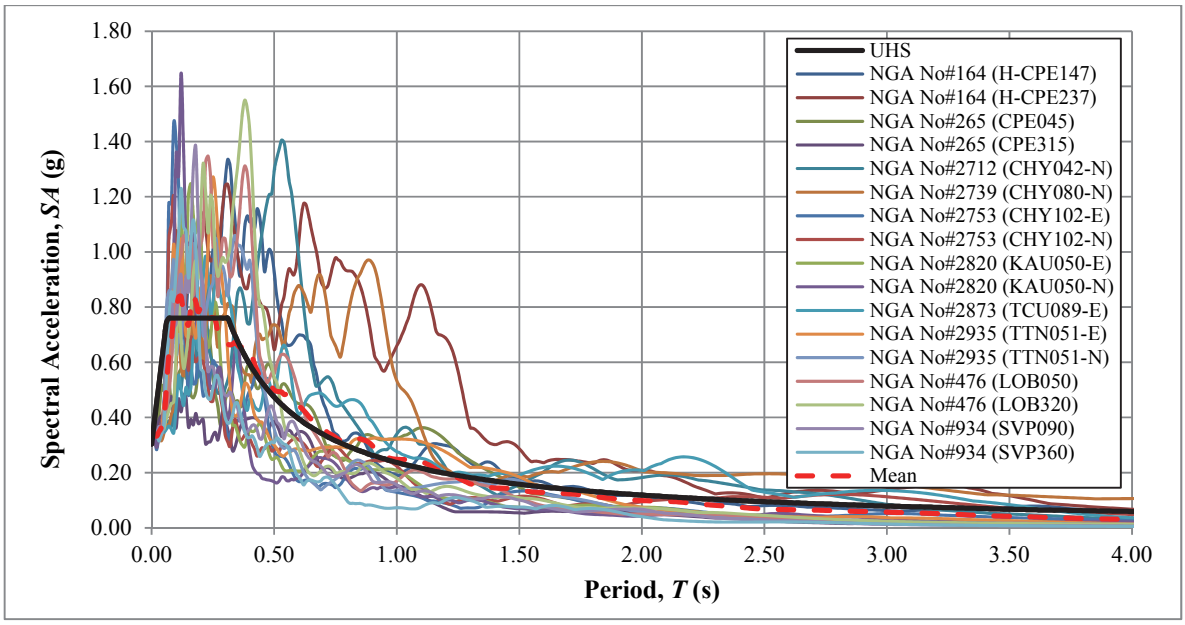

Figure 3.40. 5%-damped response spectra of earthquake record components presented in Figure 3.39 after normalization of each time series to the hazard PGA level of 0.34g

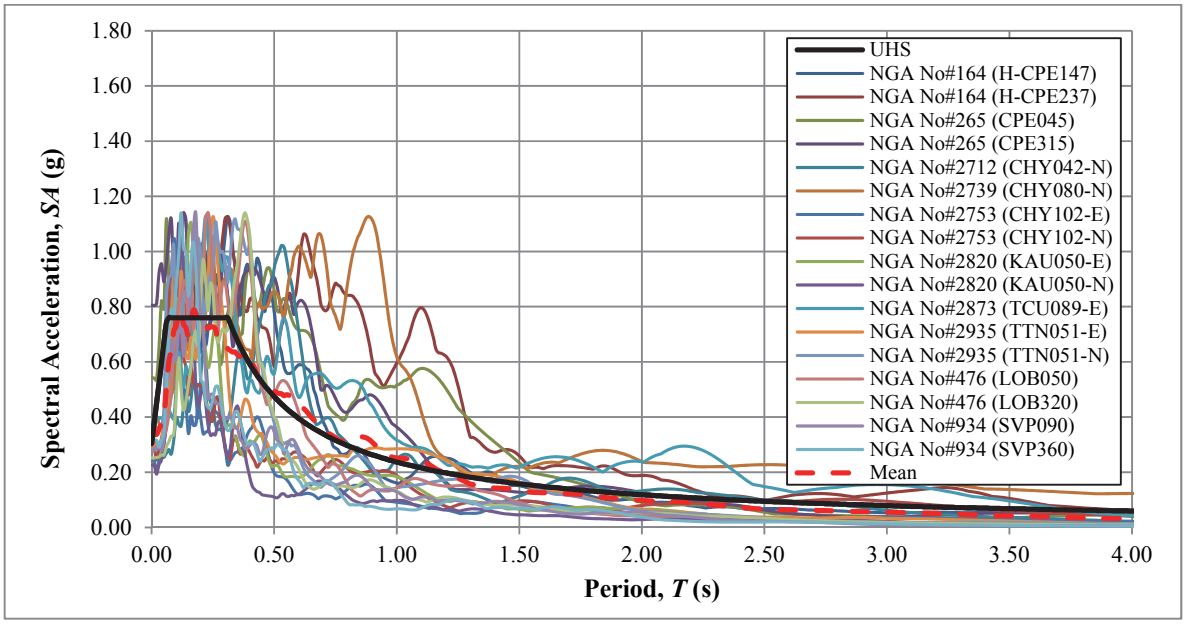

Figure 3.41. 5%-damped response spectra of earthquake record components shown in Figure 3.39 after scaling to find the mean spectrum that is best-fit with PSHA-decided UHS

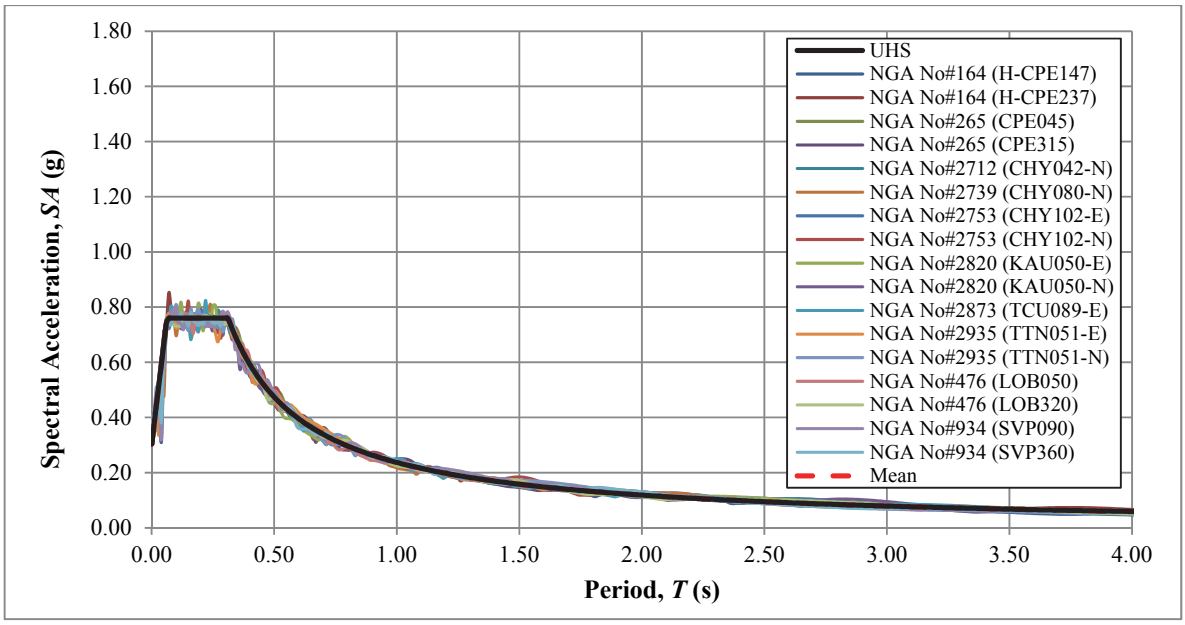

Figure 3.42. 5%-damped response spectra of earthquake record components presented in Figure 3.39 following nonstationary spectral matching as per PSHA-determined UHS

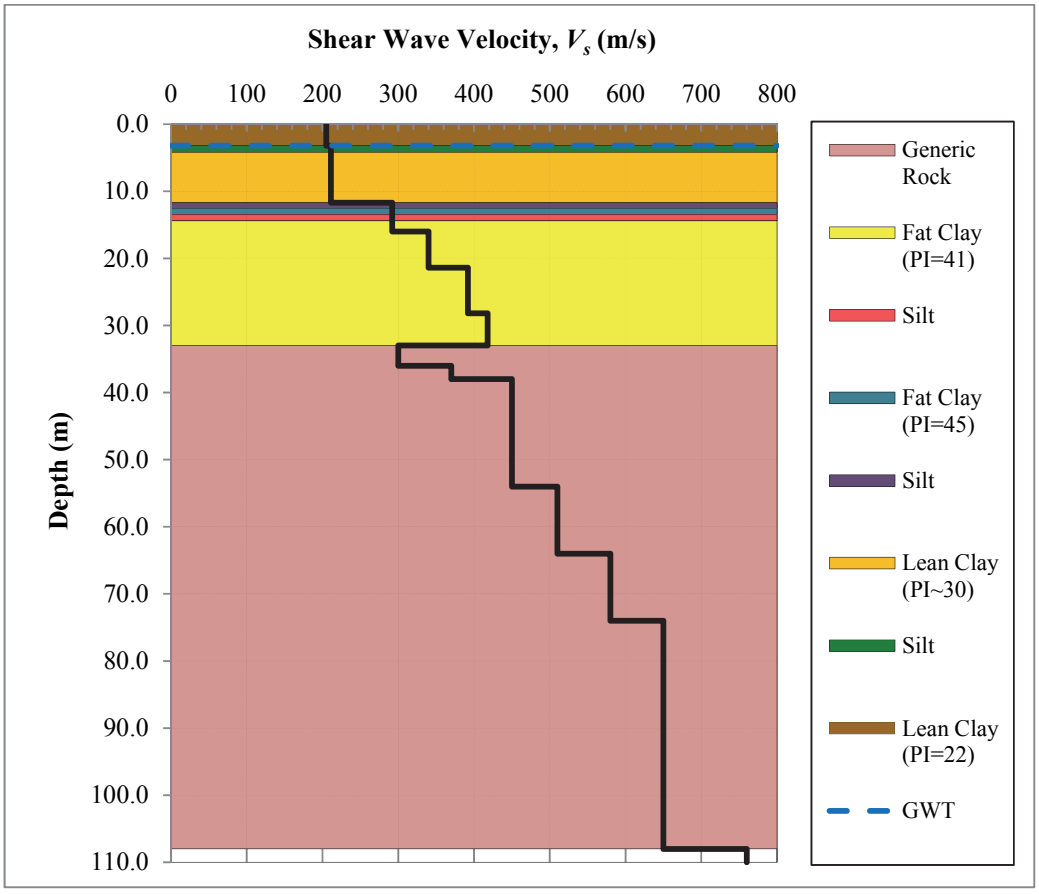

Figure 3.43. A visual depiction of soil layering and corresponding shear-wave velocity variation underneath the AI022 station; extending down to the reference site condition

In order to perform the seismic response calculations for AI022 TSGMN station, herein, the lean clay PI=22, lean clay PI~30, fat clay PI=45, silt and generic rock stratifications identified in field testing results are represented using the dynamic soil properties suggested by Vucetic and Dobry [62], Darandeli [61] and EPRI [42] respectively. Figure 3.44 provides a graphical depiction of the adopted modulus reduction/damping curves. In the performed analyses, the unit weight values of 17.30, 19.00, 20.50 and 22.00 kN/m^3 are used for clayey/silty soils, and generic rock material present between 33 to 36 m, 36 to 38 m and 38 to 108 m depths correspondingly.

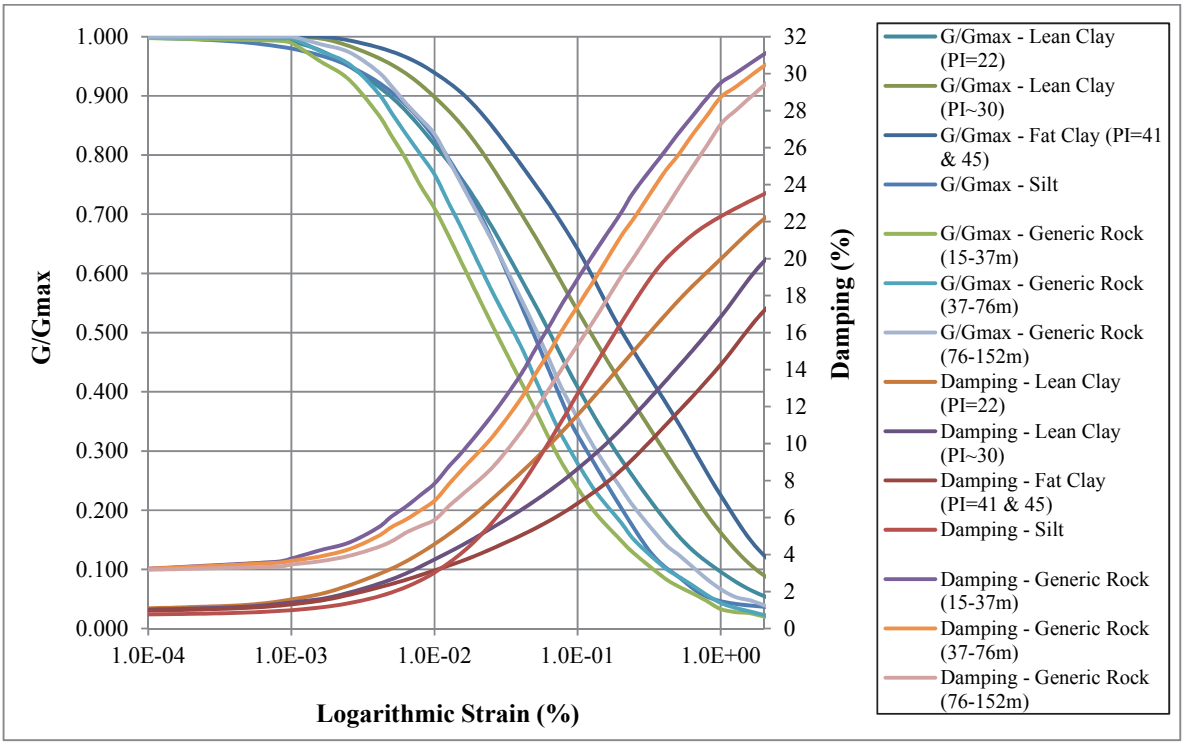

Figure 3.44. Modulus degradation and damping curves adopted for performing ground response analyses at the site of AI022 TSGMN station

Figures 3.45 and 3.46 display the ground response analysis results for AI022 TSGMN station site, obtained using each method pair. In all cases, fundamental period of the response is underestimated. Seismic response analysis indicate a predominat period value of rougly 0.29s, whereas the observed site period ranges between 0.50-0.65s. The perceived discrepancy, is most probably a consequence of the lack of long-period amplitude components in the dataset, and the unincorporated minute basin/edge effects. However, speaking in terms of the peak amplitude responses, the frequency independent calculation scheme using input motions prepared through nonstationary spectral matching technique provides a fairly comparable response with the observed behavior (i.e. a peak response ratio of approximately 1.186).

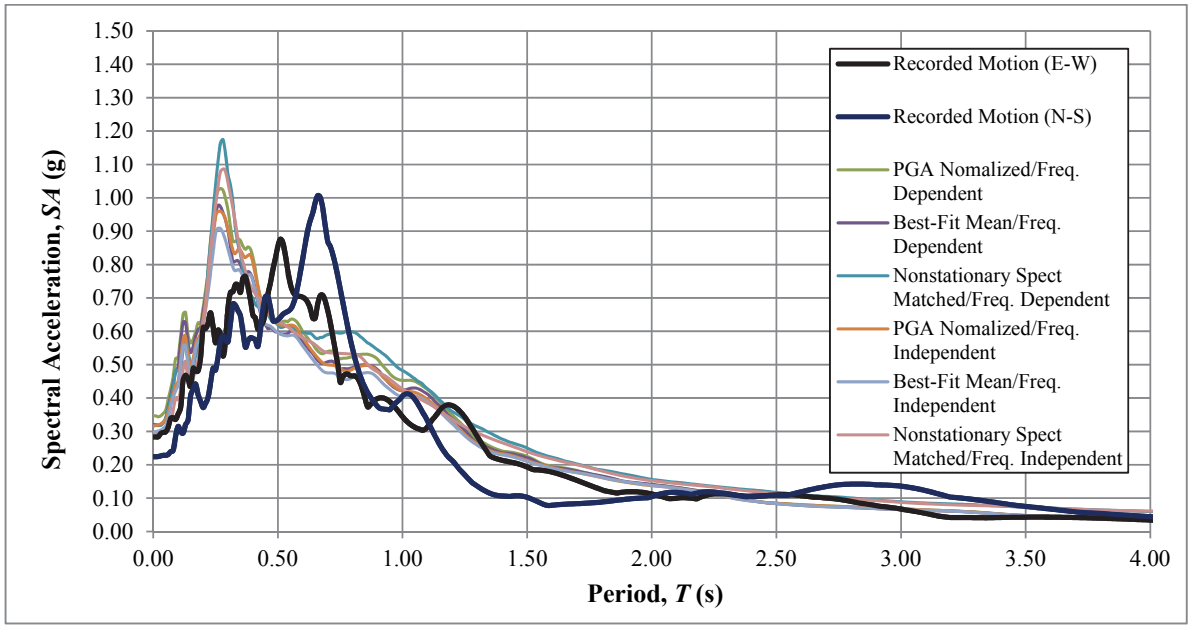

Figure 3.45. A comparison of 5%-damped mean response spectra, determined using each method pair, with the observed behavior at AI022 TSGMN station

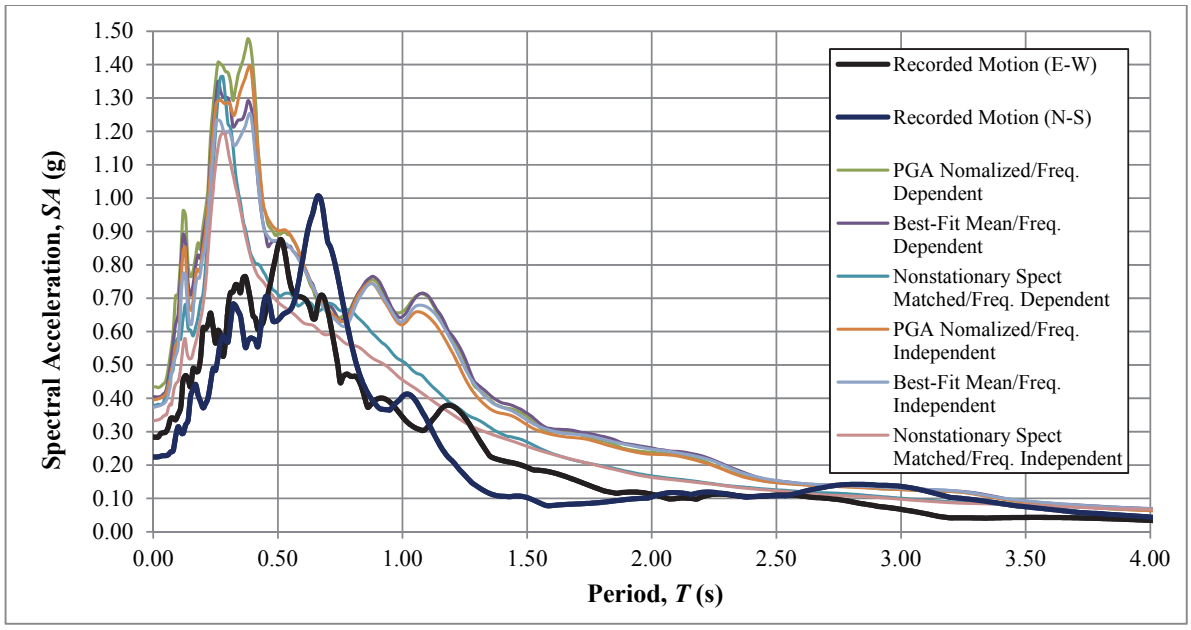

Figure 3.46. A comparison of 5%-damped mean + std. dev. response spectra, determined using each method pair, with the observed behavior at AI022 TSGMN station

3.1.6. Mersin Station (AI019)

June 27, 1998 Ceyhan, Adana earthquake resulted in considerable ground tremor in the Mersin city as well. However, in addition to the added travelling path, as a consequence of the radically different site condition in Mersin city, the same seismic event entailed a distinctive set of reference data that has significant potential use for earthquake engineering applications.

The sedimentation beneath Mersin city is generalized by a clay-layer-topped coarse-grained deposit that is founded on stiff rock formations (for the areas along the shoreline) located at a depth range of 30-40 m. Field testing conducted by TUBITAK indicates that the perceived clayey material is made up of poorly compacted deposits. However, once the strata consisting of coarse-grained settling are reached the compaction traits are detected to improve.

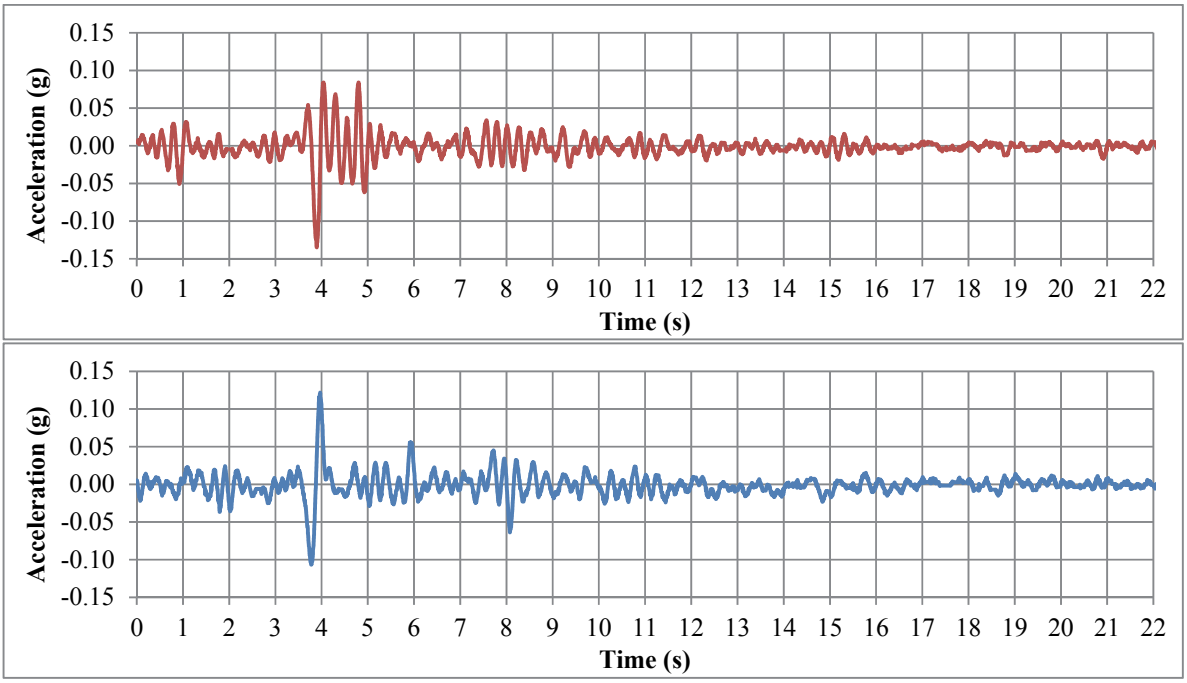

Figure 3.47. East-West (Top) and North-South (Bottom) components of the surface accelerations recorded by TSGMN Station AI019 during June 27, 1998; Ceyhan, Adana earthquake

According to the PSHA results for the subject site, acceleration time histories recorded by TSGMN station AI019, positioned in the central part of the Mersin city; off a R_{jb} distance of 57.54 km from the earthquake source mechanism, (See Figure 3.47 for East-West and North-South component recorded time histories) are nearly compatible with the design earthquake event for Mersin city. Hence, through use of the horizontal components of AI019 station records as benchmark data, and utilizing the detailed geophysical and geotechnical information published by TUBITAK, one can investigate the suitability of each method pair meant for calculating seismic ground response.

Table 3.6. List of earthquake time histories selected for use with the ground response analyses performed for AI019 TSGMN station

Record No.	Event	M_w	R_{jb} (km)	V_{s30} (m/s)	Record File	PGA
1	Imperial Valley-06 (1979)	6.53	15.2	659.6	NGA No#164 (H-CPE147)	0.170
2	Chi-Chi-Taiwan-04 (1999)	6.53	15.2	659.6	NGA No#164 (H-CPE237)	0.151
3	Chi-Chi-Taiwan-04 (1999)	6.20	12.4	680.0	NGA No#2739 (CHY080-N)	0.120
4	Victoria-Mexico (1980)	6.33	13.8	659.6	NGA No#265 (CPE045)	0.621
5	Victoria-Mexico (1980)	6.33	13.8	659.6	NGA No#265 (CPE315)	0.587
6	Chi-Chi-Taiwan-04 (1999)	6.20	39.3	679.9	NGA No#2753 (CHY102-E)	0.059
7	Chi-Chi-Taiwan-04 (1999)	6.20	39.3	679.9	NGA No#2753 (CHY102-N)	0.053
8	Chi-Chi-Taiwan-04 (1999)	6.20	34.1	680.0	NGA No#2712 (CHY042-N)	0.083
9	Chi-Chi-Taiwan-04 (1999)	6.20	27.2	680.0	NGA No#2873 (TCU089-E)	0.031
10	Chi-Chi-Taiwan-04 (1999)	6.20	37.5	680.0	NGA No#2935 (TTN051-E)	0.065
11	Chi-Chi-Taiwan-04 (1999)	6.20	37.5	680.0	NGA No#2935 (TTN051-N)	0.076
12	Morgan Hill (1984)	6.19	45.5	714.0	NGA No#476 (LOB050)	0.039
13	Morgan Hill (1984)	6.19	45.5	714.0	NGA No#476 (LOB320)	0.076
14	Chi-Chi- Taiwan-04 (1999)	6.20	39.7	680.0	NGA No#2820 (KAU050-E)	0.069
15	Chi-Chi- Taiwan-04 (1999)	6.20	39.7	680.0	NGA No#2820 (KAU050-N)	0.066
16	Big Bear-01 (1992)	6.46	[33.8]	684.9	NGA No#934 (SVP090)	0.059
17	Big Bear-01 (1992)	6.46	[33.8]	684.9	NGA No#934 (SVP360)	0.070

Assessment of the probabilistic seismic hazard for the interested site [80] estimated the PGA, S_s and S_1 values at the reference site condition as 0.10g, 0.22g and 0.07g respectively. So to conduct ground response analyses, it is vital to begin with developing a set of records, consisting of at least 10 strike-slip events that satisfy a M_w range from 5.9 to 6.5, a R_{jb} interval that spans between 10 to 50 km, and a V_{s30} range of 660-830 m/s (Note that this borderline is, in fact, somewhat different from the suggested range; as it was attuned to achieve acceptable quantity of records); compliant with the PSHA findings. Table 3.6 shows the list of 17 earthquake time histories that are found to be well-suited with the defined criteria, and, thus, judged apt for the subject application. Figures 3.48 to 3.51 show the 5%-damped response spectra of unscaled record components, and the conforming input time-histories prepared by PGA scaling, scaling to get the best-fit mean spectrum, and nonstationary spectral matching, respectively, alongside the UHS determined for the interested location, computed at the reference site condition, according to seismic hazard results.

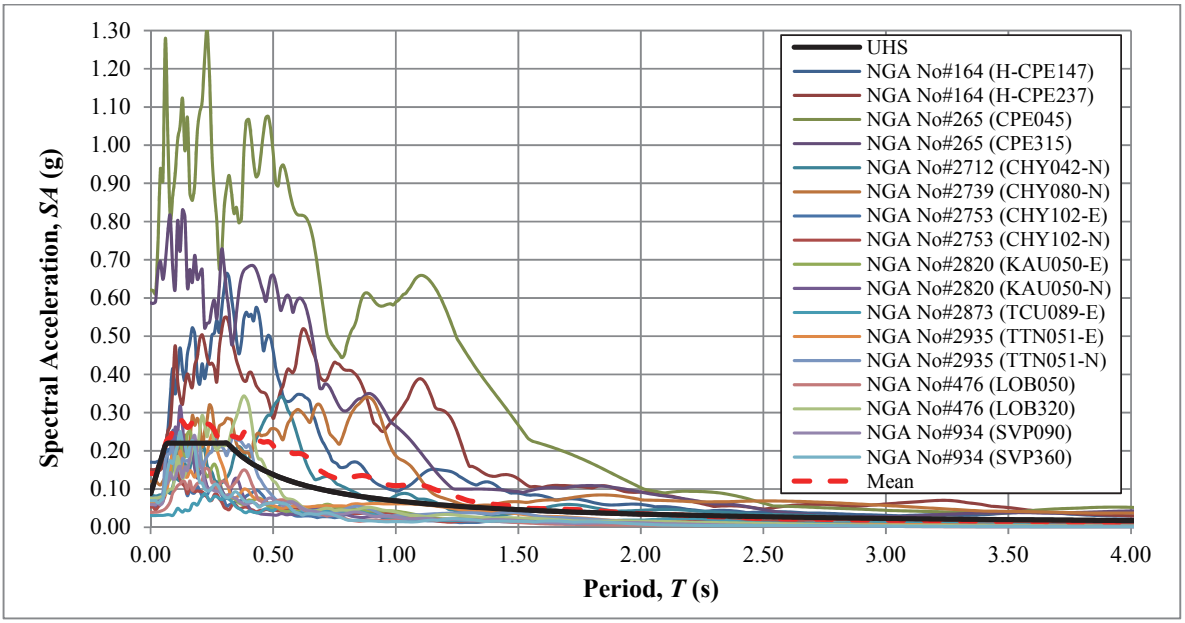

Figure 3.48. 5%-damped response spectra of earthquake record components selected for carrying out the site effects calculations for AI019 TSGMN station

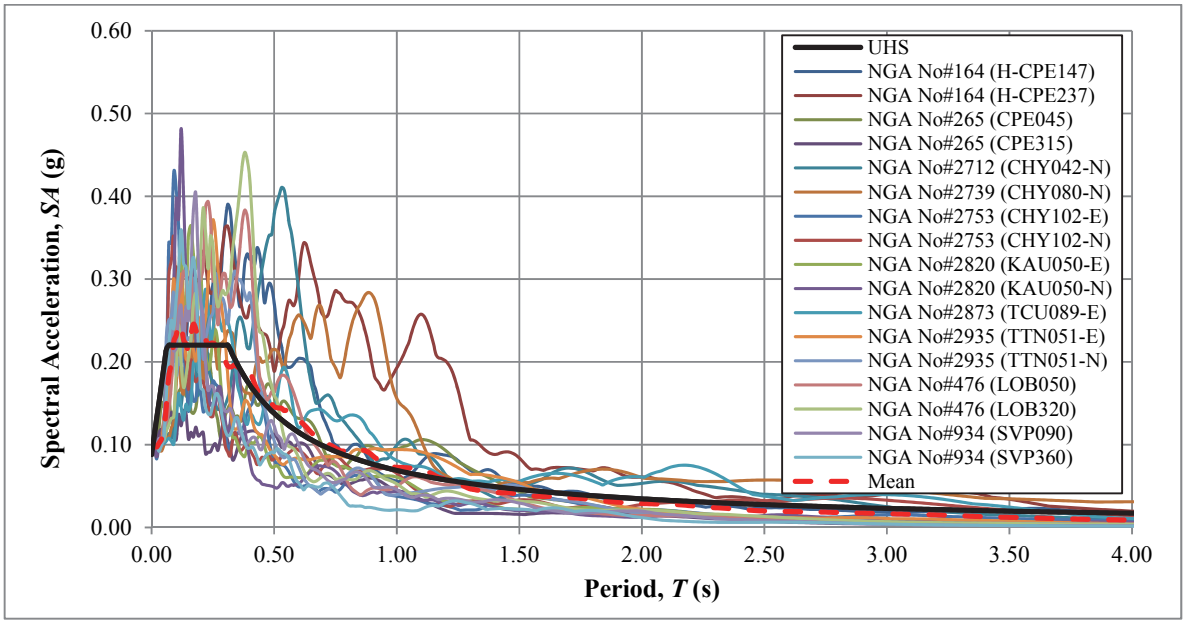

Figure 3.49. 5%-damped response spectra of earthquake record components presented in Figure 3.48 after normalization of each time series to the hazard PGA level of 0.10g

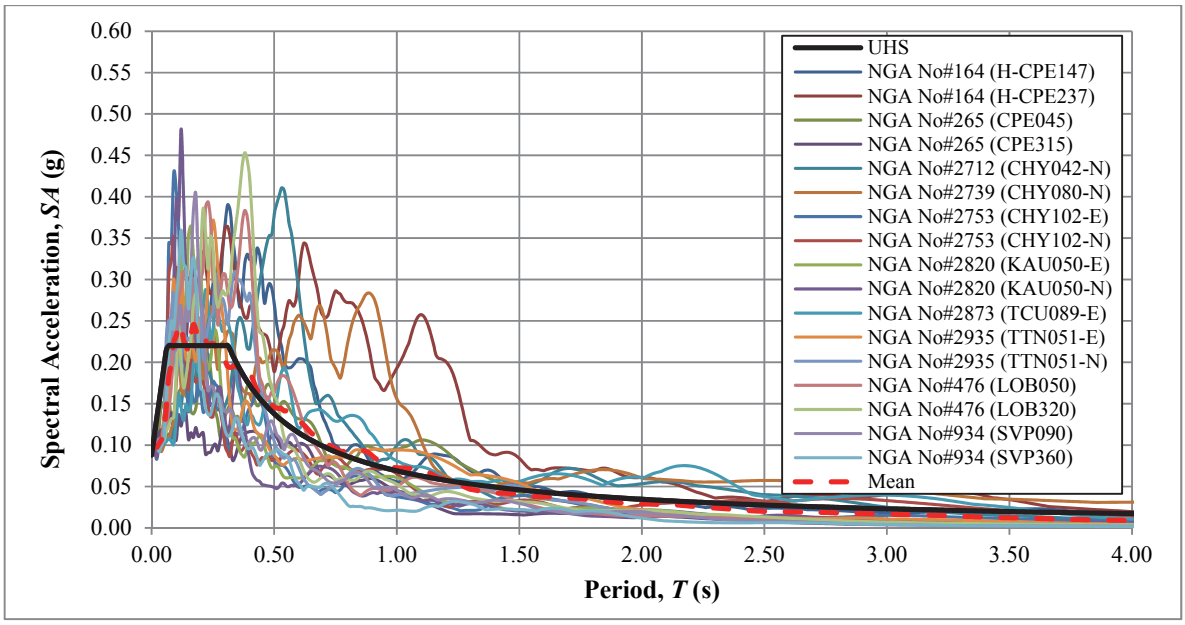

Figure 3.50. 5%-damped response spectra of earthquake record components shown in Figure 3.48 after scaling to find the mean spectrum that is best-fit with PSHA-decided UHS

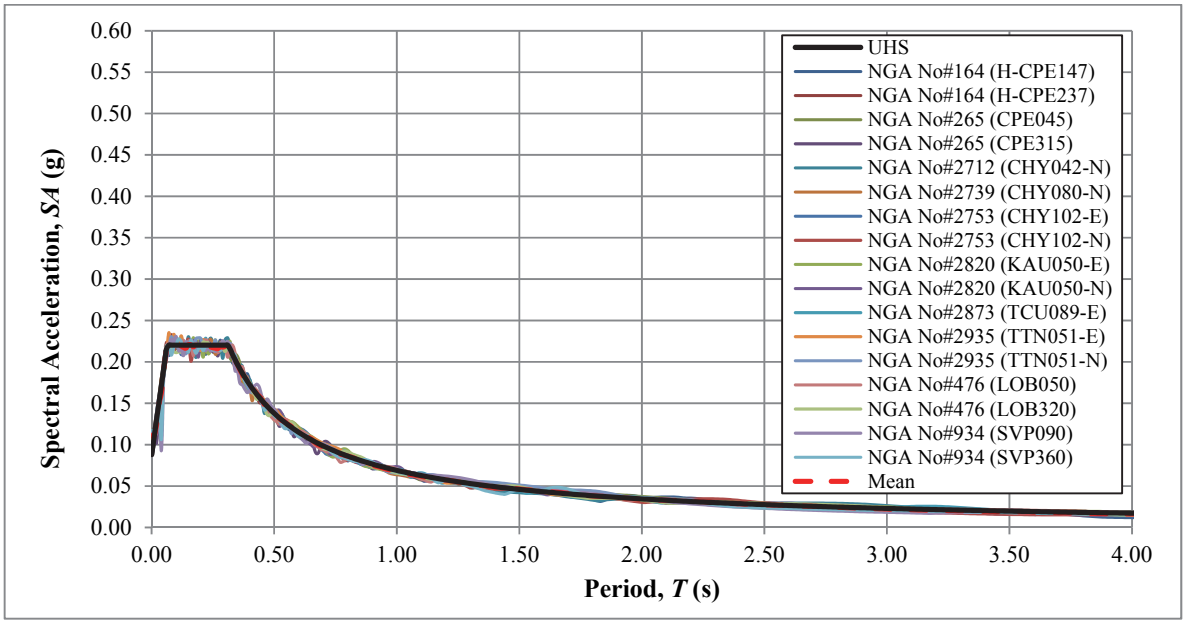

Figure 3.51. 5%-damped response spectra of earthquake record components presented in Figure 3.48 following nonstationary spectral matching as per PSHA-determined UHS

Based on the geological, geophysical and geotechnical knowledge compiled for the station site, the stratification below AI019 is characterized by a clayey structure with thin layers of clay inclusions underlain by a sand/gravel settling at the topmost 22 m. The plasticity amid clay layers are observed to be fairly consistent; merely the type of coarse-grained inclusions changing. SPT and MASW results reported for the station site indicate that except a soft layer lean clay located between 1.8 to 4 m (V_s=149 m/s), both the clayey formations and the coarse-grained deposits identified at the site are comprised of hard/stiff deposits with V_s values extending from 301 m/s on the soil surface to 583 m/s at the base of the terminating poorly-graded sand layer. The following rock-like layering is identified to display considerably higher shear resistance towards the locus; being 583 m/s at the sand/rock joint and reaching 691 m/s before the reference site condition is detected. Figure 3.52 visualizes the properties of soil layering beneath the AI019 station, down to the decided locus, discussed above.

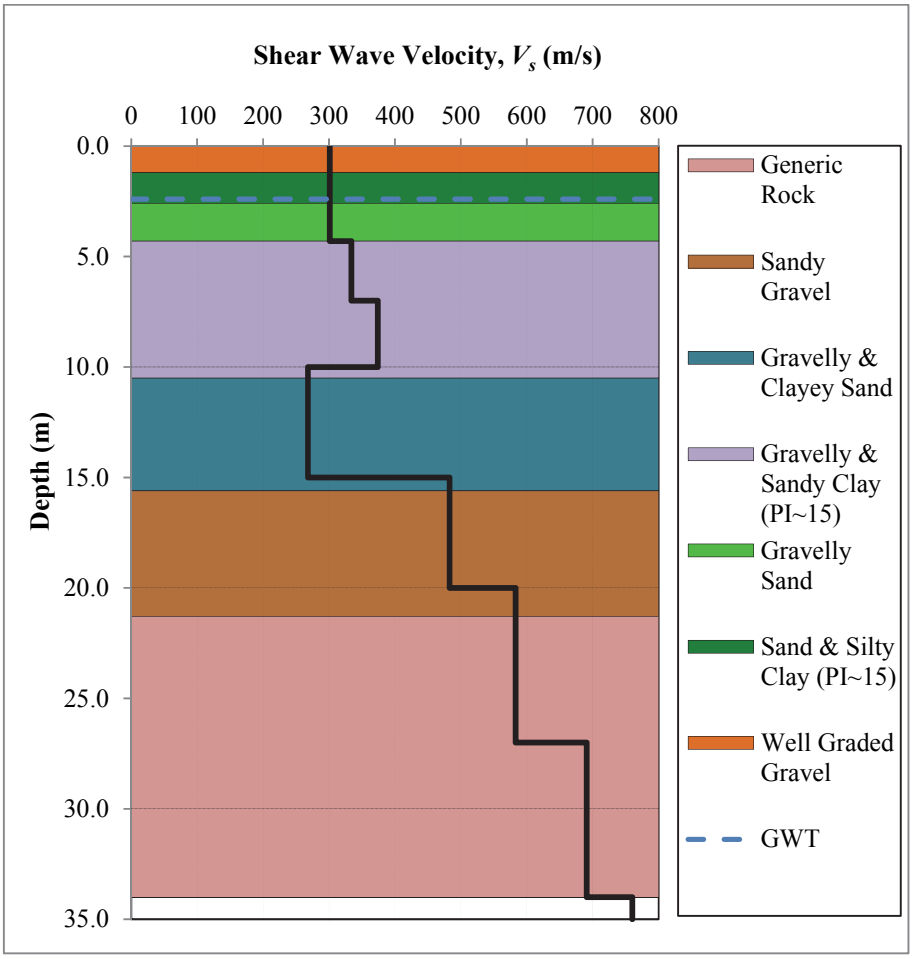

Figure 3.52. A visual depiction of soil layering and corresponding shear-wave velocity variation underneath the AI019 station; extending down to the reference site condition

Herein, so to calculate the seismic response for AI019 TSGMN station, the well-graded gravel, gravelly sand and sandy gravel; sandy & silty clay (PI~15) and gravelly & sandy clay (PI~15); gravelly & clayey sand; and generic rock stratifications identified in field testing results are modeled using the dynamic soil properties suggested by Seed et al. [64], Vucetic and Dobry [62], Darandeli [61] and EPRI [42] respectively. Figure 3.53 delivers a graphical illustration of the employed modulus reduction/damping curves. In the performed analyses, the unit weight values of 17.30, 19.00 and 20.50 are used for clayey/silty soils, gravelly soils and generic rock material present between 22 to 34 m correspondingly.

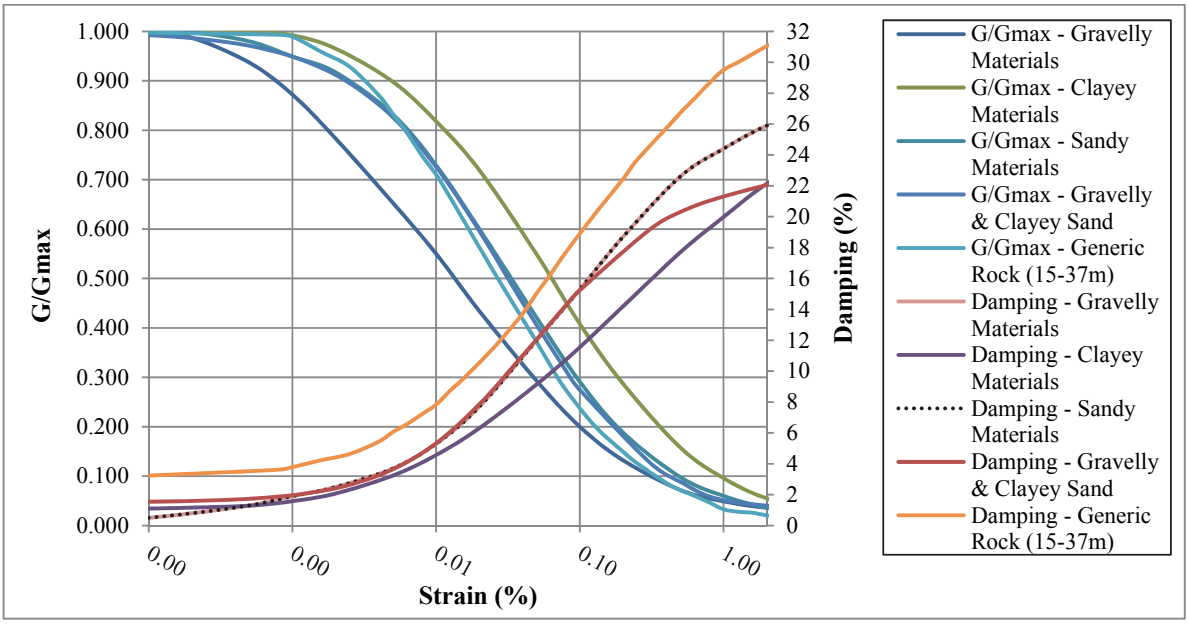

Figure 3.53. Modulus degradation and damping curves adopted for performing ground response analyses at the site of AI019 TSGMN station

Figures 3.54 and 3.55 show the results of the seismic response analyses conducted for AI022 TSGMN station site via each method pair. For all situations, obtained results approximate the fundamental period of the response in a fairly truthful manner. In case of the outcome computed through input motions generated by nonstationary matching, the amplitude traits of the recorded response spectra are very well simulated, begetting a peak response ratio of about 1.141. Merely, the spectral accelerations visible between periods of 0.5s to 1.0s are slightly underestimated by the produced peaked spectrum produced. However, as mentioned in previous sections, such an underestimation is not very significant as akin deviations are easily accounted for, through a right-tailored spectrum construction technique. As for the results obtained using remaining pairs, one can easily note that, at this instance, using such methodologies, frequency-content of the observed components are signficantly better protrayed (Even if there is an unrealistic peak visible at the period of 0.07s). Nevertheless, the vast overestimation of the actual amplitude features by these method pairs, largely impede that vital strong point; rendering the frequency independent calculation scheme using input motions established by nonstationary spectral matching technique as the best-performing pair.

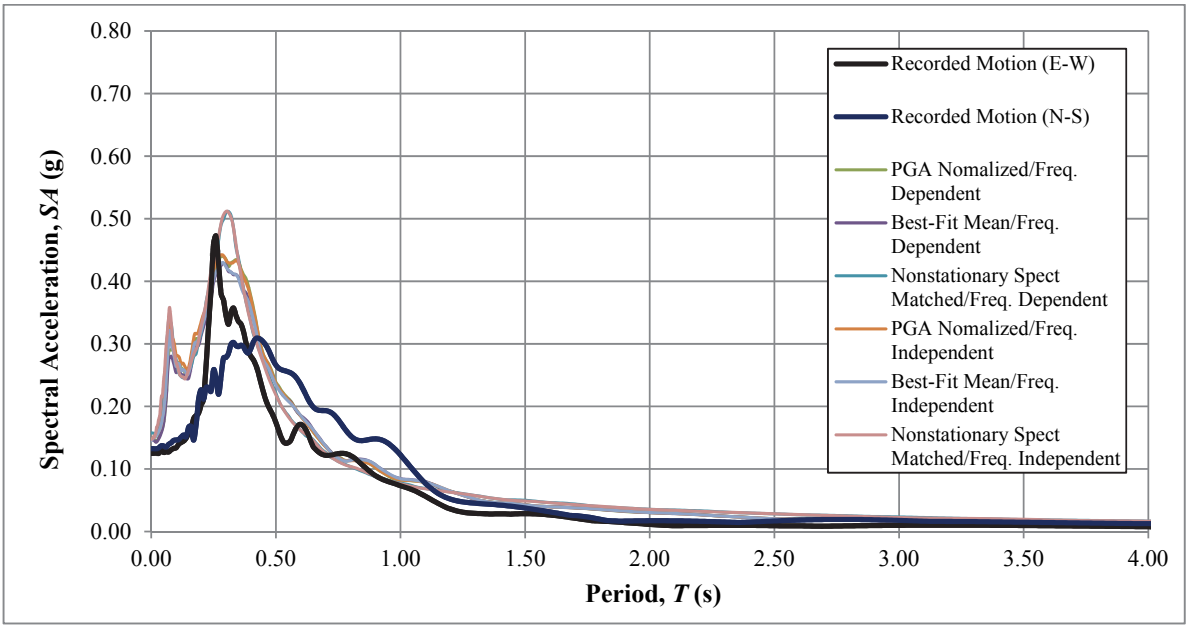

Figure 3.54. A comparison of 5%-damped mean response spectra, determined using each method pair, with the observed behavior at AI019 TSGMN station

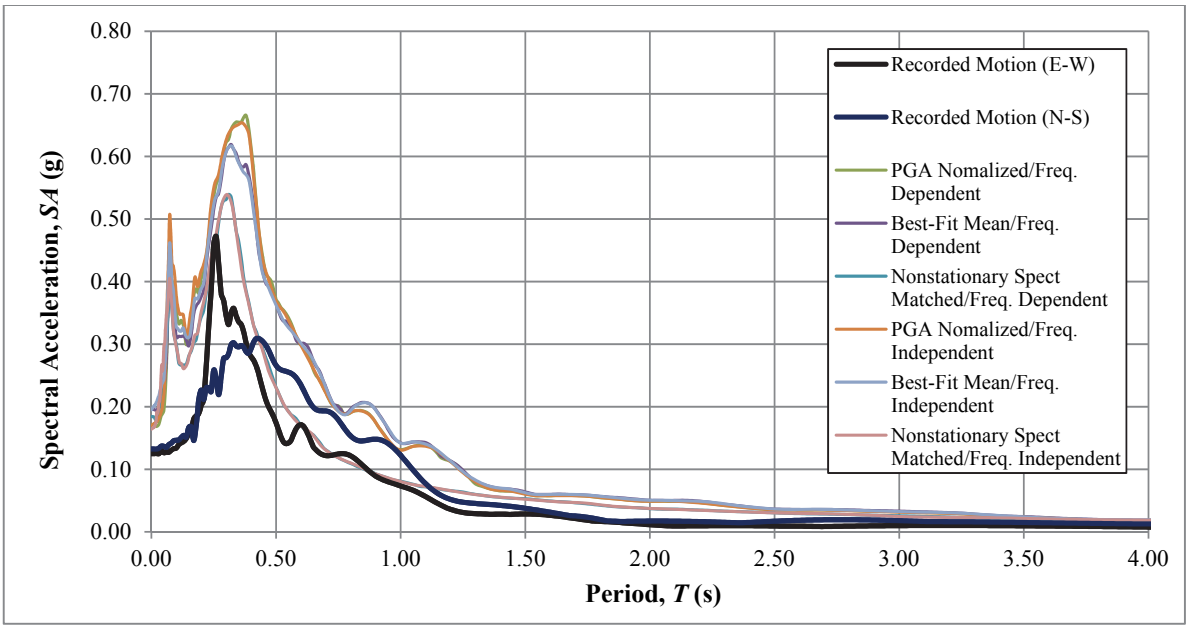

Figure 3.55. A comparison of 5%-damped mean + std. dev. response spectra, determined using each method pair, with the observed behavior at AI019 TSGMN station

3.1.7. Adapazari Station (AI005)

Adapazari, the most populous, and both economically and industrially the most vital city within the Sakarya province, is situated over a neoteric Holocene alluvial deposition that is formed by the fluvial progressions of Sakarya and Cark rivers [81]. The general geotechnical composition of the city is characterized by loose, 4 to 5 thick silts and silty sands that are underlain by silty sand strata. Even though, at various sites, a dense sand layer of thickness 4 to 5 m is observed to exist between topmost silty sand stratum and the deeper clayey sedimentation, in certain parts of the city, clayey soils supplant the surficial silty sand layering [82] [83]. Field testing conducted by the General Directorate of State Hydraulic Works of Turkey (DSI) and the findings of several private companies indicate that the thickness of Adapazari Basin changes between from 200 to 250 m roughly underneath the city center and the alluvial depth, thus the basin thickness, gradually decreases towards the mountain range in the south of the city plains.

The tectonic setting of Adapazari is shaped by, one of the most studied fault systems in Turkey, North Anatolian fault (NAF). Seventh in a progression of westward-migrating seismic occurrences along NAF, in August 17, 1999, a northern segment of this significant faulting near the city of Izmit, resulted in a M_w=7.6, pure right-lateral strike-slip earthquake. According to Bakir et al. [84], the destructive event caused 17,479 loss of life, 43,953 injuries, and collapse (or eventual demolishing) of 20,000 buildings in the cities located in close proximity of the faulting. TSGMN station AI005 enclosed inside a prefabricated structure just outside the Ministry of Public Works and Settlement building in Adapazari city center, which is about a R_{jb} distance of 3.08 km away the earthquake source, is amidst the 23 strong motion stations that recorded this event. However, due a malfunction within the installed accelerometer, only East-West component of the horizontal components of this valuable record is available for use (See Figure 3.56 for the recorded time history).

Amongst the 23 accelerogram set recorded during August 17, 1999 Izmit earthquake, the time series provided by TSGMN station AI005 is particularly significant for this application, given, the outcome of PSHA, and the succeeding deaggragation analysis performed for the site

of the strong ground motion station indicates that this seismic event, in effect, faithfully echoes the design earthquake situation for Adapazari city. Consequently, through using the East-West component ground motion recorded by AI005 station as a benchmark case, and making use of the comprehensive geophysical and geotechnical information published by TUBITAK and Bray et al. [81]; it is possible to inspect the success of each constructed method pair in assessing seismic ground response.

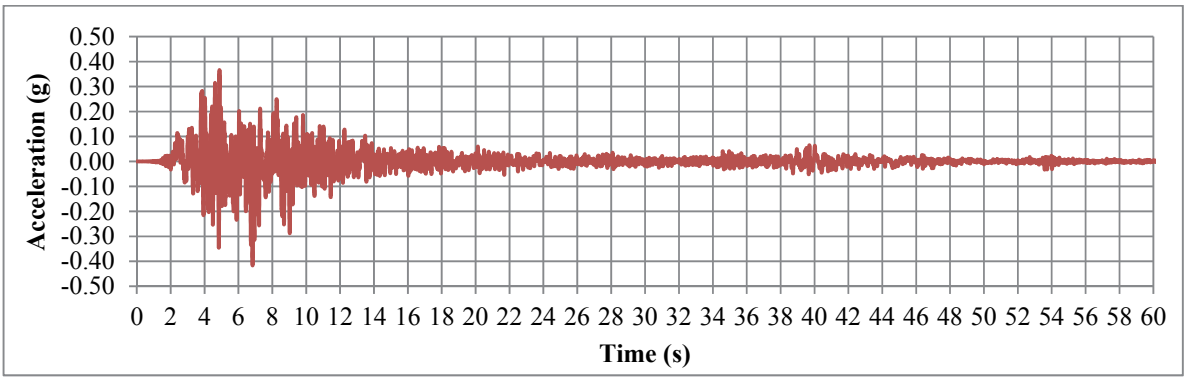

Figure 3.56. East-West component of the surface accelerations recorded by TSGMN Station AI005 during August 17, 1999; Izmit, Kocaeli earthquake

The results of the PSHA performed for the subject site [85], specify a PGA, S_s and S_1 value of 0.43g, 0.86g and 0.44g at the reference site condition, respectively. In order to perform ground response analyses, one needs to initially develop a group of records, consisting of at least 10 strike-slip earthquakes that fulfill a M_w range from 6.9 to 7.9, a R_{jb} interval that spans between 0 to 55 km and a V_{s30} range of 600-1000 m/s (Note that this interval is noticeably different from the suggested range. Herein, collecting sufficient amount of records overrules the need to comply with the defined range for record queries, thus the idea to modify the recommended span of earthquake parameters is sustained); in compliance with the PSHA results. Table 3.7 illustrates the list of 16 earthquake record components that are observed to be well-matched with the set criteria, and, as a consequence, deemed relevant for the subject task. Figures 3.57 to 3.60 show the 5%-damped response spectra of unscaled record components, and the pertaining input time-histories prepared by PGA scaling, scaling

to get the best-fit mean spectrum, and nonstationary spectral matching, correspondingly, along with the reference-site-condition-UHS determined for the interested site in terms of seismic hazard results.

Table 3.7. List of earthquake time histories selected for use with the ground response analyses performed for AI005 TSGMN station

Record No.	Event	M_w	R_{jb} (km)	V_{s30} (m/s)	Record File	PGA
1	Denali-Alaska (2002)	7.90	49.9	963.9	NGA No#2107 (5595-FN)	0.086
2	Denali-Alaska (2002)	7.90	49.9	963.9	NGA No#2107 (5595-FP)	0.078
3	Hector Mine (1999)	7.13	42.1	684.9	NGA No#1836 (22161090)	0.066
4	Hector Mine (1999)	7.13	42.1	684.9	NGA No#1836 (22161360)	0.067
5	Hector Mine (1999)	7.13	50.4	684.9	NGA No#1795 (12647090)	0.077
6	Denali-Alaska (2002)	7.90	43	963.9	NGA No#2111 (5596-FN)	0.108
7	Denali-Alaska (2002)	7.90	43	963.9	NGA No#2111 (5596-FP)	0.060
8	Landers (1992)	7.28	50.9	684.9	NGA No#891 (SIL090)	0.040
9	Hector Mine (1999)	7.13	10.3	684.9	NGA No#1787 (HEC000)	0.265
10	Hector Mine (1999)	7.13	10.3	684.9	NGA No#1787 (HEC090)	0.330
11	Sitka-Alaska	7.68	34.6	659.6	NGA No#1626 (212V5090)	0.096
12	Duzce-Turkey (1999)	7.14	8	659.6	NGA No#1618 (531-E)	0.115
13	Duzce-Turkey (1999)	7.14	8	659.6	NGA No#1618 (531-N)	0.158
14	Landers (1992)	7.28	41.4	684.9	NGA No#897 (29P000)	0.080
15	Kobe-Japan (1995)	6.90	7.1	609.0	NGA No#1111 (NIS000)	0.507
16	Kobe-Japan (1995)	6.90	7.1	609.0	NGA No#1111 (NIS090)	0.501

According to geological, geophysical and geotechnical knowledge compiled for the station site, the soil stratification below AI005 is prevailed by a clay composition, interrupted by a 2 m band of marl at a depth of 6.6 m, in the uppermost 11 m. The plasticity of the fat clay settling is detected to remain stable approximately around 25, so the dynamic behavior of the identified clayey material can be modeled by identical dynamic soil properties. Looking at the profiling beneath the location of the station, the stiffness traits within the soil profile for AI005 is observed to steadily increase, from 264 m/s on the soil surface to 663 m/s at the terminating rock-like layer. This points out to a rapid change in soil settings from soft depositions to firm

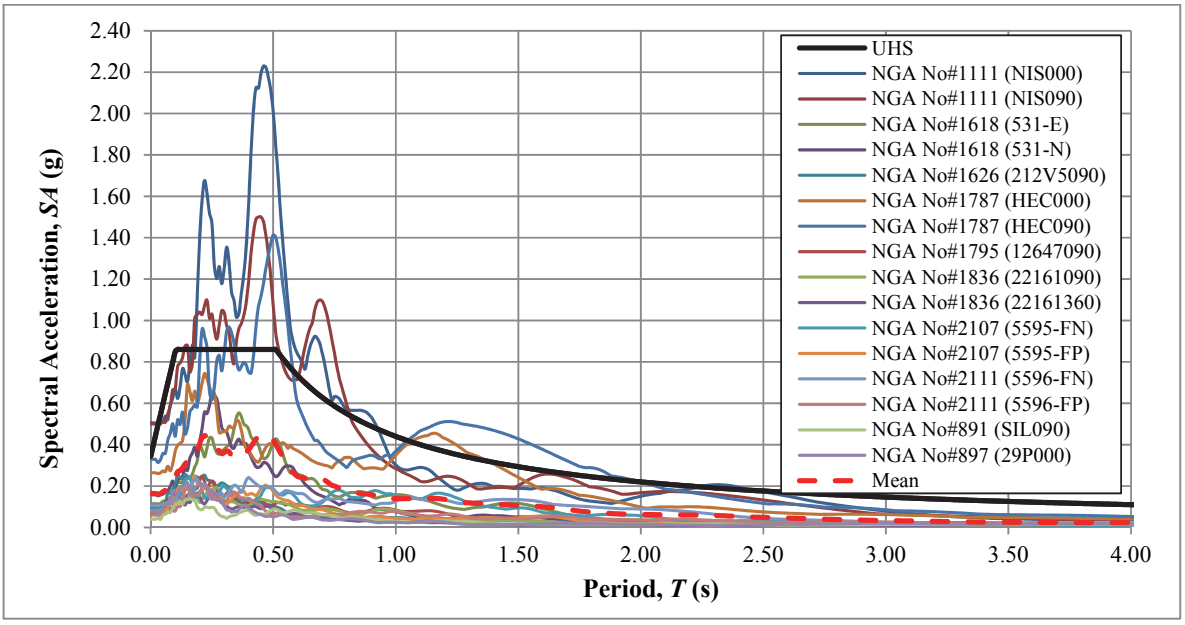

Figure 3.57. 5%-damped response spectra of earthquake record components selected for carrying out the site effects calculations for AI005 TSGMN station

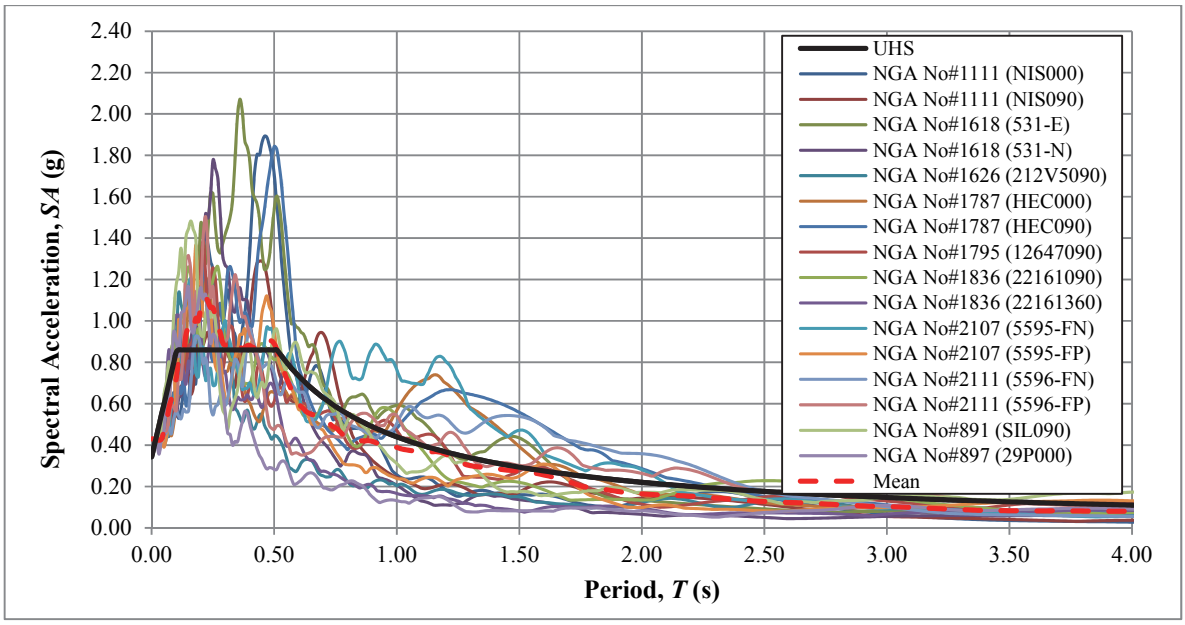

Figure 3.58. 5%-damped response spectra of earthquake record components presented in Figure 3.57 after normalization of each time series to the hazard PGA level of 0.43g

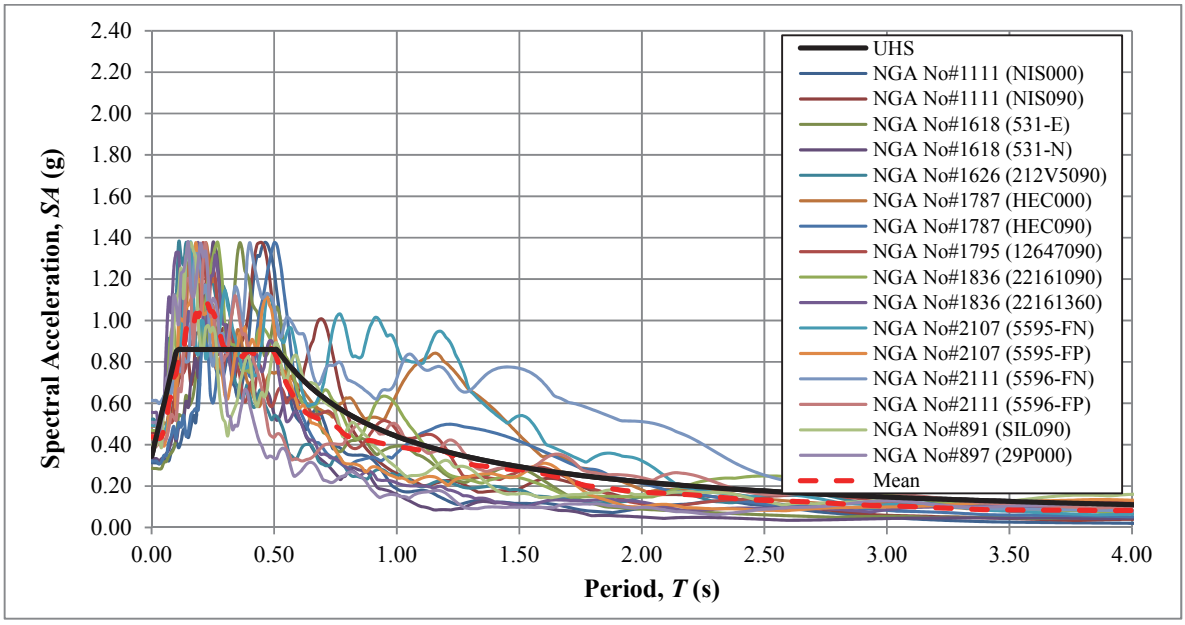

Figure 3.59. 5%-damped response spectra of earthquake record components shown in Figure 3.57 after scaling to find the mean spectrum that is best-fit with PSHA-decided UHS

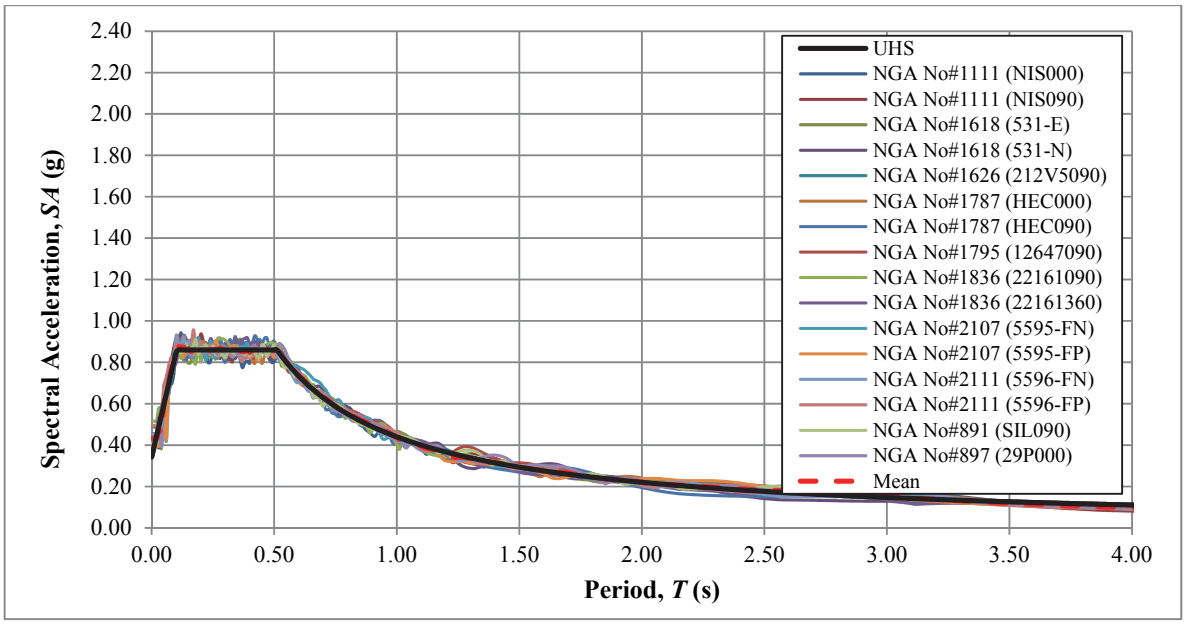

Figure 3.60. 5%-damped response spectra of earthquake record components presented in Figure 3.57 following nonstationary spectral matching as per PSHA-determined UHS

rock-resembling material. Figure 3.61 summarizes the characteristics of the soil profiling beneath the AI005 station down to the decided locus, in a visual manner.

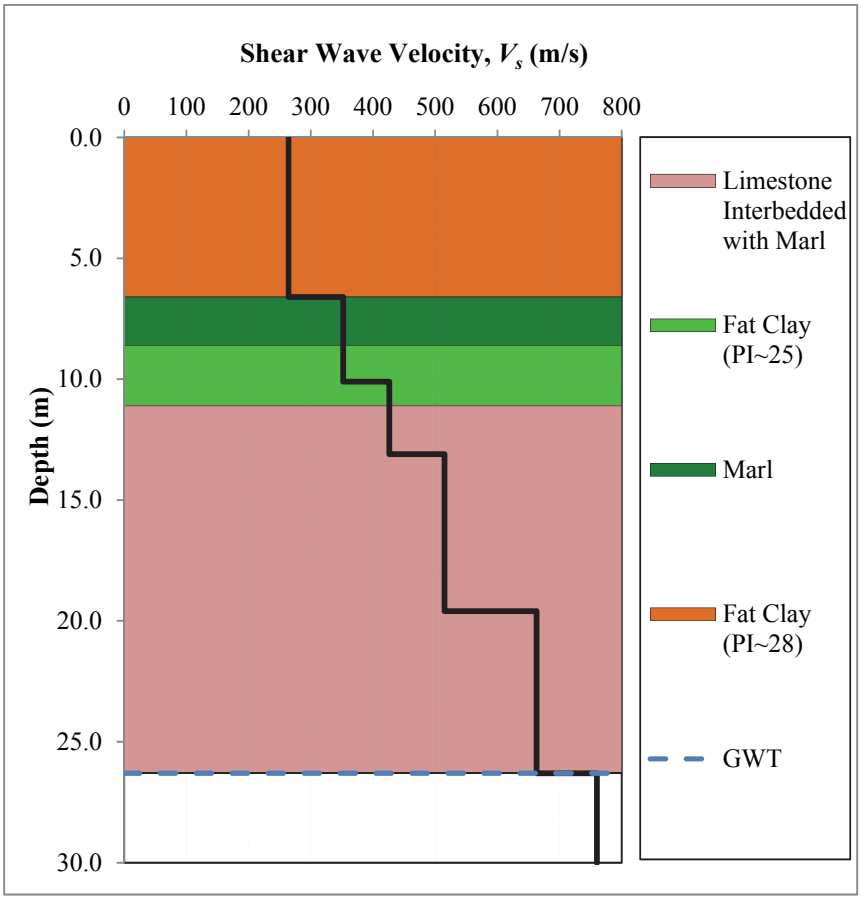

Figure 3.61. A visual depiction of soil layering and corresponding shear-wave velocity variation underneath the AI005 station; extending down to the reference site condition

In order to perform the ground response analyses for AI005 TSGMN station, herein, the fat clay PI~22 and PI~28 and generic rock formations recorded during field testing are modelled using the dynamic soil properties published by Vucetic and Dobry [62] and EPRI [42] respectively. Figure 3.62 provides a graphical depiction of the adopted modulus reduction/damping curves. In the conducted calculations, the unit weight values of 17.30 and 20.50 kN/m^3 are used for clayey soils and generic rock materials correspondingly. The unit weight value for the reference site condition is assumed as 22.00 kN/m^3.

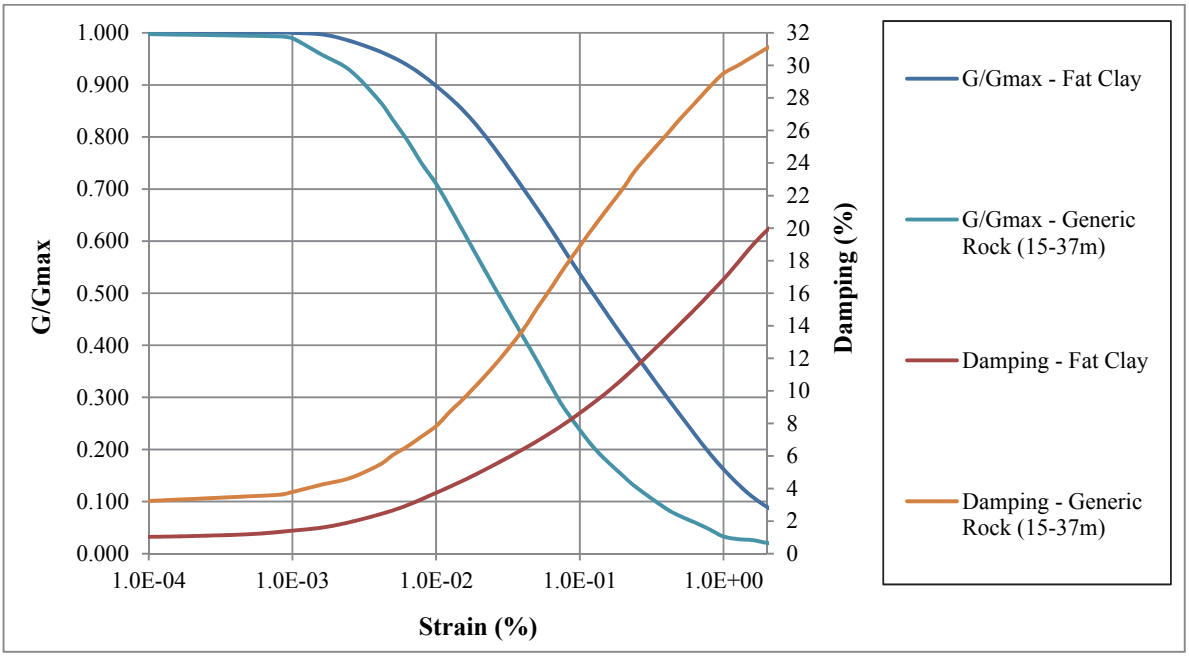

Figure 3.62. Modulus degradation and damping curves adopted for performing ground response analyses at the site of AI005 TSGMN station

Figures 3.63 and 3.64 display the analysis results for AI005 TSGMN station site, obtained using each method pair. In all cases, fundamental period of the response is overestimated. Seismic response analysis indicate a predominat period value of rougly 0.23s, whereas the observed fundamental site period is just about 0.09s. Whether this alteration between calculated and observed spectal behavior is a conseuqence of the lack of short-period amplitude values within the input dataset or the uncertainty in determination of Vs cannot be decided. However, speaking in terms of the peak amplitude responses, the frequency independent calculation scheme utilizing input motions established via nonstationary spectral matching method offers a reasonably analogous response with the observed behavior (i.e. a peak response ratio of approximately 1.186).

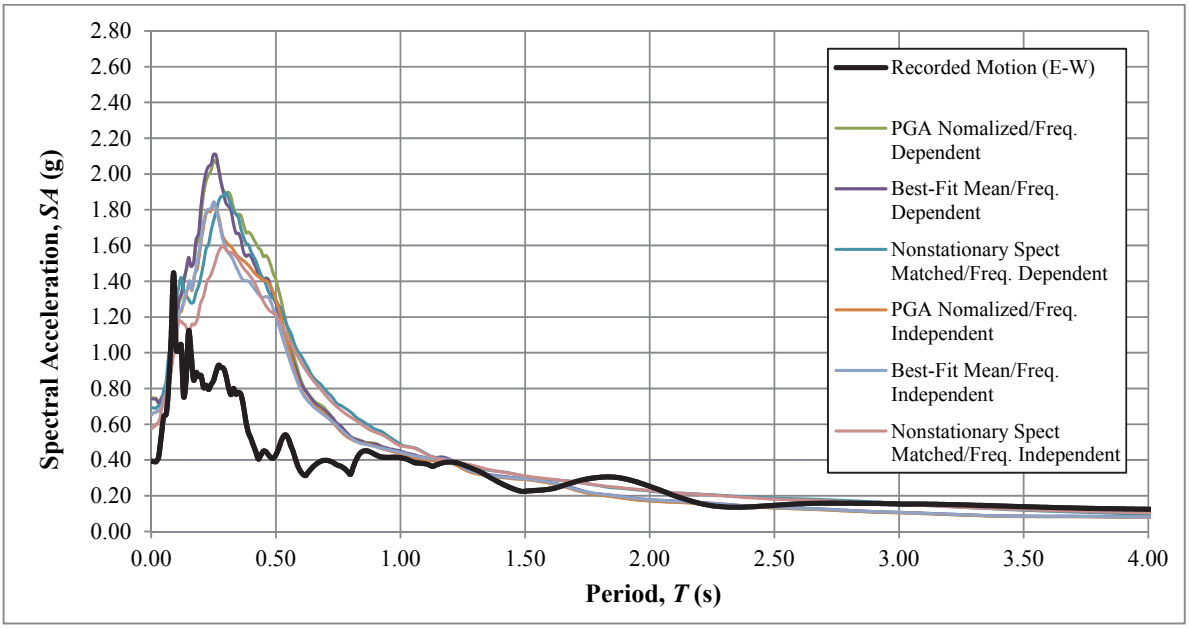

Figure 3.63. A comparison of the 5%-damped response spectra of mean surface response, determined using each method pair, with the observed behavior at AI005 TSGMN station

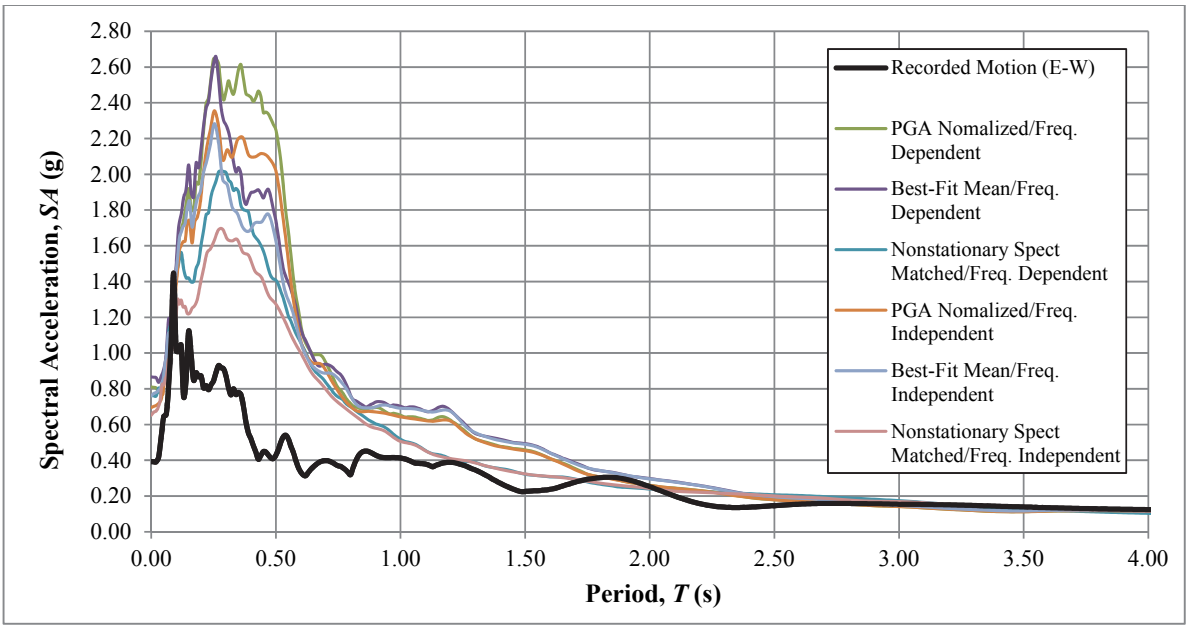

Figure 3.64. A comparison of the 5%-damped response spectra of mean + std. dev. surface response, determined via each method pair, with the observed behavior at AI005 station

3.1.8. Bolu Station (AI010)

Bolu city, a central administrative division of the Bolu province, is founded on a pull-apart type basin. The basin structure is composed of Quaternary alluvium, alluvium fan, and recent-Pliocene alluvium terraces (comprising of uncemented sand and gravel) in and on the proximity of the city. The city is smoothly sloped towards south; the clayey and silty depositions along flood plains and gravelly and sandy settlings transported by Buyuksu creek being in transition with each other [86]. Maximum thickness of these Quaternary alluvial deposits is determined to be 230m in the city proper [87]. Nonetheless, based on geophysical testing results published in various resources, the locus-type rock formations can be said to lie at a depth around 70-80m just beneath Bolu city.

Tectonic environment of Bolu is characterized by the strike-slip North Anatolian fault (NAF). 87 days after the Izmit earthquake, in November 12, 1999, a section of this substantial faulting, 6 km off the city of Duzce, caused a M_w=7.1, pure strike-slip earthquake. The powerful event caused 894 casualties, 4,948 injuries, and widespread structural/geotechnical damage within the surrounding cities. TSGMN station AI010 installed within a building near the Ministry of Public Works and Settlement headquarters in Bolu; roughly about a R_{jb} distance of 8.01 km away the earthquake source, is among the 19 accelerograph stations that recorded this vital event (See Figure 3.65 for East-West and North-South component recorded time histories).

Based on PSHA, and the subsequent deaggragation calculations performed for the site of the AI010 seismograph station, the earthquake event that took place on November 12 is in reality, fairly compliant with the design earthquake event for Bolu city. Hence, through utilizing horizontal components of Bolu station records as benchmark data, and adopting the detailed geophysical and geotechnical information published by TUBITAK, Rathje et al. [88], Hobiger et al. [89] and Basokur [90], one can to investigate the suitability of each method pair for calculating seismic ground response.

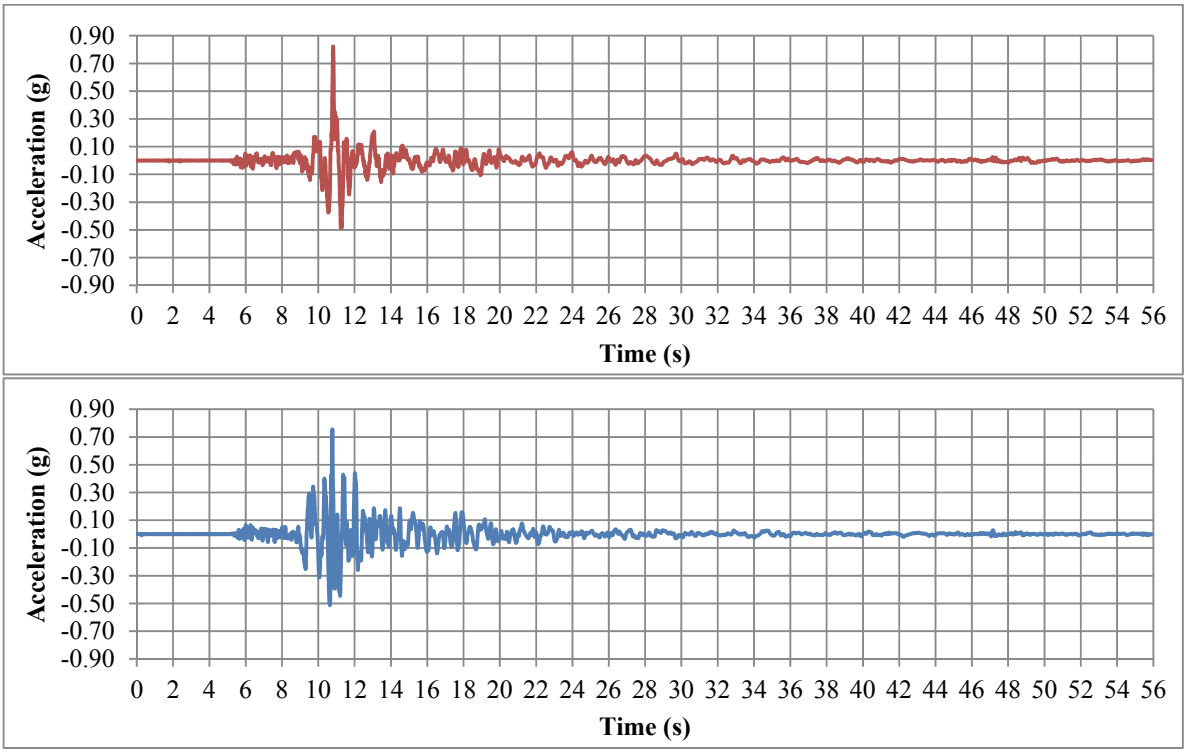

Figure 3.65. East-West (Top) and North-South (Bottom) components of the surface accelerations recorded by TSGMN Station AI010 during November 12, 1999; Duzce earthquake

The PSHA calculation results for the subject site [17], point to PGA, S_s and S_1 values of 0.67g, 1.49g and 0.65g at the reference site condition, respectively. So to carry out seismic response analyses, it is necessary to first develop a group of records, consisting of at least 10 strike-slip events that satisfy a M_w range from 6.5 to 7.7, a R_{jb} interval that spans between 5 to 55 km and a V_{s30} range of 600-820 m/s (This range is a slight modification of the suggested interval that is adjusted to obtain adequate amount of time series, for computing a stable seismic response outcome); in compliance with the PSHA conclusions. Table 3.8 displays the list of the 17 earthquake record components that are observed to comply with the stipulated measures, and, accordingly, considered apt for the subject study. Figures 3.66 to 3.69 demonstrate the 5%-damped response spectra of unscaled record components, and the pertaining input time series prepared by PGA scaling, scaling to get the best-fit mean

spectrum, and nonstationary spectral matching, respectively, alongside the UHS calculated for the subject location, described at the locus site condition according to seismic hazard results.

Table 3.8. List of earthquake time histories selected for use with the ground response analyses performed for AI010 TSGMN station

Record No.	Event	M_w	R_{jb} (km)	V_{s30} (m/s)	Record File	PGA
1	Hector Mine (1999)	7.13	50.4	684.9	NGA No#1795 (12647090)	0.077
2	Hector Mine (1999)	7.13	42.1	684.9	NGA No#1836 (22161360)	0.067
3	Landers (1992)	7.28	50.9	684.9	NGA No#891 (SIL000)	0.050
4	Sitka-Alaska (1972)	7.68	34.6	659.6	NGA No#1626 (212V5090)	0.096
5	Sitka-Alaska (1972)	7.68	34.6	659.6	NGA No#1626 (212V5180)	0.086
6	Duzce-Turkey (1999)	7.14	8	659.6	NGA No#1618 (531-E)	0.115
7	Hector Mine (1999)	7.13	11.7	684.9	NGA No#1787 (HEC000)	0.265
8	Hector Mine (1999)	7.13	11.7	684.9	NGA No#1787 (HEC090)	0.330
9	Imperial Valley-06 (1979)	6.53	15.2	659.6	NGA No#164 (H-CPE147)	0.170
10	Imperial Valley-06 (1979)	6.53	15.2	659.6	NGA No#164 (H-CPE237)	0.151
11	Duzce-Turkey (1999)	7.14	25.9	782.0	NGA No#1613 (1060-E)	0.053
12	Duzce-Turkey (1999)	7.14	34.3	659.6	NGA No#1619 (MDR000)	0.119
13	Duzce-Turkey (1999)	7.14	34.3	659.6	NGA No#1619 (MDR090)	0.056
14	Landers (1992)	7.28	41.4	684.9	NGA No#897 (29P000)	0.080
15	Landers (1992)	7.28	41.4	684.9	NGA No#897 (29P090)	0.060
16	Kobe-Japan (1995)	6.90	7.1	609.0	NGA No#1111 (NIS000)	0.507
17	Kobe-Japan (1995)	6.90	7.1	609.0	NGA No#1111 (NIS090)	0.501

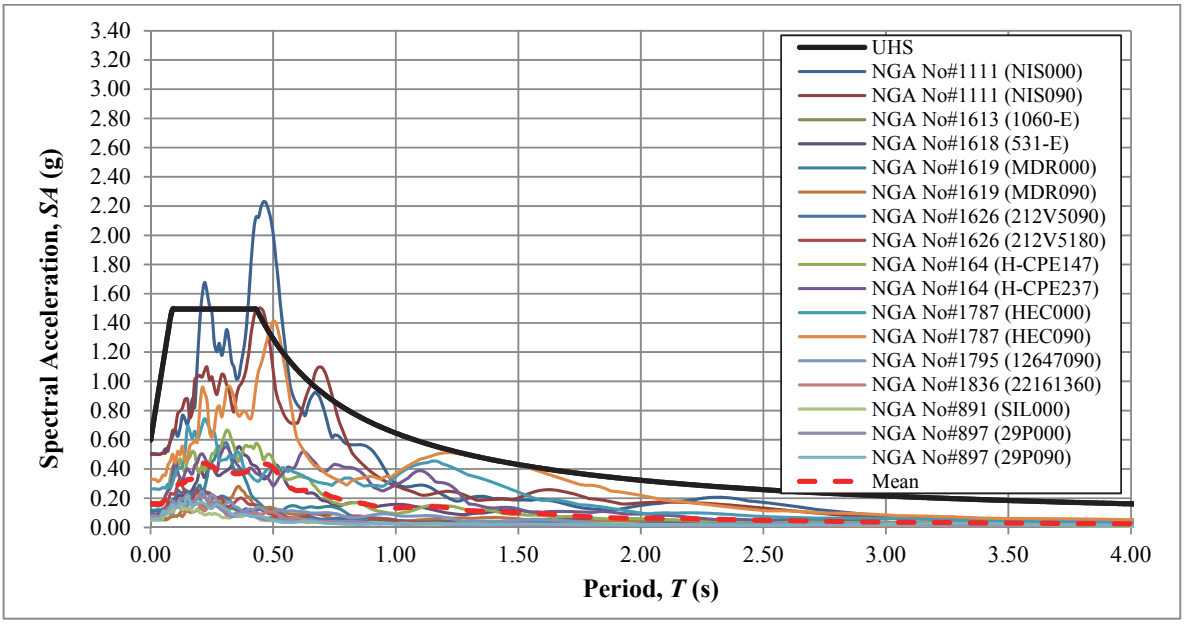

Figure 3.66. 5%-damped response spectra of earthquake record components selected for carrying out the site effects calculations for AI010 TSGMN station

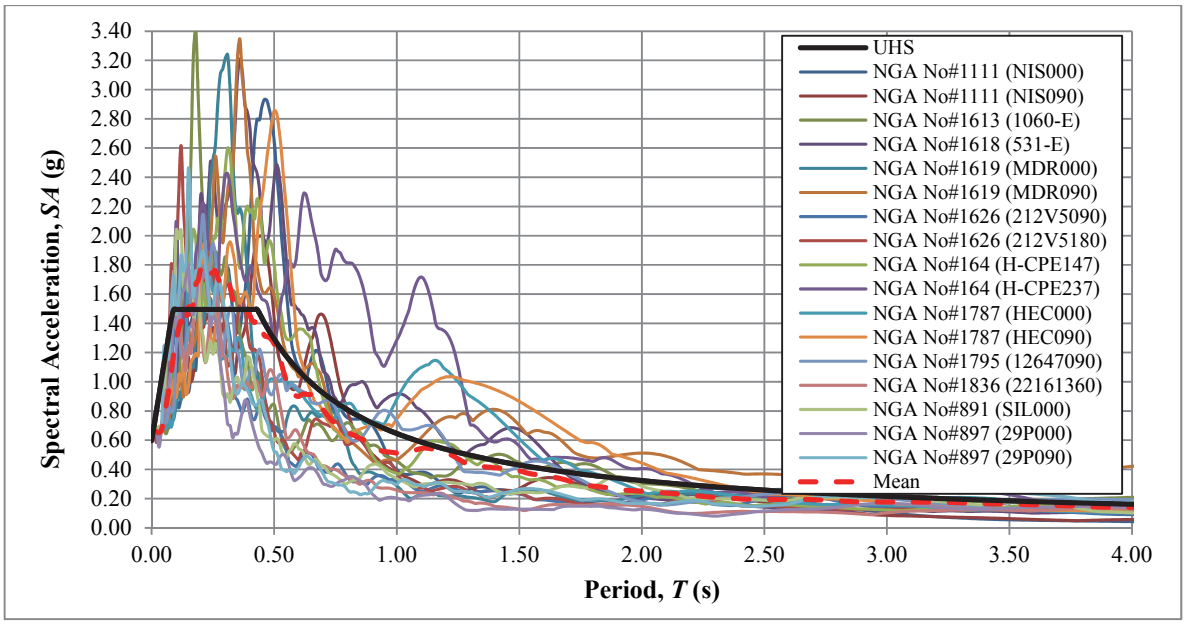

Figure 3.67. 5%-damped response spectra of earthquake record components presented in Figure 3.66 after normalization of each time series to the hazard PGA level of 0.67g

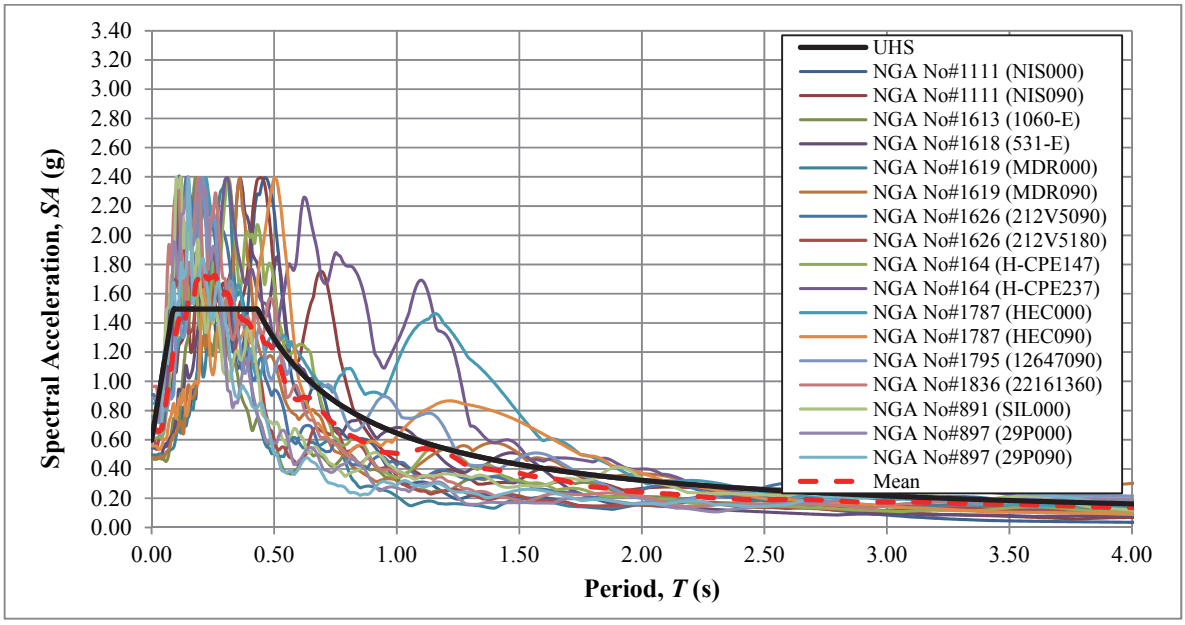

Figure 3.68. 5%-damped response spectra of earthquake record components shown in Figure 3.66 after scaling to find the mean spectrum that is best-fit with PSHA-decided UHS

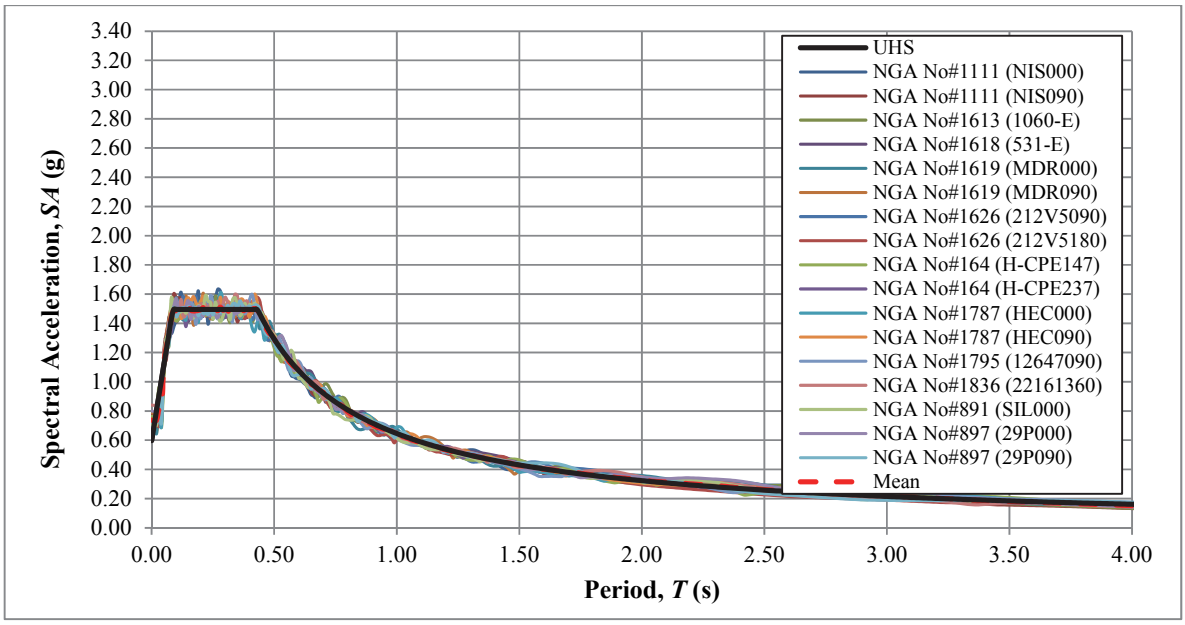

Figure 3.69. 5%-damped response spectra of earthquake record components presented in Figure 3.66 following nonstationary spectral matching as per PSHA-determined UHS

As per the geological, geophysical and geotechnical knowledge brought together for the station site, the soil stratification just below AI010 is dominated by a clayey material with slight silt inclusions at the topmost 40 m. Within this depth interval, the plasticity traits of the involved settling shows broad variability, thus even if the comprising materials are fundamentally the same, the hysteretic behavior exhibited at each depth, to some extent, differs. The SPT-N and V_s values reported for the subject location suggests that the observed clay formation is composed of very soft layers of material that stiffens with increasing depth; measured V_s values ranging from 163 m/s at the ground surface to 495 m/s at 40 m depth. The ensuing weak-rock layering displays considerably higher shear resistance that steadily escalates towards the locus. Figure 3.70 outlines the features of the soil layering beneath the AI010 station down to the reference site conditions, in a visual manner.

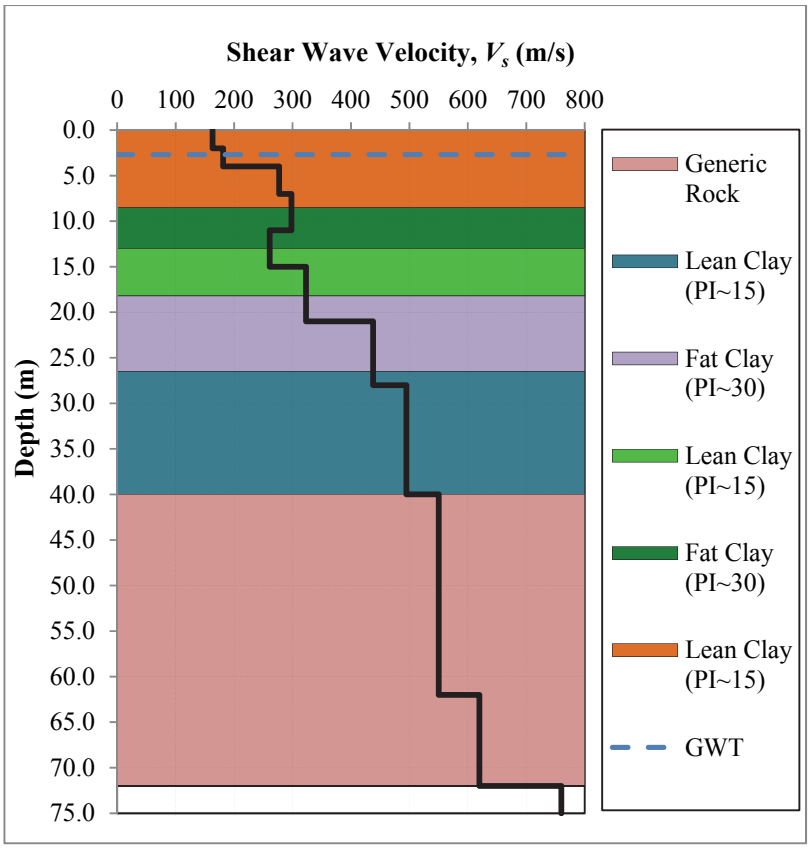

Figure 3.70. A visual depiction of soil layering and corresponding shear-wave velocity variation underneath the AI010 station; extending down to the reference site condition

So to conduct ground response analysis for AI010 TSGMN station, herein, the lean clay PI=15, lean clay PI~30 and generic rock stratifications identified through field testing are modeled via the dynamic soil properties suggested by Vucetic and Dobry [62] and EPRI [42] respectively. Figure 3.71 provides a graphical representation of the adopted modulus reduction/damping curves. In the performed analyses, the unit weight values of 17.30 and 22.00 kN/m^3 are used for clayey soils, and generic rock material present between 40 to 72 m depths correspondingly.

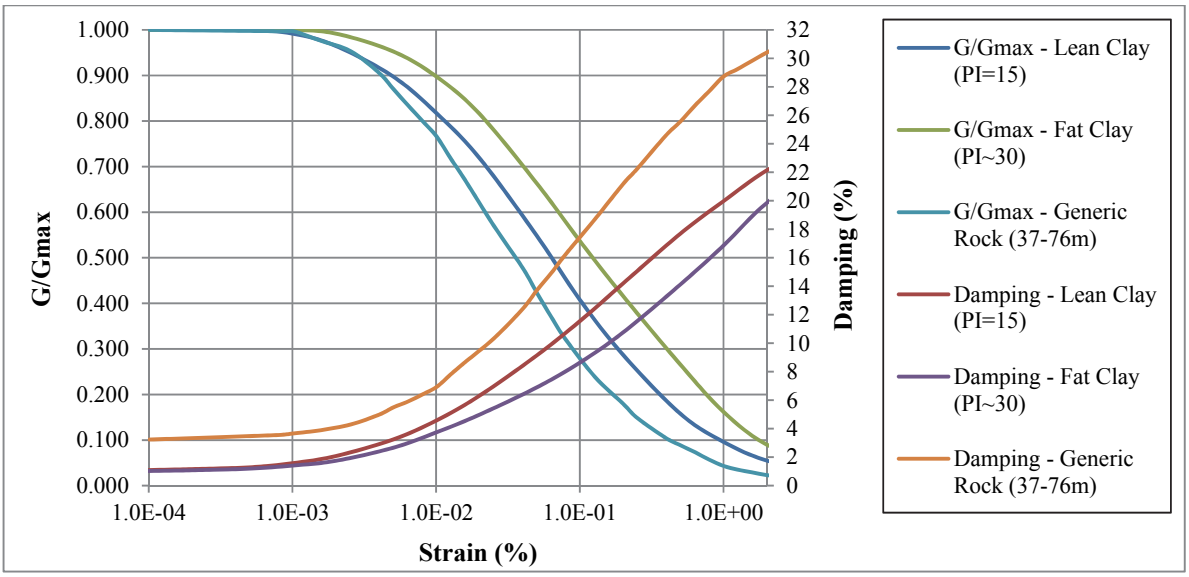

Figure 3.71. Modulus degradation and damping curves adopted for performing ground response analyses at the site of AI010 TSGMN station

Figures 3.72 and 3.73 show the analysis results for AI010 TSGMN station site, attained using each method pair. In all cases, fundamental period of the response is overestimated, very likely, as a result of the uncertainties in determination of stiffness traits of a soil profile. Nevertheless, in terms of the peak amplitude responses, the frequency independent calculation process adopting input motions established via nonstationary spectral matching method provides a fairly close response with the spectra for recorded ground motions (i.e. a peak response ratio of approximately 1.094).

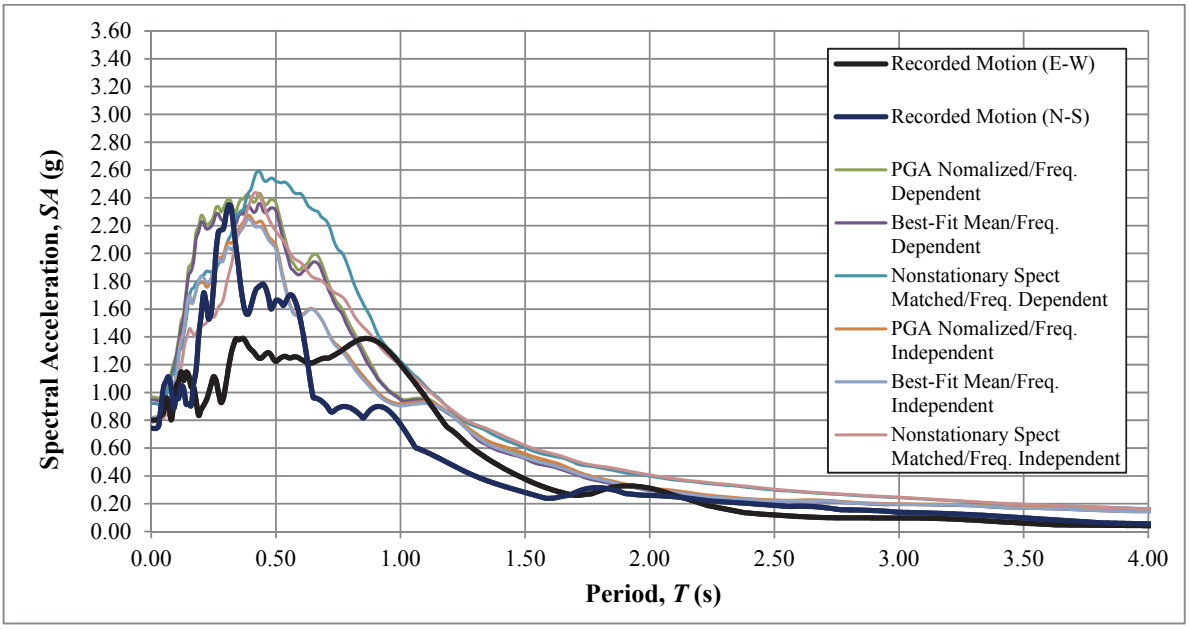

Figure 3.72. A comparison of the 5%-damped response spectra of mean surface response, determined using each method pair, with the observed behavior at AI010 TSGMN station

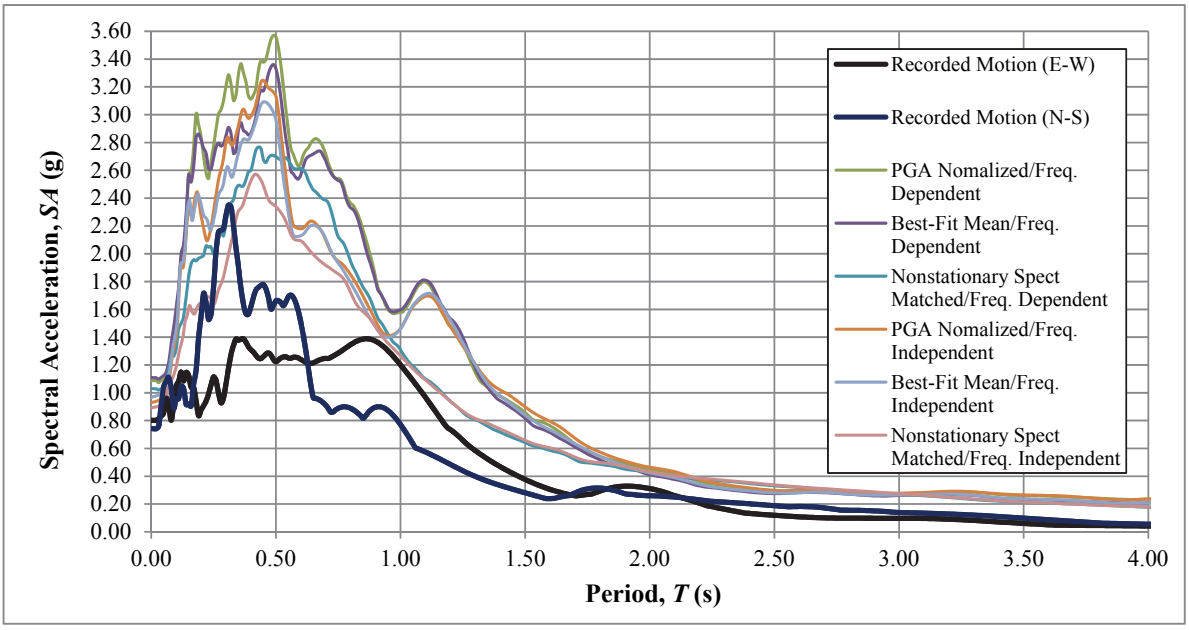

Figure 3.73. A comparison of the 5%-damped response spectra of mean + std. dev. surface response, determined via each method pair, with the observed behavior at AI010 station

3.1.9. Duzce Station (AI011)

The greatest extent of damage resulting from the November 12, 1999 Duzce earthquake occurred in Duzce city, now the primary economic center of Duzce province (prior to Duzce earthquake, officially, the city was a part of Bolu province). The city is located very close to the source mechanism of the event and is situated on a site that is, both from geotechnical and geophysical aspects, drastically different from Bolu city. Hence the same seismic event triggered a unique set of benchmark case that is outright valuable for engineering uses.

Duzce proper is a dynamic subsidence and deposition region that is bounded by Quaternary-aged andesitic and diabasic volcanic rock formations on the perimeters. The deposition just beneath Duzce city is generalized by surficial clay layers overlying coarse-grained material residing on stiff rock formations, lying approximately at a depth range of 120-150 m. Field investigations carried out by various entities show that the perceived clayey material is made up of loosely-structured deposits. Nonetheless, once the strata containing coarse-grained settlings are reached the compaction properties of observed material is detected to improve.

According to the PSHA results for the station site, the seismic occurrence recorded by TSGMN station AI011, located in a central part of the Duzce city that is particularly close to the source mechanism of Duzce seismic occurrence, i.e. a R_{jb}=0 km, (See Figure 3.74 for East-West and North-South component recorded time histories) is fairly well-suited with the design earthquake for Duzce city. Henceforth, by making use of the horizontal components of AI011 station records as reference ground motions, and adopting the detailed geophysical and geotechnical information published by TUBITAK, Rathje et al. [88] and Hobiger et al. [89]; it is possible to investigate the appropriateness of each assembled method pair in appraising seismic ground response.

According to the PSHA findings for the subject site [17], estimated PGA, S_s and S_1 values at the reference site condition are 0.56g, 1.24g and 0.56g respectively. So to conduct seismic response analyses, it is vital to initially develop a set of records that comprises of at

least 10 strike-slip events that satisfy a M_w range from 6.5 to 7.7, a R_{jb} interval that spans between 0 to 55 km and a V_{s30} range of 600-820 m/s (Note that this selection range is slightly different from the proposed interval of values. However, as the number of records used in analyses has a larger impact on attained results, herein, decision to modify selection criteria is warranted); in-line with PSHA indications. Table 3.9 displays the list of 17 earthquake record components that are satisfactory with the specified criteria, and, as a consequence, reasoned appropriate for the subject application. Figures 3.75 to 3.78 exhibit the 5%-damped response spectra of unscaled record components, and the corresponding input time-histories prepared by PGA scaling, scaling to obtain the best-fit mean spectrum, and nonstationary spectral matching, respectively, along with the UHS calculated for the subject location, determined at the locus site condition according to seismic hazard results.

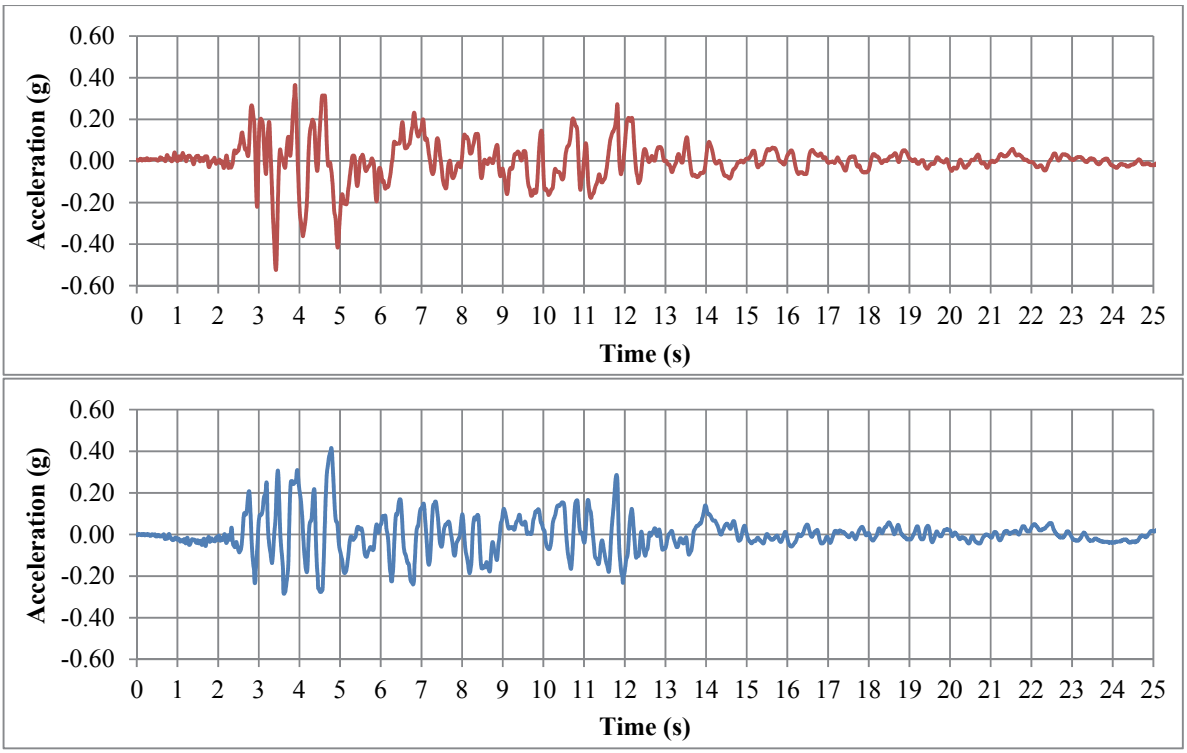

Figure 3.74. East-West (Top) and North-South (Bottom) components of the surface accelerations recorded by TSGMN Station AI011 during November 12, 1999; Duzce earthquake

Table 3.9. List of earthquake time histories selected for use with the ground response analyses performed for AI011 TSGMN station

Record No.	Event	M_w	R_{jb} (km)	V_{s30} (m/s)	Record File	PGA
1	Hector Mine (1999)	7.13	50.4	684.9	NGA No#1795 (12647090)	0.077
2	Hector Mine (1999)	7.13	42.1	684.9	NGA No#1836 (22161360)	0.067
3	Landers (1992)	7.28	50.9	684.9	NGA No#891 (SIL000)	0.050
4	Sitka-Alaska (1972)	7.68	34.6	659.6	NGA No#1626 (212V5090)	0.096
5	Sitka-Alaska (1972)	7.68	34.6	659.6	NGA No#1626 (212V5180)	0.086
6	Duzce-Turkey (1999)	7.14	8	659.6	NGA No#1618 (531-E)	0.115
7	Hector Mine (1999)	7.13	11.7	684.9	NGA No#1787 (HEC000)	0.265
8	Hector Mine (1999)	7.13	11.7	684.9	NGA No#1787 (HEC090)	0.330
9	Imperial Valley-06 (1979)	6.53	15.2	659.6	NGA No#164 (H-CPE147)	0.170
10	Imperial Valley-06 (1979)	6.53	15.2	659.6	NGA No#164 (H-CPE237)	0.151
11	Duzce-Turkey (1999)	7.14	25.9	782.0	NGA No#1613 (1060-E)	0.053
12	Duzce-Turkey (1999)	7.14	34.3	659.6	NGA No#1619 (MDR000)	0.119
13	Duzce-Turkey (1999)	7.14	34.3	659.6	NGA No#1619 (MDR090)	0.056
14	Landers (1992)	7.28	41.4	684.9	NGA No#897 (29P000)	0.080
15	Landers (1992)	7.28	41.4	684.9	NGA No#897 (29P090)	0.060
16	Kobe-Japan (1995)	6.90	7.1	609.0	NGA No#1111 (NIS000)	0.507
17	Kobe-Japan (1995)	6.90	7.1	609.0	NGA No#1111 (NIS090)	0.501

According to field investigations performed in the periphery of station site, the soil stratification below AI011 is characterized by three distinct soil material; that is clayey deposits at the uppermost 12 m, sandy settling extending down to 37 m, and rock-like formations observed down to 128 m depth, at which locus site condition is observed. The clayey deposits are prevailed by especially loose, lean clay material with a plasticity index around 15. The V_s values within this depth range are reported as 154 m/s on the ground surface and 276 m/s at the clay/sand junction. The following poorly-graded sand stratum are particularly stiffer compared to the perceived clayey material, with a V_s interval between 305 to 449 m/s. Nonetheless, the weak-rock formations witnessed between 37 to 128 m show markedly higher shear resistance (i.e. V_s= 449 to 660 m/s). Figure 3.75 graphically visualizes the characteristics of soil layering below the AI011 station down to the decided locus.

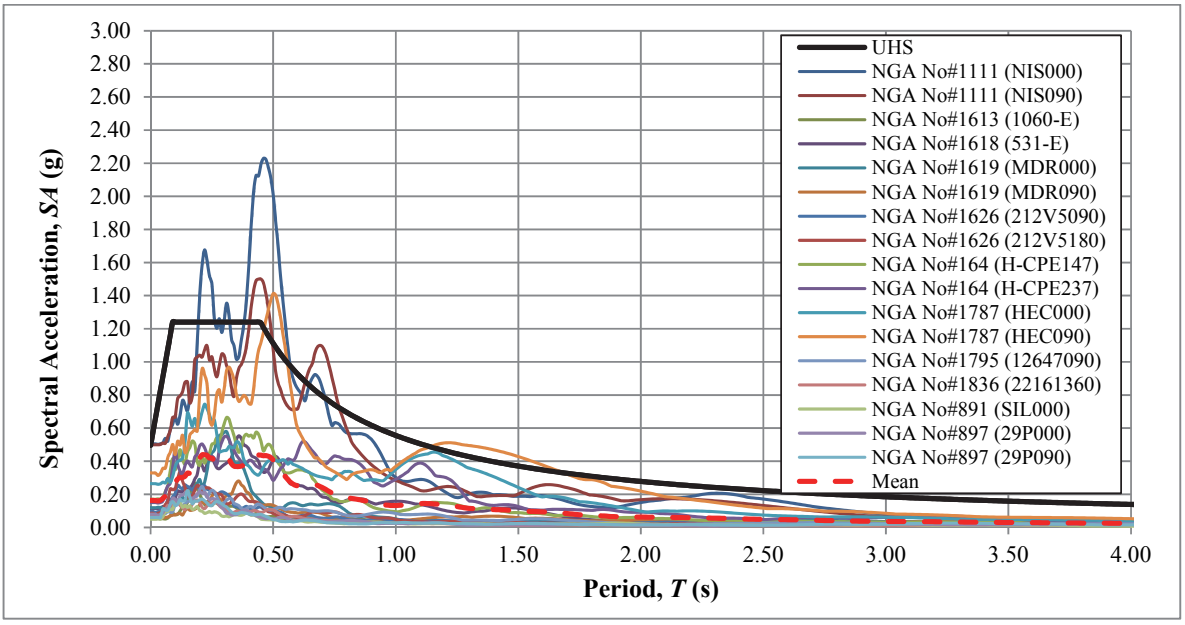

Figure 3.75. 5%-damped response spectra of earthquake record components selected for carrying out the site effects calculations for AI011 TSGMN station

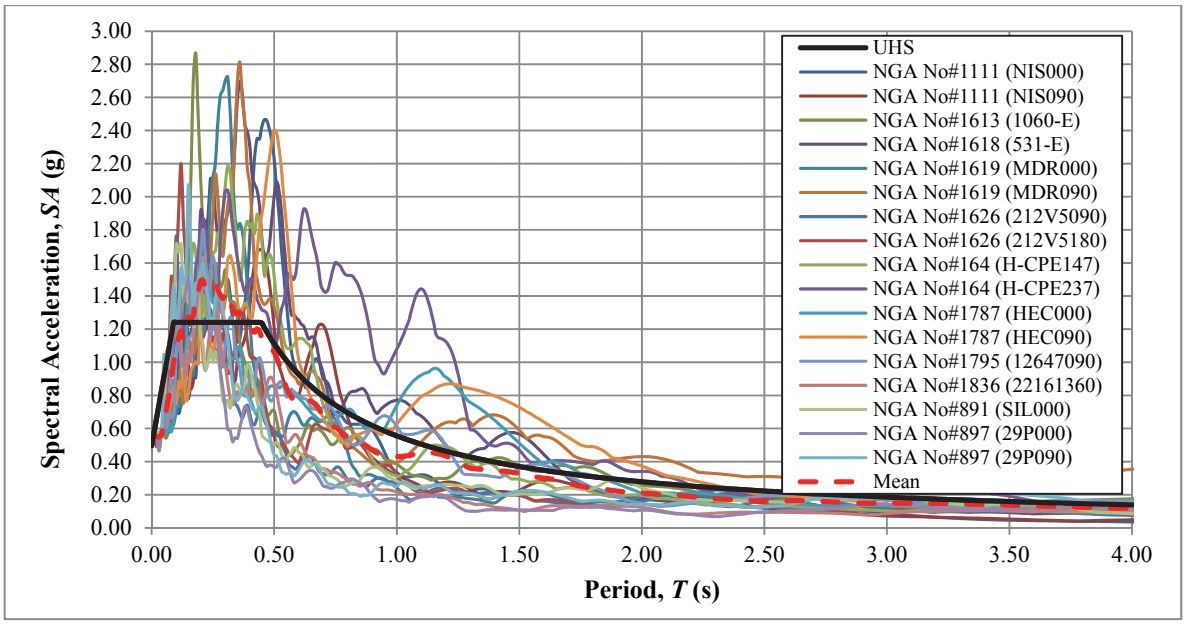

Figure 3.76. 5%-damped response spectra of earthquake record components presented in Figure 3.75 after normalization of each time series to the hazard PGA level of 0.56g

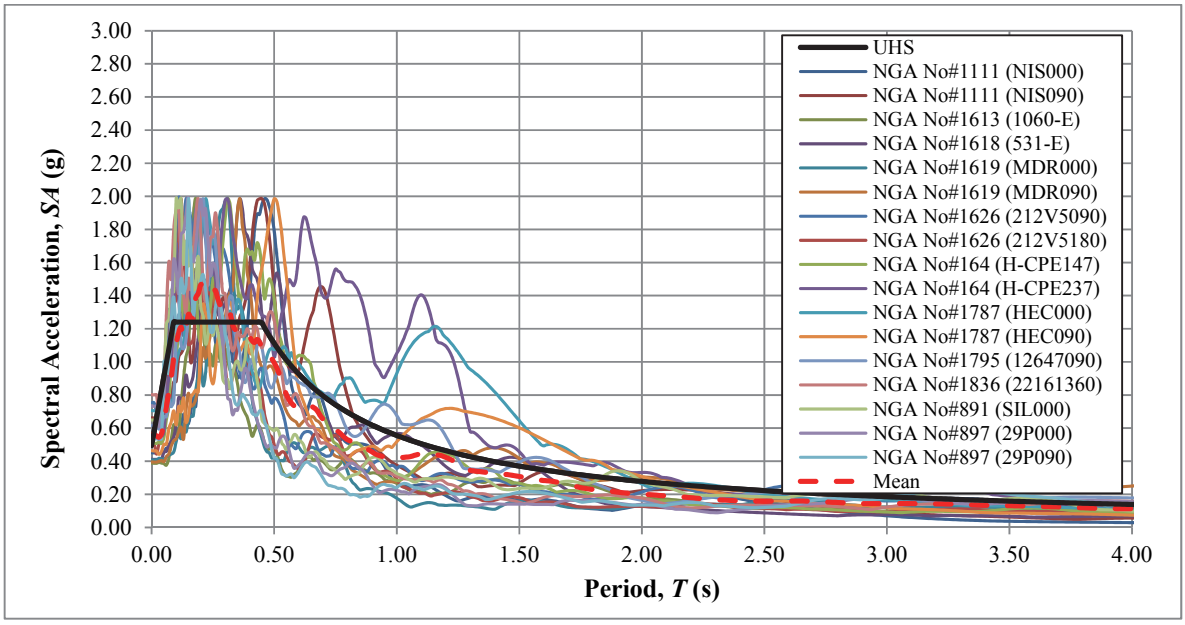

Figure 3.77. 5%-damped response spectra of earthquake record components shown in Figure 3.75 after scaling to find the mean spectrum that is best-fit with PSHA-decided UHS

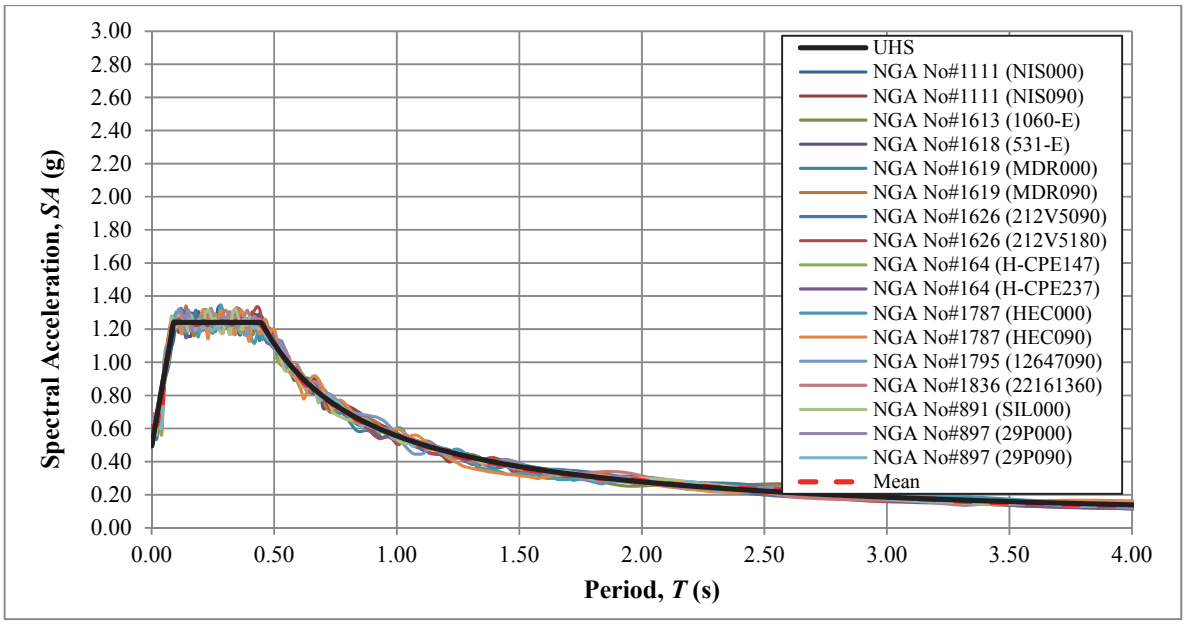

Figure 3.78. 5%-damped response spectra of earthquake record components presented in Figure 3.75 following nonstationary spectral matching as per PSHA-determined UHS

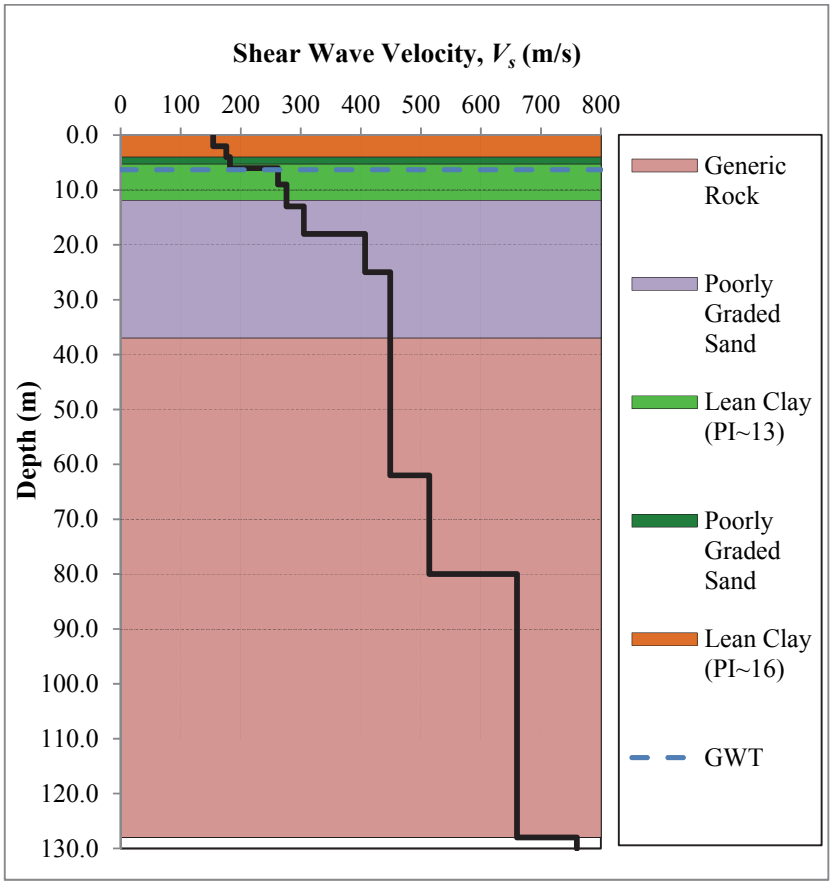

Figure 3.79. A visual depiction of soil layering and corresponding shear-wave velocity variation underneath the AI011 station; extending down to the reference site condition

In order to perform the seismic response calculations for AI011 TSGMN station, herein, the lean clay PI~13/16, poorly graded sand and generic rock layering reported via field testing are represented using the dynamic soil properties suggested by Vucetic and Dobry [62], Seed et al. [64] and EPRI [42] respectively. Figure 3.80 provides a graphical description of the adopted modulus reduction/damping curves. In the performed analyses, the unit weight values of 17.30 and 22.00 kN/m^3 are used for clayey/sandy soils, and generic rock material present between 37 to 128 m depths correspondingly.

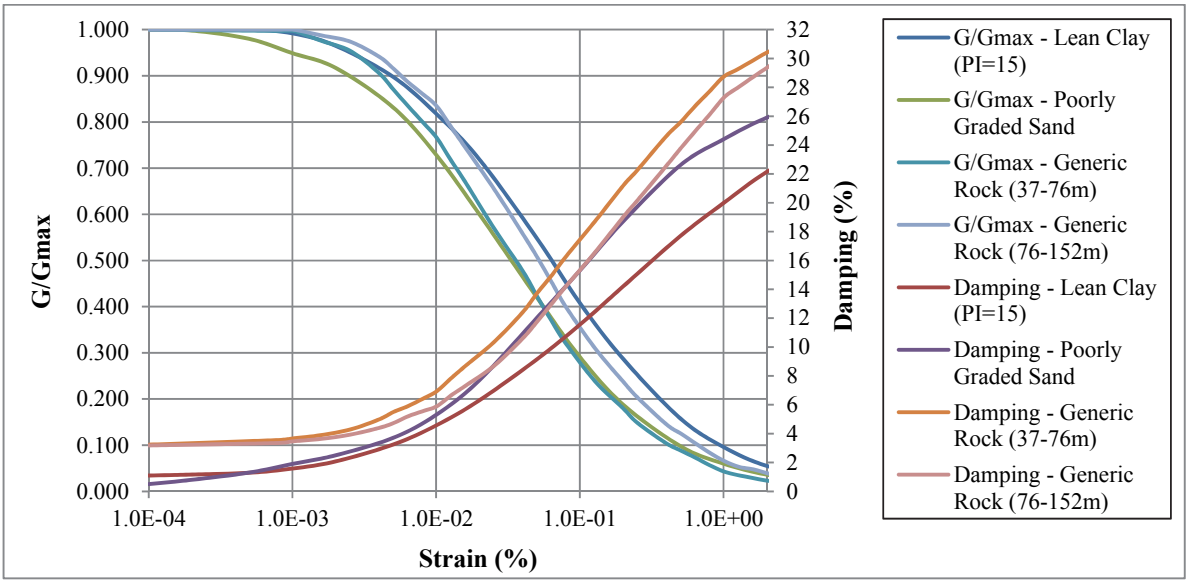

Figure 3.80. Modulus degradation and damping curves adopted for performing ground response analyses at the site of AI011 TSGMN station

Figures 3.81 and 3.82 display the results of ground response analyses for AI011 TSGMN station site, computed using each method assemble. In all calculation situations, the period value that corresponds to the critical spectral response, that is approximately 0.41s, is more or less simulated. However, the remaining significant peaks, at which the spectral amplitudes are specifically concentrated within the response spectrum for each observed record component, was captured to a limited extent, even if each of the mean + standard deviation spectrum, effectively enveloped, almost all of these peaks. By also taking into account the agreement between the peak spectral accelerations of the calculated and the observed response spectra, this understanding can be clearly said to pronounce the need for adopting a spectrum construction method, in connection with ground response methodologies implemented for testing in this study. As, for instance, in the case of ground response analysis technique using the frequency independent calculation mode employing input motions prepared via nonstationary spectral matching technique (i.e. best-performing case), a response that is remarkably similar with the observed behavior, with a peak response ratio of approximately 0.973, was attained, while the frequncy-content of the actual events was very poorly modeled as a matter of involved uncertainties.

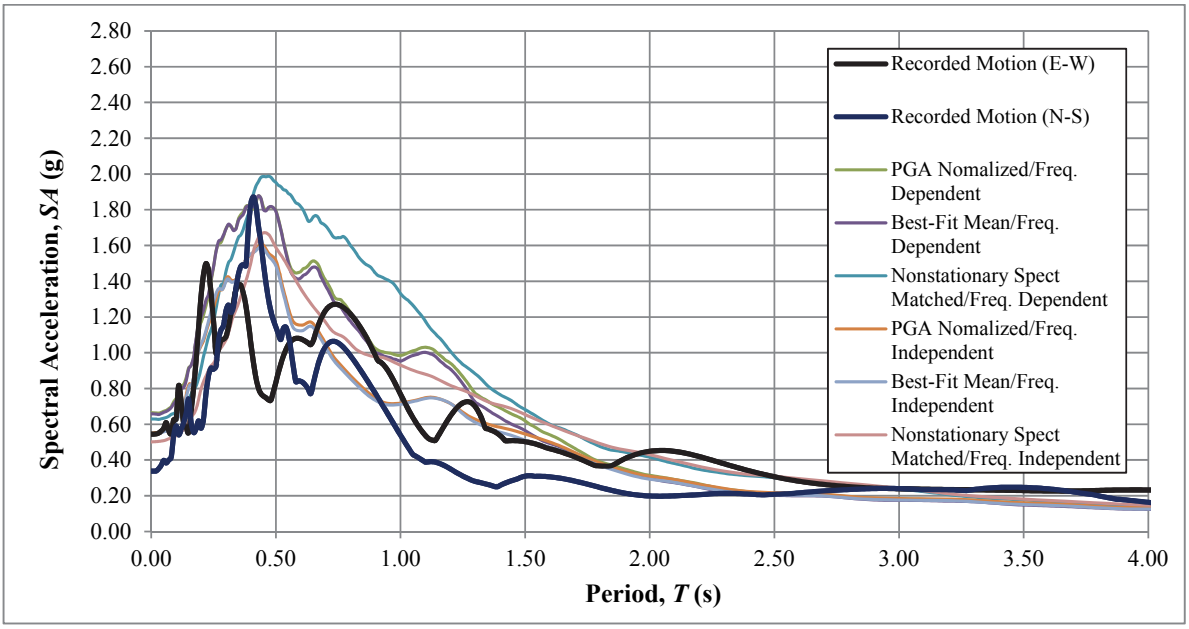

Figure 3.81. A comparison of the 5%-damped response spectra of mean surface response, determined using each method pair, with the observed behavior at AI011 TSGMN station

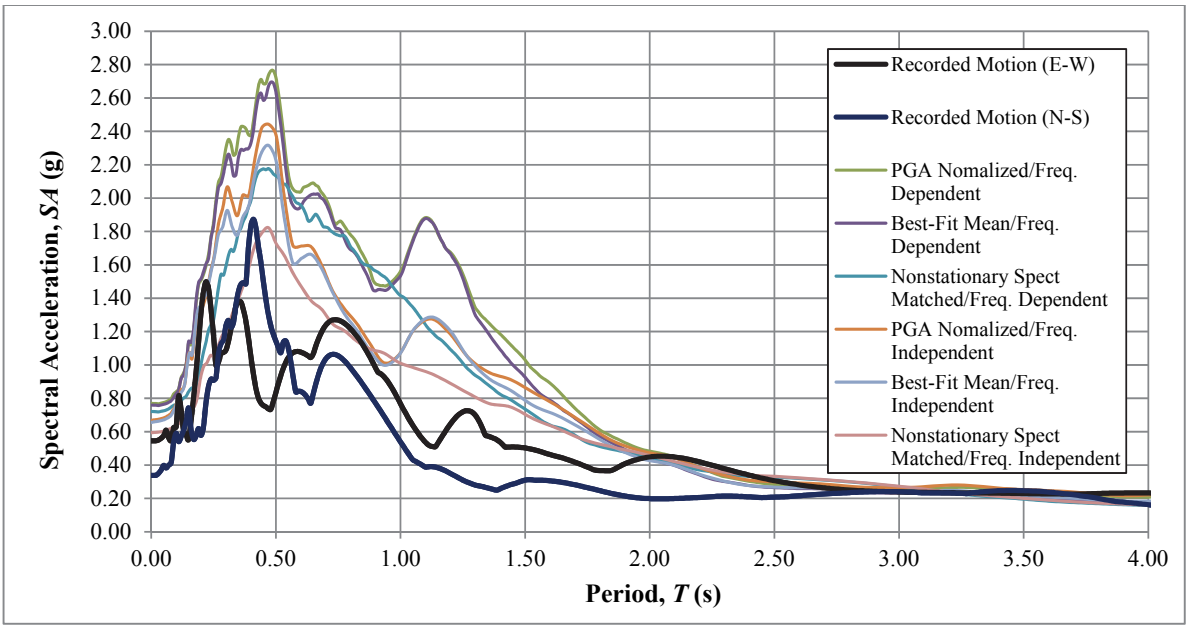

Figure 3.82. A comparison of the 5%-damped response spectra of mean + std. dev. surface response, determined via each method pair, with the observed behavior at AI011 station

3.1.10. Fethiye Station (AI127)

Seismic setting of the city of Fethiye, i.e. one of the 12 cities within Mugla province, is controlled by a number of extensional and strike-slip mechanisms that were observed to produce seismic occurrences as large as magnitude 7.1. In June 10, 2012, one of the active tectonic systems in the region, Hellenic-Cyprus Arc created a M_L=6.0, left-lateral strike-slip earthquake bearing extensional components. The event resulted in 51 injuries and minor structural damage in the area. TSGMN station AI127 situated within the boundaries of Fethiye city, positioned at a R_{jb} distance of approximately 32.6 km from surface projection of the earthquake, is one of the 43 ground motion stations that recorded this event (See Figure 3.83 for East-West and North-South component recorded time histories).

Based on PSHA and the succeeding deaggragation analysis carried out for the site of the AI127 strong motion station, the earthquake event that took place on November 12 is very much below the ranks of the design event for Fethiye city, both from distance and magnitude aspects. However, even for such a smaller size event, a raw PGA value of 0.235g was observed in the E-W component ground motion recording retrieved from AI127 station. Such a large-amplitude motion has the potential to induce considerable nonlinear behavior within the terminal soil stratification, thus, from a seismic response analysis perspective, trigger a significant behavior.

In section 3.1.4, a vital limitation of the utilized seismic response methodologies, and the consequences of applying the suggested techniques outside the defined area of applicability, was demonstrated. In this section using the ground motion records of AI127 station as benchmark data, seismic ground response analysis are performed to visualize the effect of another vital restriction; the potential overestimation by a method pair if hazard-compatibility of input motions is not ensured during analyses. Herein, this is achieved by conducting each calculation case through adopting time series that are modified to comply with the 475-year-return-period-UHS determined at the subject site, and then comparing the analysis results with the reference data that is, as per deaggragation analysis, proved to be a product of a source mechanism that is critically smaller than the relevant design event.

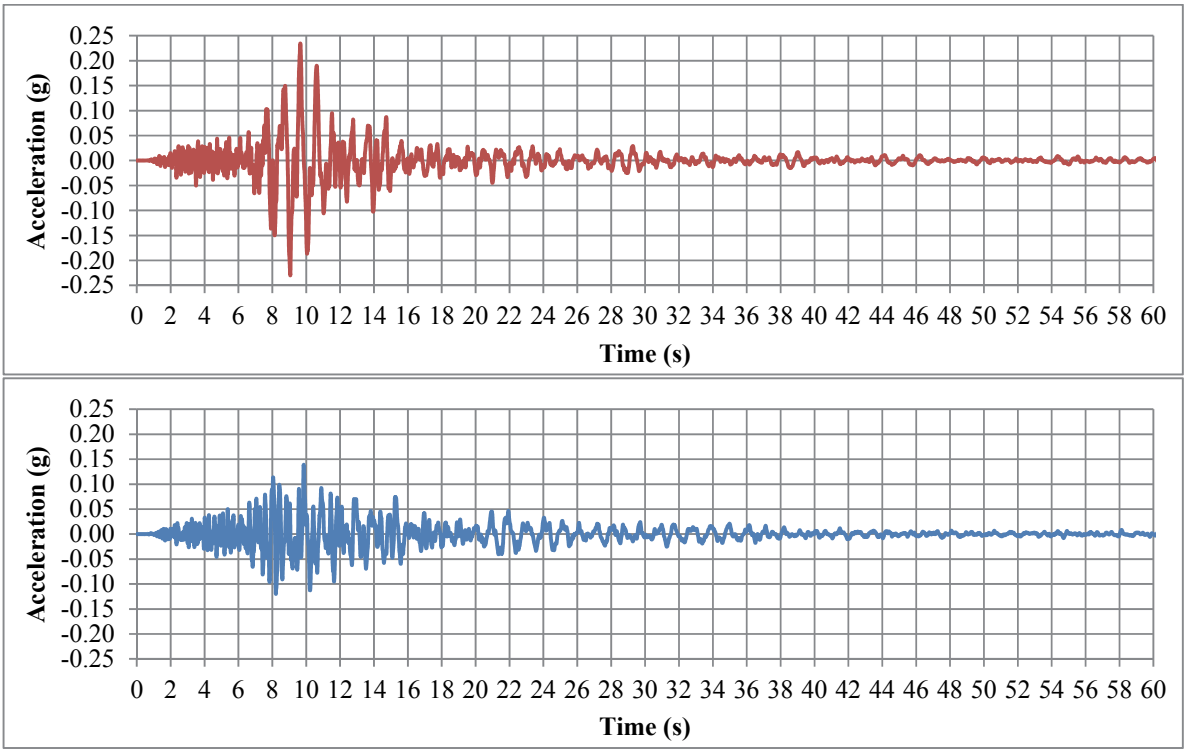

Figure 3.83. East-West (Top) and North-South (Bottom) components of the surface accelerations recorded by TSGMN Station AI127 during June 10, 2012; Fethiye earthquake

PGA, S_s and S_1 values at the locus site condition, determined for a 10% exceedance rate in 50 years, are defined as 0.32g, 0.71g and 0.22g, respectively, for Fethiye Station site [17]. In order to conduct ground response analyses, it is necessary to first develop a set of records, consisting of at least 10 strike-slip/normal events that satisfy a M_w range from 5.5 to 6.5, a R_{jb} interval that extends between 10 to 50 km, and a V_{s30} range of 600-1000 m/s; in agreement with the PSHA findings. Table 3.10 demonstrates the list of 22 earthquake time series that are found to be well-suited with the stipulated criteria, and, thus, deemed right for the subject application. Figures 3.84 to 3.87 show the 5%-damped response spectra of unscaled record components, and the pertaining input time-histories prepared by PGA scaling, scaling to obtain the best-fit mean spectrum, and nonstationary spectral matching, respectively, along with the UHS determined for the interested location, computed at the reference site condition in terms of seismic hazard results.

Table 3.10. List of earthquake time histories selected for use with the ground response analyses performed for AI127 TSGMN station

Record No.	Event	M_w	R_{jb} (km)	V_{s30} (m/s)	Record File	PGA
1	Chi-Chi-Taiwan-04 (1999)	6.2	12.4	680.0	NGA No#2739 (CHY080-N)	0.120
2	Victoria-Mexico (1980)	6.33	13.8	659.6	NGA No#265 (CPE045)	0.621
3	Morgan Hill (1984)	6.19	31.9	622.9	NGA No#471 (SJL360)	0.069
4	Morgan Hill (1984)	6.19	31.9	622.9	NGA No#472 (SJR270)	0.078
5	Morgan Hill (1984)	6.19	14.9	1428.0	NGA No#455 (G01230)	0.069
6	Morgan Hill (1984)	6.19	14.9	1428.0	NGA No#455 (G01320#2)	0.096
7	Chi-Chi-Taiwan-04 (1999)	6.2	33.5	652.9	NGA No#2897 (TCU138-W)	0.047
8	Chi-Chi-Taiwan-04 (1999)	6.2	39.3	679.9	NGA No#2753 (CHY102-E)	0.059
9	Chi-Chi-Taiwan-04 (1999)	6.2	39.3	679.9	NGA No#2753 (CHY102-N)	0.053
10	Irpinia- Italy-02 (1980)	6.2	14.7	1000.0	NGA No#297 (B-BIS000)	0.075
11	Irpinia- Italy-02 (1980)	6.2	20.4	1000.0	NGA No#303 (B-STU270)	0.077
12	Chi-Chi-Taiwan-04 (1999)	6.2	27.2	680.0	NGA No#2873 (TCU089-E)	0.031
13	Irpinia- Italy-02 (1980)	6.2	17.8	1000.0	NGA No#296 (B-BAG000)	0.048
14	Coyote Lake (1979)	5.74	10.2	1428.0	NGA No#146 (G01320#1)	0.133
15	Chi-Chi-Taiwan-04 (1999)	6.2	37.5	680.0	NGA No#2935 (TTN051-E)	0.065
16	Chi-Chi-Taiwan-04 (1999)	6.2	37.5	680.0	NGA No#2935 (TTN051-N)	0.076
17	Norcia- Italy (1979)	5.9	[1.7]	659.6	NGA No#156 (F-CSC-NS)	0.161
18	Chi-Chi-Taiwan-04 (1999)	6.2	39.7	680.0	NGA No#2820 (KAU050-E)	0.069
19	Little Skull Mtn-NV (1992)	5.65	23.8	659.6	NGA No#1741 (Lsm2270)	0.086
20	Big Bear-01 (1992)	6.46	[33.8]	684.9	NGA No#934 (SVP090)	0.059
21	Big Bear-01 (1992)	6.46	[33.8]	684.9	NGA No#934 (SVP360)	0.070
22	Norcia- Italy (1979)	5.9	[31.4]	1000.0	NGA No#155 (F-BEV-NS)	0.040

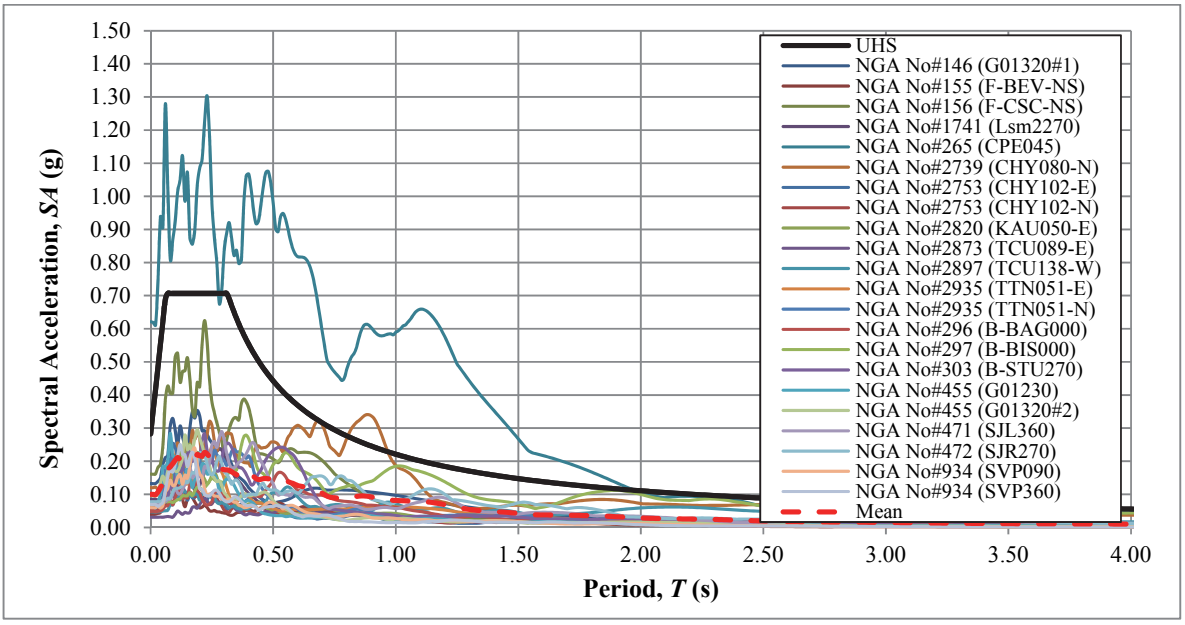

Figure 3.84. 5%-damped response spectra of earthquake record components selected for carrying out the site effects calculations for AI127 TSGMN station

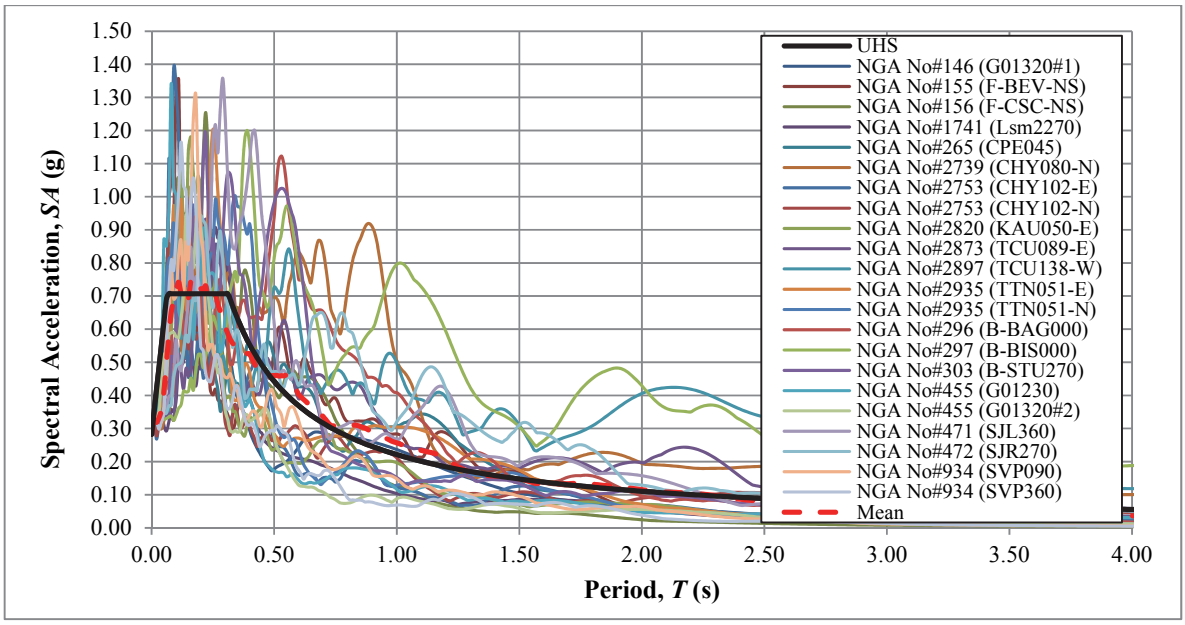

Figure 3.85. 5%-damped response spectra of earthquake record components presented in Figure 3.84 after normalization of each time series to the hazard PGA level of 0.32g

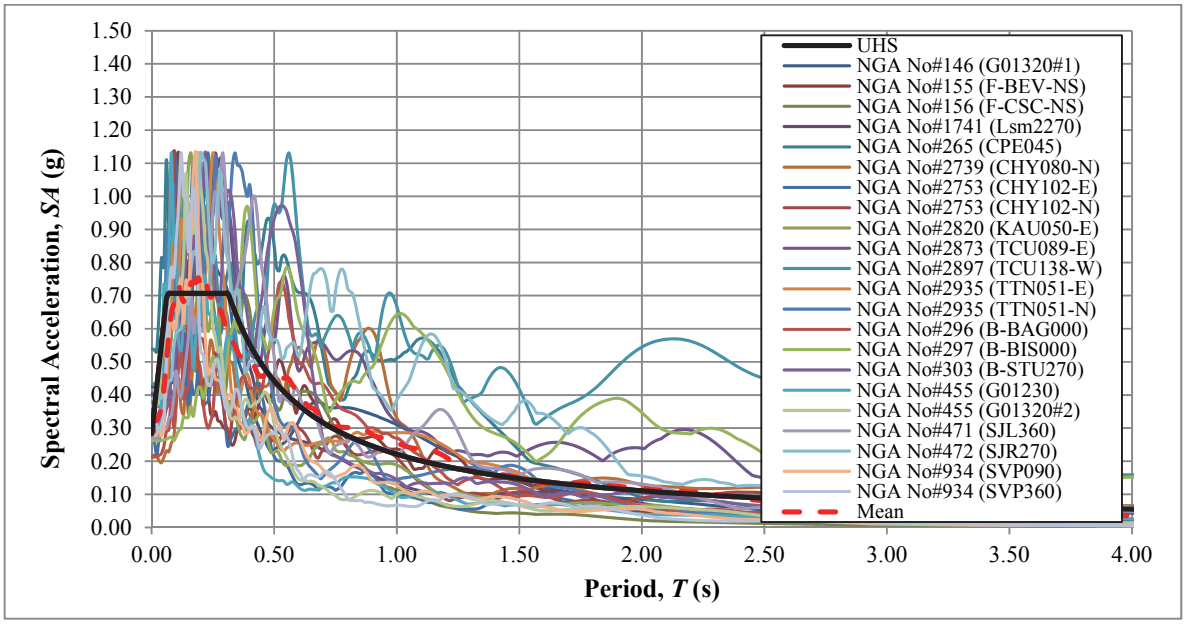

Figure 3.86. 5%-damped response spectra of earthquake record components shown in Figure 3.84 after scaling to find the mean spectrum that is best-fit with PSHA-decided UHS

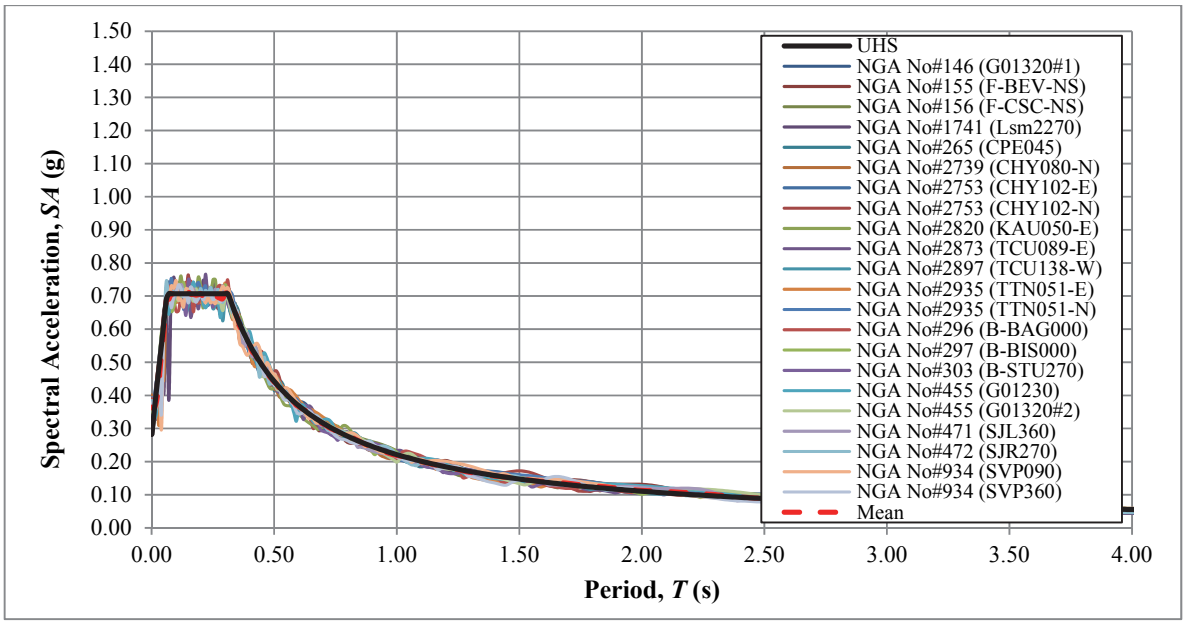

Figure 3.87. 5%-damped response spectra of earthquake record components presented in Figure 3.84 after nonstationary spectral matching as per the PSHA-determined UHS

Speaking in terms of the geological, geophysical and geotechnical information compiled for the station site, at the uppermost 34 m, the soil stratification beneath AI127 is prevailed by a clayey material that includes thin layers of coarse-grained-containing soils. The plasticity traits of the observed sedimentation show a wide changeability within this depth range, so even if the constituting materials are essentially the same, the dynamic soil properties at each depth differ in certain ways. The field testing results reported for the subject location suggests that the observed clay formations are made up of very soft layers of material that rather stiffens with increasing depth; measured V_s values extending from 170 m/s at the ground surface to 448 m/s at 34 m depth. The following weak-rock layering shows noticeably higher shear resistance that gradually grows toward the locus. Figure 3.88 graphically summarizes the properties of soil layering beneath the AI127 station down to reference site conditions

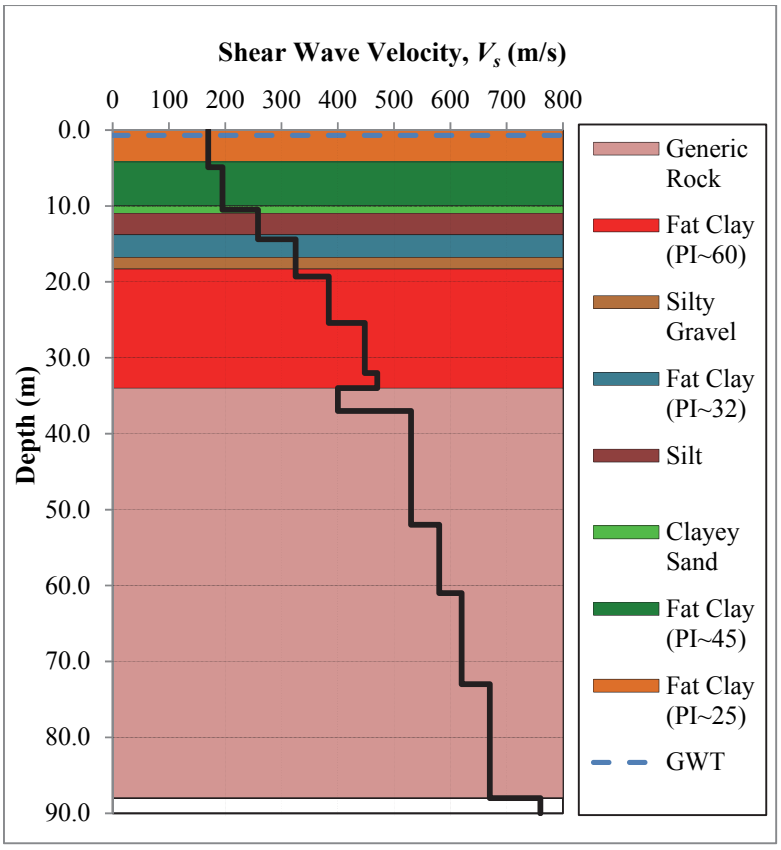

Figure 3.88. A visual depiction of soil layering and corresponding shear-wave velocity variation underneath the AI127 station; extending down to the reference site condition

In order to carry out the site effects calculations for AI127 TSGMN station, here, the lean clay PI=25 & 32, fat clay=45 and fat clay=60; silt/silty gravel; and generic rock layering recognized via field testing are simulated using the dynamic soil properties reported by Vucetic and Dobry [62], Darendeli [61], and EPRI [42] respectively. Figure 3.89 conveys a graphical representation of the adopted modulus reduction/damping curves. In the performed computations, the unit weight values of 17.30, 20.50 and 22.00 kN/m^3 are used for the topmost soil stratification and the following generic rock material present between 37 to 45 m, and 45 to 88m depths correspondingly.

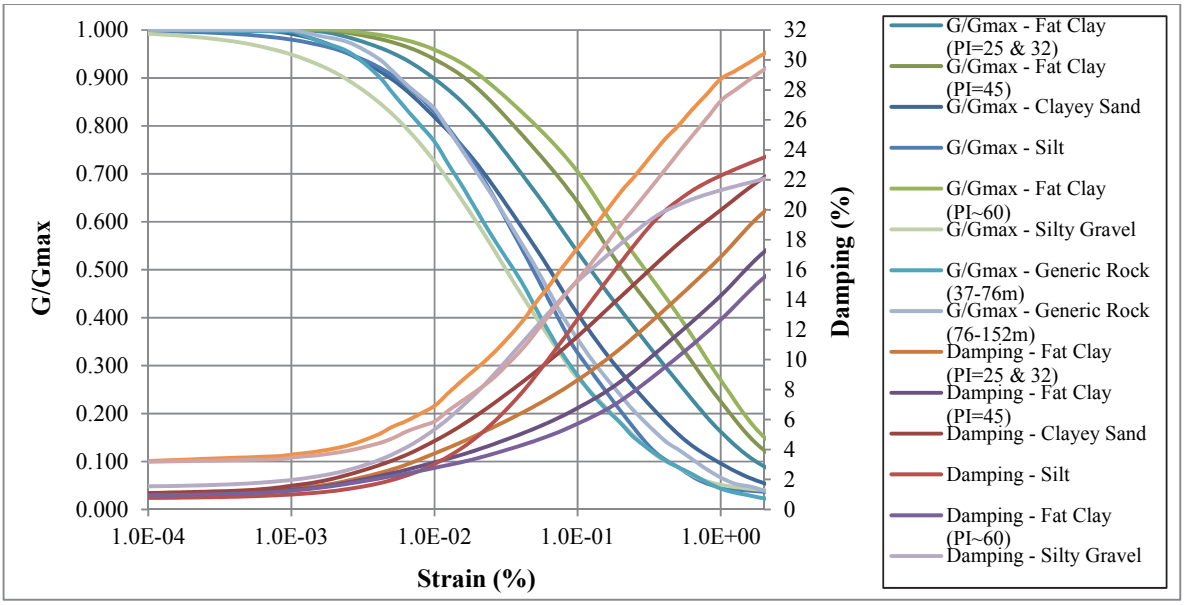

Figure 3.89. Modulus degradation and damping curves adopted for performing ground response analyses at the site of AI127 TSGMN station

Figures 3.90 and 3.91 demonstrate the mean and mean mean + standard deviation surface response results for AI127 TSGMN station site attained using each method pair. In each analysis situation, the initial peak witnessed on the response spectra for the observed ground motions, occuring at a period of roughly 0.70s, is fairly well simulated. Whereas, the fundamental peak generating the greatest spectral amplitude among the two components, i.e. peak spectral response of the E-W component time-history perceived at the period value of

just about 1.00s, is misidentified virtually in all analysis cases; often leading to spectrum patterns that stand to be significantly different from the recorded spectral behavior. One can easily conceive that this specific discrepancy is most probably a product of the unavoidable uncertainty in description of the velocity structure for a soil profile, coupled with the inevitable vagueness in definition of the depth of reference layer at the station site, as a consequence of the scarcity of accesible data for the subject area.

Judging as per the analysis results obtained to this point,for different station sites, the evident effect of both unpredicatibilities can be simply eliminated. In this specific application, however, the sizeable overestimation of spectral amplitudes (i.e. in the best-performing case of nonstationary spectral matching method\frequency independent computation process, a peak response ratio of about 1.466 was attained) appear to be naturally inescapable, owing to the incompatibility between calculation inputs (thus computed seismic responses) and the adopted benchmark data. This enunciates the importance of ensuring suitability between the projected hazard rate and the selected input to establish reasonable approximates of seismic response.

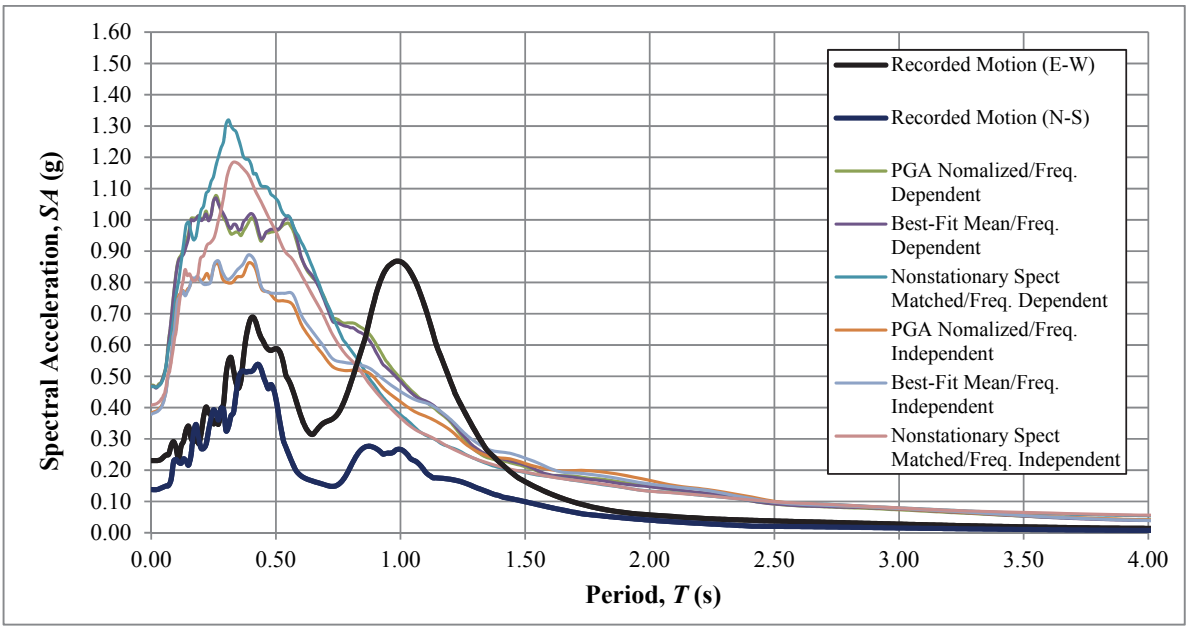

Figure 3.90. A comparison of the 5%-damped response spectra of mean surface response, determined using each method pair, with the observed behavior at AI127 TSGMN station

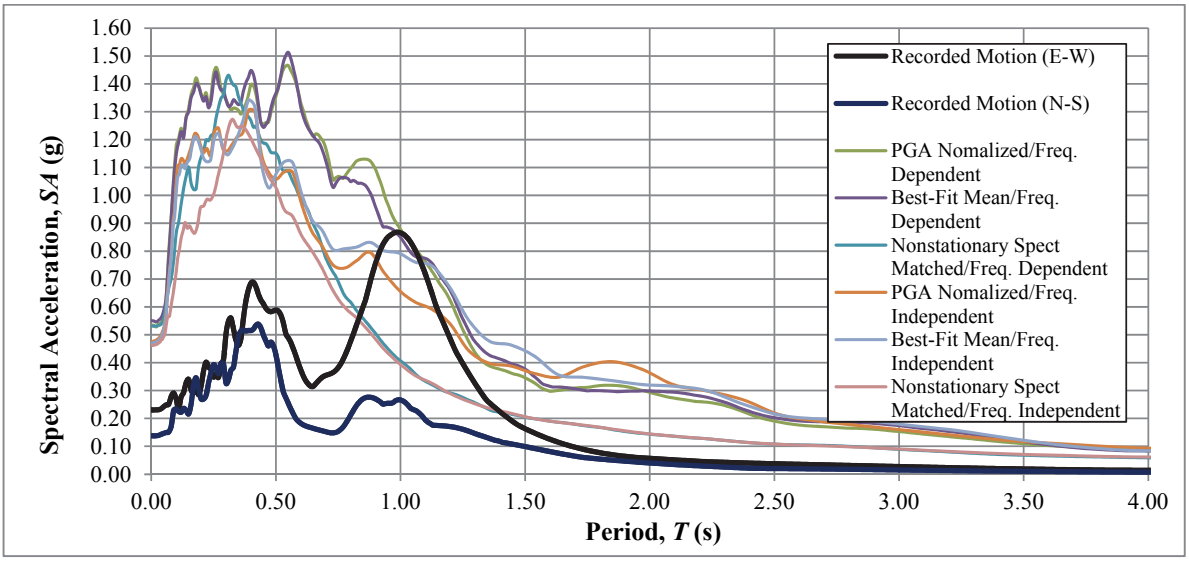

Figure 3.91. A comparison of the 5%-damped response spectra of mean + std. dev. surface response, determined via each method pair, with the observed behavior at AI127 station

3.2. Ground-Response-Analyses-Based Site-Specific UHS Results

Based on the analysis results displayed in the previous section, one can easily conclude that through using a frequency independent calculation mode adopting input motions prepared via nonstationary spectral matching technique, very close approximations of the spectral amplitude ranks of a seismic response, observed during actual seismic events, can be established. Thus, by proposing a proficient spectrum construction scheme to eliminate the witnessed discrepancies between the frequency-content estimation of a calculated response and the perceived seismic response, one can in fact develop exceptionally close predictions of the actual behavior.

In this study a NEHRP-inspired two-point site specific Uniform Hazard Spectra is recommended for spectrum assembling purposes, given this approach appear to be well-suited for a quick description of site-specific design spectra, by means of a procedure such as conditional mean spectrum, without a compromise from the anticipated frequency-characteristics. The fundamental outset here is to maintain the procedure at the simplest extent

possible while providing effective solutions for the studied problem, hence a spectrum construction method that develops a UHS merely based on definition of any two parameters required for spectrum calculations appear to be perfectly suited for the subject application.

Herein, a piecewise spectrum construction procedure that utilizes the calculation output as following is developed for using in connection with the proposed seismic response calculation method. In this technique the parameter definitions for S_s *and* S_1 are very straightforward. In the event that the peak spectral acceleration calculated using the suggested procedure exceeds the 1.50g mark;

$$S_s = \max(SA) \tag{3.1}$$

and

$$S_1 = SA(1s) \tag{3.2}$$

else

$$S_1 = SA(0.7s) \tag{3.3}$$

where *SA*(1s) and *SA*(0.7s) denote the spectral acceleration values obtained at 1.0s and 0.7s period values respectively. The reason for this adjustment in the spectra for smaller amplitude levels stems from the observation that if identical parameter definitions are adopted in both situations, the long-period responses are, at certain times, slightly miscalculated; requiring a slightly conservative setting for S_1 values.

Figures 3.92 to 3.101 demonstrate the two-point site specific UHS calculated for Denizli (AI107), Dursunbey (AI145), Horasan (AI059), Dinar (AI137), Ceyhan (AI022), Yenisehir (AI019), Adapazari (AI005), Bolu (AI010), Duzce (AI011), and Fethiye (AI127) TSGMN stations, respectively, using the spectrum construction process defined above, alongside the standardized spectrums proposed in FEMA P-750 [54], Eurocode 8 [55] and TSC07 [56]. This implementation is particularly significant, as it points out the existing inadequacies of current code procedures, and how the proposed technique can create an alternative path to estimate

seismic ground response, and eventually design spectrums; therefore, serve as an efficient tool to amend current practice to better estimate the effect of seismic tremors.

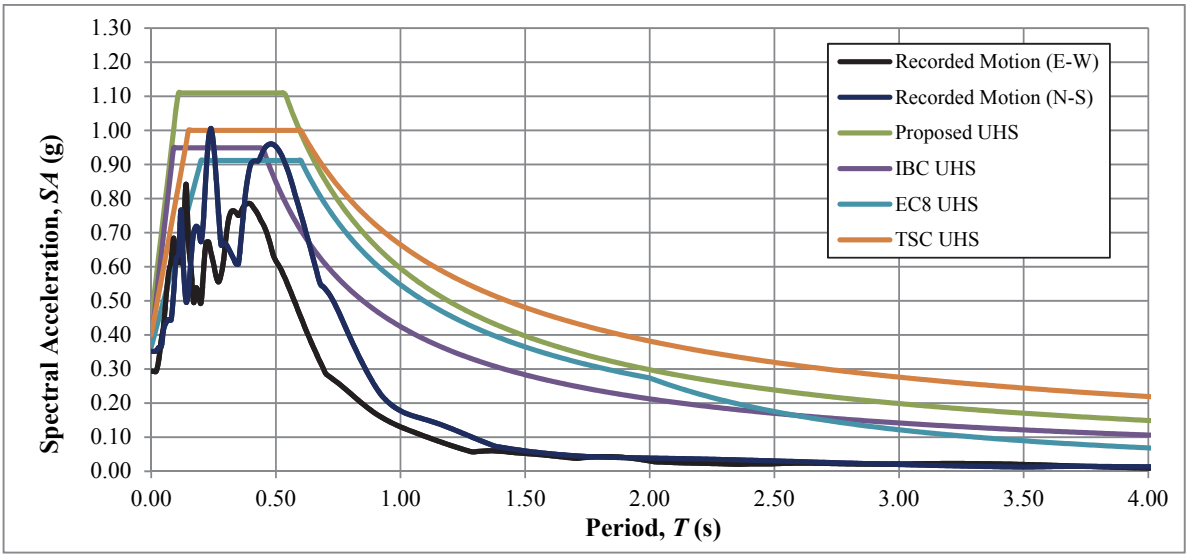

Figure 3.92. A comparison of the 5%-damped UHS determined via suggested methodology with the observed behavior at AI107 station and the relevant code-based spectra

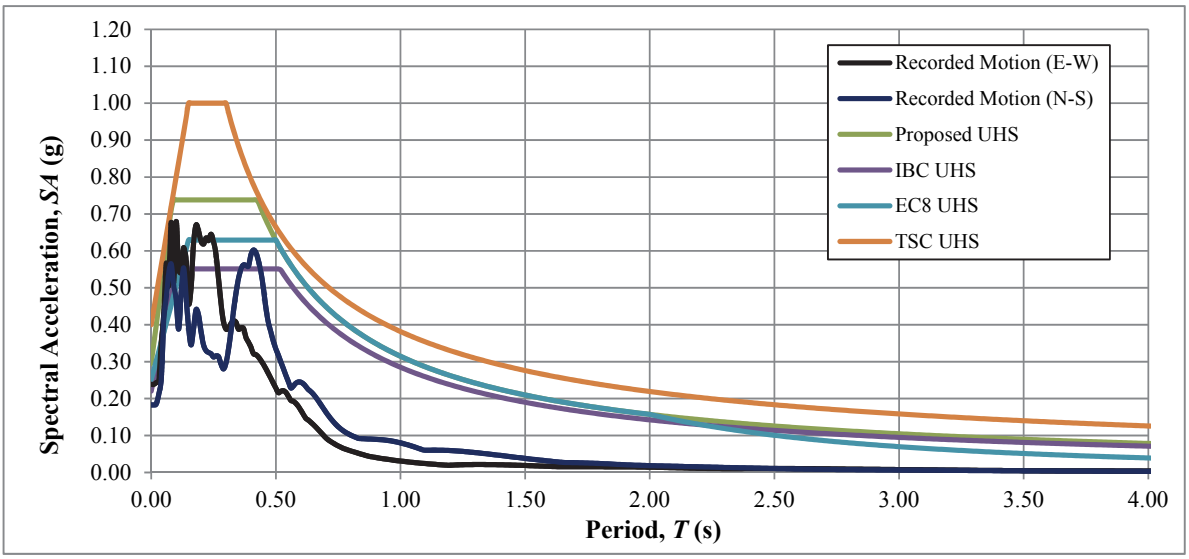

Figure 3.93. A comparison of the 5%-damped UHS determined via suggested methodology with the observed behavior at AI145 station and the relevant code-based spectra

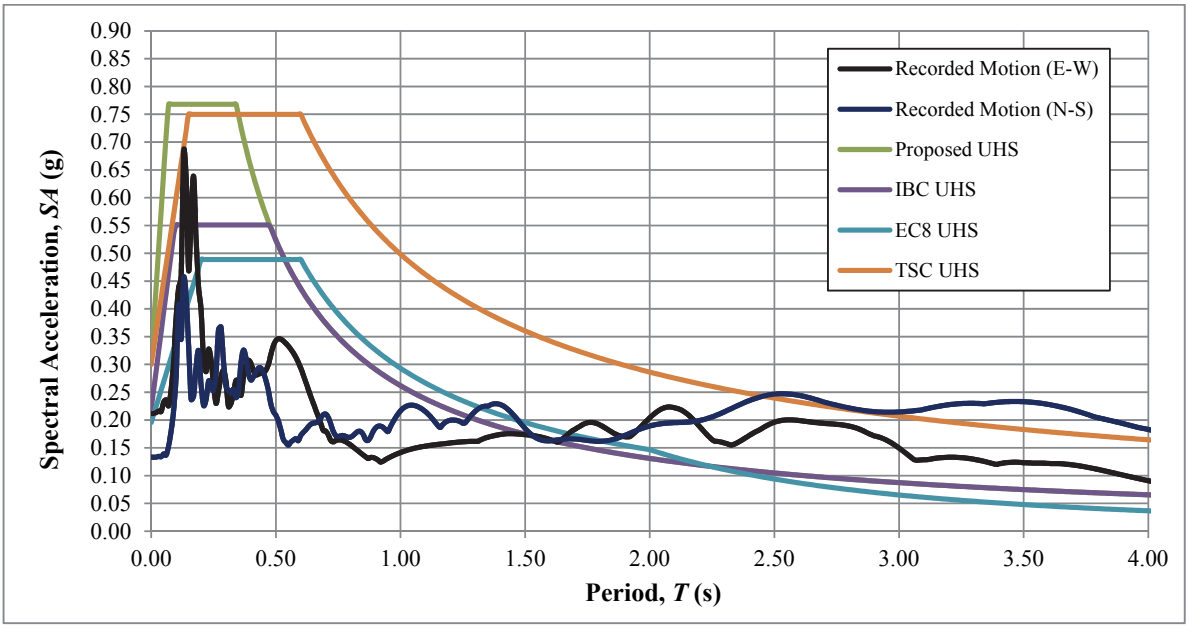

Figure 3.94. A comparison of the 5%-damped UHS determined via suggested methodology with the observed behavior at AI059 station and the relevant code-based spectra

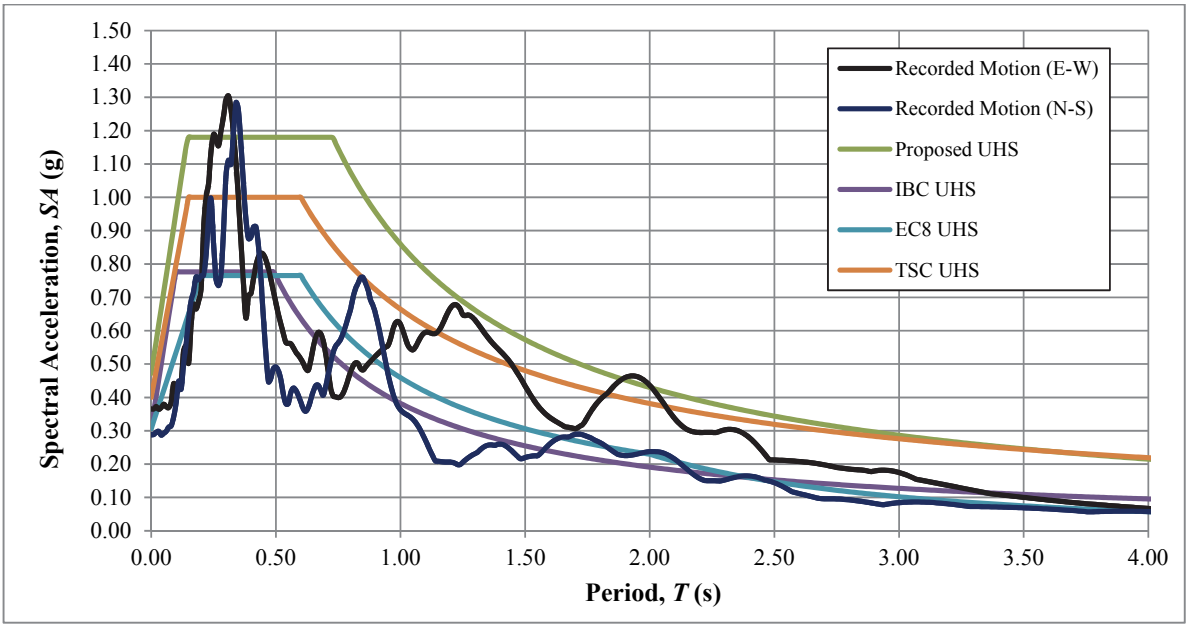

Figure 3.95. A comparison of the 5%-damped UHS determined via Method#4 with the observed behavior at AI137 station and the relevant code-based spectra

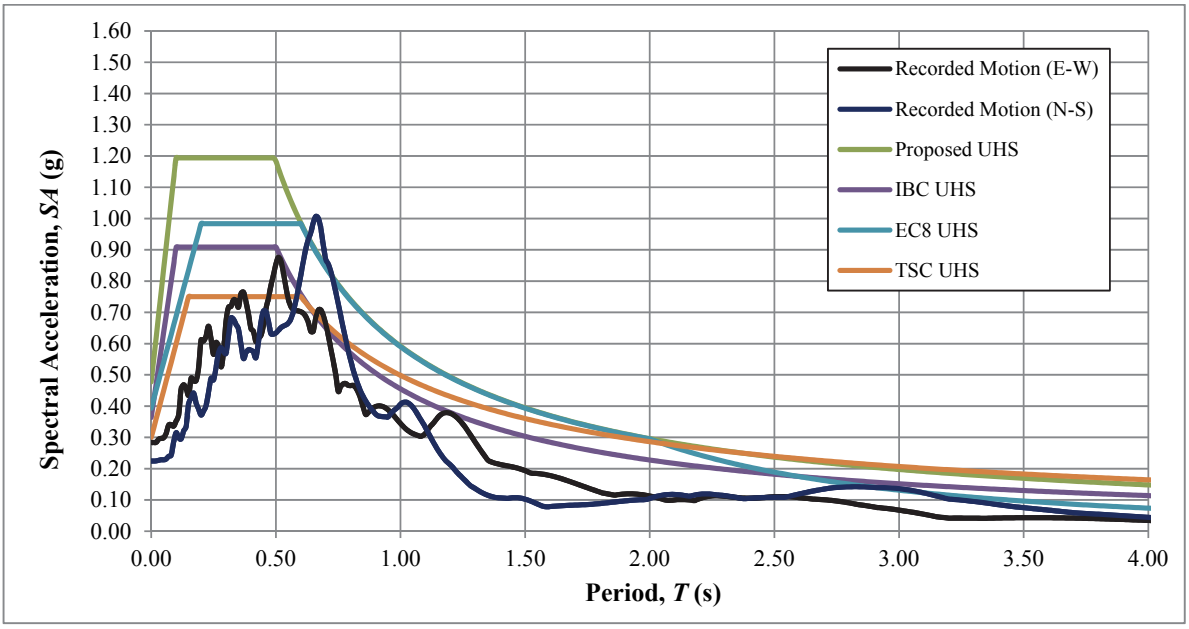

Figure 3.96. A comparison of the 5%-damped UHS determined via suggested methodology with the observed behavior at AI022 station and the relevant code-based spectra

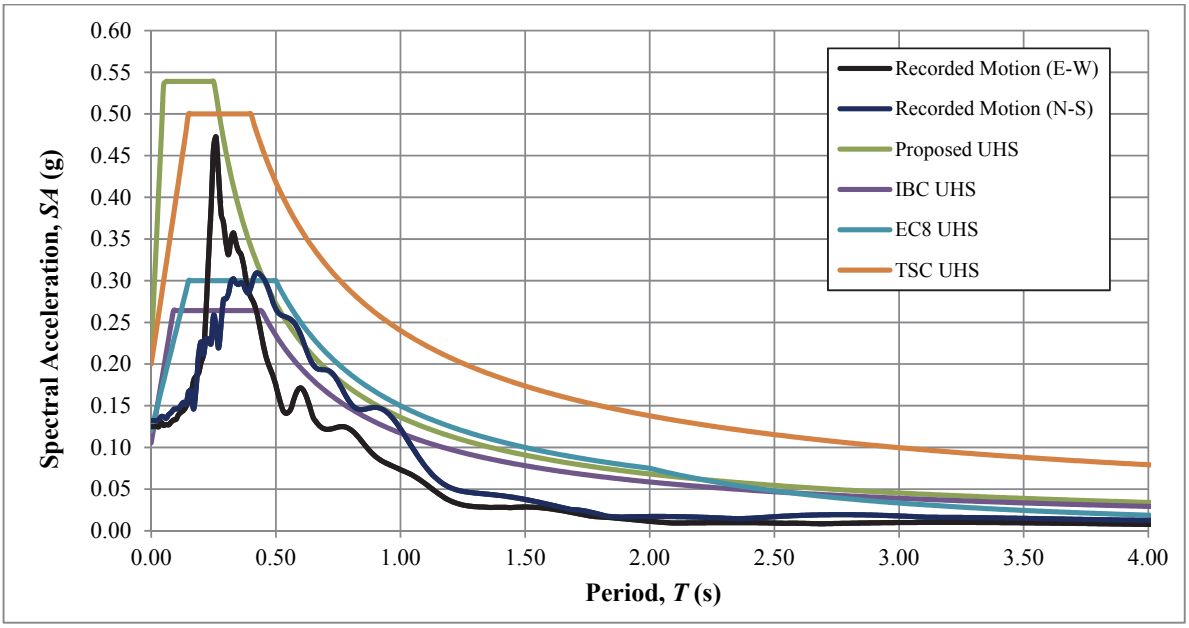

Figure 3.97. A comparison of the 5%-damped UHS determined via suggested methodology with the observed behavior at AI019 station and the relevant code-based spectra

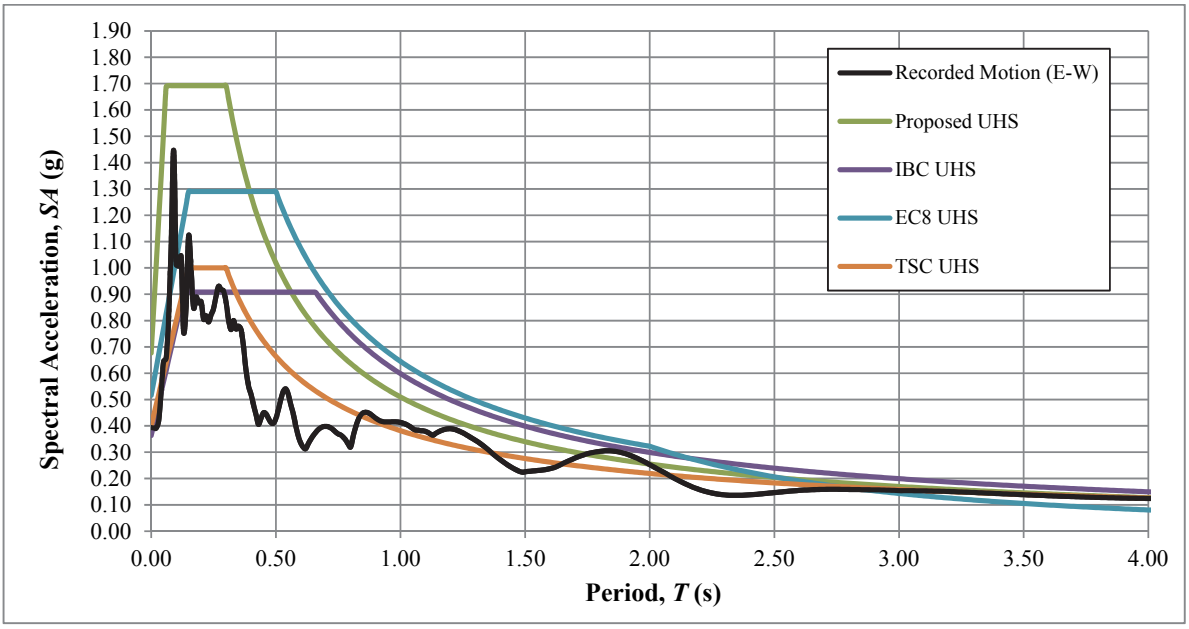

Figure 3.98. A comparison of the 5%-damped UHS determined via suggested methodology with the observed behavior at AI005 station and the relevant code-based spectra

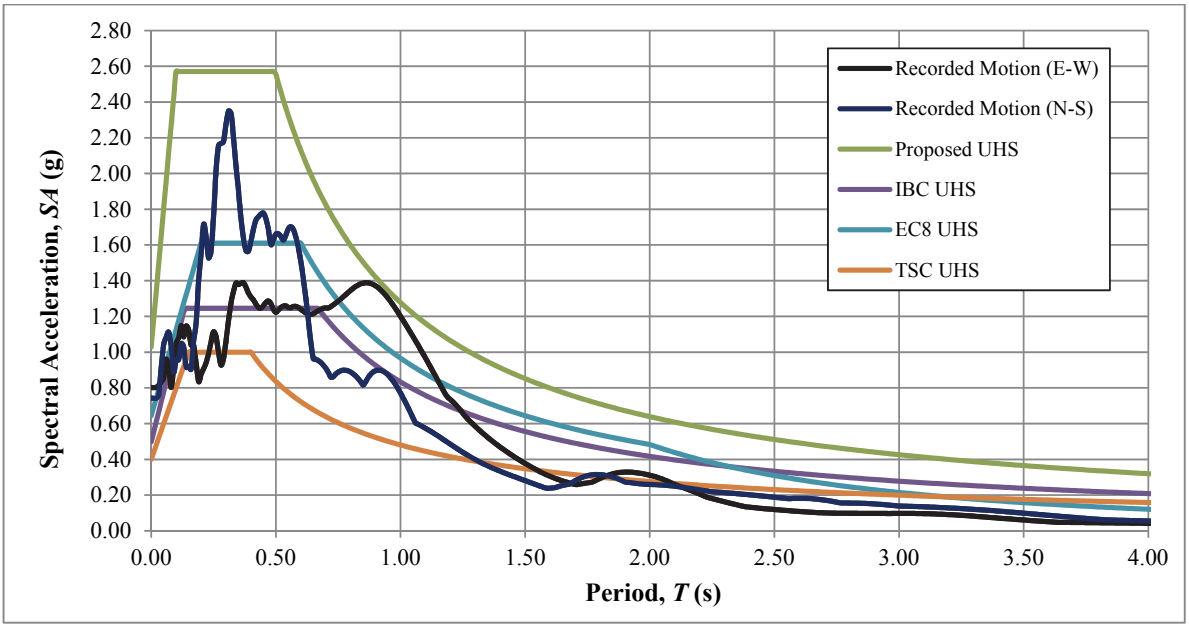

Figure 3.99. A comparison of the 5%-damped UHS determined via suggested methodology with the observed behavior at AI010 station and the relevant code-based spectra

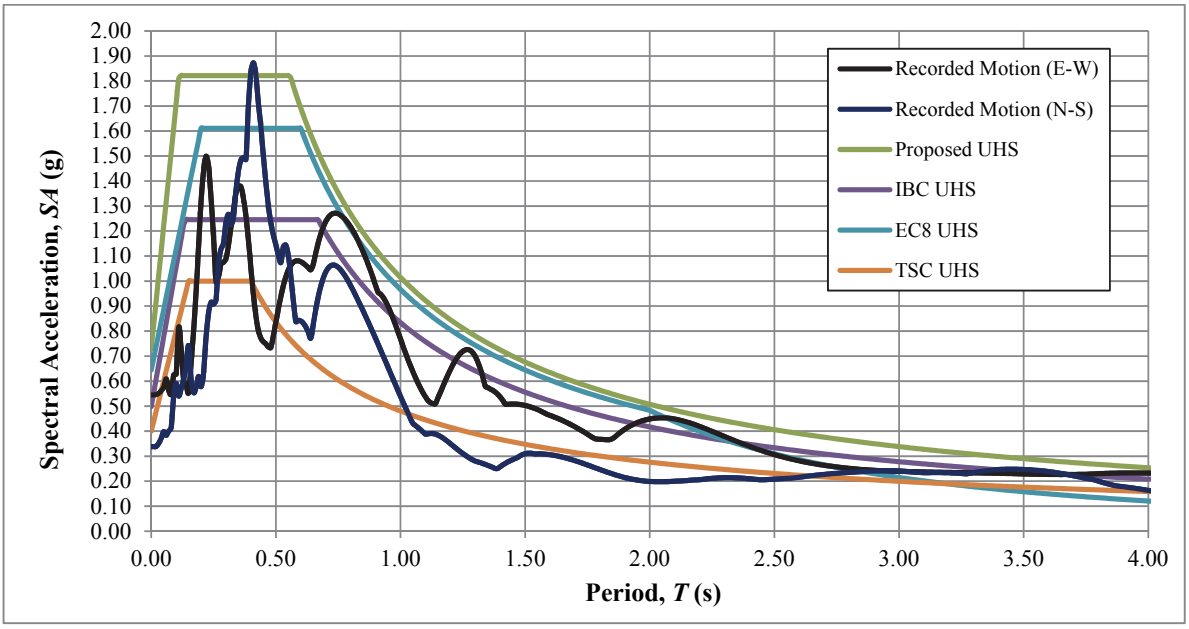

Figure 3.100. A comparison of the 5%-damped UHS determined via suggested methodology with the observed behavior at AI011 station and the relevant code-based spectra

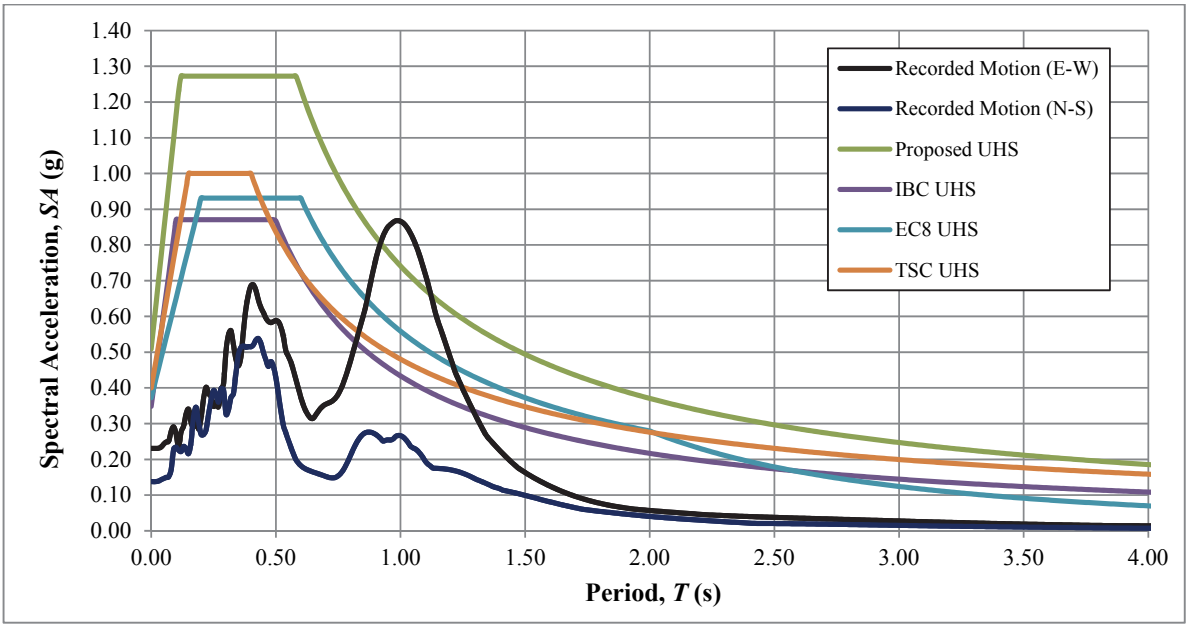

Figure 3.101. A comparison of the 5%-damped UHS determined via suggested methodology with the observed behavior at AI127 station and the relevant code-based spectra

4. CONCLUSIONS

In order to approximate the seismic ground response at an interested location, it is necessary to first establish an objective site effects calculation procedure, which will serve as an accurate tool preordained for the purpose. This study focused on constructing a practice-oriented method intended to address this aspect of the seismic response problem.

Herein, the effectiveness of six different site effects calculation methodologies, assembled from three different input motion selection (namely PGA scaling, scaling to obtain the best-fit mean spectrum, and nonstationary spectral matching) and two distinct frequency dependent/independent 1-D site response analysis codes are evaluated using 10 benchmark cases extracted from separate TSGMN-recorded events. The results of the performed analysis indicate that a site effects calculation procedure composed of a nonstationary spectral matching technique and a frequency independent 1-D wave propagation solution based calculation routine, in fact, very closely resembles the earthquake shaking triggered by a design event. For the assessed situations, such a pair led to an approximation extent ranging from roughly 2-16%. Isolating the effects of each component, this is a consequence of the reduced scatter around the target UHS at the reference site condition ensured by the effective wavelet manipulations and the appropriate damping modeling warranted through frequency-independent solution.

UHS developed using such a technique result in a truthful representation of the ground response induced by a design event. This also justifies the use of such a system as a tool to rehabilitate current code spectra; observed to perform very poorly compared to the determined resemblance levels.

APPENDIX: INDIVIDUAL SURFACE RESPONSES CALCULATED DURING GROUND RESPONSE ANALYSES

In order to sustain the displayed outcomes at an easy-to-read layout, during discussions, only the calculation results for mean and mean + standard deviation spectra were displayed. In this chapter, so to not leave out an important constituent of the overall findings, resultant spectra attained via each method, also including responses attained for individual time histories, are illustrated.

For simplicity in defining figure captions, following notation is designated to describe the adopted method pairs;

- Method#1: Frequency independent calculation scheme using input motions scaled to hazard PGA
- Method#2: Frequency independent calculation method utilizing input motions scaled to obtain best-fit mean spectrum
- Method#3: Frequency independent calculation mode adopting input motions prepared through nonstationary spectral matching technique
- Method#4: Frequency dependent calculation scheme using input motions scaled to hazard PGA
- Method#5: Frequency dependent calculation method utilizing input motions scaled to obtain best-fit mean spectrum
- Method#6: Frequency dependent calculation mode adopting input motions prepared through nonstationary spectral matching technique

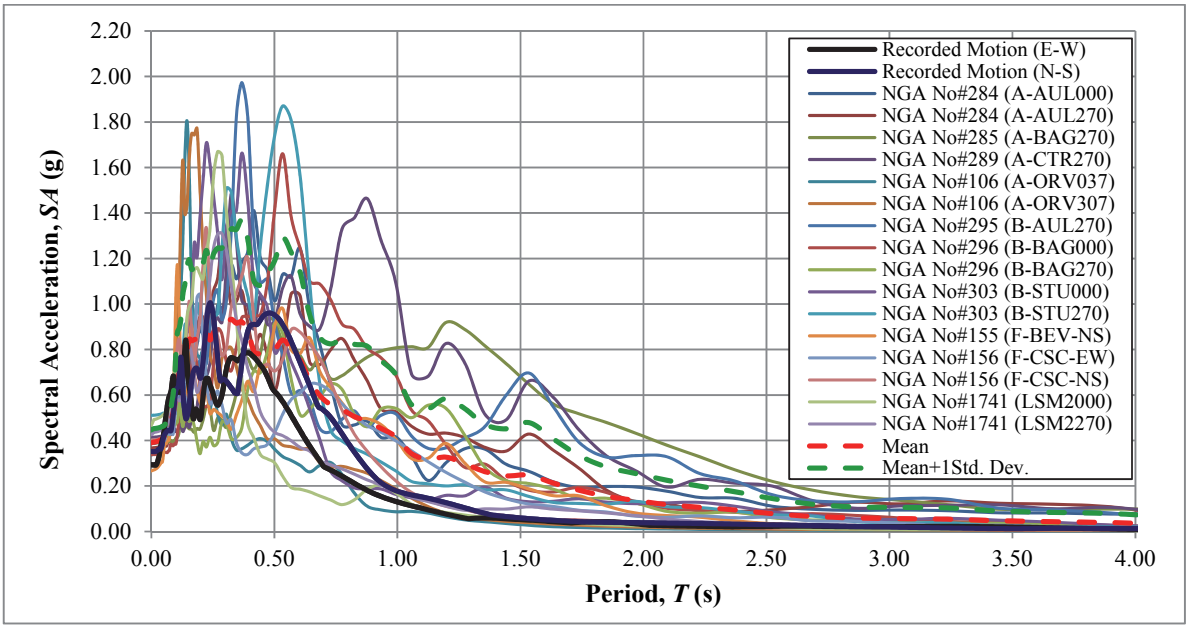

Figure A.1. A comparison of the mean and mean+1 standard deviation response spectrums, determined using Method#1, with the spectral response observed at AI107 TSGMN station

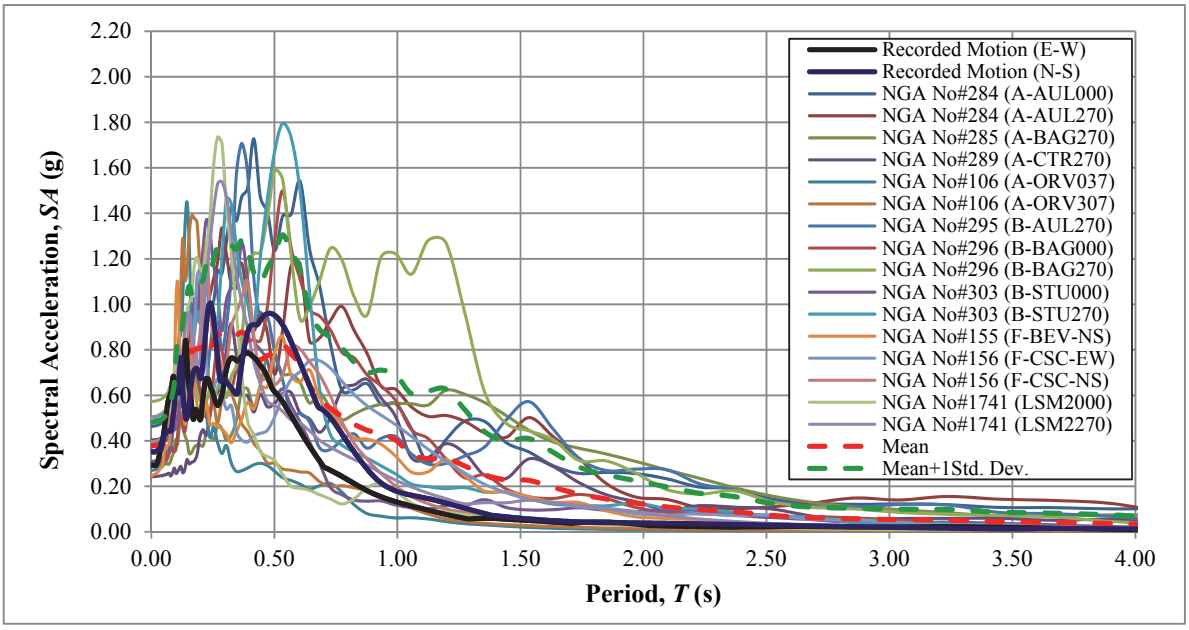

Figure A.2. A comparison of the mean and mean+1 standard deviation response spectrums, determined using Method#2, with the spectral response observed at AI107 TSGMN station

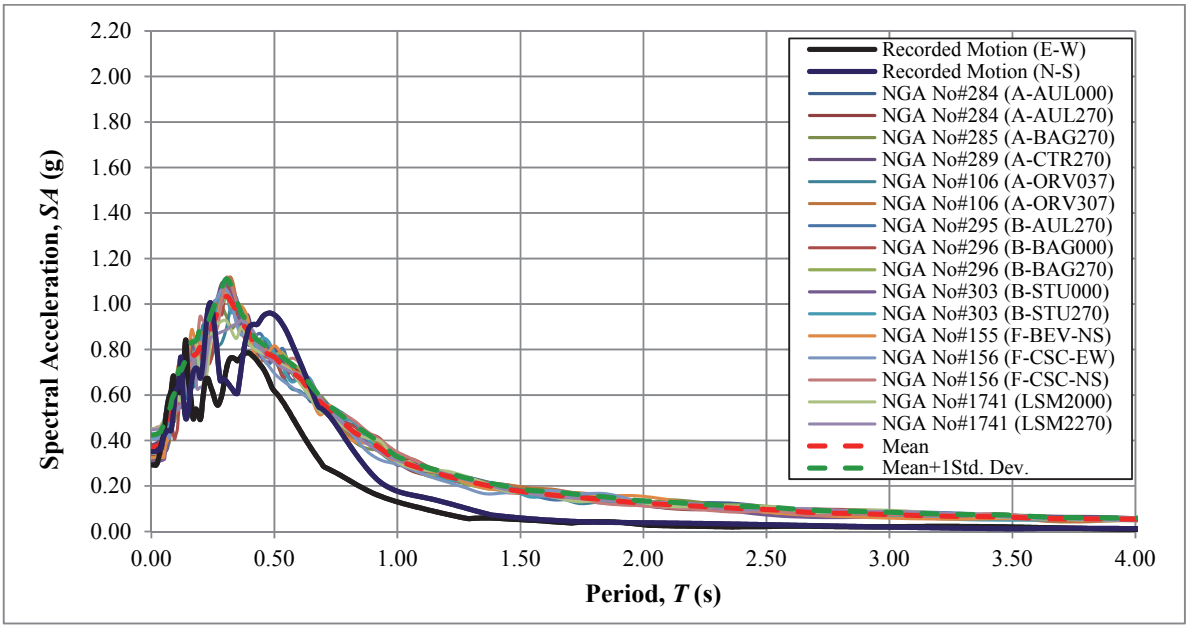

Figure A.3. A comparison of the mean and mean+1 standard deviation response spectrums, determined using Method#3, with the spectral response observed at AI107 TSGMN station

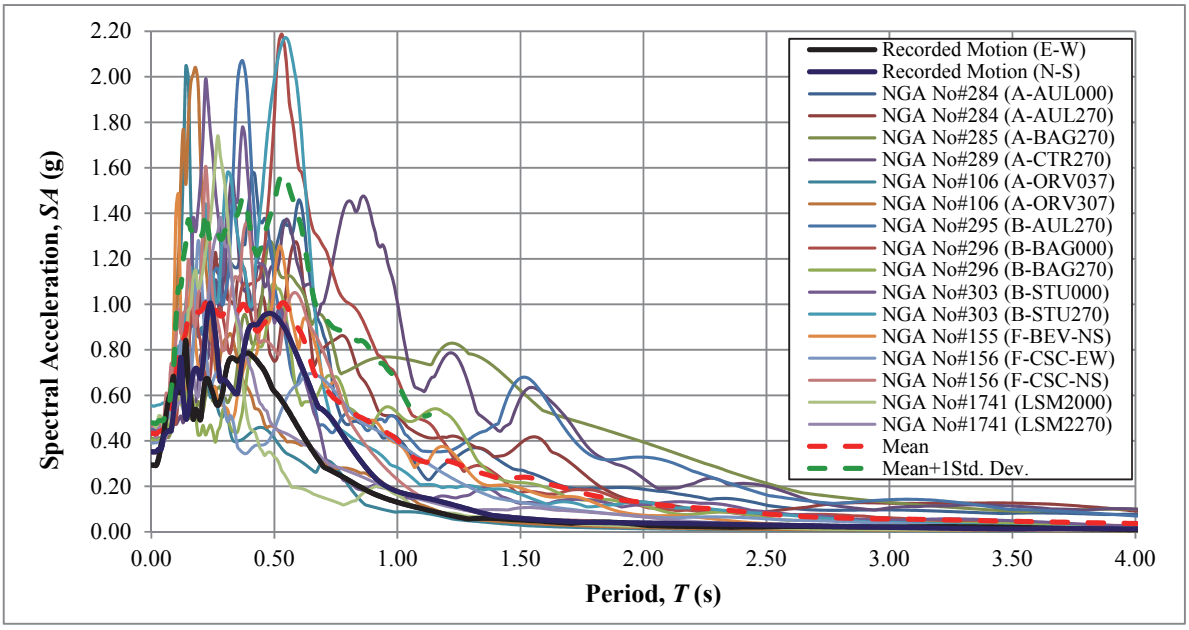

Figure A.4. A comparison of the mean and mean+1 standard deviation response spectrums, determined using Method#4, with the spectral response observed at AI107 TSGMN station

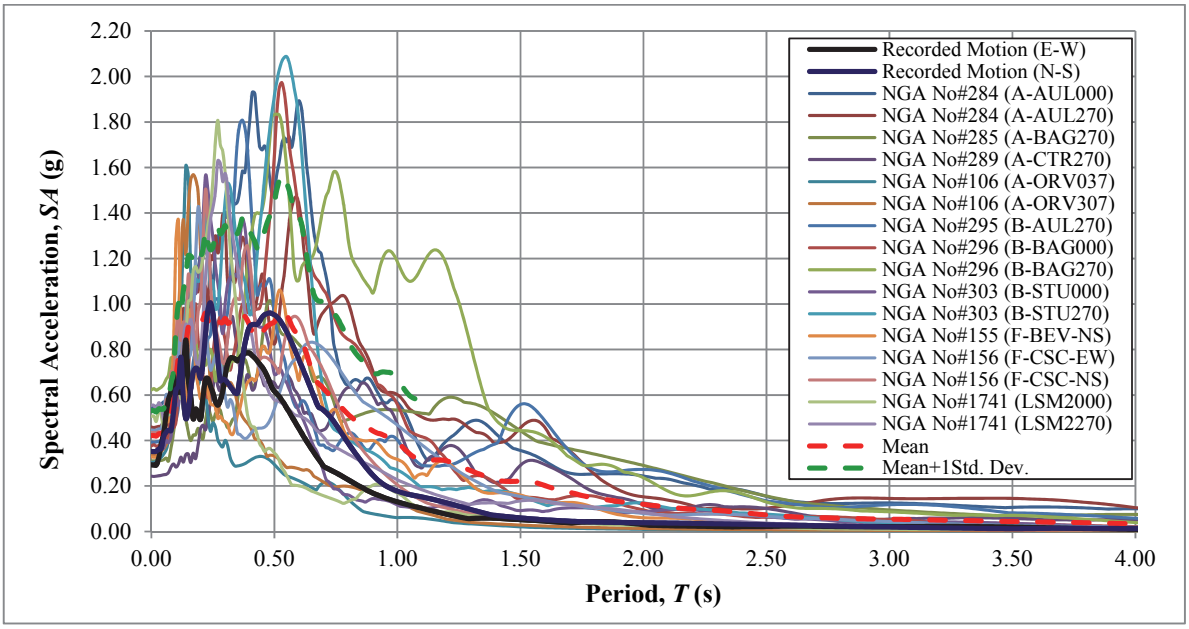

Figure A.5. A comparison of the mean and mean+1 standard deviation response spectrums, determined using Method#5, with the spectral response observed at AI107 TSGMN station

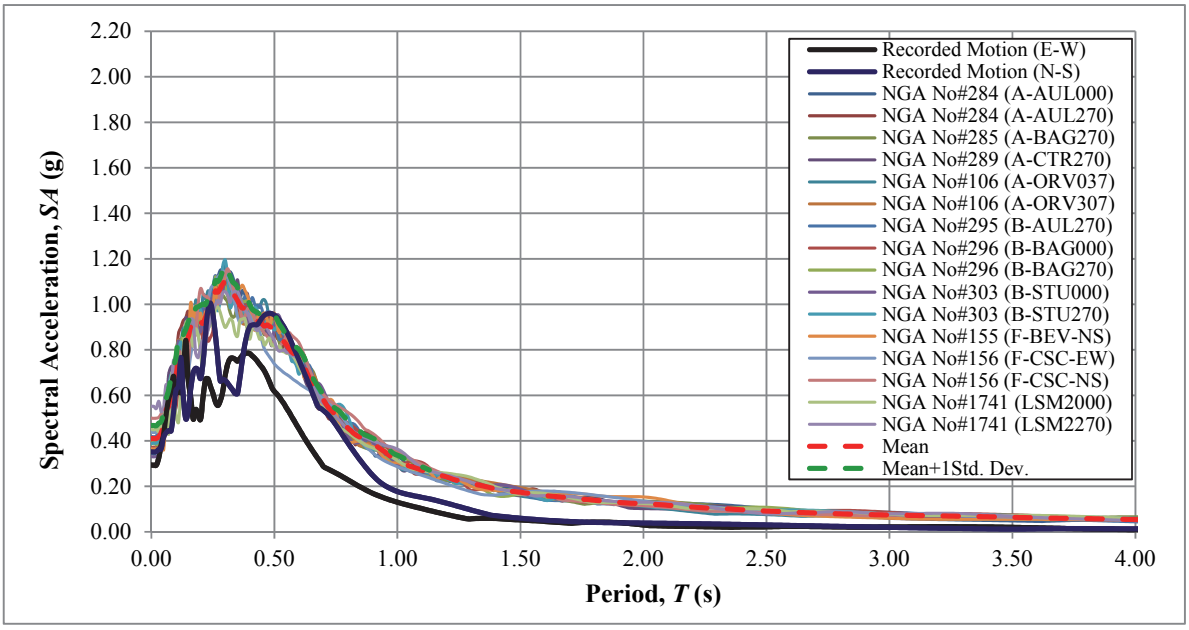

Figure A.6. A comparison of the mean and mean+1 standard deviation response spectrums, determined using Method#6, with the spectral response observed at AI107 TSGMN station

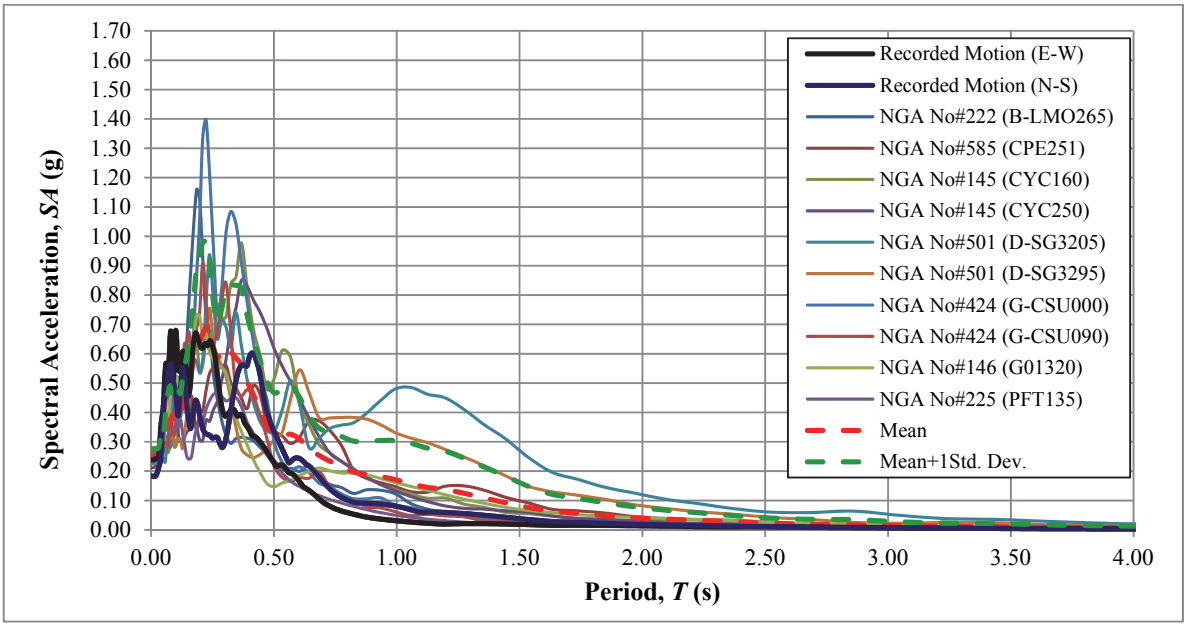

Figure A.7. A comparison of the mean and mean+1 standard deviation response spectrums, determined using Method#1, with the spectral response observed at AI145 TSGMN station

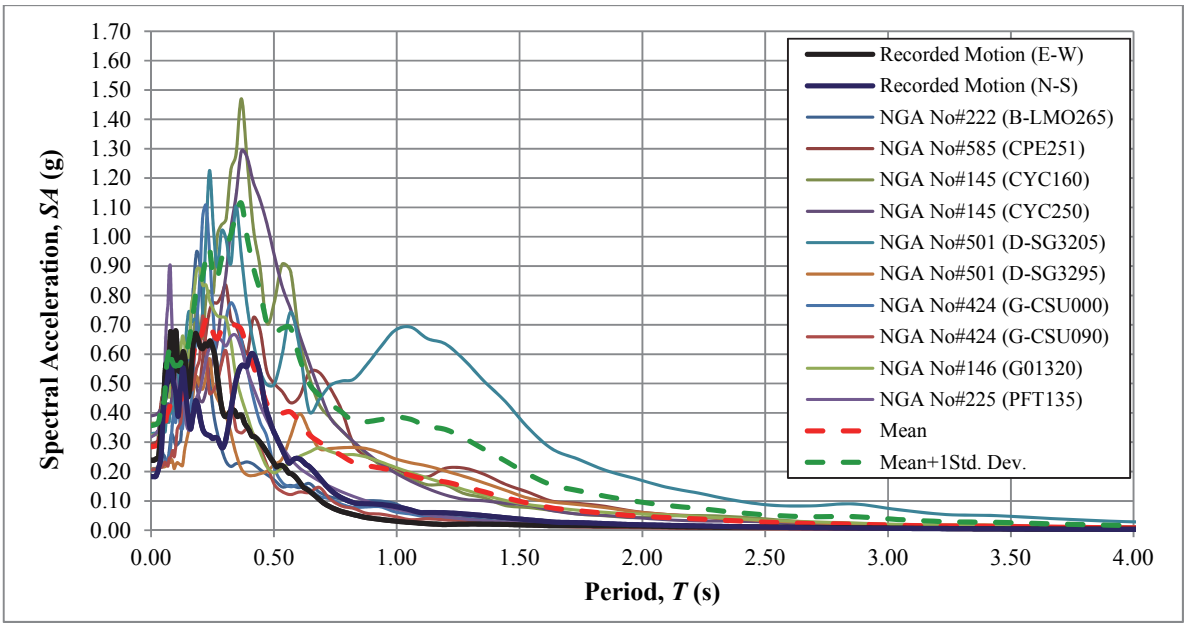

Figure A.8. A comparison of the mean and mean+1 standard deviation response spectrums, determined using Method#2, with the spectral response observed at AI145 TSGMN station

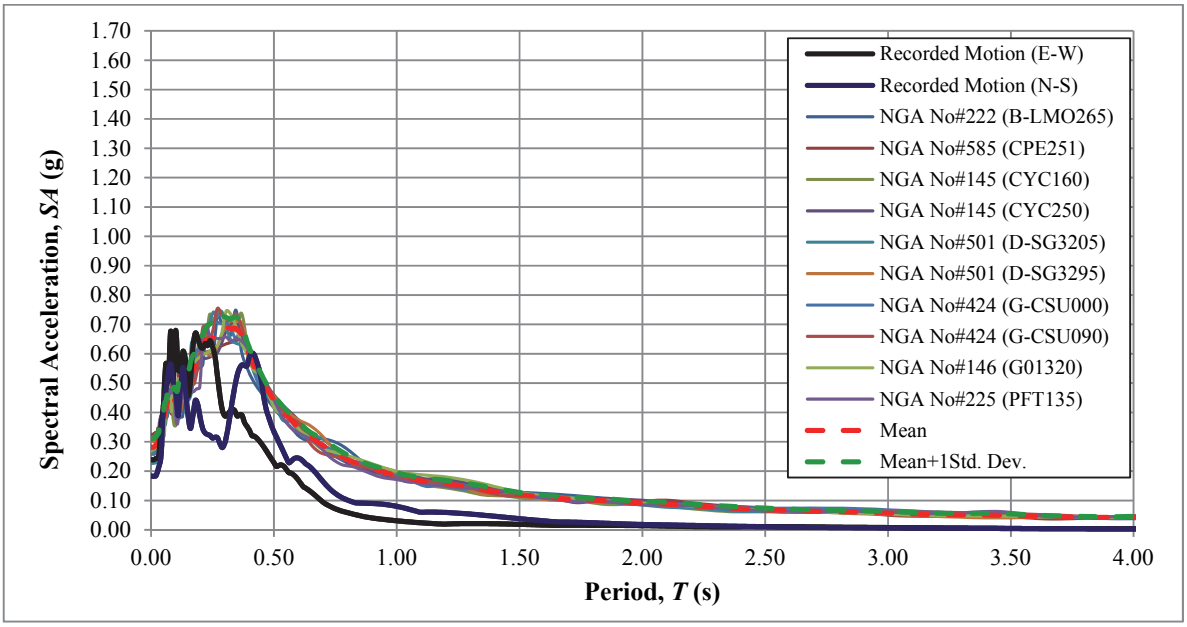

Figure A.9. A comparison of the mean and mean+1 standard deviation response spectrums, determined using Method#3, with the spectral response observed at AI145 TSGMN station

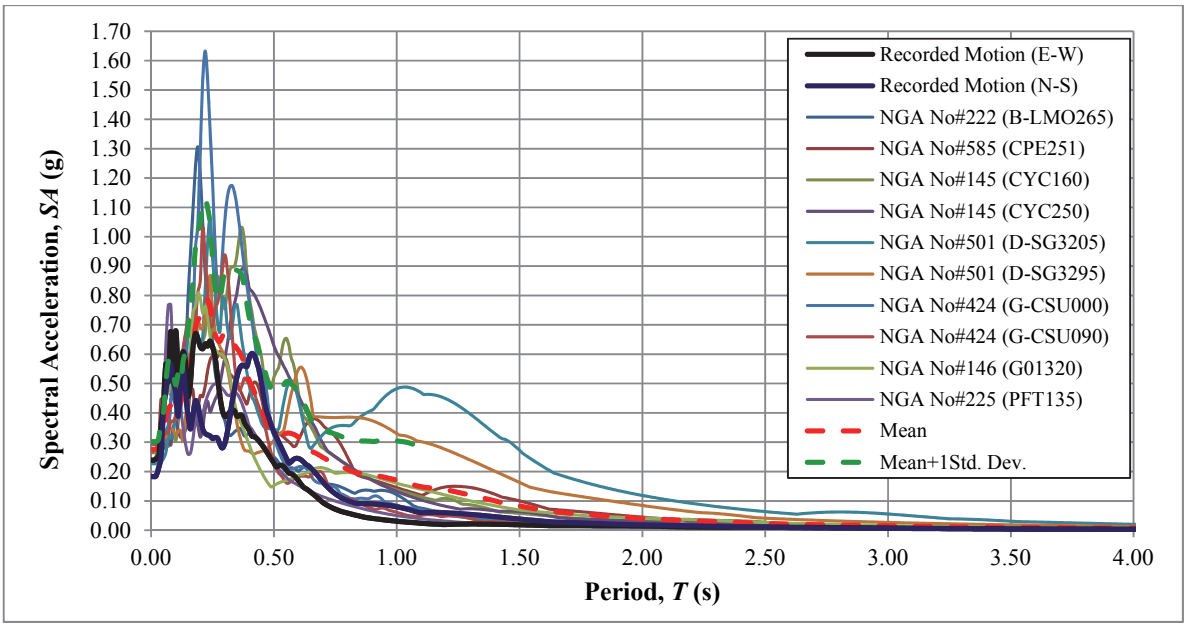

Figure A.10. A comparison of the mean and mean+1 standard deviation response spectrums, determined using Method#4, with the spectral response observed at AI145 TSGMN station

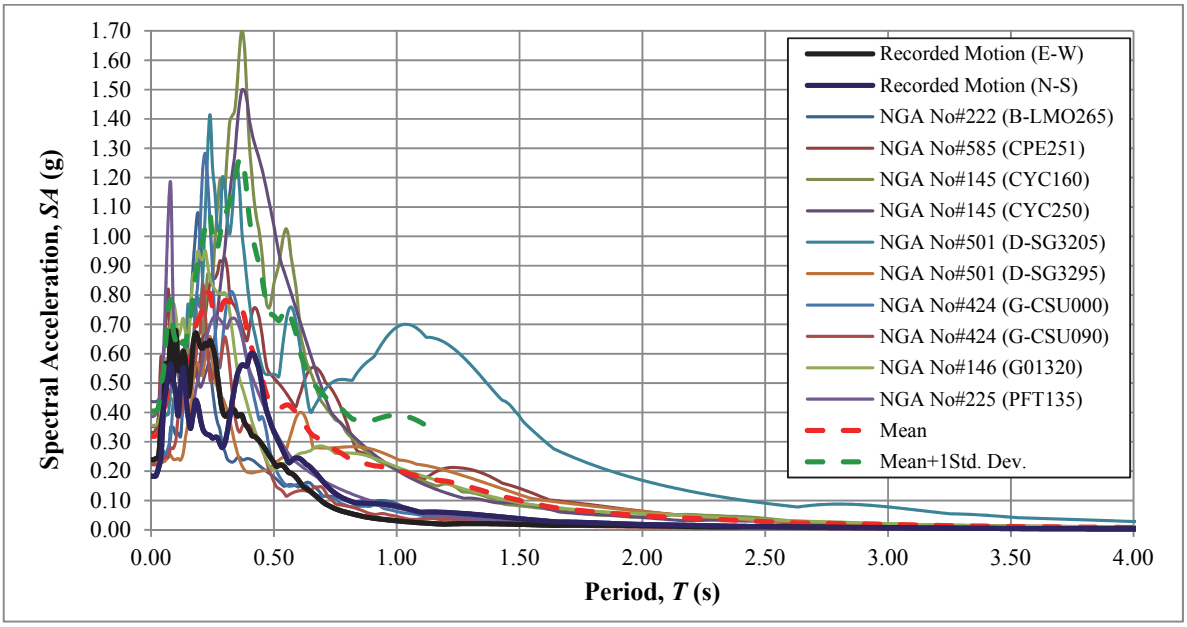

Figure A.11. A comparison of the mean and mean+1 standard deviation response spectrums, determined using Method#5, with the spectral response observed at AI145 TSGMN station

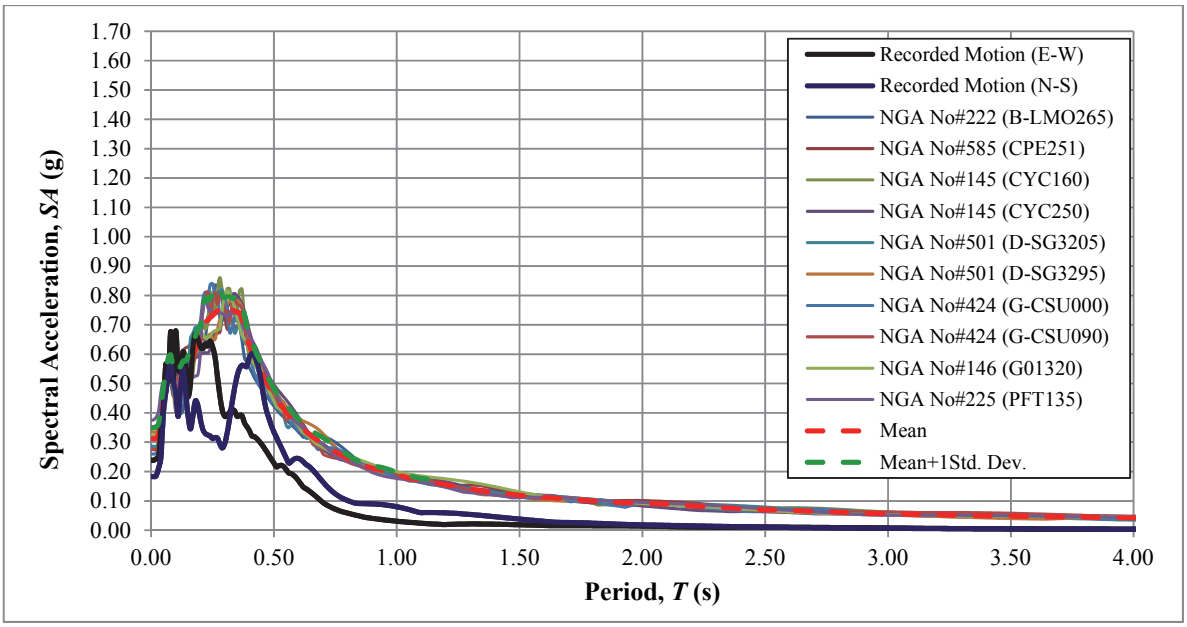

Figure A.12. A comparison of the mean and mean+1 standard deviation response spectrums, determined using Method#6, with the spectral response observed at AI145 TSGMN station

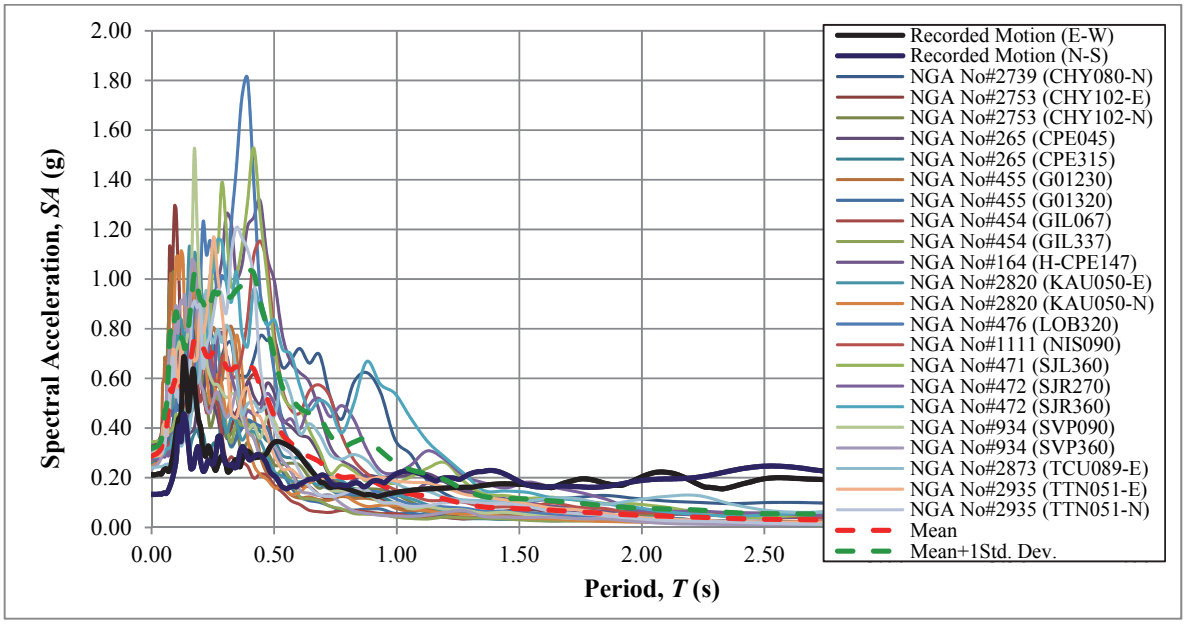

Figure A.13. A comparison of the mean and mean+1 standard deviation response spectrums, determined using Method#1, with the spectral response observed at AI059 TSGMN station

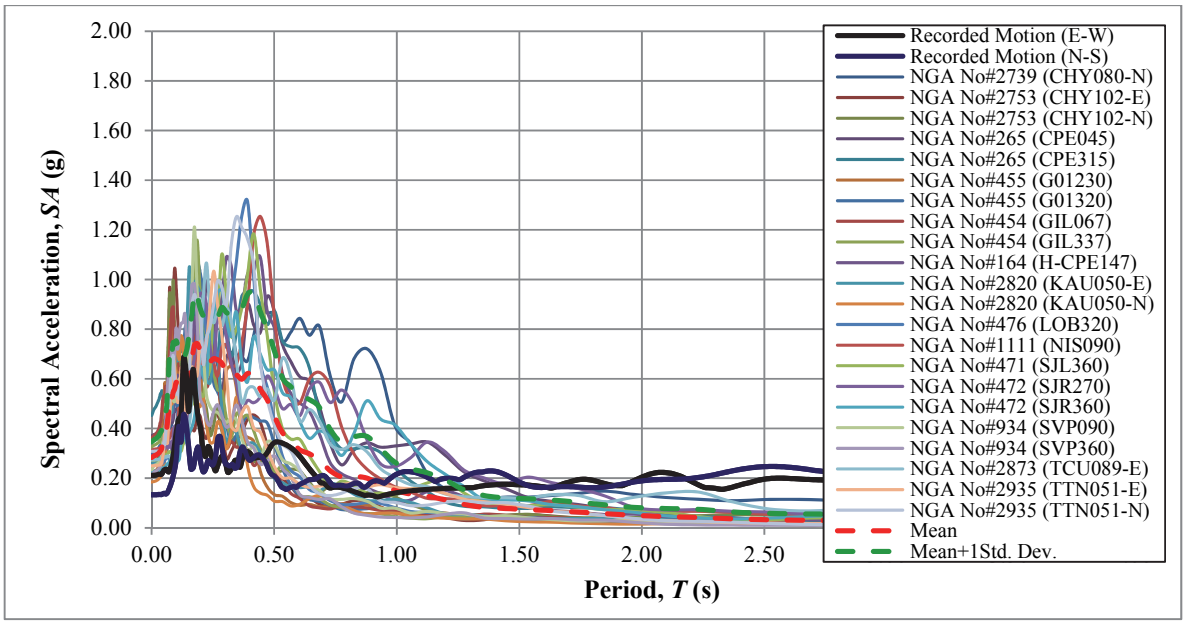

Figure A.14. A comparison of the mean and mean+1 standard deviation response spectrums, determined using Method#2, with the spectral response observed at AI059 TSGMN station

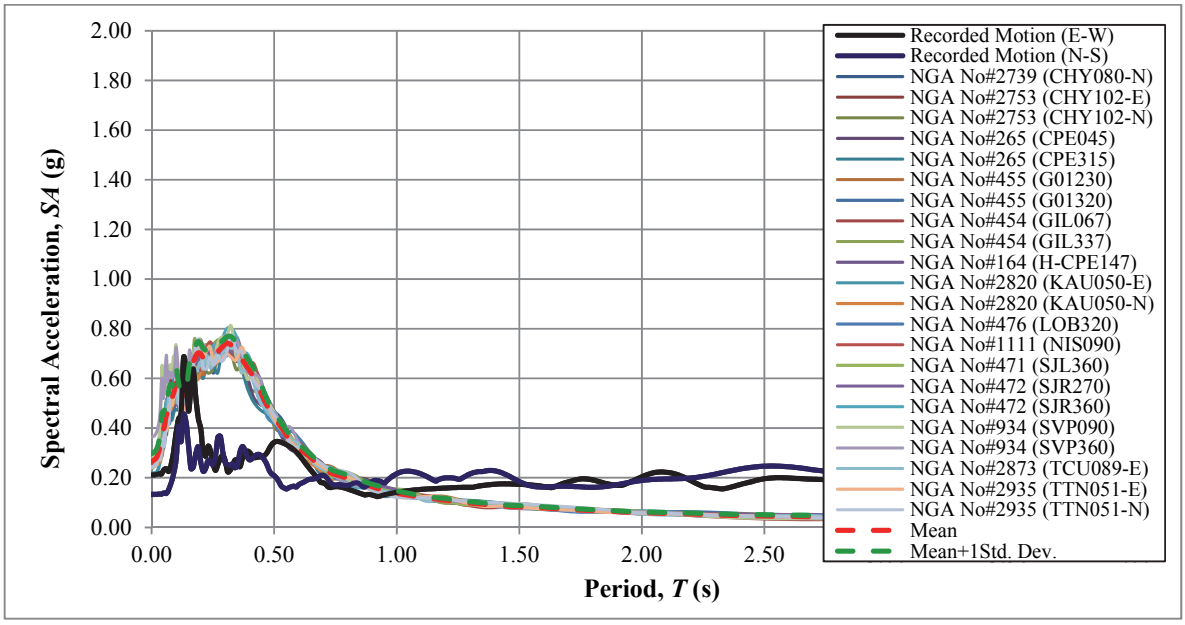

Figure A.15. A comparison of the mean and mean+1 standard deviation response spectrums, determined using Method#3, with the spectral response observed at AI059 TSGMN station

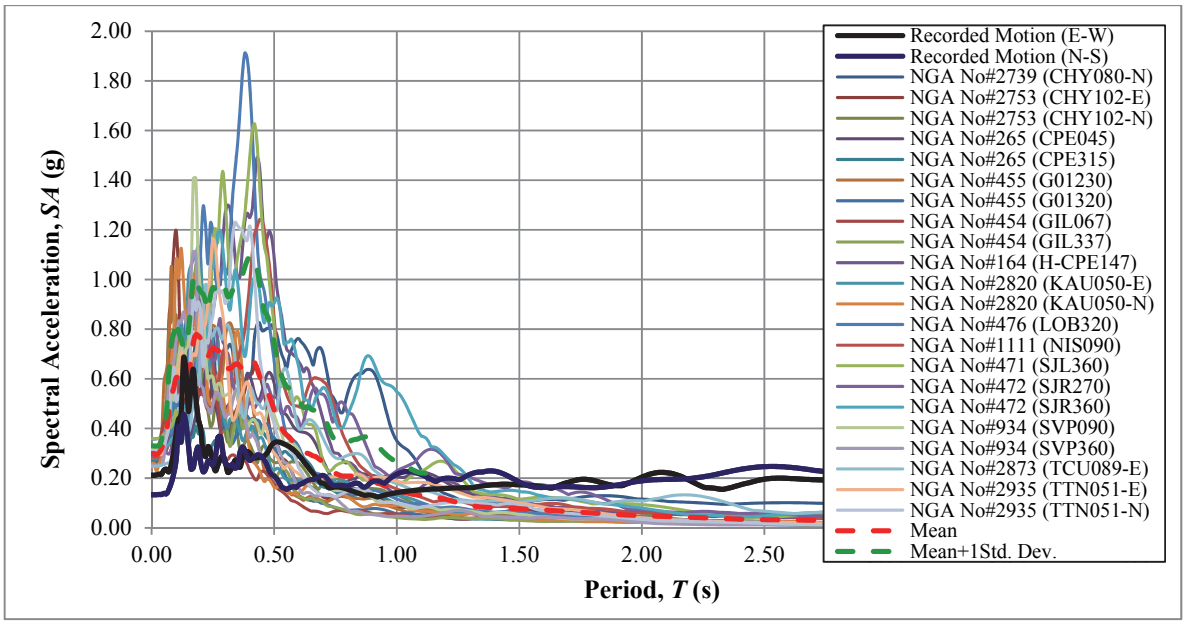

Figure A.16. A comparison of the mean and mean+1 standard deviation response spectrums, determined using Method#4, with the spectral response observed at AI059 TSGMN station

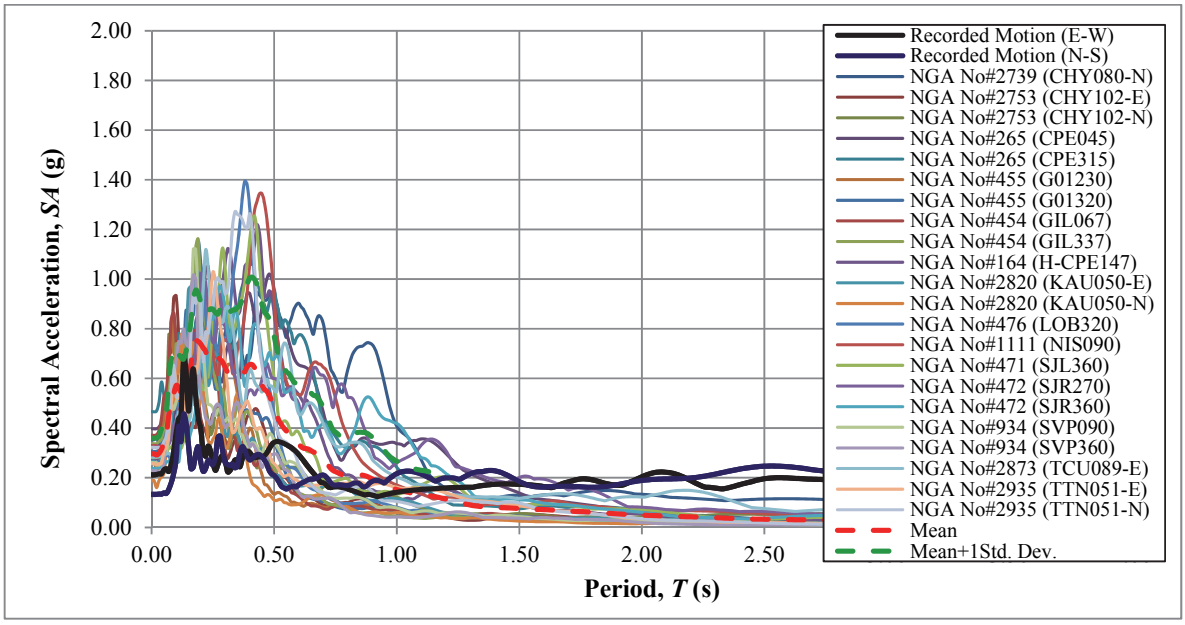

Figure A.17. A comparison of the mean and mean+1 standard deviation response spectrums, determined using Method#5, with the spectral response observed at AI059 TSGMN station

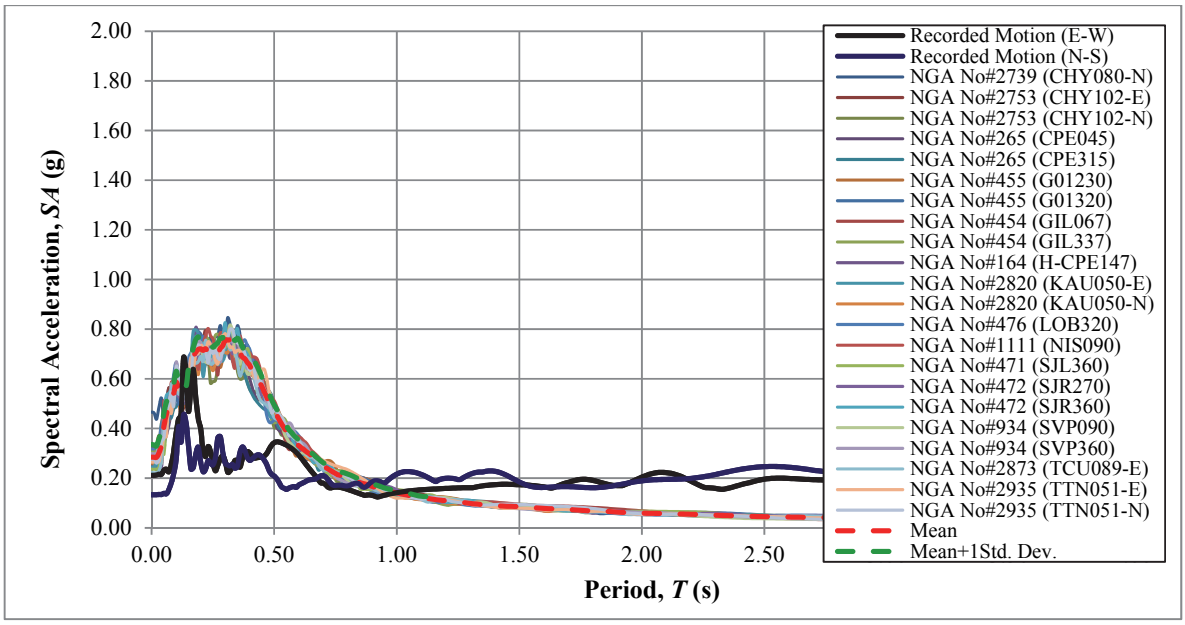

Figure A.18. A comparison of the mean and mean+1 standard deviation response spectrums, determined using Method#6, with the spectral response observed at AI059 TSGMN station

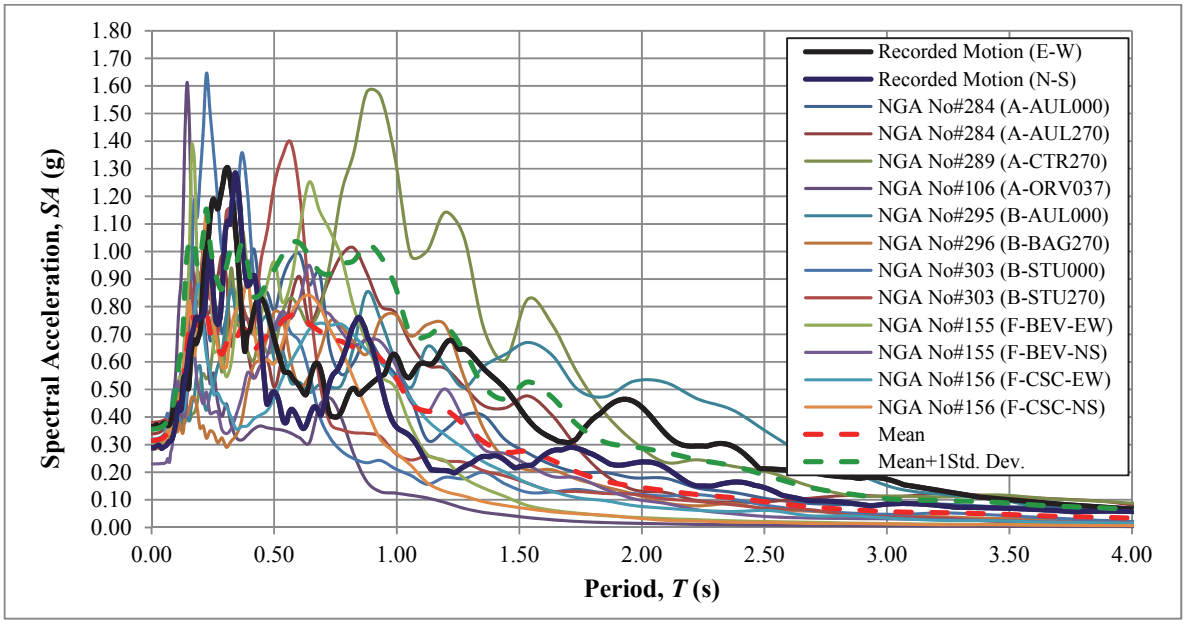

Figure A.19. A comparison of the mean and mean+1 standard deviation response spectrums, determined using Method#1, with the spectral response observed at AI137 TSGMN station

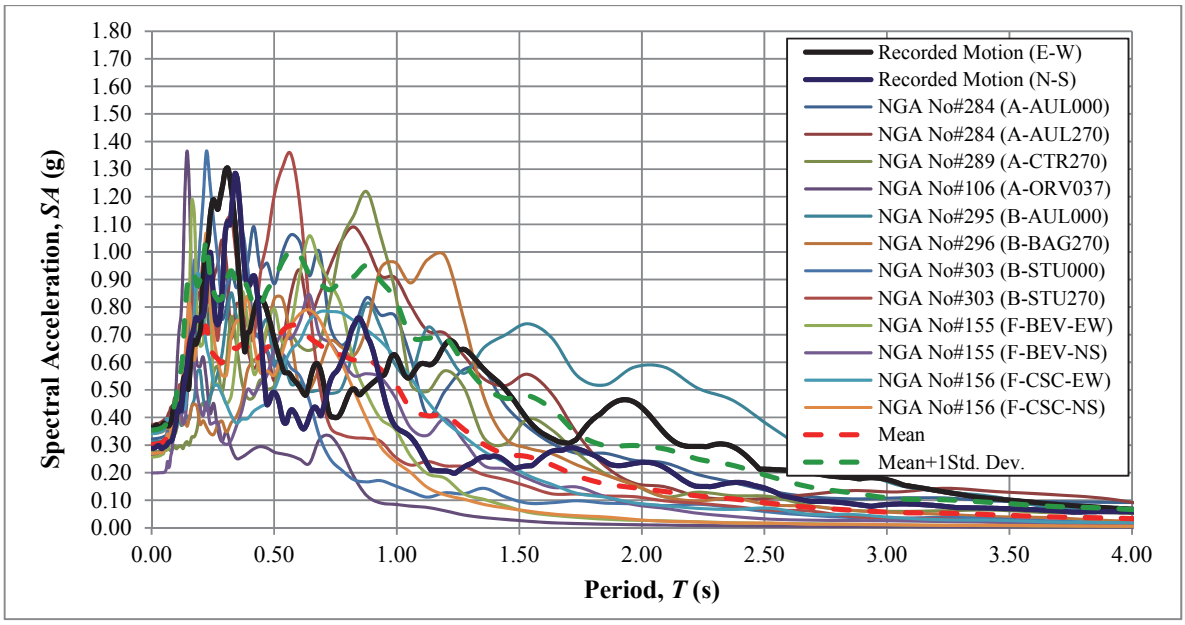

Figure A.20. A comparison of the mean and mean+1 standard deviation response spectrums, determined using Method#2, with the spectral response observed at AI137 TSGMN station

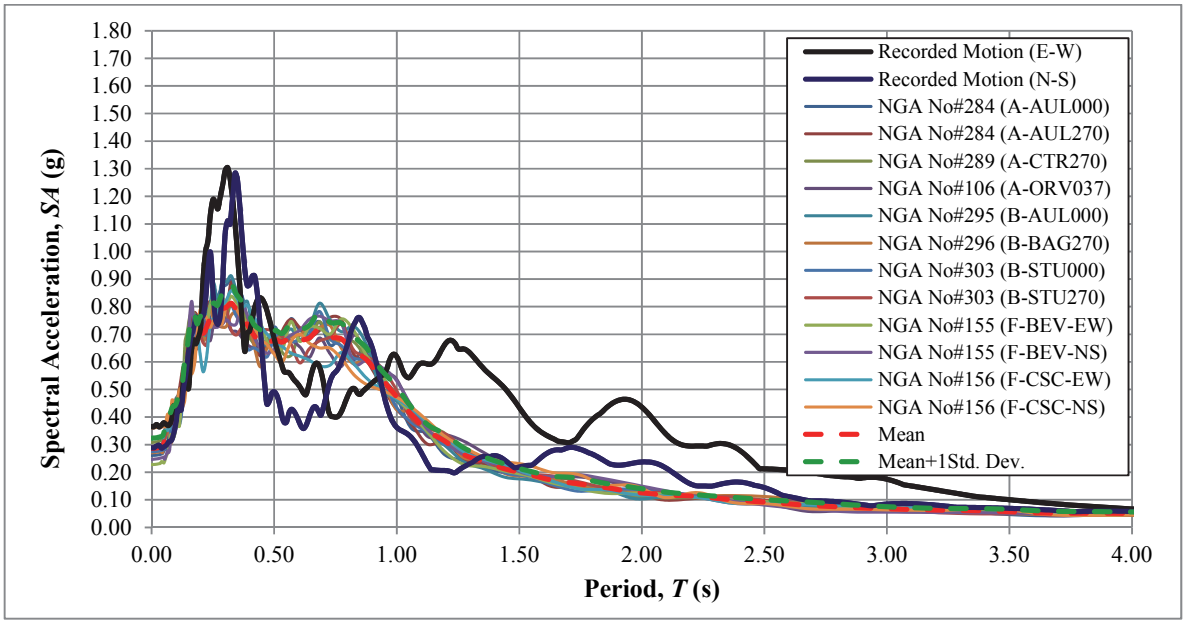

Figure A.21. A comparison of the mean and mean+1 standard deviation response spectrums, determined using Method#3, with the spectral response observed at AI137 TSGMN station

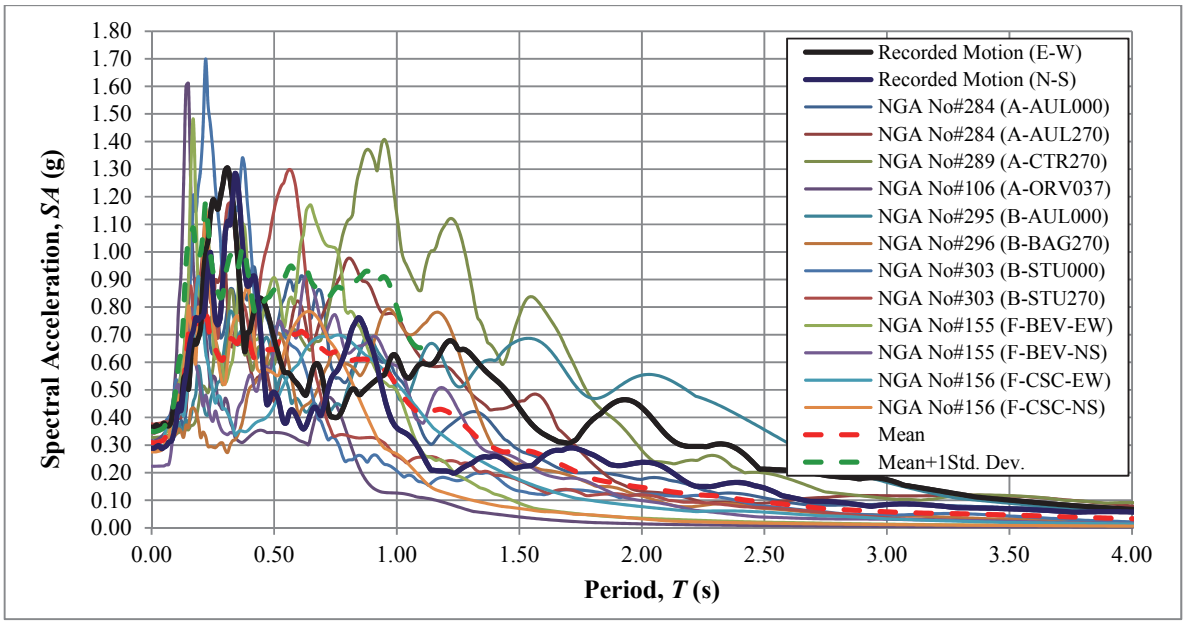

Figure A.22. A comparison of the mean and mean+1 standard deviation response spectrums, determined using Method#4, with the spectral response observed at AI137 TSGMN station

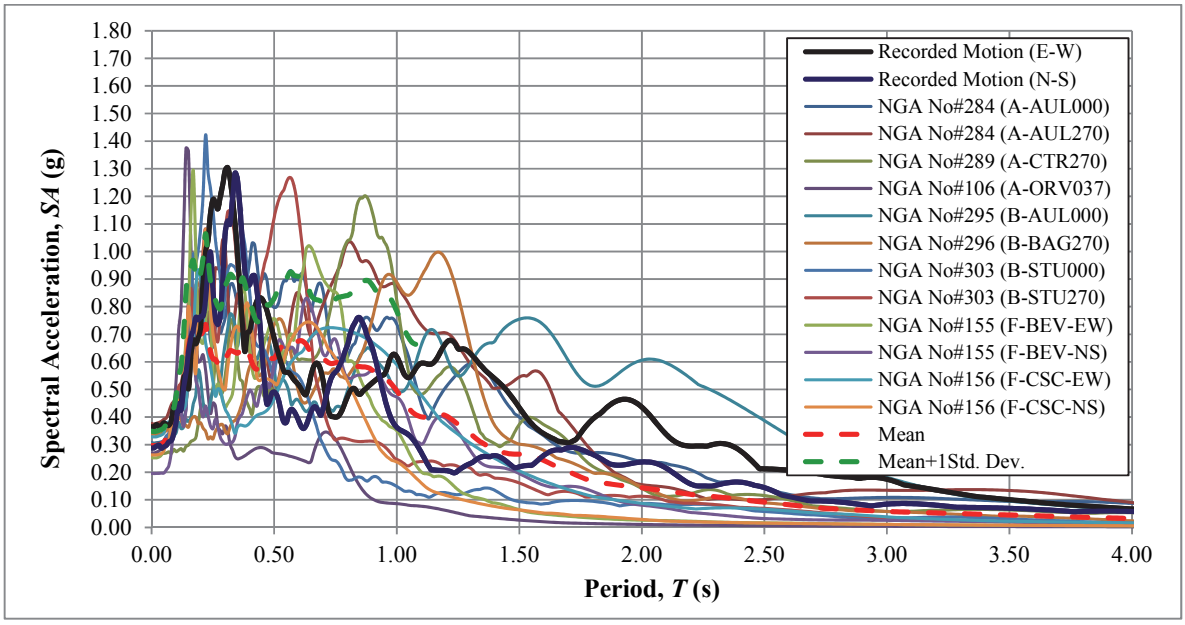

Figure A.23. A comparison of the mean and mean+1 standard deviation response spectrums, determined using Method#5, with the spectral response observed at AI137 TSGMN station

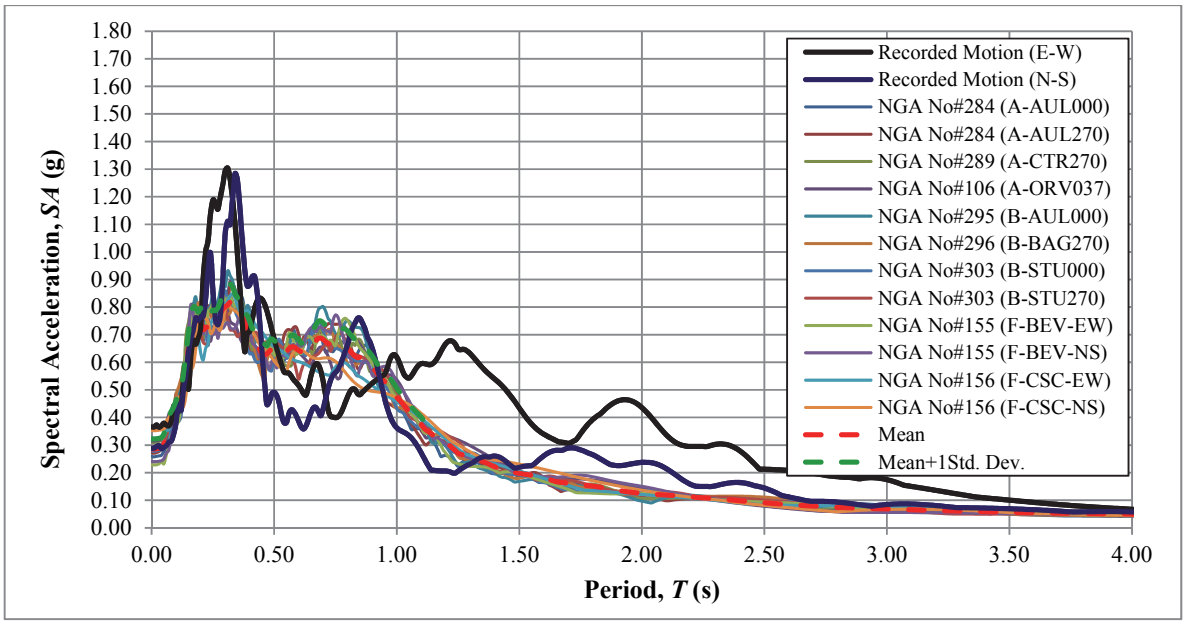

Figure A.24. A comparison of the mean and mean+1 standard deviation response spectrums, determined using Method#6, with the spectral response observed at AI137 TSGMN station

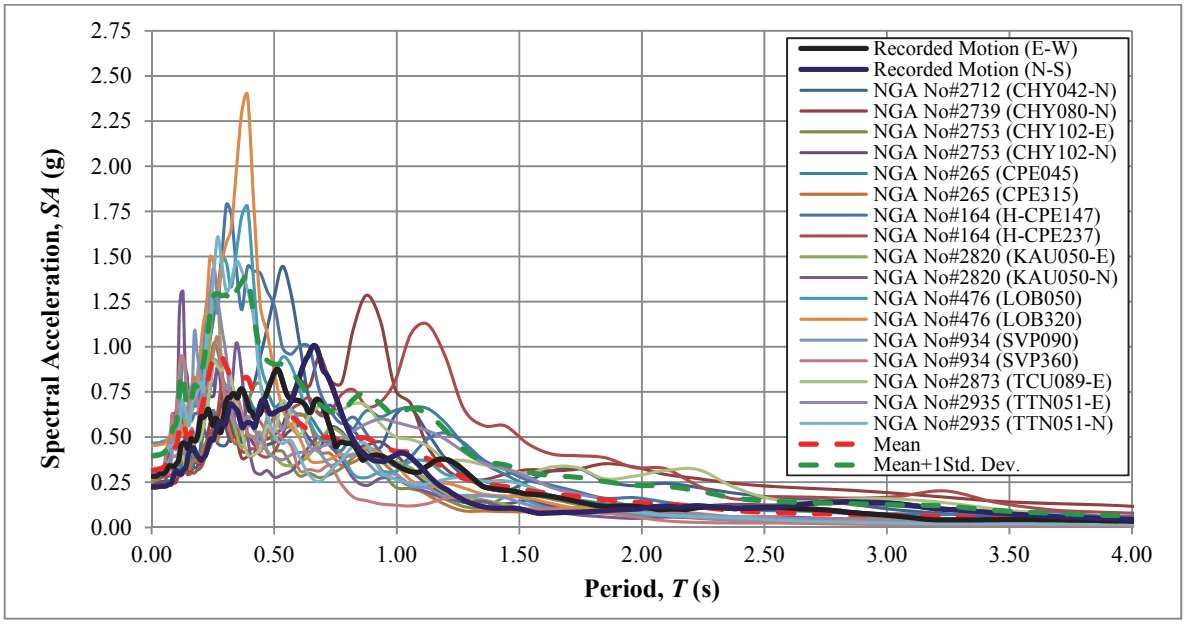

Figure A.25. A comparison of the mean and mean+1 standard deviation response spectrums, determined using Method#1, with the spectral response observed at AI022 TSGMN station

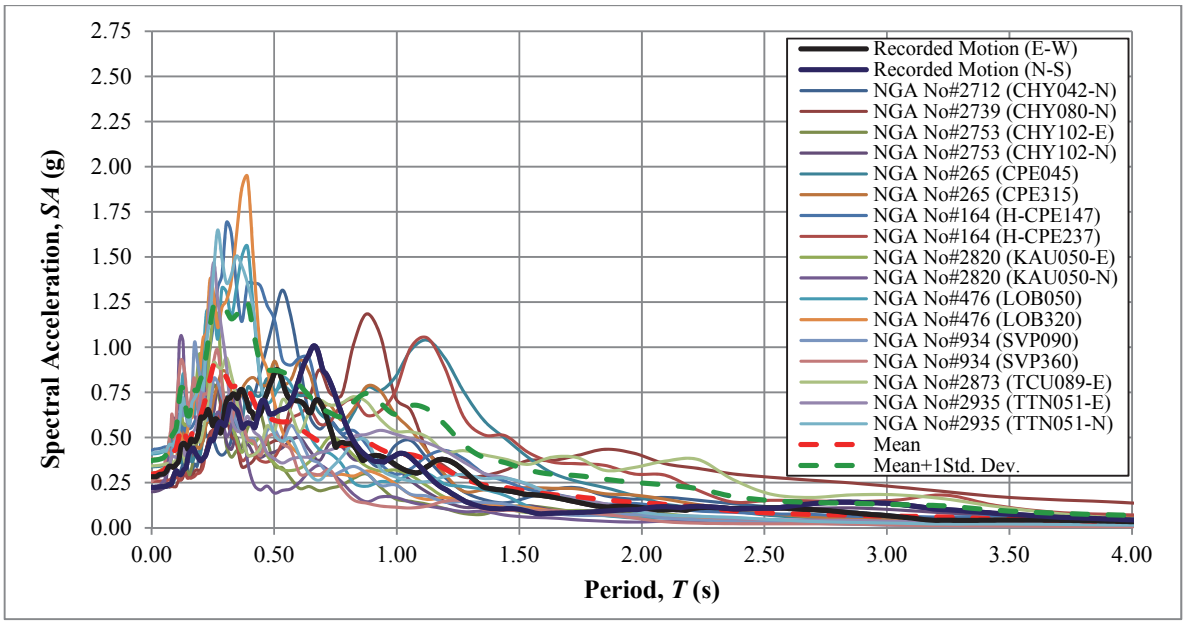

Figure A.26. A comparison of the mean and mean+1 standard deviation response spectrums, determined using Method#2, with the spectral response observed at AI022 TSGMN station

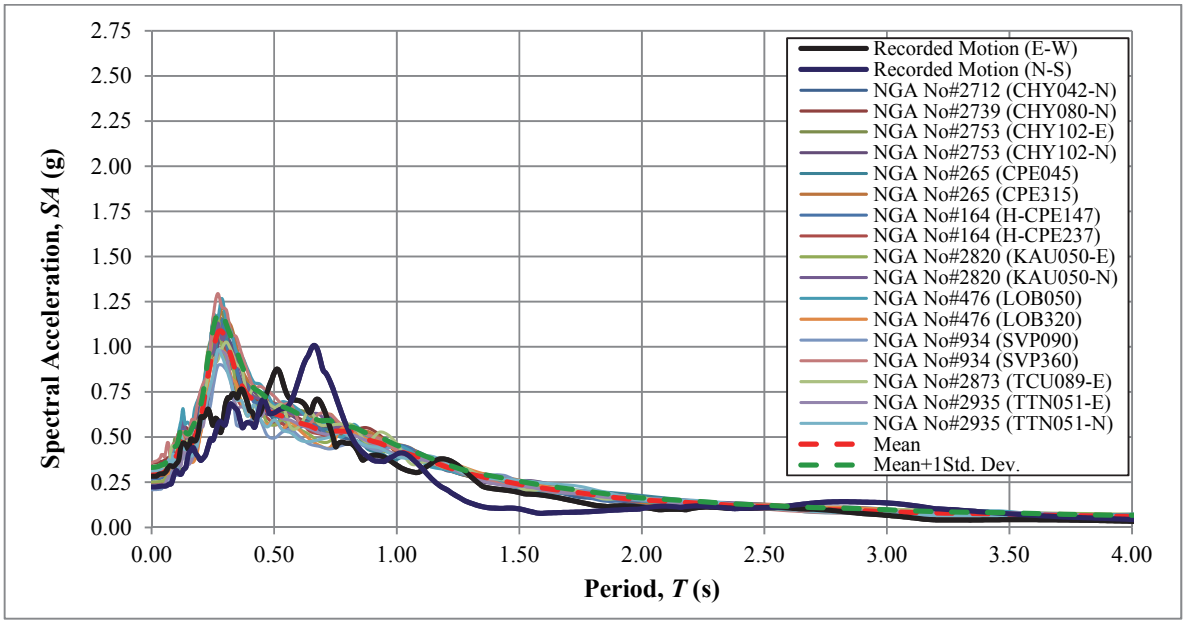

Figure A.27. A comparison of the mean and mean+1 standard deviation response spectrums, determined using Method#3, with the spectral response observed at AI022 TSGMN station

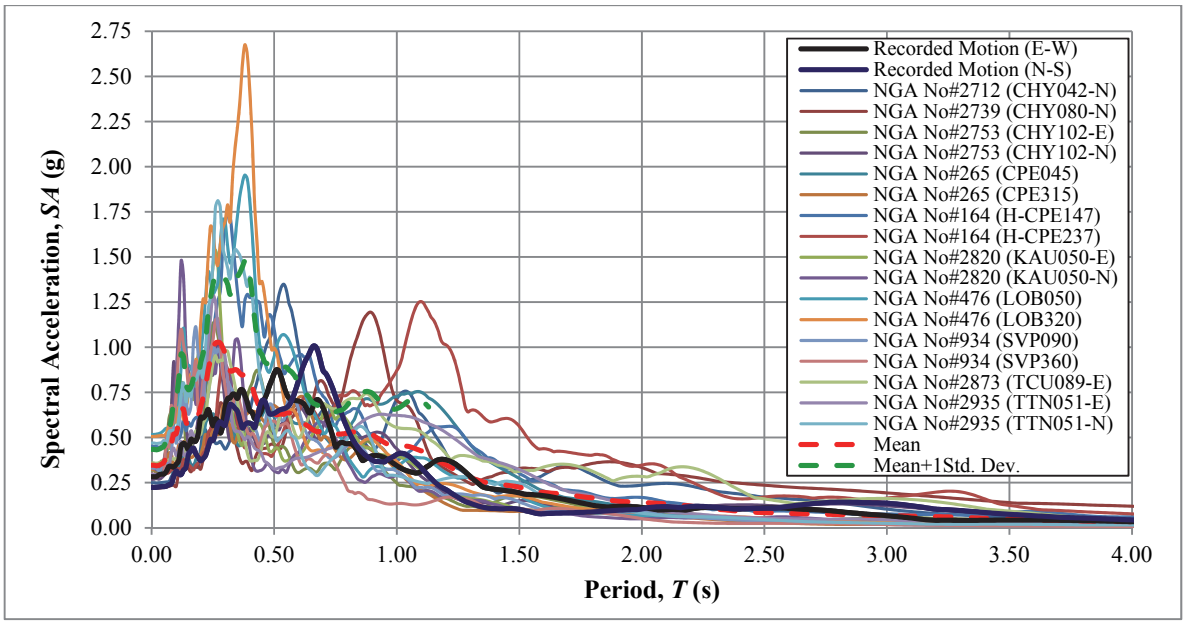

Figure A.28. A comparison of the mean and mean+1 standard deviation response spectrums, determined using Method#4, with the spectral response observed at AI022 TSGMN station

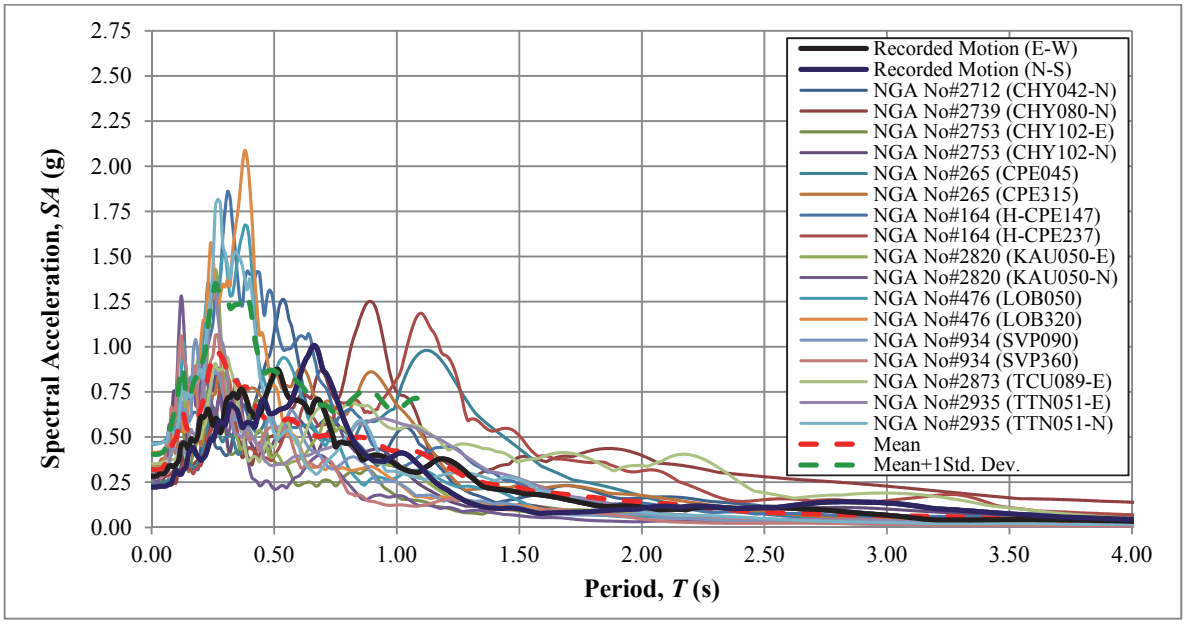

Figure A.29. A comparison of the mean and mean+1 standard deviation response spectrums, determined using Method#5, with the spectral response observed at AI022 TSGMN station

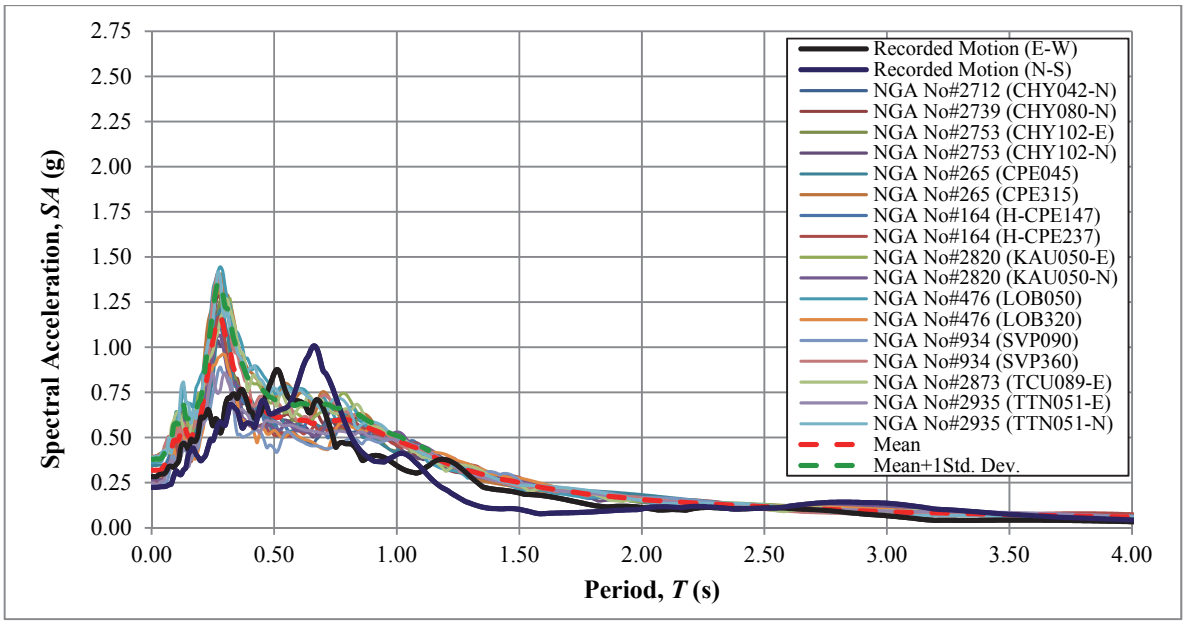

Figure A.30. A comparison of the mean and mean+1 standard deviation response spectrums, determined using Method#6, with the spectral response observed at AI022 TSGMN station

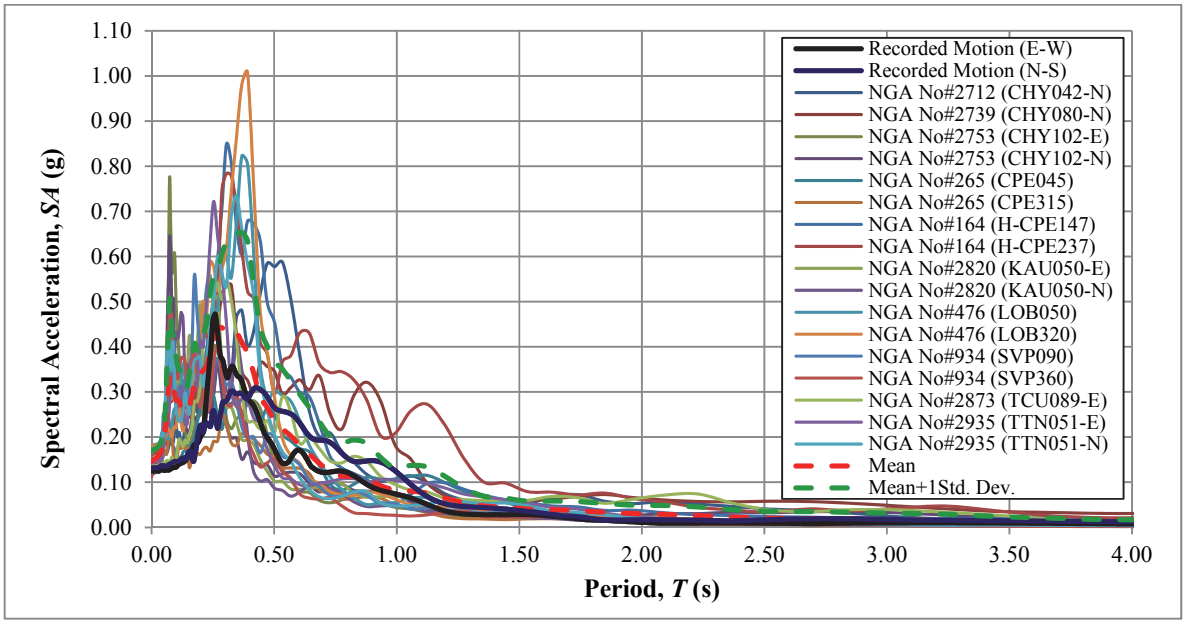

Figure A.31. A comparison of the mean and mean+1 standard deviation response spectrums, determined using Method#1, with the spectral response observed at AI019 TSGMN station

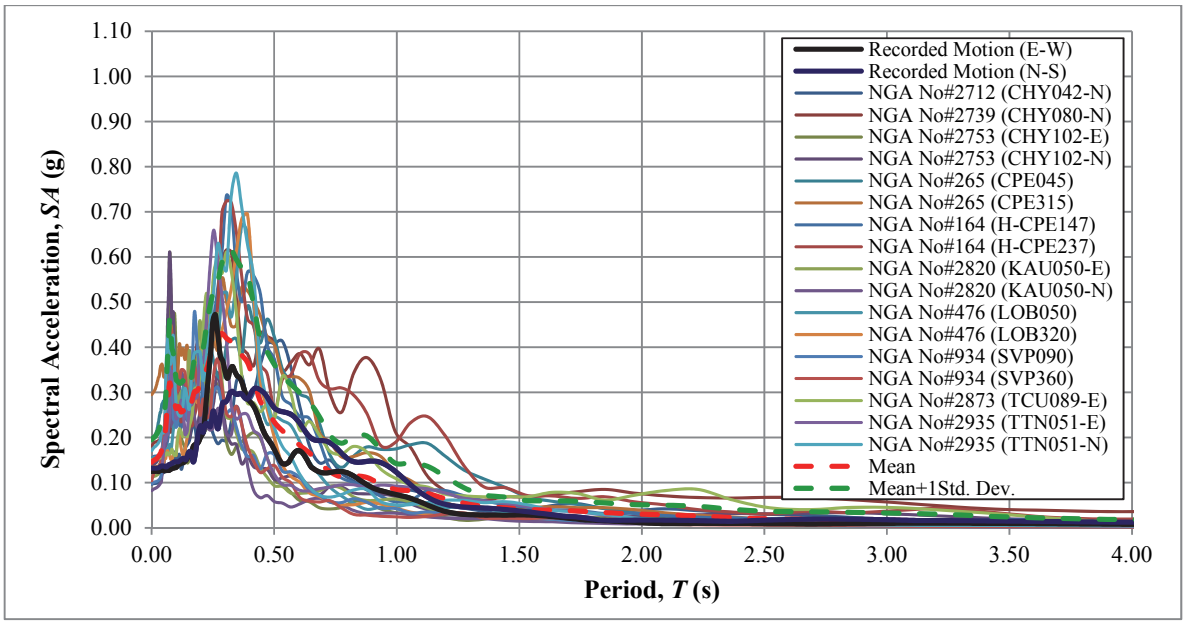

Figure A.32. A comparison of the mean and mean+1 standard deviation response spectrums, determined using Method#2, with the spectral response observed at AI019 TSGMN station

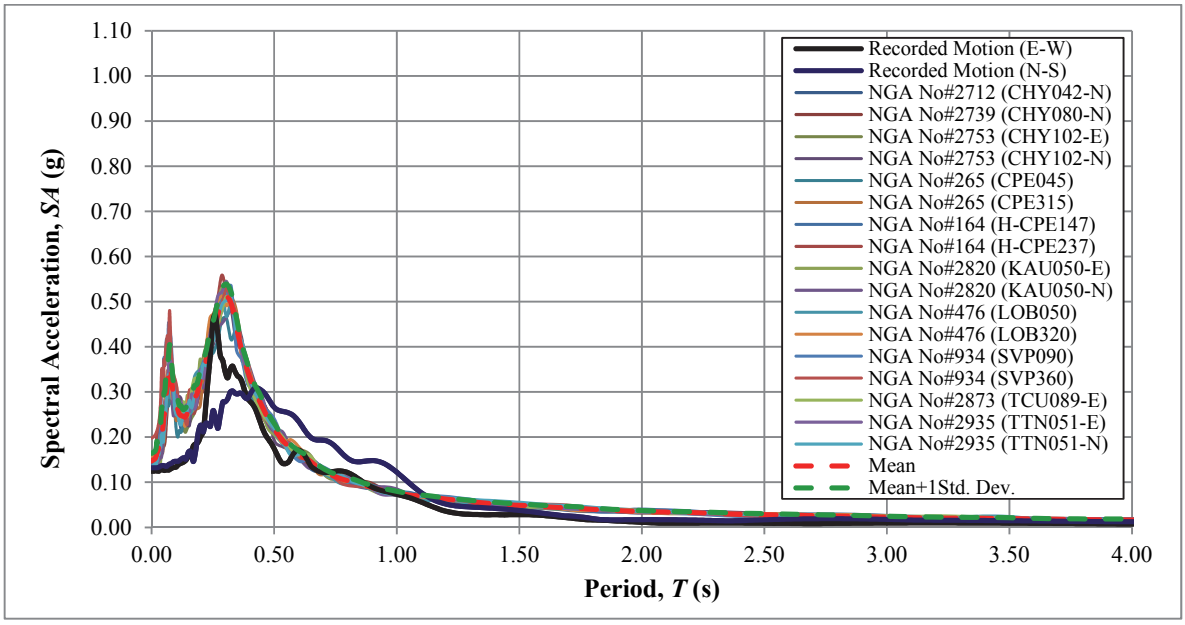

Figure A.33. A comparison of the mean and mean+1 standard deviation response spectrums, determined using Method#3, with the spectral response observed at AI019 TSGMN station

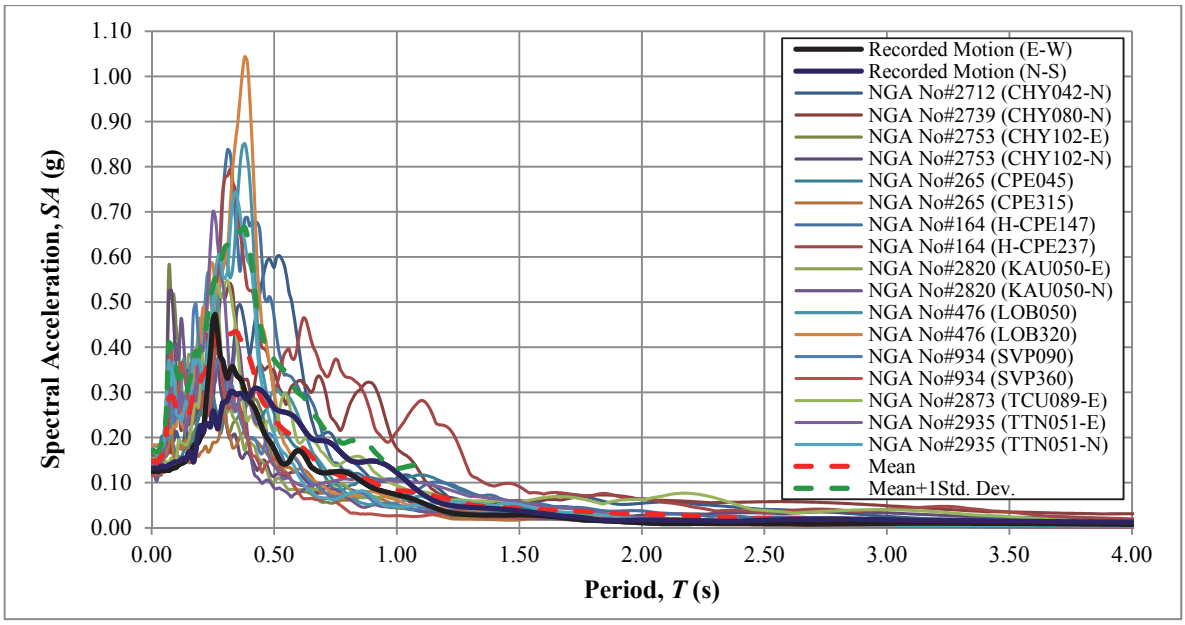

Figure A.34. A comparison of the mean and mean+1 standard deviation response spectrums, determined using Method#4, with the spectral response observed at AI019 TSGMN station

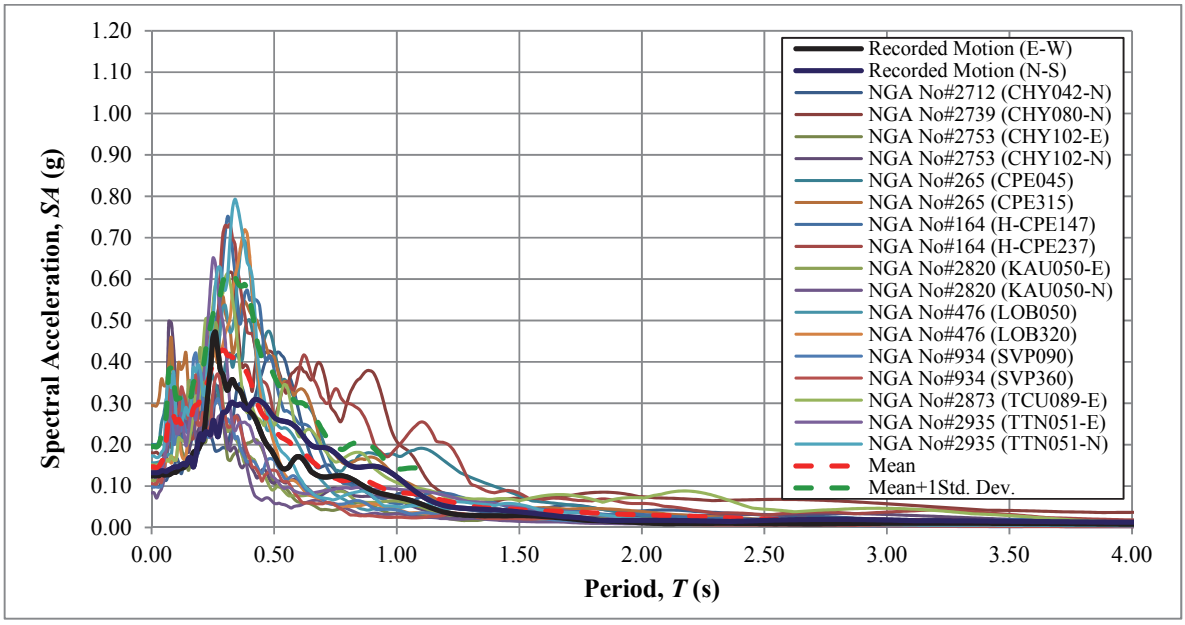

Figure A.35. A comparison of the mean and mean+1 standard deviation response spectrums, determined using Method#5, with the spectral response observed at AI019 TSGMN station

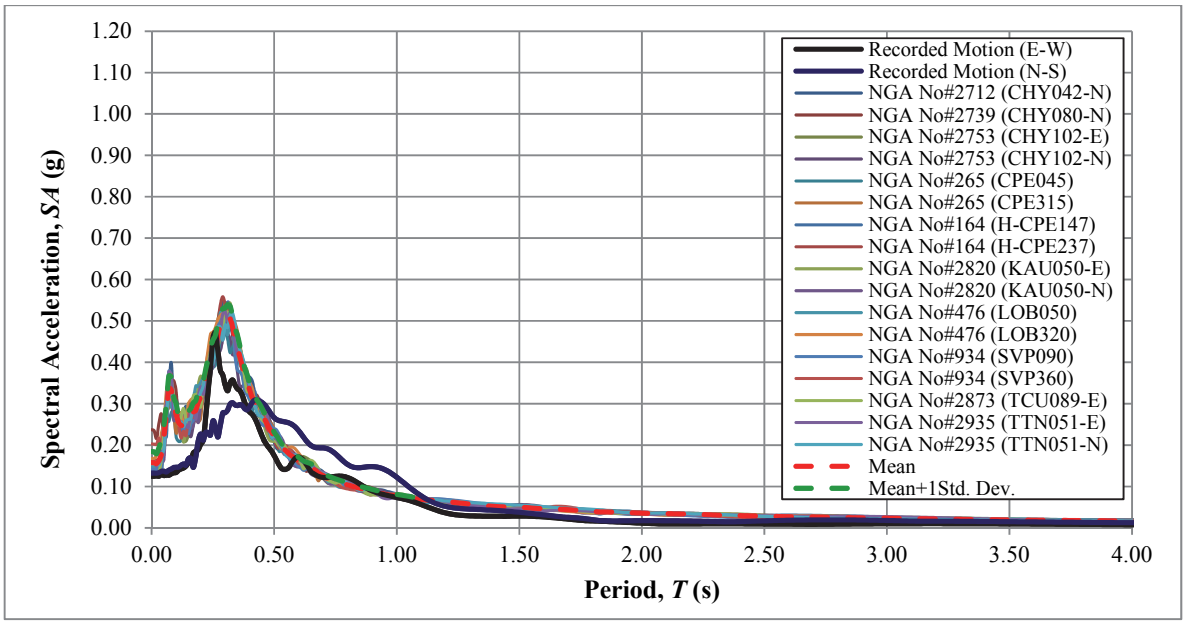

Figure A.36. A comparison of the mean and mean+1 standard deviation response spectrums, determined using Method#6, with the spectral response observed at AI019 TSGMN station

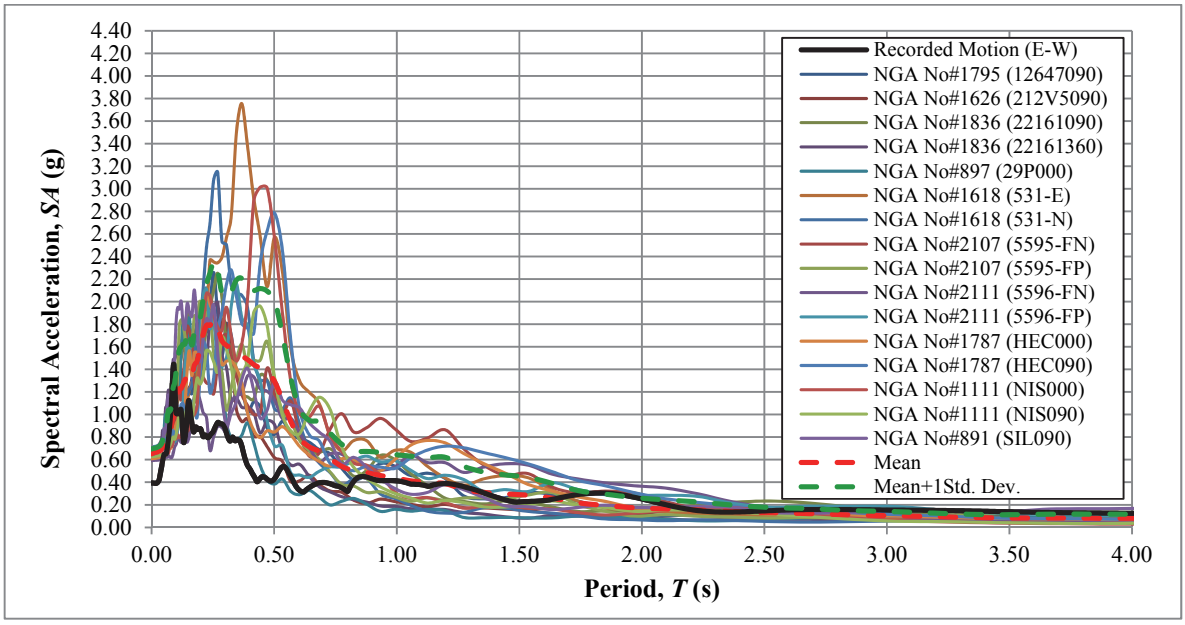

Figure A.37. A comparison of the mean and mean+1 standard deviation response spectrums, determined using Method#1, with the spectral response observed at AI005 TSGMN station

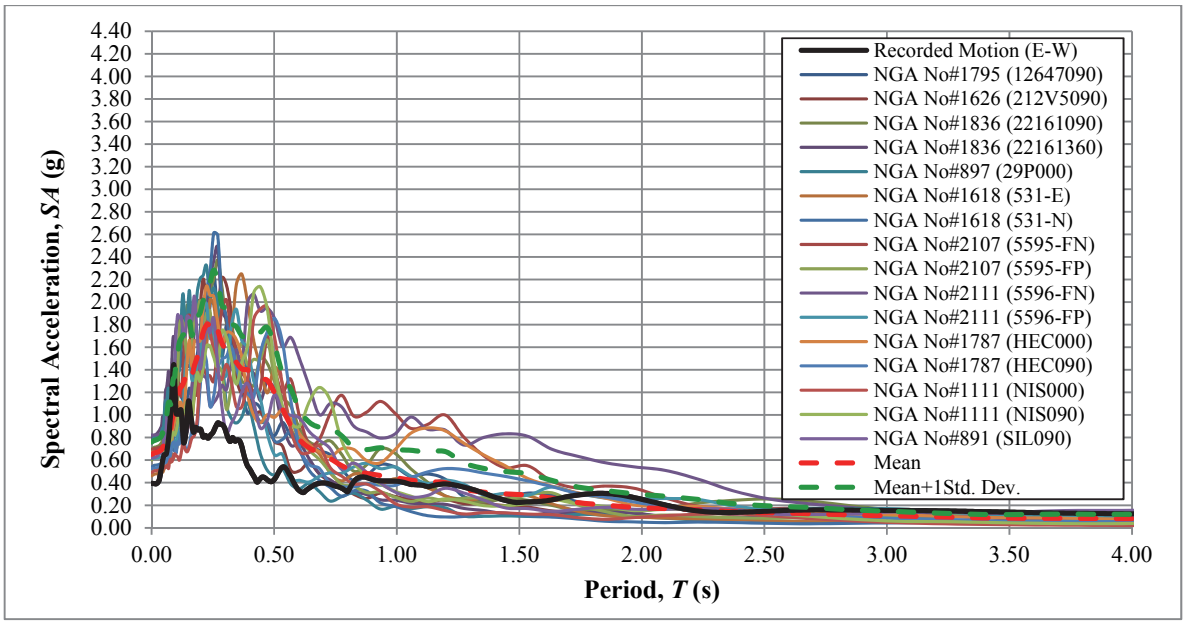

Figure A.38. A comparison of the mean and mean+1 standard deviation response spectrums, determined using Method#2, with the spectral response observed at AI005 TSGMN station

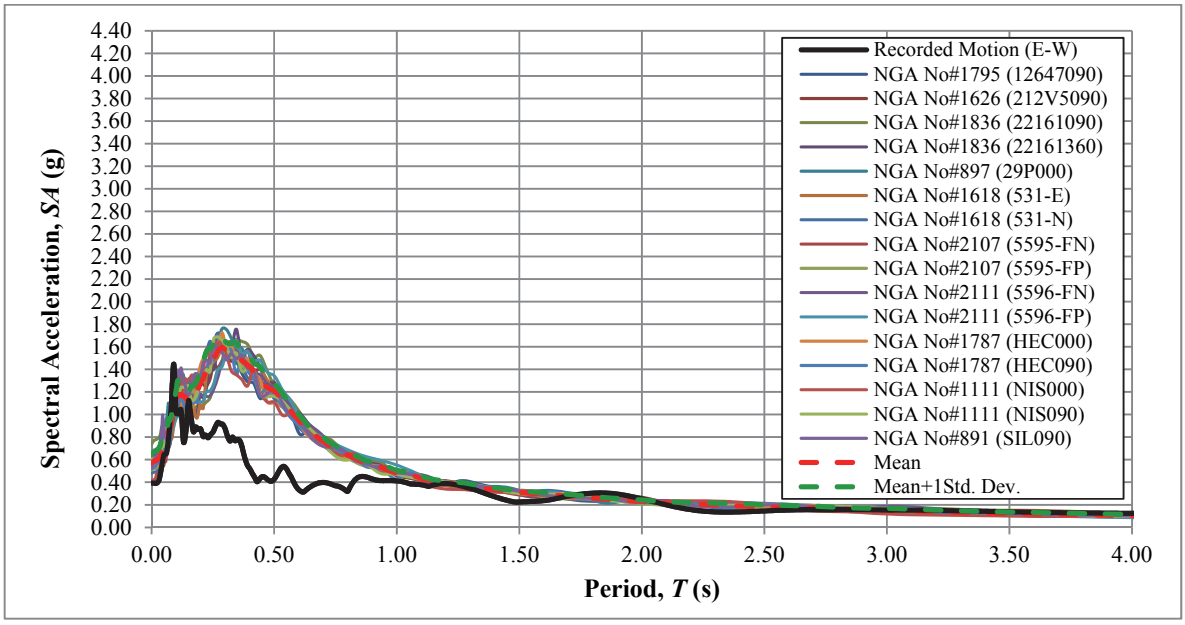

Figure A.39. A comparison of the mean and mean+1 standard deviation response spectrums, determined using Method#3, with the spectral response observed at AI005 TSGMN station

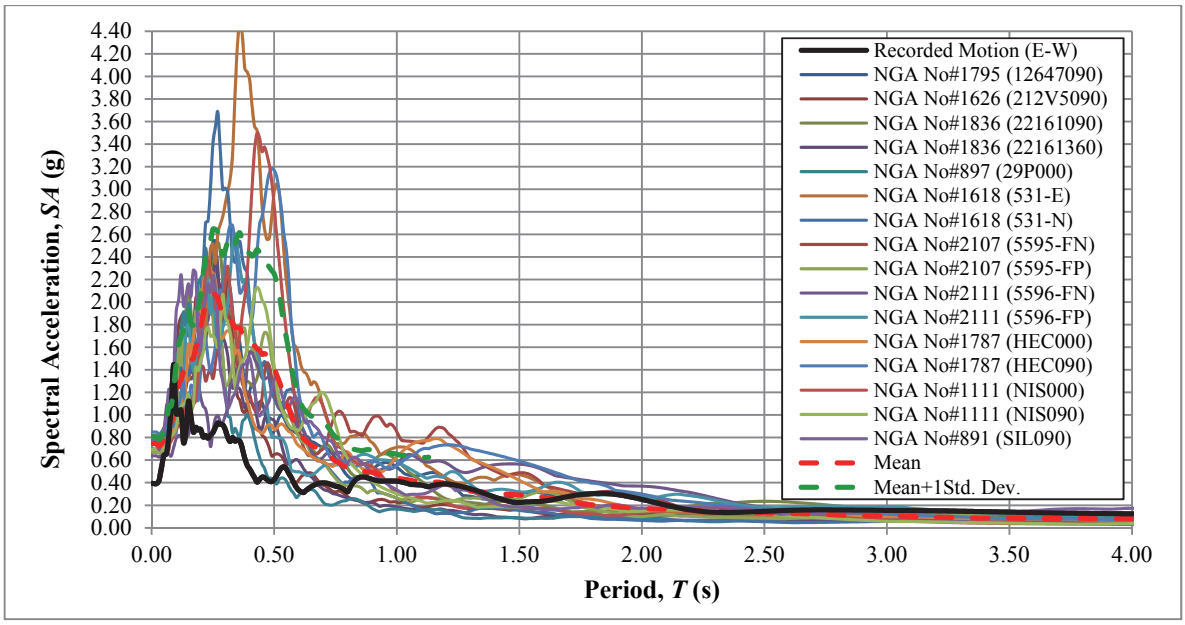

Figure A.40. A comparison of the mean and mean+1 standard deviation response spectrums, determined using Method#4, with the spectral response observed at AI005 TSGMN station

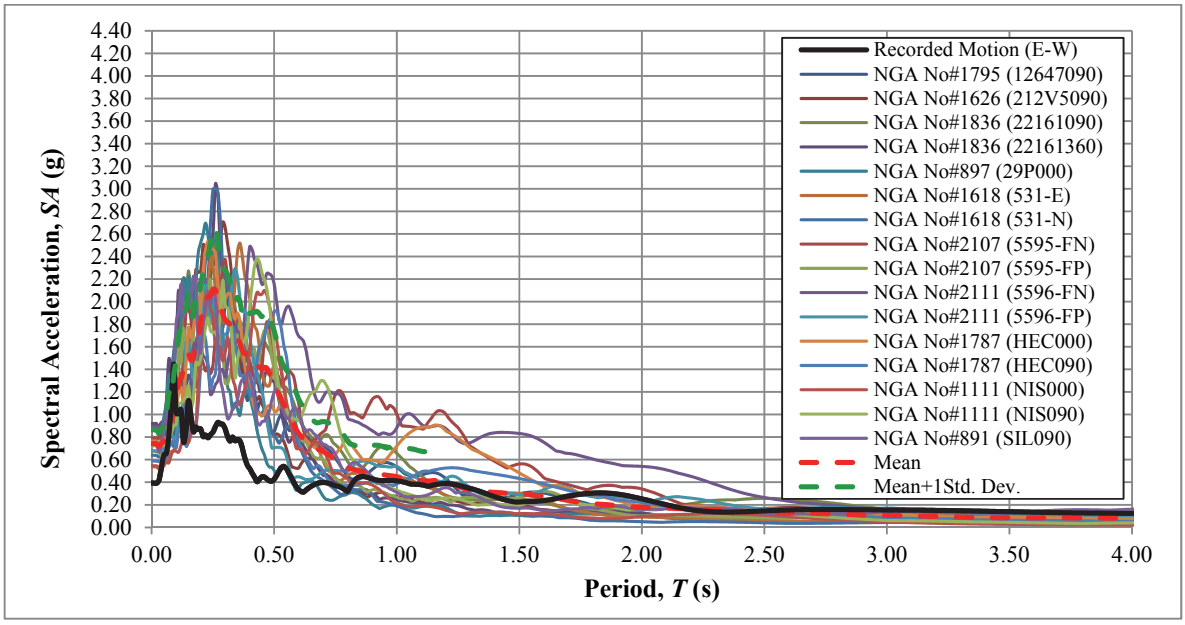

Figure A.41. A comparison of the mean and mean+1 standard deviation response spectrums, determined using Method#5, with the spectral response observed at AI005 TSGMN station

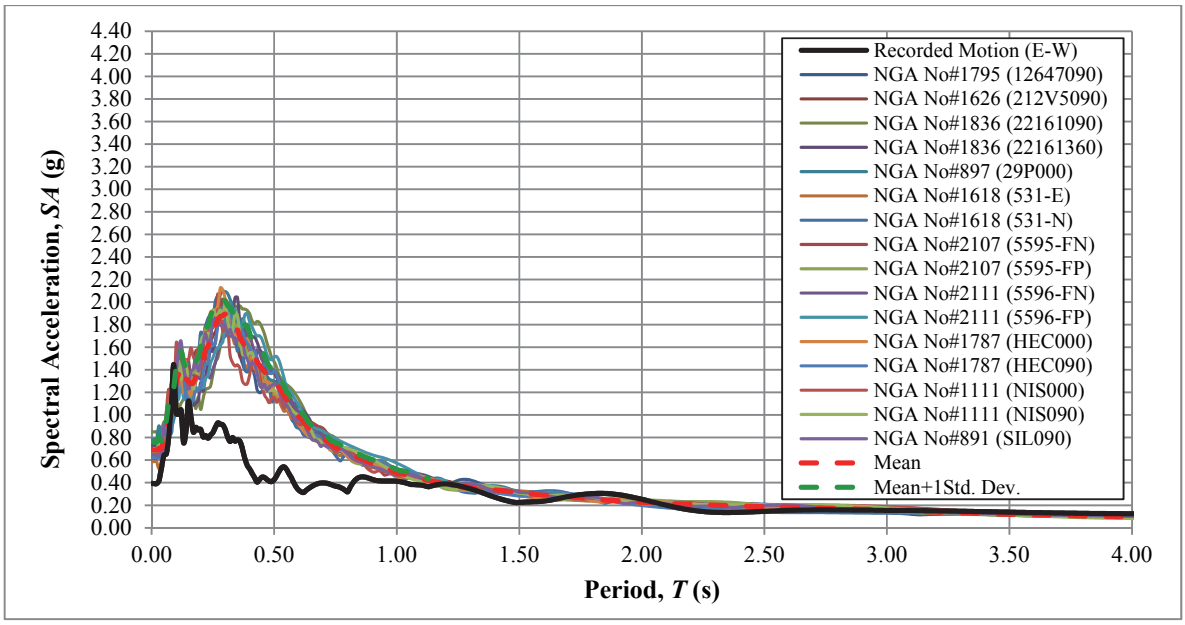

Figure A.42. A comparison of the mean and mean+1 standard deviation response spectrums, determined using Method#6, with the spectral response observed at AI005 TSGMN station

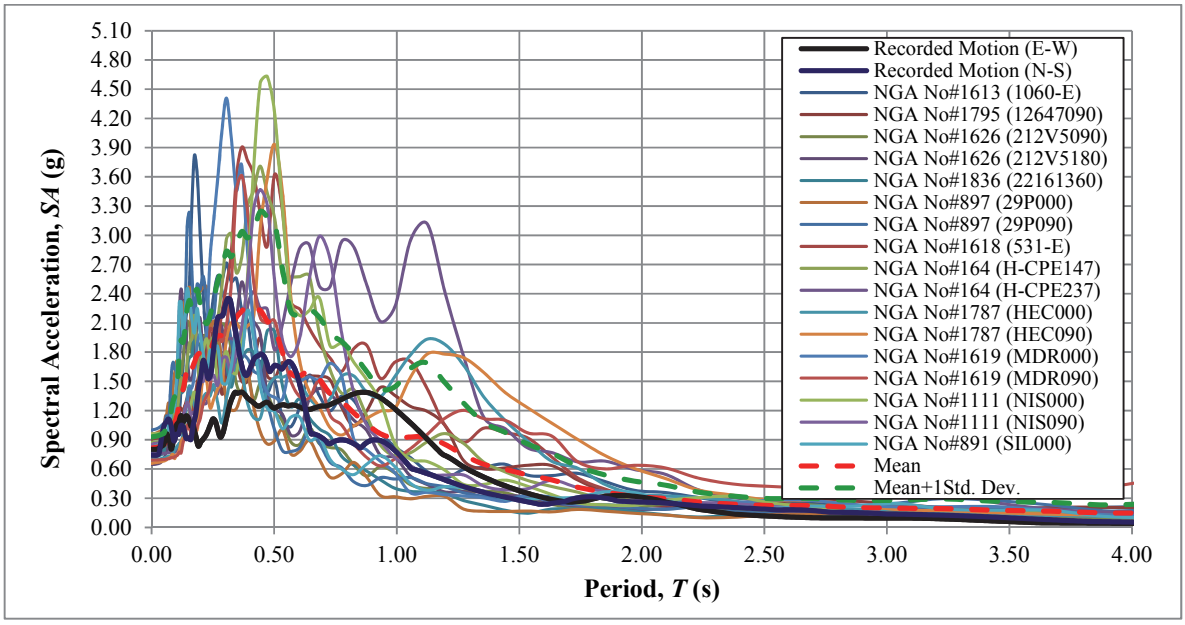

Figure A.43. A comparison of the mean and mean+1 std. deviation response spectrums, determined using Method#1, with the spectral response observed at AI010 TSGMN station

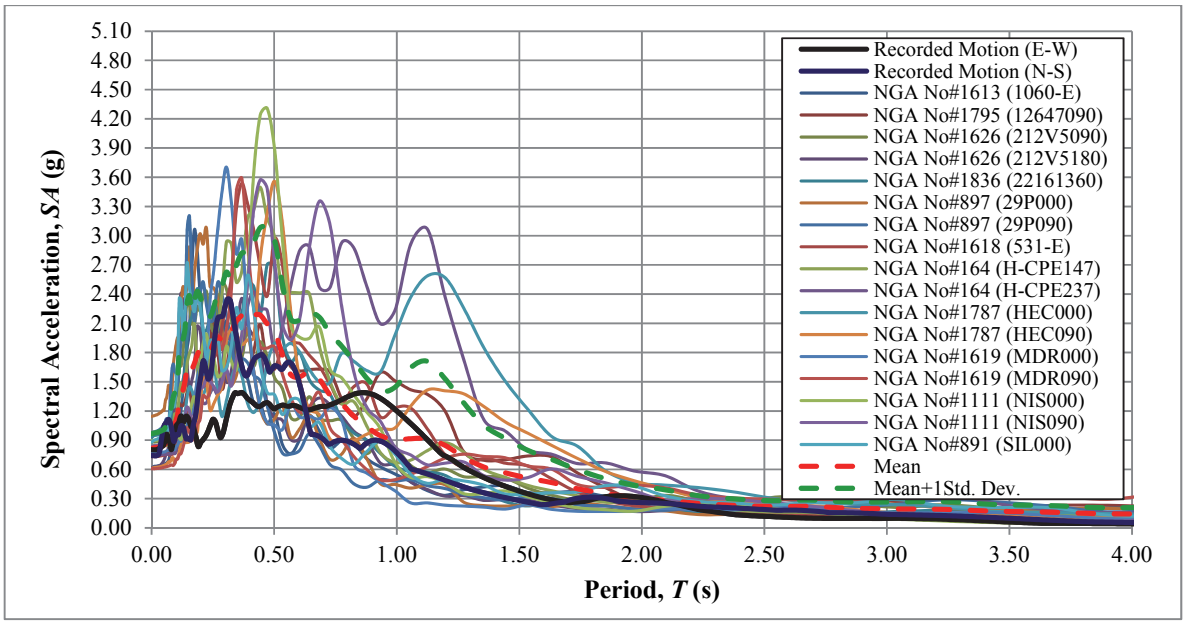

Figure A.44. A comparison of the mean and mean+1 std. deviation response spectrums, determined using Method#2, with the spectral response observed at AI010 TSGMN station

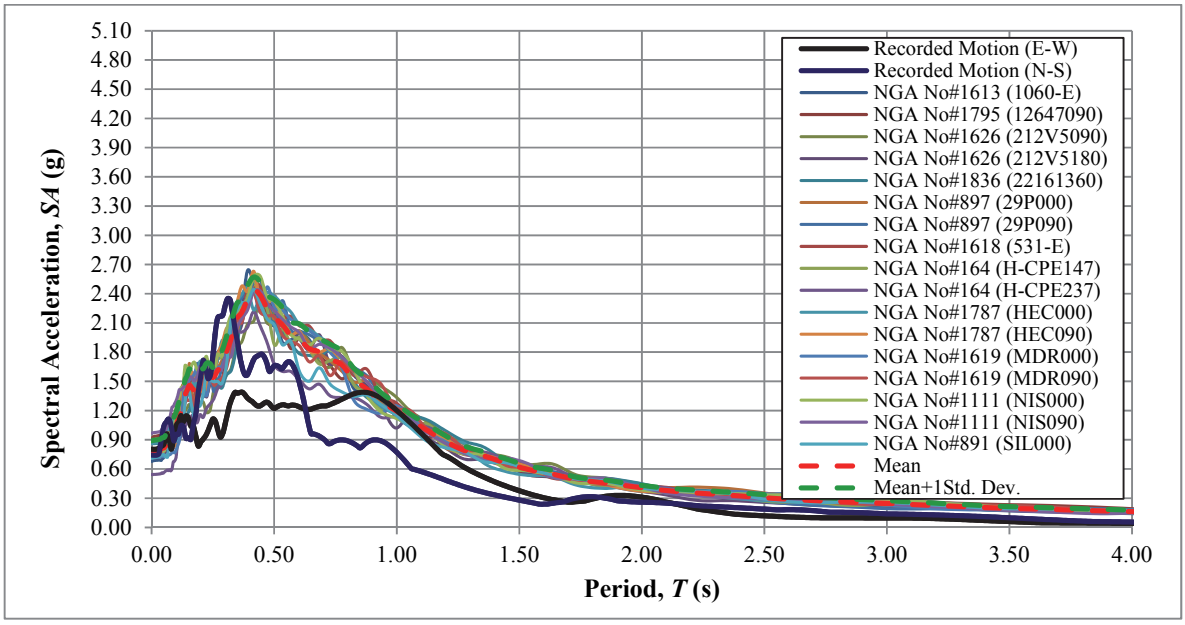

Figure A.45. A comparison of the mean and mean+1 std. deviation response spectrums, determined using Method#3, with the spectral response observed at AI010 TSGMN station

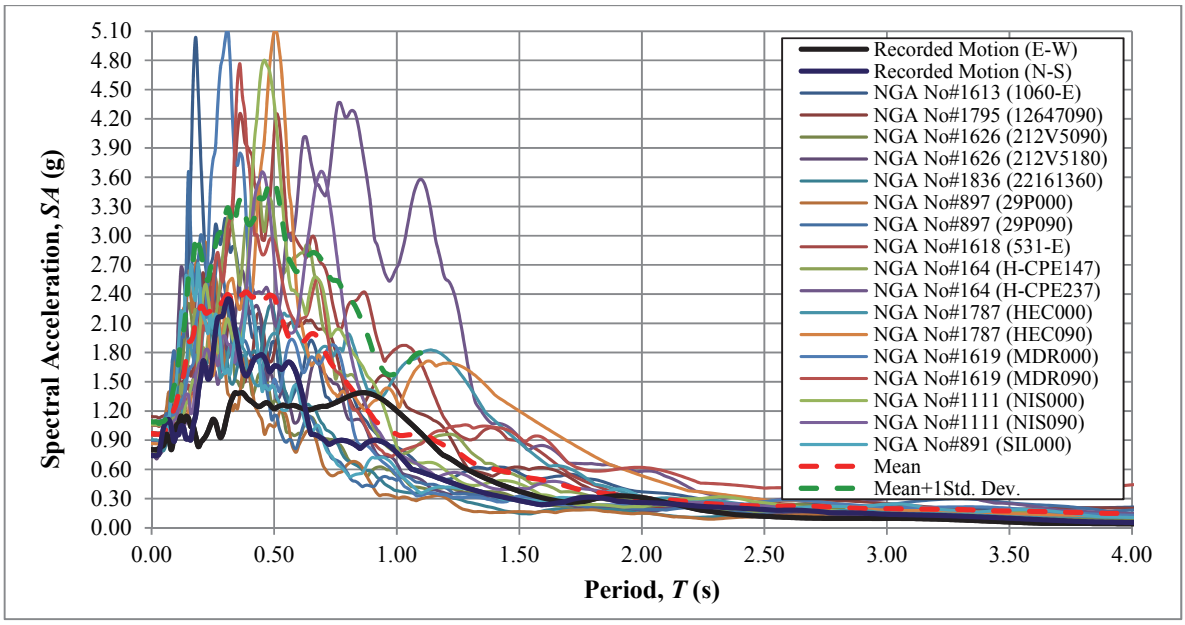

Figure A.46. A comparison of the mean and mean+1 std. deviation response spectrums, determined using Method#4, with the spectral response observed at AI010 TSGMN station

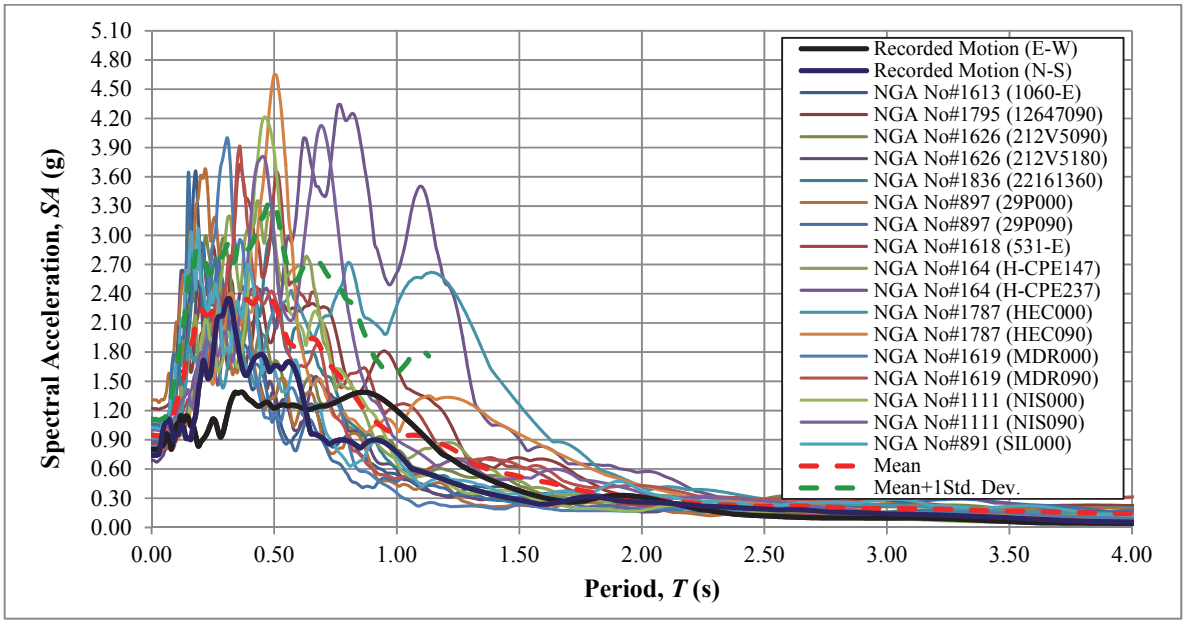

Figure A.47. A comparison of the mean and mean+1 std. deviation response spectrums, determined using Method#5, with the spectral response observed at AI010 TSGMN station

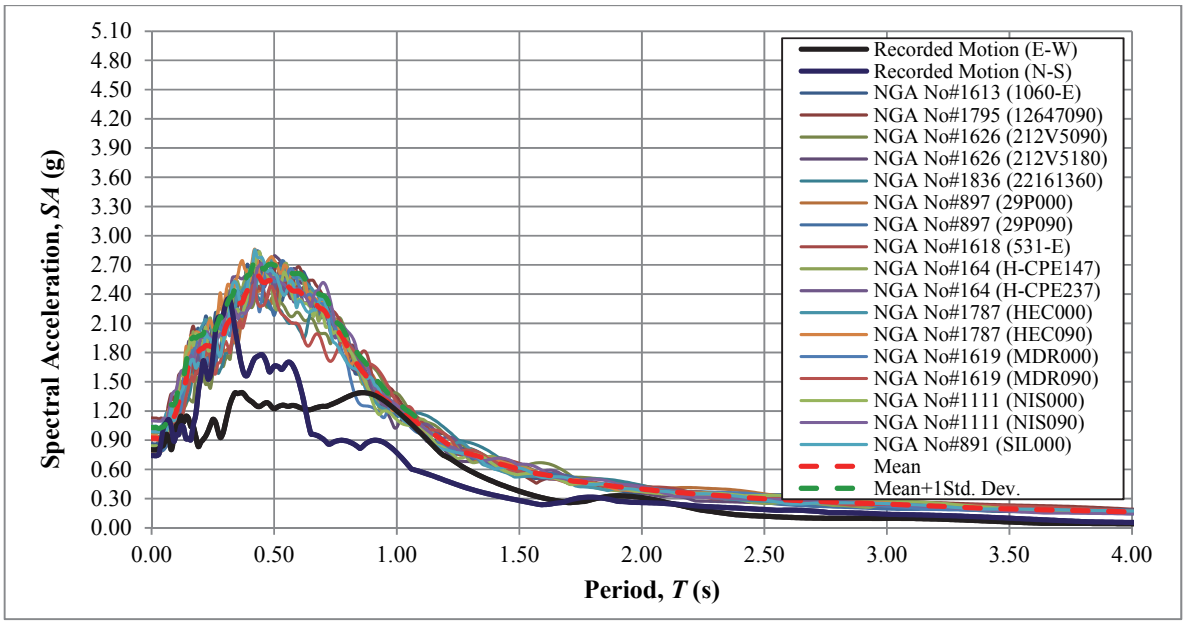

Figure A.48. A comparison of the mean and mean+1 std. deviation response spectrums, determined using Method#6, with the spectral response observed at AI010 TSGMN station

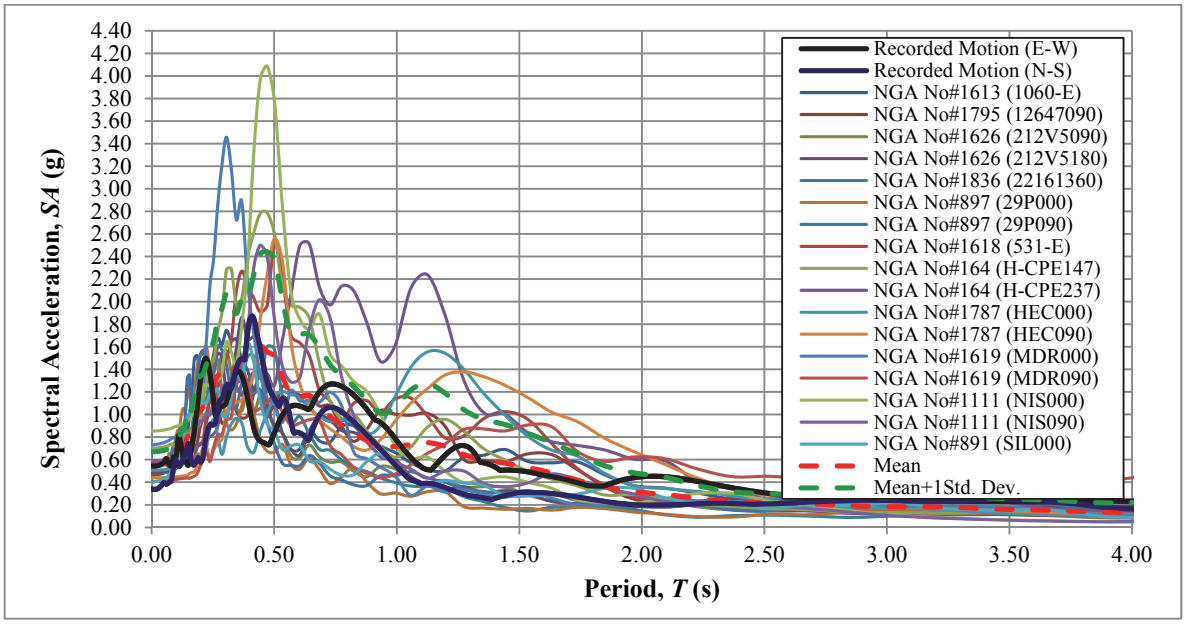

Figure A.49. A comparison of the mean and mean+1 std. deviation response spectrums, determined using Method#1, with the spectral response observed at AI011 TSGMN station

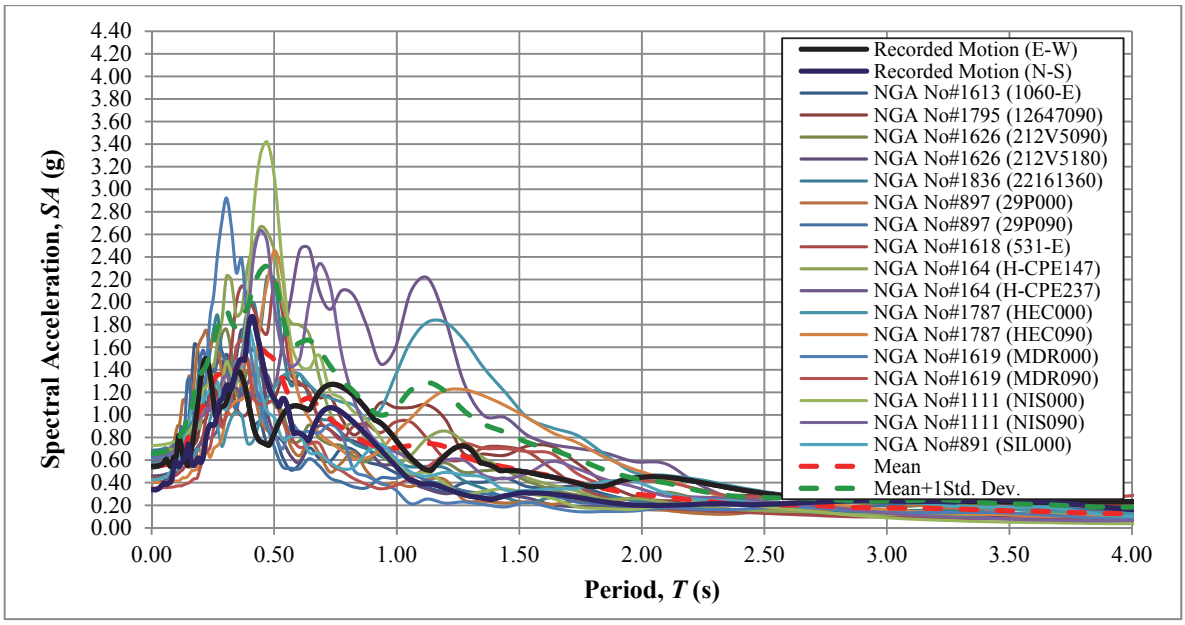

Figure A.50. A comparison of the mean and mean+1 std. deviation response spectrums, determined using Method#2, with the spectral response observed at AI011 TSGMN station

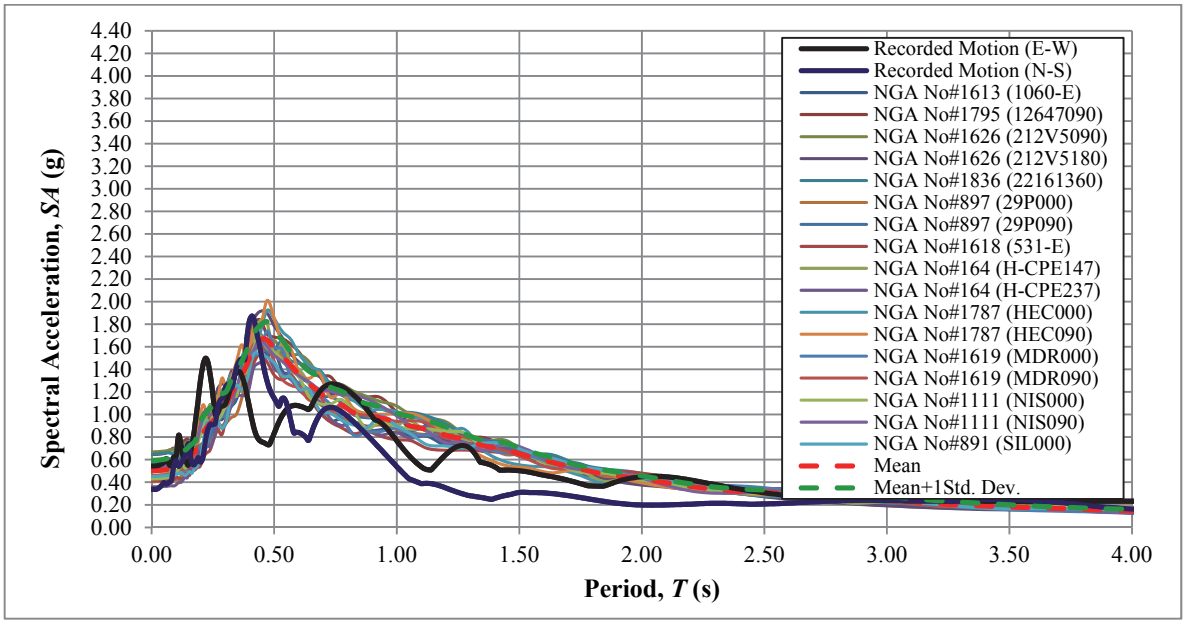

Figure A.51. A comparison of the mean and mean+1 std. deviation response spectrums, determined using Method#3, with the spectral response observed at AI011 TSGMN station

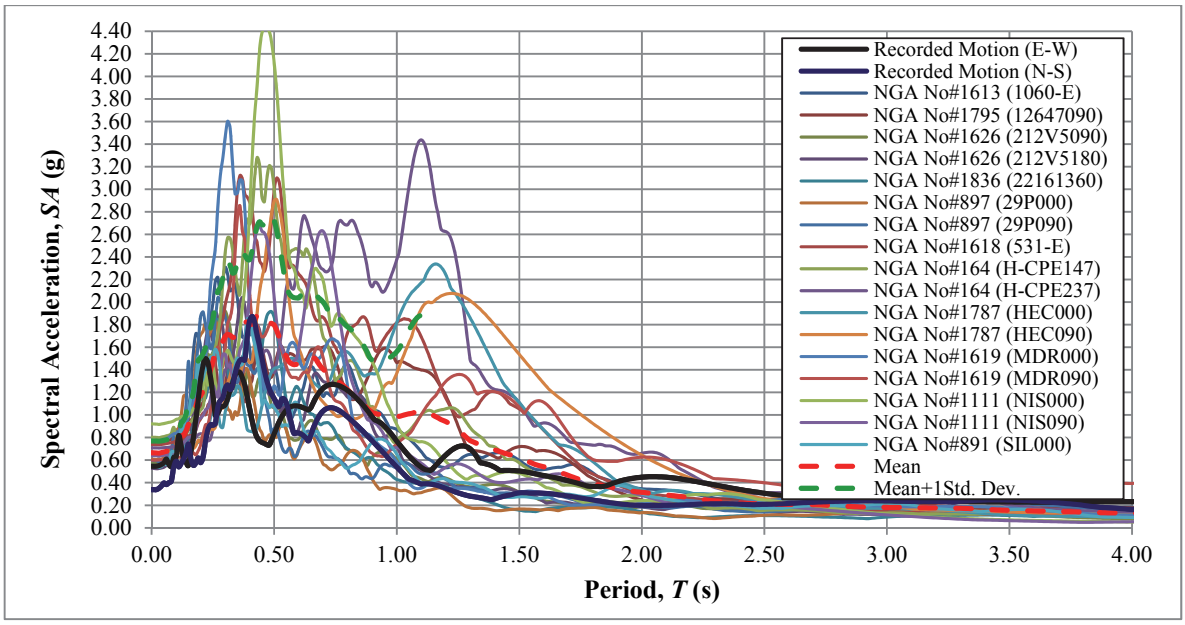

Figure A.52. A comparison of the mean and mean+1 std. deviation response spectrums, determined using Method#4, with the spectral response observed at AI011 TSGMN station

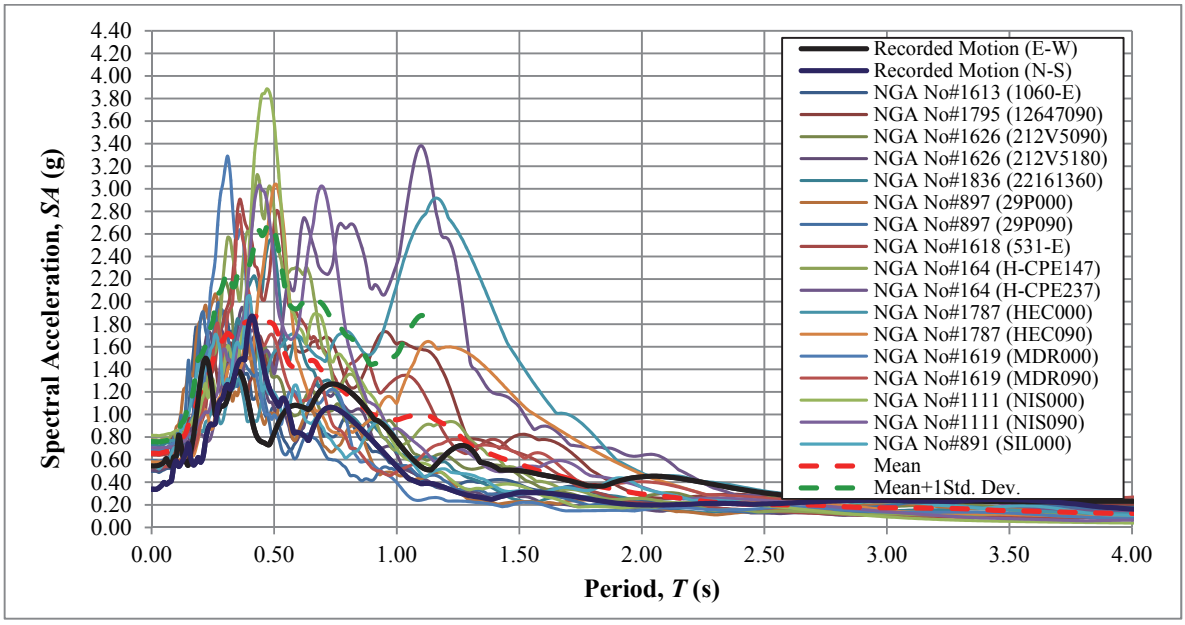

Figure A.53. A comparison of the mean and mean+1 std. deviation response spectrums, determined using Method#5, with the spectral response observed at AI011 TSGMN station

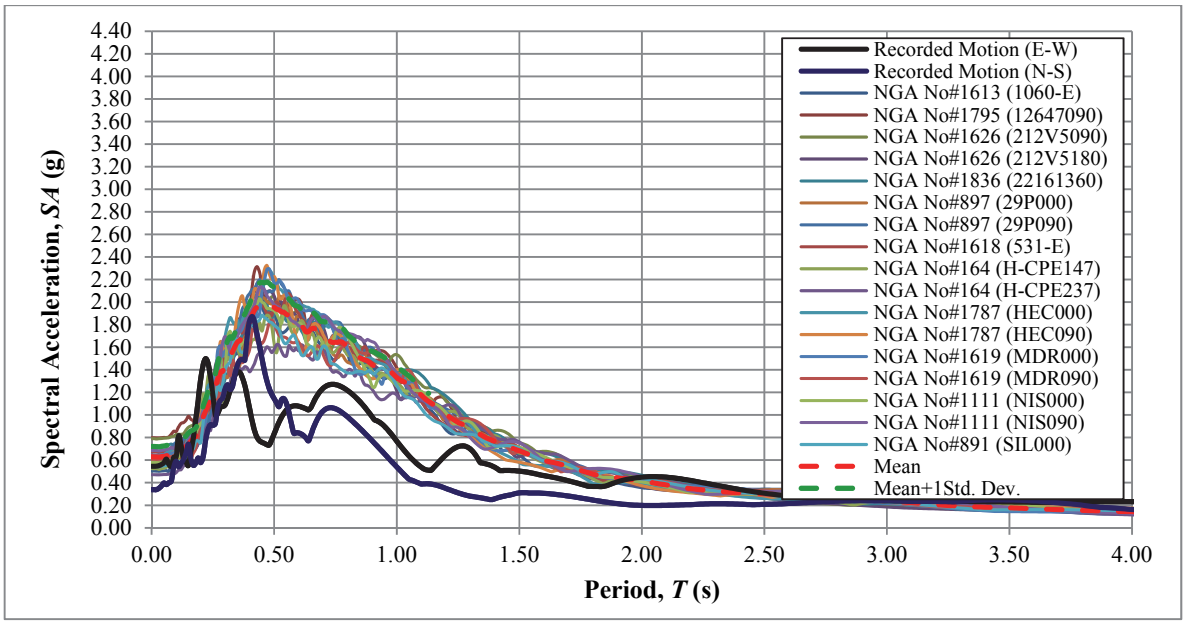

Figure A.54. A comparison of the mean and mean+1 std. deviation response spectrums, determined using Method#6, with the spectral response observed at AI011 TSGMN station

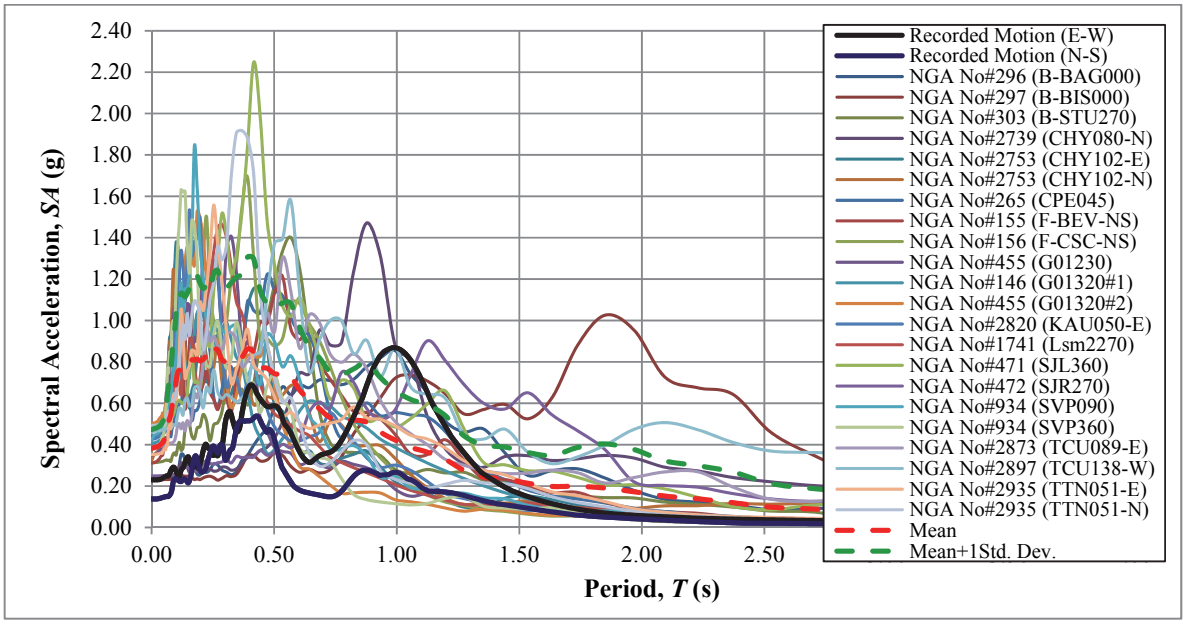

Figure A.55. A comparison of the mean and mean+1 standard deviation response spectrums, determined using Method#1, with the spectral response observed at AI127 TSGMN station

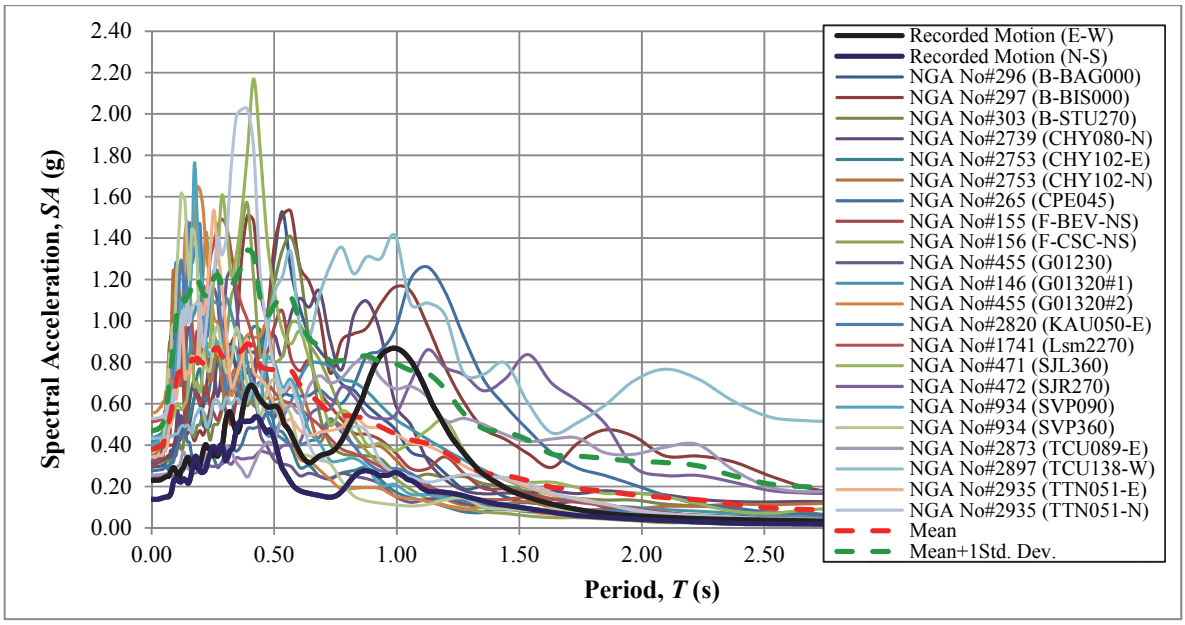

Figure A.56. A comparison of the mean and mean+1 standard deviation response spectrums, determined using Method#2, with the spectral response observed at AI127 TSGMN station

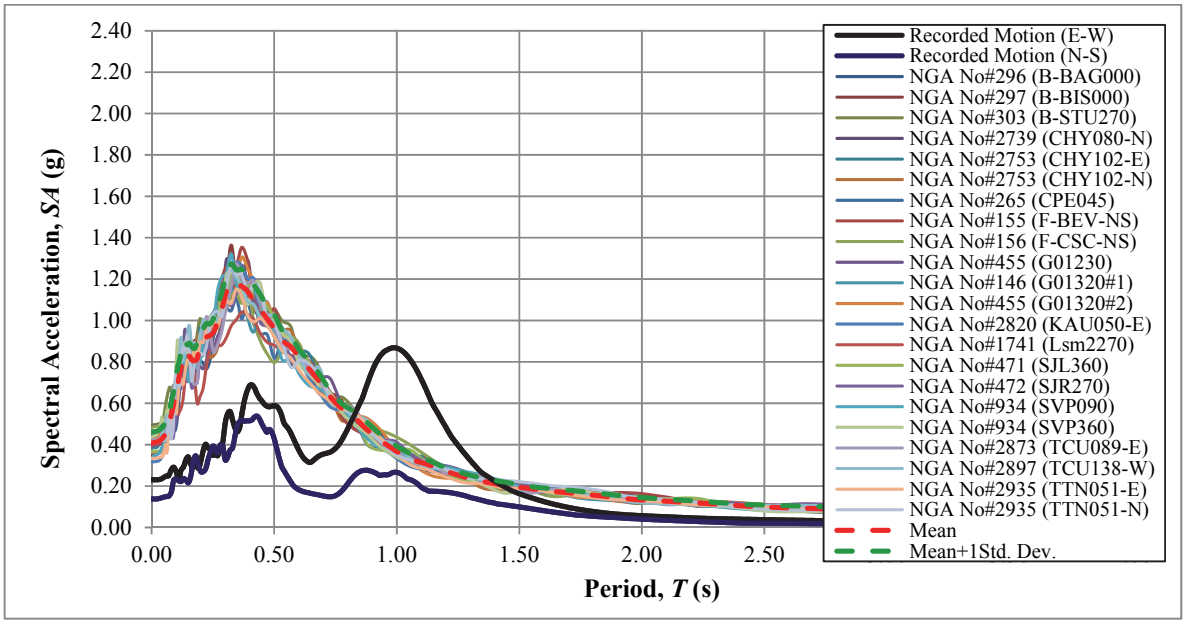

Figure A.57. A comparison of the mean and mean+1 standard deviation response spectrums, determined using Method#3, with the spectral response observed at AI127 TSGMN station

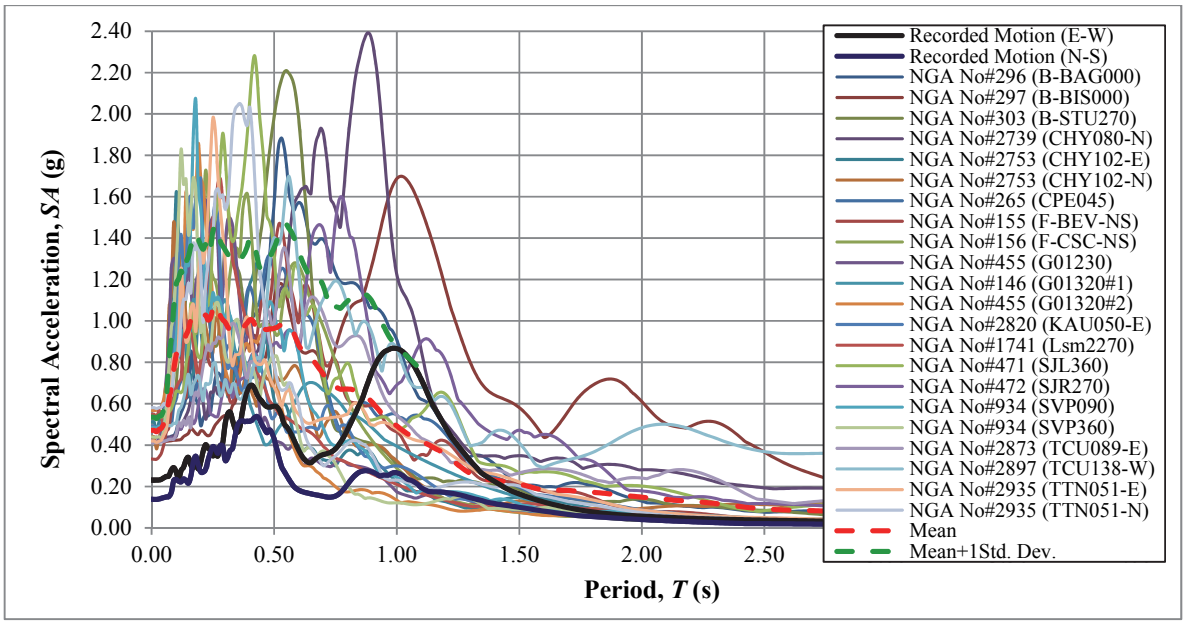

Figure A.58. A comparison of the mean and mean+1 standard deviation response spectrums, determined using Method#4, with the spectral response observed at AI127 TSGMN station

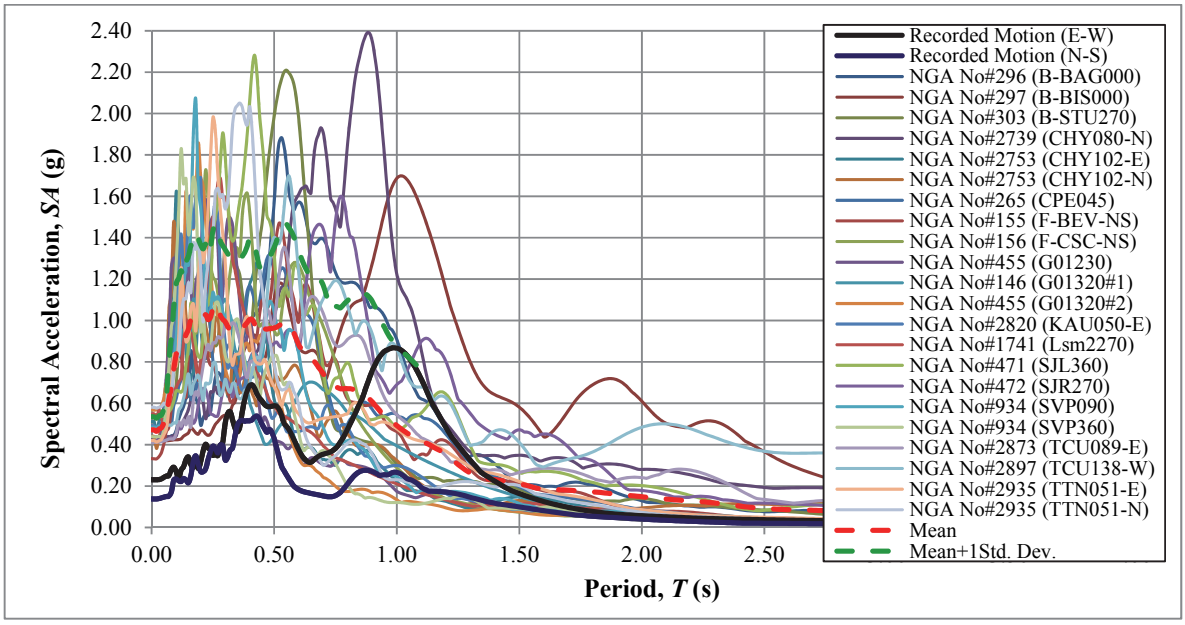

Figure A.59. A comparison of the mean and mean+1 standard deviation response spectrums, determined using Method#5, with the spectral response observed at AI127 TSGMN station

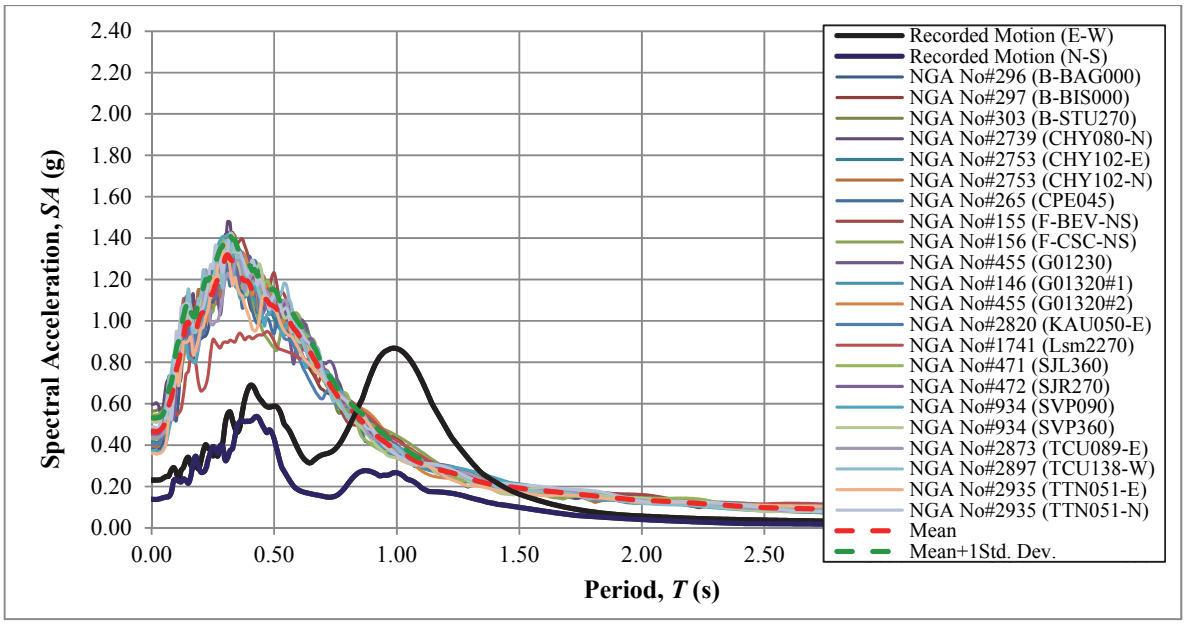

Figure A.60. A comparison of the mean and mean+1 standard deviation response spectrums, determined using Method#6, with the spectral response observed at AI127 TSGMN station

REFERENCES

[1] L. Reiter, Earthquake Hazard Analysis: Issues and Insights, 1st ed., New York, NY: Columbia University Press, 1991.

[2] R. K. McGuire, Seismic Hazard and Risk Analysis, 1st ed., Berkeley, CA: Earthquake Engineering Research Institute, 2004.

[3] K. Aki and P. G. Richards, Quantitative Seismology, 2nd ed., Sausalito, CA: University Science Books, 2009.

[4] J. H. Steidl, "Site Response in Southern California for Probabilistic Seismic Hazard Analysis," *Bulletin of the Seismological Society of America,* vol. 90, no. 6B, p. S149–S169, 2000.

[5] K. Pitilakis, C. Gazepis and A. Anastasiadis, "Design Response Spectra and Soil Classification for Seismic Code Provosions," in *Proceedings of 13th World Conference in Earthquake Engineering*, Vancouver, 2004.

[6] D. Di Giacomo, M. R. Gallipoli, M. Mucciarelli, S. Parolai and M. S. Richwalski, "Analysis and Modeling of HVSR in the Presence of a Velocity Inversion: The Case of Venosa, Italy," *Bulletin of the Seismological Society of America,* vol. 95, no. 6, p. 2364–2372, 2005.

[7] T. Kokusho and K. Sato, "Surface-to-Base Amplification Evaluated from KiK-net Vertical Array Strong Motion Records," *Soil Dynamics and Earthquake Engineering,* vol. 28, no. 9, p. 707–716, 2008.

[8] V. W. Lee and M. D. Trifunac, "Should Average Shear-Wave Velocity in the top 30m of Soil Be Used to Describe Seismic Amplification," *Soil Dynamics and Earthquake Engineering,* vol. 30, no. 11, p. 1250–1258, 2010.

[9] K. Pitilakis, E. Riga and A. Anastasiadis, "New Code Site Classification, Amplification Factors and Normalized Response Spectra Based on a Worldwide Ground-Motion Database," *Bulletin of Earthquake Engineering,* 2013.

[10] N. A. Abrahamson, W. J. Silva and R. Kamai , "PEER 2013/04 – Update of the AS08 Ground-Motion Prediction Equations Based on the NGA-West2 Data Set," Pacific Earthquake Engineering Research Center, Berkeley, 2013.

[11] D. M. Boore, J. P. Stewart and E. Seyhan, "PEER 2013/05 – NGA-West2 Equations for Predicting Response Spectral Accelerations for Shallow Crustal Earthquakes," Pacific Earthquake Engineering Research Center, Berkeley, 2013.

[12] K. W. Campbell and Y. Bozorgnia, "PEER 2013/06 – NGA-West2 Campbell-Bozorgnia Ground Motion Model for the Horizontal Components of PGA, PGV, and 5%-Damped Elastic Pseudo-Acceleration Response Spectra for Periods Ranging from 0.01 to 10 sec," Pacific Earthquake Engineering Research Center, Berkeley, 2013.

[13] B. S. Chiou and R. R. Youngs , "PEER 2013/07 – Update of the Chiou and Youngs NGA Ground Motion Model for Average Horizontal Component of Peak Ground Motion and Response Spectra," Pacific Earthquake Engineering Research Center, Berkeley, 2013.

[14] I. M. Idriss, "PEER 2013/08 – NGA-West2 Model for Estimating Average Horizontal Values of Pseudo-Absolute Spectral Accelerations Generated by Crustal Earthquakes," Pacific Earthquake Engineering Research Center, Berkeley, 2013.

[15] FEMA, "P-750 NEHRP recommended seismic provisions for new buildings and other structures," Building Seismic Safety Council, Washington DC, 2009.

[16] M. D. Petersen, A. D. Frankel, S. C. Harmsen, C. S. Mueller, K. M. Haller, R. L. Wheeler, R. L. Wesson, Y. Zeng, O. S. Boyd, D. M. Perkins, N. Luco, E. H. Field, C. J. Wills and K. S. Rukstales, "Documentation for the 2008 Update of the United States National Seismic Hazard Maps: U.S. Geological Survey Open-File Report 2008–1128," United States Geological Survey, Reston, 2008.

[17] M. Erdik, K. Sesetyan, M. B. Demircioğlu and E. Durukal, "Identification of Earthquake Hazards for Ministry of Transportation, Directorate of Harbor, Railroad and Airfield Assemblages Seismic Provisions for Harbor, Railroad and Airfield Facility Constructions (In Turkish)," Kandilli Observatory and Earthquake Research Institute, Istanbul, 2006.

[18] INGV, "DPC-INGV S1: Continuation of Assistance to DPC for Improving and Using the Seismic Hazard Map Compiled According to the Prime Minister "Ordinanza" 3274 of 2003 and Planning Future Initiatives," Italian National Institute of Geophysics and Volcanology, Rome, 2007a.

[19] G. A. Tselentis and L. Danciu, "Probabilistic Seismic Hazard Assessment in Greece – Part 1: Engineering Ground Motion Parameters," *Natural Hazards and Eart System Sciences,* vol. 10, no. 1, pp. 25-39, 2010.

[20] P. B. Schnabel, J. Lysmer and H. B. Seed, "UCB/EERC-72/12 - SHAKE: A Computer Program for Earthquake Response Analysis of Horizontally Layered Sites," Earthquake Engineering Research Center, University of California, Berkeley, Berkeley, 1972.

[21] I. M. Idriss and J. I. Sun, "SHAKE91: A Computer Program for Conducting Equivalent Linear Seismic Response Analyses of Horizontally Layered Soil Deposits," Center for

Geotechnical Modelling, Department of Civil and Environmental Engineering, University of California, Davis, Davis, 1992.

[22] Y. M. Hashash, D. Groholski and C. A. Phillips, "DEEPSOIL 5.1, User Manual and Tutorial," University of Illinois at Urbana-Champaign, Urbana-Champaign, 2012.

[23] T. Udaka, Analysis of Response of Large Embankments to Traveling Base Motions, Berkeley, CA: University of California Berkeley, 1975.

[24] S. L. Kramer, Geotechnical Earthquake Engineering, 1st Edition ed., Upper Saddle River, New Jersey: Prentice Hall, 1996, p. 653.

[25] P. Stoica and R. L. Moses, Spectral Analysis of Signals, 1st ed., Upper Saddle River, NJ: Prentice Hall, 2005.

[26] J. Dewey and P. Byerly, "The Early History of Seismometry (to 1900)," *Bulletin of Seismological Society of America,* vol. 59, no. 1, pp. 183-227, 1969.

[27] E. L. Krinitzsky and F. K. Chang, "S-73-1: State-of-the-Art for Assessing Earthquake Hazards in the United States; Report 7, Specifying Peak Motions for Design Earthquakes," Soils and Pavements Laboratory - U. S. Army Engineer Waterways Experiment Station, Vicksburg, 1977.

[28] V. W. Lee, "Empirical Scaling of Strong Earthquake Ground Motion - Part I: Attenuation and Scaling of Response Spectra," *ISET Journal of Earthquake Technology,* vol. 39, no. 4, pp. 219-254, 2002.

[29] M. D. Trifunac and A. G. Brady, "On the Correleation of Seismic Intensity with Peaks of Recorded Strong Ground motion," *Bulletion of Seismological Society of America,* vol. 65,

no. 1, pp. 139-162, 1975.

[30] E. L. Krinitzsky and F. K. Chang, "State-of-the-Art for Assessing Earthquake Hazards in the United States. Report 25 - Parameters for Specifying Intensity-Related Earthquake Ground Motions," Army Engineer Waterways Experiment Station Vicksburg, MS Geotechnical Laboratory, Vicksburg, 1987.

[31] G. F. Panza, R. Cazzaro and F. Vaccari, "Correlation Between Macroseismic Intensities and Seismic Ground Motions," *Annals of Geophysics,* vol. 40, no. 5, 1997.

[32] D. J. Wald, V. Quitoriano, T. H. Heaton and H. Kanamori, "Relationships Between Peak Ground Acceleration, Peak Ground Velocity, and Modified Mercalli Intensity in California," *Earthquake Spectra,* vol. 15, no. 3, pp. 557-564, 1999.

[33] K. R. Karim and F. Yamazaki, "Correlation of JMA Instrumental Seismic Intensity with Strong Motion Parameters," *Earthquake Engineering and Structural Dynamics,* vol. 31, no. 5, p. 1191–1212, 2002.

[34] A. G. Tselentis and L. Danciu, "Empirical Relationships between Modified Mercalli Intensity and Engineering Ground-Motion Parameters in Greece," *Bulletin of the Seismological Society of America,* vol. 98, no. 4, p. 1863–1875, 2008.

[35] E. M. Rathje, A. R. Kottke and W. L. Trent, "Influence of Input Motion and Site Property Variabilities on Seismic Site Response Analysis," *Journal of Geotechnical and Geoenvironmental Engineering,* vol. 136, no. 4, pp. 607-619, 2010.

[36] M. A. Biot, "Theory of Elastic Systems Vibrating under Transient Impulse with an Application to Earthquake-Proof Buildings," *Proceedings of the National Academy of Sciences of the United States of America,* vol. 19, no. 2, pp. 262-268, 1933.

[37] E. Safak, "Discrete-Time Analysis of Seismic Site Amplification," *Journal of Engineering Mechanics,* vol. 121, no. 7, p. 801–809, 1995.

[38] L. S. Lasdon, R. L. Fox and M. W. Ratner, "Nonlinear Optimization Using the Generalized Reduced Gradient Method," National Technical Information Service, Springfield, 1973.

[39] E. H. Vanmarcke, "Representation of Earthquake Ground Motion: Scaled Accelerograms and Equivalent Response Spectra," U.S. Army Engineer Waterways Experiment Station, Vicksburg, 1979.

[40] Y. M. A. Hashash and D. Park, "Non-linear One-Dimensional Seismic Ground Motion Propagation in the Mississippi Embayment," *Engineering Geology,* vol. 62, no. 1-3, pp. 185-206, 2001.

[41] R. Dobry, W. G. Pierce, R. Dyvik, G. E. Thomas and R. S. Ladd, "Pore Pressure Model for Cyclic Straining of Sand," Rensselaer Polytechnic Institute - Civil Engineering Department, Troy, 1985.

[42] Electric Power Research Institute, "Guidelines for Determining Design Basis Ground Motions - Volume 1: Method and Guidelines for Estimating Earthquake Ground Motion in Eastern North America," EPRI, Palo Alto, 1993.

[43] N. A. Abrahamson and W. J. Silva, "Empirical Response Spectral Attenuation Relations for Shallow Crustal Earthquakes," *Seismological Research Letters,* vol. 68, no. 1, pp. 94-127, 1997.

[44] P. Bazzurro and N. Luco, "Do Scaled and Spectrum-Matched Near-Source Records Produce Biased Nonlinear Structural Responses?," in *Proceesings of the 8th U.S.*

National Conference on Earthquake Engineering, San Fransisco, 2006.

[45] L. Al Atik and N. Abrahamson, "An Improved Method for Nonstationary Spectral Matching," *Earthquake Spectra,* vol. 26, no. 3, pp. 601-617, 2010.

[46] K. Lilhanand and S. W. Tseng, "Development and Application of Realistic Earthquake Time Histories Compatible with Multiple Damping Response Spectra," in *9th World Conference on Earthquake Engineering*, Tokyo, 1988.

[47] I. Elishakoff, Probabilistic Theory of Structures, 2nd ed., Toronto, Ontario: Dover Publications, 1999.

[48] R. I. Borja, H.-Y. Chao, F. J. Montans and C.-H. Lin, "Nonlinear Ground Response at Lotung LSST Site," *Journal of Geotechnical and Geoenvironmental Engineering,* vol. 125, no. 3, pp. 187-197, 1999.

[49] M. B. Baturay and J. P. Stewart, "Uncertainty and Bias in Ground-Motion Estimates from Ground Response Analyses," *Bulletin of the Seismological Society of America,* vol. 93, no. 5, p. 2025–2042, 2003.

[50] A. Meslem, F. Yamazaki, Y. Maruyama, D. Benouar, N. Laouami and N. Benkaci, "Site-Response Characteristics Evaluated from Strong Motion Records of the 2003 Boumerdes, Algeria, Earthquake," *Earthquake Spectra,* vol. 26, no. 3, p. 803–823, 2010.

[51] B. Kim and Y. M. Hashash, "Site Response Analysis Using Downhole Array Recordings during the March 2011 Tohoku-Oki Earthquake and the Effect of Long-Duration Ground Motions," *Earthquake Spectra,* vol. 29, no. S1, p. S37–S54, 2013.

[52] A. K. Chopra, Dynamics of Structures: Theory and Applications to Earthquake Engineering, Upper Saddle River, NJ: Prentice Hall, 2007.

[53] M. A. Sandıkkaya, M. T. Yılmaz, B. S. Bakır and Ö. Yılmaz, "Site Classification of Turkish National Strong Motion Stations," *Journal of Seismology,* vol. 14, no. 3, pp. 543-563, 2010.

[54] Building Seismic Safety Council, "NEHRP RecommendeSeismic Provisions for New Buildings and Other Structures: FEMA P-750," Federal Emergency Management Agency, Washington DC, 2009.

[55] European Committee for Standardisation, "Eurocode 8: Design Provisions for Earthquake Resistance of Structures, Part 1.1: General Rules, Seismic Actions and Rules for Buildings," CEN, Brussels, 2003.

[56] "Specification for Structures to be Built in Seismic Zones," Ministry of Public Works and Settlement, Government of the Republic of Turkey, Ankara, 2007.

[57] M. Inel, S. M. Senel, S. Toprak and Y. Manav, "Seismic Risk Assessment of Buildings in Urban Areas: A Case Study for Denizli, Turkey," *Natural Hazards,* vol. 46, no. 3, pp. 265-285, 2008.

[58] R. Ulusay, O. Aydan, H. Kumsar and H. Tano, "Is There a Relation Between the Temperature Changes of Thermal Waters in Denizli Region and the Behavior of Earth Crust at the Denizli Fault Zone? (In Turkish)," in *Jeoteknik-III*, Izmir, 2001.

[59] G. Vannucci and P. Gasperini, "A Database of Revised Fault Plane Solutions for Italy and Surrounding Regions," *Computers & Geosciences,* vol. 29, no. 7, pp. 903-909, 2003.

[60] R. C. Ates and N. Bayulke, "The 19 August 1976 Denizli, Turkey Earthquake: Evaluation of the Strong Motion Accelerograph Record," *Bulletin of the Seismological Society of America,* vol. 72, no. 5, pp. 1635-1649, 1982.

[61] M. B. Darendeli, Development of a New Family of Normalized Modulus Reduction and Material Damping Curves, Austin: The University of Texas at Austin, 2001.

[62] M. Vucetic and R. Dobry, "Effect of Soil Plasticity on Cyclic Response," *Journal of Geotechnical Engineering,* vol. 117, no. 1, pp. 89-107, 1991.

[63] C. Erentoz, "A General Review of the Geology of Turkey," *MTA Bulletin,* vol. 48, pp. 40-58, 1956.

[64] H. B. Seed, R. T. Wong, I. M. Idriss and K. Tokimatsu, "Moduli and Damping Factors for Dynamic Analyses of Cohesionless Soils," *Journal of Geotechnical Engineering,* vol. 112, no. 11, pp. 1016-1032, 1986.

[65] K. Gelisli and N. Maden, "Analysis of Potential Field Anomalies in Pasinler-Horasan Basin, Eastern Turkey," *Journal of the Balkan Geophysical Society,* vol. 9, no. 1, pp. 1-7, 2006.

[66] A. Barka and M. S. Bayraktutan, "Active Fault Systems Affecting the Erzurum Basin and Surroundings (In Turkish)," in *Proceedings of the Turkish Geology Congress*, Ankara, 1985.

[67] H. Eyidogan, S. S. Nalbant, A. Barka and G. C. P. King, "Static Stress Changes Induced by the 1924 Pasinler (M=6.8) and 1983 Horasan-Narman (M=6.8) Earthquakes, Northeastern Turkey," *Terra Nova,* vol. 11, no. 1, pp. 38-44, 1999.

[68] Y. F. Aysan, "The Erzurum-Kars Earthquake of Eastern Turkey (1983)," *Disasters,* vol. 8, no. 1, pp. 21-32, 1984.

[69] L. Selcuk, A. S. Selcuk and T. Beyaz, "Probabilistic Seismic Hazard Assessment for Lake Van Basin Turkey," *Natural Hazards,* vol. 54, no. 3, p. 949–965, 2010.

[70] B. S. Bakir, M. Y. Ozkan and S. Cılız, "Effects of Basin Edge on the Distribution of Damage in 1995 Dinar, Turkey Earthquake," *Soil Dynamics and Earthquake Engineering,* vol. 22, no. 4, pp. 335-345, 2002.

[71] R. Iyisan and M. E. Hasal, "The Basin Edge Effect on Dynamic Response: Dinar Basin Model (In Turkish)," *Teknik Dergi,* vol. 22, no. 3, pp. 5559-5578, 2011.

[72] H. Eyidogan and A. Barka, "The 1 October 1995 Dinar Earthquake, SW Turkey," *Terra Nova,* vol. 8, no. 52, pp. 479-485, 1996.

[73] Afet İşleri Genel Müdürlüğü, Deprem Araştırma Dairesi Bakanlığı, "Disaster Management Report," Sismoloji Şube Müdürlüğü, Ankara, 1995.

[74] A. I. Kanli, P. Tildy, Z. Pronay, A. Pınar and L. Hermann, "Vs30 Mapping and Soil Classification for Seismic Site Effect Evaluation in Dinar Region, SW Turkey," *Geophysical Journal International,* vol. 165, no. 1, pp. 223-235, 2006.

[75] R. Ulusay, H. Sönmez, Ö. Aydan and H. Kumsar, "Engineering Geological Characteristics of the 1998 Adana-Ceyhan Earthquake, with Particular Emphasis on Liquefaction Phenomena and the Role of Soil Behaviour," *Bulletin of Engineering Geology and the Environment,* vol. 59, no. 2, pp. 99-118, 2000.

[76] M. Çelebi, "Revelations from a Single Strong-Motion Record Retrieved during the 27

June 1998 Adana (Turkey) Earthquake," *Soil Dynamics and Earthquake Engineering,* vol. 20, no. 5, p. 283–288, 2000.

[77] H. Sucuoğlu, T. Gür and P. Gülkan, "The Adana–Ceyhan Earthquake of 27 June 1998: Seismic Retrofit of 120 R/C Buildings," in *Proceedings of 12th World Conference on Earthquake Engineering*, Auckland, 2000.

[78] A. Ayhan and A. Z. Bilgin, "1/100,000 Scale Stratigraphy Map of Kozan-Adana (In Turkish)," Mineral Research and Exploration General Directorate of Turkey, Ankara, 1988.

[79] C. Yetis, "Reorganization of the Tertiary Stratigraphy in the Adana Basin, Southern Turkey," *Newsletters on Stratigraphy,* vol. 20, no. 1, pp. 43-58, 1988a.

[80] R. F. Kartal, T. Kilic and F. T. Kadiroglu, "Prediction of Seismic Hazard for the Province of Mersin using Probabilistic and Statistical Methods (In Turkish)," in *1st Earthquake Engineering and Seismology Conference (Turkey)*, Ankara, 2011.

[81] J. D. Bray, R. B. Sancio, T. Durgunoglu, A. Onalp, T. L. Youd, J. P. Stewart, R. B. Seed, K. O. Cetin, E. Bol, M. B. Baturay, C. Christensen and T. Karadayilar, "Subsurface Characterization at Ground Failure Sites in Adapazari Turkey," *Journal of Geotechnical and Geoenvironmental Engineering,* vol. 130, no. 7, pp. 673-685, 2004.

[82] A. Onalp, E. Arel and E. Bol, "A General Assessment of the Effects of 1999 Earthquake on the Soil-Structure Interaction in Adapazari," in *Jubilee Papers in Honor of Prof. Ergun Togrul*, Istanbul, 2001.

[83] R. B. Sancio, "Ground Failure and Building Performance in Adapazari, Turkey," University of California at Berkeley, Berkeley, 2003.

[84] B. S. Bakir, H. Sucuoglu and T. Yılmaz, "An Overview of Local Site Effects and the Associated Building Damage in Adapazarı during the 17 August 1999 Izmit Earthquake," *Bulletin of the Seismological Society of America,* vol. 92, no. 1, p. 509–526, 2002.

[85] E. Kalkan, P. Gulkan, N. Yilmaz and M. Celebi, "Reassessment of Probabilistic Seismic Hazard in the Marmara Region," *Bulletin of the Seismological Society of America,* vol. 99, no. 4, pp. 2127-2146, 2009.

[86] K. Ulamis and R. Kilic, "Liquefaction Potential of Quaternary Alluvium in Bolu Settlement Area, Turkey," *Environmental Geology,* vol. 55, no. 5, pp. 1029-1038, 2008.

[87] DSI, "Borehole Logs and Explanations of the Water Well Drilling within Bolu Proper (In Turkish)," General Directorate of State Hydraulic Works, Ankara, 1962.

[88] E. M. Rathje, K. H. Stokoe II and B. Rosenblad, "Strong Motion Station Characterization and Site Effects During the 1999 Earthquakes in Turkey," *Earthquake Spectra,* vol. 19, no. 3, p. 653–675, 2003.

[89] M. Hobiger, C. Cornou , M. Wathelet , G. Di Giulio, B. Knapmeyer-Endrun , F. Renalier, P.-Y. Bard, A. Savvaidis , S. Hailemikael , N. Le Bihan , M. Ohrnberger and N. Theodoulidis, "Ground Structure Imaging by Inversions of Rayleigh Wave Ellipticity: Sensitivity Analysis and Application to European Strong-Motion Sites," *Geophysical Journal International,* vol. 192, no. 1, pp. 207-229, 2013.

[90] A. T. Basokur, "Determination of Shear Wave Velocity Profile at a Construction Site using REMI Method (In Turkish)," in *Kocaeli Earthquake Symposium*, Kocaeli, 2005.